Dissertation

submitted to the
Combined Faculties for the Natural Sciences and for Mathematics
of the Ruperto-Carola University of Heidelberg, Germany
for the degree of
Doctor of Natural Sciences

Put forward by
Dipl. Phys. Christian Eberhard
born in Freudenstadt, Germany

Oral examination: December 11, 2012

Development of a Model System to Study Cell Adhesion and Cell Mechanics

Referees:
Prof. Dr. Joachim P. Spatz
Prof. Dr. Rainer H. A. Fink

Zusammenfassung

In dieser Arbeit wurde ein vereinfachtes Modell zur experimentellen Untersuchung der physikalischen Prozesse, welche der Zelladhäsion zugrunde liegen, entwickelt. Die Komplexität der Zelle wurde reduziert auf drei grundlegende Komponenten: die Lipidmembran, das Zelladhäsionsmolekül Integrin und das Protein Aktin, welches Teil des zellulären Zytoskeletts ist. Integrin wurde in kugelförmige Lipidmembran, sogenannte Riesenvesikel, eingebaut, welche zusätzlich mit Aktin gefüllt waren.

Integrin $\alpha_{\mathrm{IIb}}\beta_3$ wurde mit hoher Ausbeute aus Blutplättchenmembranen aufgereinigt. Zunächst wurde dieses Integrin in kleine, einschalige Vesikel rekonstituiert. Durch Variation von Lipidzusammensetzung, Vesikeldurchmesser und Detergenskonzentration konnten grundlegende Parameter für einen effizienten Einbau gefunden, und die Effizienz der Rekonstitution erhöht werden.

Zum Wachsen von Riesenvesikeln wurden zwei verschiedene Herangehensweisen verglichen, zum einen Elektroschwellen und zum anderen spontanes Wachstum auf Agarose-Lipidfilmen. Neben der biochemischen Charakterisierung wurde die Bildung von Riesenvesikeln mit einem konfokalen Laserscanning Mikroskop untersucht. Dadurch konnte der erfolgreiche Einbau von Integrin in die Doppelschicht der Riesenvesikel bestätigt werden.

Des Weiteren wurde eine neue Methode zur Herstellung von Riesenvesikeln aus Blutplättchenmembranen etabliert. Dies gelingt durch die direkte Aufreinigung von Blutplättchenmembranen und anschließendem Elektroschwellen. Die Wechselwirkung dieser Riesenvesikel mit nanostrukturierten und biofunktionalisierten Oberflächen wurde untersucht. Die Adhäsion dieser mit Integrin bedeckten Vesikel in Abhängigkeit der Ligandendichte wurde erstmals mittels Interferenzreflexionsmikroskopie charakterisiert. Somit konnte eine mittlere Adhäsionsenergie der mit Integrin funktionalisierten Vesikel abgeschätzt werden.

Abstract

Within this work, a simplified model system was developed for the experimental investigation of physical mechanisms underlying cell adhesion. Cellular complexity was reduced to three essential components: the lipid bilayer, the cell adhesion molecule integrin and the cytoskeletal protein actin. Integrin was integrated in spherical lipid bilayers, called giant unilamellar vesicles (GUVs), which were additionally filled with actin.

Integrin $\alpha_{\mathrm{IIb}}\beta_3$ was purified from human platelet membranes with high yield. Initially, this integrin was reconstituted in small unilamellar vesicles (SUVs). By variation of lipid composition, vesicle size and detergent concentration, crucial parameters for efficient integration could be determined and incorporation efficiency was enhanced.

Two different approaches were compared to grow GUVs: electroformation and spontaneous swelling on agarose-lipid films. Besides biochemical characterization, formation of GUVs was investigated by means of confocal laser scanning microscopy confirming successful integration of integrin into the bilayer of the giant vesicles.

A novel method for the preparation of GUVs from purified platelet membranes was established. Platelet membranes were directly purified and grown to giant vesicles by electroformation. Interaction of these GUVs with nano-structured and bio-functionalized surfaces was investigated. Adhesion of these integrin-coated vesicles was characterized for the first time by reflection interference contrast microscopy (RICM), which allowed estimation of an average adhesion energy.

Contents

1 Motivation

The human body is comprised of about 100 trillion cells [21], which fulfill many different tasks and functions. Cell adhesion and subsequent spreading are thereby of fundamental importance. These two processes ensure not only adequate cell growth, but rather are indispensable for their survival. Establishing a dynamic interface between the environment and adjacent cell bodies is thus the prerequisite for multicellular life [1].

Cells adhere with the help of cell adhesion molecules (CAMs) to a surrounding protein-rich interconnected structure, the so-called extracellular matrix (ECM). The ECM is built from various heterogeneous proteins like collagens or fibronectin providing structure and stability to the tissue as well as serving as ligands to CAMs [93,200]. CAM-mediated adhesion processes are involved in essential physiological processes like blood clotting, wound healing and immunity. Malfunction or dysregulation can therefore lead to diseases like rheumatoid arthritis and stroke [78]. One important class of CAMs, integrins, can influence tumor metastasis and neovascularization of tumor tissue [121]. Therefore, a better understanding of the interaction between integrins and the ECM might be essential on the way to new therapies for cancer.

Integrins are tightly interacting with a meshwork of filamentous biopolymers and their associated regulatory proteins. This physical connection enables cells to sense the mechanical properties of their environment actively adapting and rearranging the surrounding ECM by generation of directed forces [215]. A correlation between altered cellular responses to mechanical cues and various diseases could be established in multiple studies [84].

Spatio-temporal regulation of cell adhesion molecules requires a highly orchestrated interplay between various signaling pathways creating a complex, multi-dimensional network of interactions [227]. In order to understand the underlying basic mechanisms of adhesion a simplified biomimetic model system with few important variables is required. This reductionists' concept might help to discern physical processes from active biological responses. Identification of key players is thereby paving the ground for an understanding-by-construction approach creating a universal model system for cell adhesion processes. Such systems could be the base for creation of bio-inspired autonomous machines in the far future, as already envisioned by Richard Feynman in the early sixties [52].

This work aims to develop the before mentioned low dimensional model system which imitates cell adhesion, but also allows control of its mechanical properties. Therefore the technique of forming giant unilamellar vesicles, an established model

system for the cell membranes, is combined with in-vitro reconstitution of cytoskeleton building blocks.

This bottom-up approach opens up tremendous opportunities to add more and more components in the future, gradually increasing complexity. One could even attempt to synthetically reconstitute focal adhesion complexes build from more than 150 components [226, 227] by reverse engineering.

This thesis is divided into three major parts: Introduction, Experimental Design and Measurement Techniques as well as Results and Discussion. The introduction reviews some basic concepts regarding cell adhesion and cell structure. Established model systems to investigate cell adhesion processes are summarized in the next section leading to reconstitution of membrane proteins in vesicles and relevant microscopy and biochemistry techniques applied within this study. Subsequent chapters address the experimental design as well as protocols and assays developed. In the third part, key findings are presented and discussed starting with a closer look on the biochemistry of the system. Results concerning the incorporation of integrin in small and giant vesicles are discussed in the fourth section. The final chapter gives attention to first measurements on the adhesive properties of the model system. This work closes with concluding remarks and ideas on future experiments.

Part I

Introduction

2 Cell Adhesion and Mechanics

Adhesion of cells to their surroundings and to each other is an essential process in the development of complex multi-cellular life. It is essential in the regulation of many intra- and extracellular phenomena such as cell motility, differentiation and apoptosis [149,150,201]. Cell adhesion is closely related to cell mechanics and thereby to cell structure [181, 215] which is described in the first section of this chapter. In the second chapter, cell adhesion in general and particularly the integrins as one important class of adhesion proteins are subsequently discussed. A brief literature review of model systems providing insight into the physics of adhesion is given in the third section.

2.1 Cell Structure

Cells can be separated in four major components: membrane, cytoskeleton, cytosol with it's many organelles, and the nucleus. The plasma membrane is a selectively permeable barrier between the cell's interior and the outside environment. It consists of a phospholipid double layer with a thickness of around 5 nm [27]. In this context the term leaflet is used to address only one lipid layer. The membrane's barrier function allows the establishment and maintenance of gradients of ions, nutrients and metabolites. Polar as well as large molecules have to be actively transported across the bilayer by specialized protein complexes. A system of membrane-bound or membrane-integrated proteins, like adhesion receptors or ion channels, can be approximated as a solution of proteins in a two dimensional (2D), viscous lipid fluid - a model known as the fluid mosaic model [189]. On the outer side of the cell membrane, glycoproteins and other polymeric sugars connected to the extracellular leaflet of the bilayer form a coat preventing unspecific adhesion due to steric hindrance which is called glycocalyx. Glycoproteins are proteins with at least one covalently bound sugar.

A cell's physical integrity and overall shape is maintained by the cytoskeleton. It is composed of three biopolymers - filamentous actin (F-actin), microtubules, and intermediate filaments - with different mechanical properties and many associated proteins that cross-link, bundle, cap or severe the polymers [17].

A common feature of actin filaments and microtubules is their assembly from globular monomers, called G-actin and tubulin, making their structure highly dynamic. In contrast, intermediate filaments are build up from fibrous subunits forming a coiled-

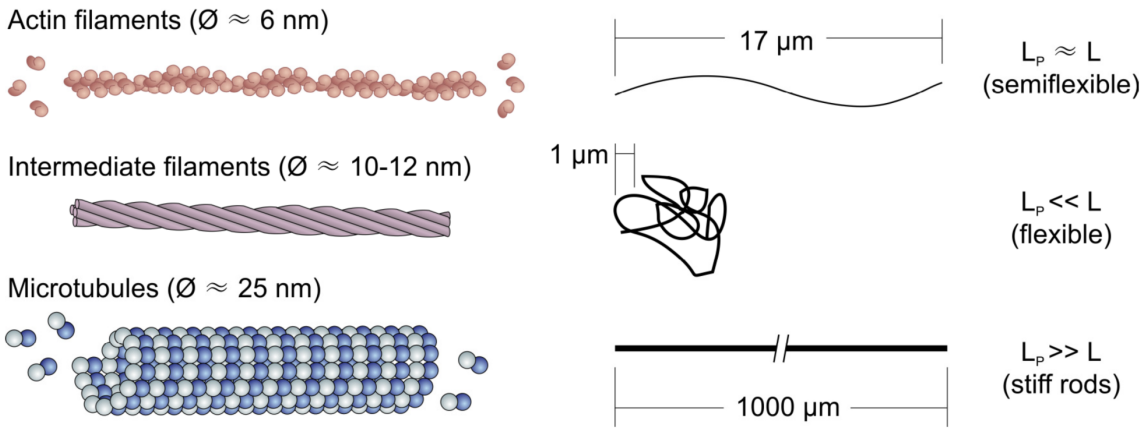

Figure 2.1: General properties of cytoskeletal components. Semi-flexible actin filaments are assembled from G-actin monomers. Protofilaments are the major constituents of intermediate filaments which display a high structural flexibility. Microtubules are pipe-like structures built from α/β-tubulin heterodimers, exhibiting an extraordinary persistence length L_P. (Sketches to the right are drawn to scale. The indicated length represents the persistence length l_P). Courtesy of Martin Deibler [37].

coil structure [7]. Their name is deduced from their diameter d of 10 nm, which is in between the diameters of actin filaments $d = 7$ nm and microtubules $d = 24$ nm [111]. The polymers' diverse mechanical behavior is reflected in their persistence lengths l_P. The persistence length gives the length scale over which a polymer behaves like a rigid rod. Actin is semi-flexible ($l_P = 17$ µm), while microtubules form rigid pipe-like structures with $l_P = 1$ mm. Intermediate filaments are highly flexible ($l_P = 1$ µm structures [89]. A summary of structure and mechanical properties of cytoskeletal proteins is found in figure 2.1.

Due to their unique features, each polymer is serves different functions. Actin gives the membrane stability without constraining its flexibility by forming a thin meshwork of actin fibers, termed "actin cortex", underneath the plasma membrane. Combination of motor proteins, in the case of actinmyosins, and filamentous actin (F-actin) builds actomyosin-fibrils. These multi-protein complexes are involved in cell contraction and motility [143].

Intermediate filaments help to resist mechanical forces via their rope-like structure that can bear high tensile strain. This class of cytoskeleton proteins can be found throughout the cell. In contrast, microtubules, being tube-like and rigid, serve as intracellular transport paths and establish a mechanical abutment for the process of cell division, the mitotic spindle.

The cytosol is the viscous, protein-rich fluid within cells. It is an aqueous, dense solution of ions, molecules of various size, proteins and protein-complexes. Eukaryotic cells are characterized by the presence of compartments called organelles.

The majority of the hereditary information is stored as deoxyribonucleic acid (DNA) highly condensed into chromatin, a complex mixture of DNA and different proteins, inside of the nucleus. A scheme of an eukaryotic cell is depicted in figure 2.2.

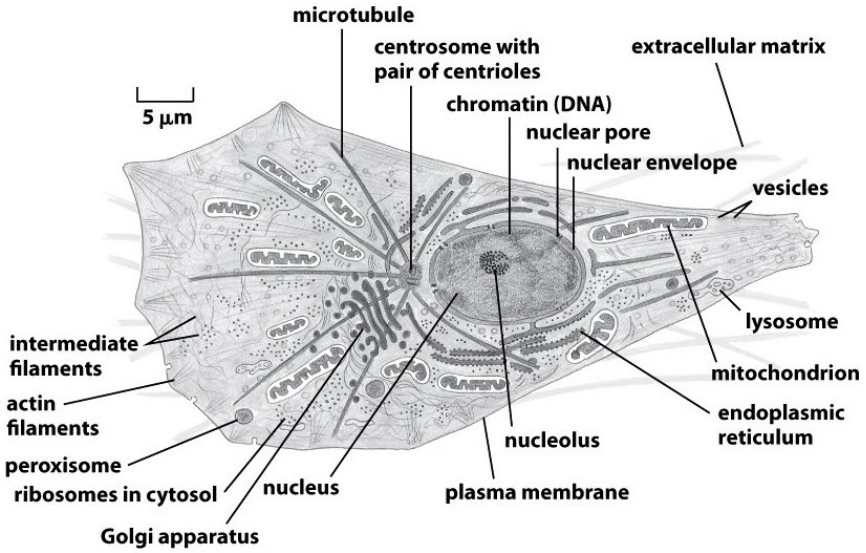

Figure 2.2: Schematic showing an eukaryotic cell with many of its organelles. Taken from [146].

2.2 Cell Adhesion

The adhesion of cells to surfaces and to each other is governed by the complex interplay between specific binding and non-specific forces mediated by various interactions [173]. These generic forces include capillary forces also determining a liquid's wetting or dewetting of a surface. On the other hand, the molecules of the glycocalyx result in repulsive forces due to steric hindrance. Elastic, resulting from the mechanical properties of the membrane, as well as undulation forces can both enhance or reduce binding. Undulation forces arise from oscillations of the cell membrane. Since cells are able to control the density of the glycocalyx and the composition of their membrane they can actively regulate cell adhesion in space and time.

Specific binding of CAMs, usually transmembrane proteins, to molecule on adjacent cells or the ECM, works like a key matching its lock. Specificity arises from geometrical constraints (receptor and ligand should have complementary molecular shapes) and the amino acid sequence of both molecules. The sequences have to match in such a way to maximize electrostatic interactions between oppositely charged amino acids of CAM and ligand as well as to maximize number of hydrogen bonds between both proteins.

CAMs can be divided in four protein superfamilies: integrins, selectins, cadherins and immunoglobulins. Most of them exhibit a large extracellular domain and a helical transmembrane domain. The intracellular domain often is able to bind to the cytoskeleton.

Selectins form relatively weak bonds with carbohydrates. This weak binding is important for the rolling and adhesion of leukocytes in the blood stream which is dependent on transient adhesion of selectins to the vessel wall. Cadherins are homophilic molecules characterized by the restriction to solely interact with members of the same family. They are responsible for the formation of stable cell-cell contacts in the presence of calcium ions [147]. Immunoglobulins mediate interactions with integrins but also with their own kind. Since integrins are of major interest for this study, they are illuminated in section 2.2.1 in more detail.

Cell adhesion can be described as a two-step process [174]: initially, binding occurs with an aggregation of adhesion molecules over time. Thereafter, biochemical signaling contributes to a strengthening of the adhesion sites via the binding of the cytoskeleton to intracellular domains of CAMs. Other proteins like talin or vinculin can be recruited to the adhesion clusters maturing the signaling platform to multi-protein complexes termed focal adhesions (FAs) [62]. These sophisticated multi-protein structures are not only important in adhesion but are also involved in the sensing of the cellular environment [181]. A schematic model of a FA is shown in figure 2.3. The scheme is based on measurements with an interferometric variant of the super-resolution technique photoactivated localization microscopy (PALM). This advanced method allows to determine the position of a fluorophore in three dimensions with around 10 nm accuracy [88].

2.2.1 Integrins

Integrins are transmembrane proteins consisting of two subunits: an α-subunit linked non-covalently to a β-subunit. There are 18 known α- and 8 β-subunits assembling into 24 heterodimers [83]. Their small intracellular domain binds to the cytoskeleton forming an important link for signaling between ECM and cytoskeleton: Cells do not only sense their chemical environment via integrins (outside-in signaling) but also the integrin's conformation changes upon intracellular signals (inside-out signaling or activation) thereby actively regulating cell adhesion [72]. Both processes require forces to be transmitted across the membrane through this linkage [181]. This force propagation and conversion is termed "mechanotransduction".

Each integrin has a specific cluster of ligands on other cells or more often in the surrounding ECM which is bound with high affinity [82]. The short sequence arginine-glycine-aspartic acid (RGD) is found in the amino acid sequence of several of these macromolecules. Integrins selectively recognize different forms of artificially synthesized RGD-containing peptides [145]. Fibrinogen, an ECM-protein, is the preferred binding partner of integrin $\alpha_{\mathrm{IIb}}\beta_3$ (also known as glycoprotein IIb/IIIa or short GPI-

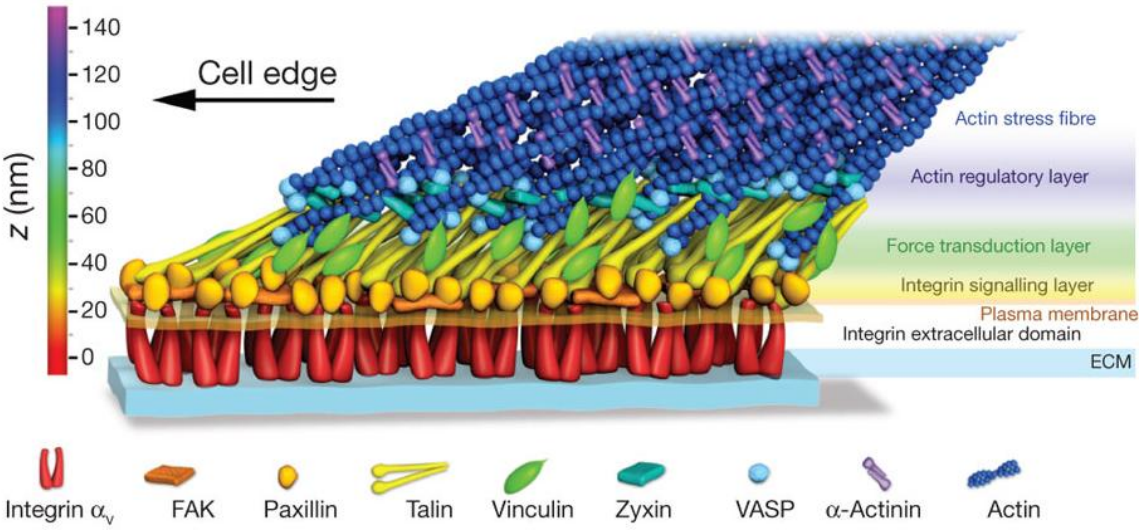

Figure 2.3: Schematic model of molecular assembly of focal adhesion. The scheme is constructed from experimentally determined protein positions. Protein stoichiometry is not depicted in the model. Taken from [88].

Ib/IIIa) [19, 29], the most abundant membrane protein in blood platelets [26]. It appears obvious that purification of integrins from thrombocyte concentrate [54, 71] is the preferred method applied within this work.

Platelets are about 2 µm in diameter and carry approximately 80000 copies of GPIIb/IIIa on their membrane [29]. Estimating the surface area, this implies an average distance of 20 nm between each receptor-couple. This is remarkable, especially since the extracellular part measures approximately 10 nm in size with the integrin spanning roughly 20 nm at full length (compare figure 2.4a). Integrin $\alpha_{\mathrm{IIb}}\beta_3$ is responsible for clot formation during hemostasis. It is tightly regulated to prevent spontaneous, often harmful thrombus formation [19]. Genetic defects in the gene of integrin $\alpha_{\mathrm{IIb}}\beta_3$ lead to a bleeding disorder due to the platelets' reduced or absent mutual adhesion [63].

The structure of integrins was investigated in several by means of either X-ray diffraction or cryo electron microscopy [2, 216, 220, 222]. Figure 2.4 depicts a structural model of the protein $\alpha_{\mathrm{IIb}}\beta_3$. A debate is going on about the conformation leading to integrin activation [229]. The deadbolt model describes enabling of ligand binding despite of a bent integrin head domain [221]. The switchblade model in contrast requires an elongated conformation for successful binding [204], whereas in the deadbolt model, extension of integrin occurs after the ligand is bound. The deadbolt model is corroborated by experiments not able to show a change in height of the integrins embedded in liposomes after incubation with Mn^{2+} [221,225], which results in the activation of integrin [83]. In contrast, the switchblade model is supported by investigations finding the majority of integrins in the upright conformation when

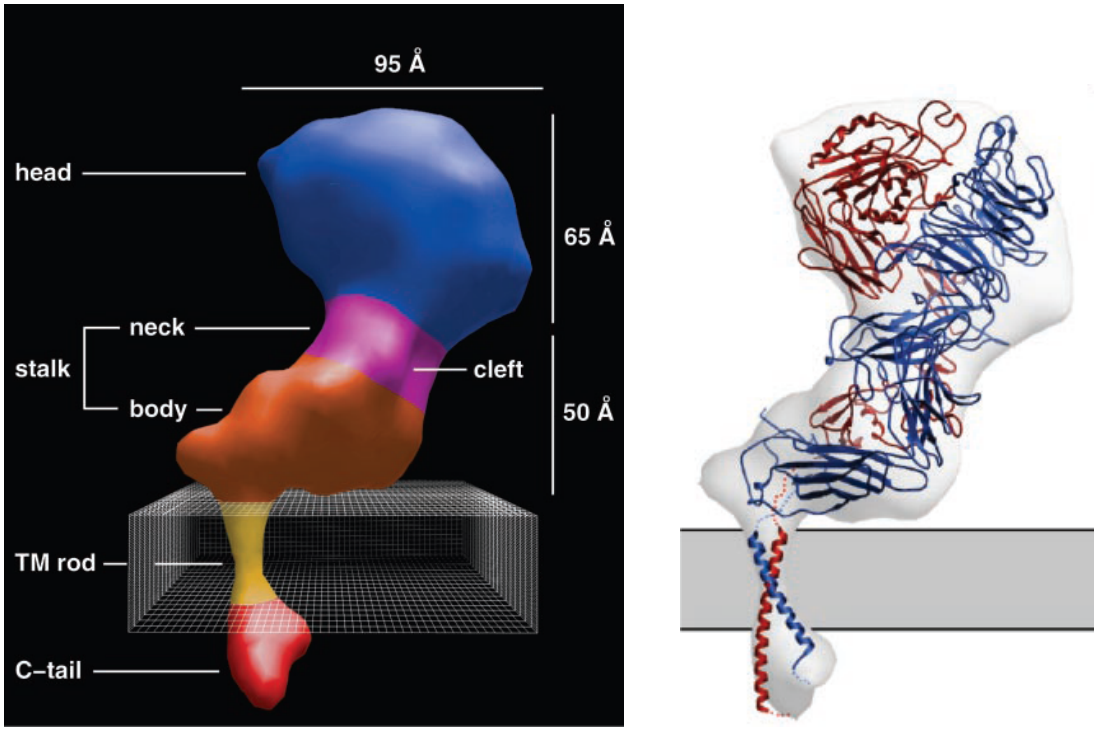

Figure 2.4: Structure of integrin $\alpha_{\mathrm{IIb}}\beta_3$ from data obtained with X-ray crystallography and cryo TEM. Images taken from [2].
(a) Surface-shaded 3D density map. The shaded box depicts the membrane with a thickness of 30 Å.
(b) Ribbon model with the α_{IIb} subunit in blue and the β_3 subunit in red.

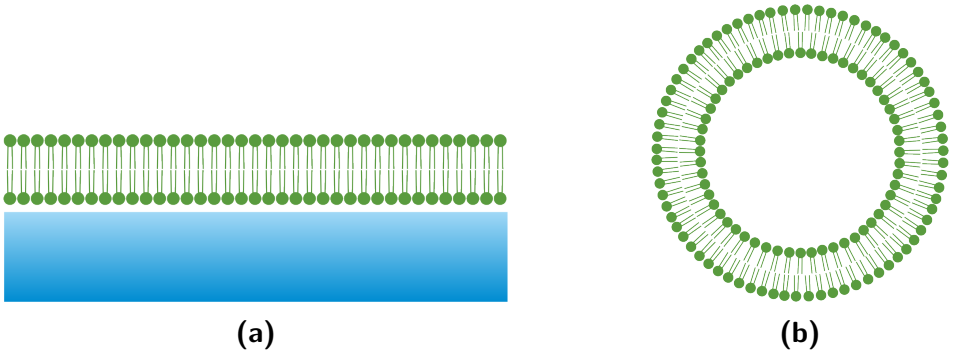

Figure 2.5: Different forms of bilayers depending on their environment.
(a) Planar lipid bilayer on a glass support.
(b) Spherical closed lipid bilayer in aqueous environment.

activated [2, 204].

2.3 Model Systems

In recent years so-called "synthetic biology" became more and more popular [110, 182]. Top-down approaches use genetic engineering to attenuate or switch off certain cellular processes, while other functions are amplified. Despite recent advances in the field of molecular biology, it remains difficult to create a functional cellular model to investigate cellular adhesion phenomena in detail. An alternative approach is to design bio-inspired artificial model systems being simple enough for quantitative data acquisition and modeling. Until now only few examples can be found in literature applying this strategy to the field of cell adhesion [193]. A selection of studies will be presented in more detail in the following section with a special focus on systems that use integrin or actin.

Phospholipid bilayers serve as a minimal model of the cell membrane, either in the form of a planar (see figure 2.5a) or a spherical closed bilayer (depicted in figure 2.5b). Bilayers form spontaneously in aqueous environments due to the amphiphilic nature of lipids, provided their concentration exceeds a certain concentration often called critical micelle concentration (CMC). For a typical lipid like phosphatidylcholine the CMC lies within the range of nanomols per liter [12].

Frequently found lipid components of cellular membranes are phospholipids, sphingolipids and cholesterol [111]. Phospholipids consist of a hydrophilic headgroup and two hydrophobic fatty acid chains. These two chains are covalently linked to a phosphate group via a glycerol backbone. Different phospholipids are distinguished depending on residue bound to the phosphate. For instance, figure 2.6 shows a phosphatidylcholine with two different fatty acid tails: the saturated one - without double bonds - is palmitic acid, the unsaturated one is known as oleic acid. This depicted

lipid was chosen for it is the main component in the lipid mixtures used in this study. Table 2.1 lists some common phospholipids relevant for this thesis.

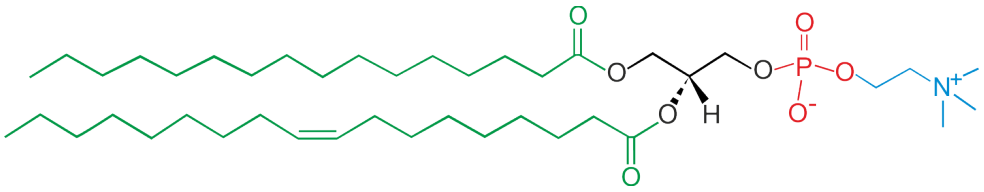

Figure 2.6: Skeletal formula of palmitoyl-oleyl-sn-phosphatidylcholine, one variant of phosphatidylcholine: the choline headgroup is shown in blue, the phosphate group in red and the glycerol backbone in black as well as both fatty acid tails in green.

The molecular geometry of lipids determines their assembly in micelles, bilayers or non-bilayer structures in aqueous environment [27, 56]. The packing parameter $P = V/(a\,l)$ describes the geometry with the volume V occupied by the tails, the cross sectional area a of the lipid heads and the tails' length l [56]. Typical values for a and l are $0.5\,\mathrm{nm}^2$ and about $2\,\mathrm{nm}$ respectively. Phospholipids having a cylindrical shape (e.g. phosphatidylcholine) self-assemble in a double layer exposing their hydrophilic headgroups and shielding the hydrophobic tails from getting in contact with surrounding water molecules. Conical shapes (e.g. phosphatidylethanolamines) result in non-bilayer arrangement of lipids, while inverted cone-like lipids (e.g. lysophosphatidylcholine; lysolipids lack one of the two fatty acids) arrange in micelles as depicted in figure 3.4.

Membrane proteins can be incorporated in both, planar or spherical closed bilayers. The latter are also known as vesicles or liposomes. Depending on their diameter d they are typically grouped in small ($d < 100\,\mathrm{nm}$), large ($0.1\,\mu\mathrm{m} < d < 1\,\mu\mathrm{m}$) or giant vesicles ($d > 10\,\mu\mathrm{m}$). In figure 2.7 two images of GUVs are shown. When there is only one bilayer the term unilamellar is used. More than one layer is termed multilamellar or in some cases oligolamellar.

In order to model its mechanical properties, a bilayer is considered to be an elastic sheet [74]. Its parameters also determine the bilayer's overall shape [183], which depends on the packing of lipids in the double layer, an intrinsic property also known

Table 2.1: Common phospholipids relevant for this study. The charge of zwitterionic molecules depends on the pH of the solvent.

name	headgroup	charge
phosphatidylcholine (PC)	R-$OCH_2CH_2N^+(CH_3)_3$	zwitterionic
phosphatidylethanolamine (PE)	R-$OCH_2CH_2NH_3^+$	zwitterionic
phosphatidic acid (PA)	R-OH	negative
phosphatidylserine (PS)	R-$OCH_2CHNH_2COO^-$	negative

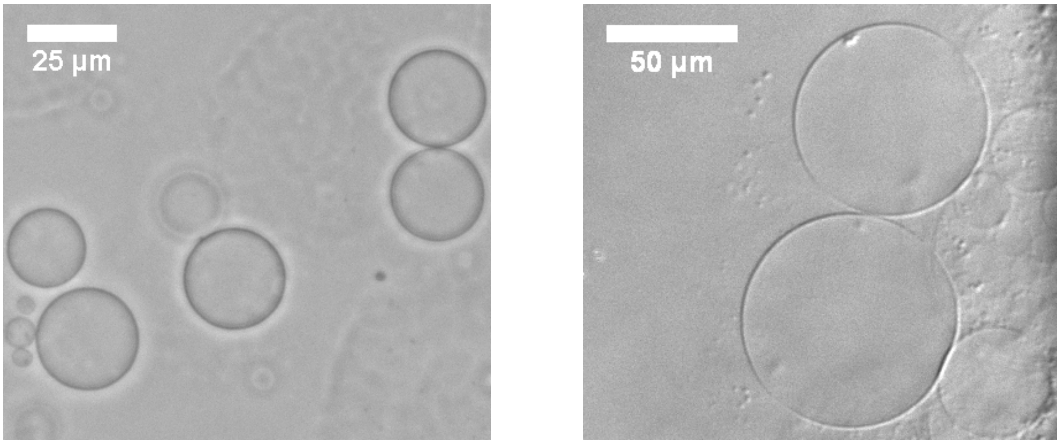

Figure 2.7: Pictures of GUVs imaged by optical microscopy with different contrast methods. Both techniques are described in more detail in the appendix in A.
(a) Phase contrast
(b) Differential interference contrast

as phase behavior. In the fluid phase, lipid molecules diffuse freely in the two dimensional membrane. Their position is fixed in the gel phase leading to a higher rigidity of the bilayer. In analogy to the melting of ice, bilayers in the gel phase melt at the phase transition temperature and lipids are in the fluid phase above this temperature. Longer fatty acid chains increase the phase transition temperature due to enhanced Van der Waals interaction between tails. Unsaturated tails - fatty acids with at least one double bond - decrease the phase transition temperature. Saturated molecules have no multiple bonds between atoms.

Planar bilayers frequently serve as a model of the ECM. They are normally formed on hydrophilic, solid supports, like glass, by rupturing tensed SUVs [87]. In order to facilitate an unhindered diffusion of membrane proteins in the double layer, they are tethered to the glass with linker polymers [156] or peptide spacers [190]. Otherwise, only a very thin film of water separates glass and lipids and large proteins incorporated in the bilayer get stuck on the surface. Thin cushions of cellulose were also employed to enhance diffusion of integrin in supported lipid bilayers (SLBs) [66]. To mimic the glycocalyx of cells and to prevent unspecific adhesion, lipids with a poly(ethylene glycol) (PEG) chain covalently attached to their headgroup were incorporated in the double layer of synthetic systems [131]. PEG-lipids also strongly enhance the stability of vesicles in aqueous solution due to steric stabilization [90].

GUVs often serve as models for cells because of their comparable size also making them easily observable in the optical microscope. Until now, various adhesion molecules have been incorporated in the membranes of GUVs. The first binding partners to be utilized in adhesion studies was biotin and avidin. The small molecule

biotin is easily bound to lipids, PEG chains or other proteins like casein. Thus, biotin was frequently incorporated in lipid bilayers or crafted on glass surfaces. The tetrameric proteins streptavidin or neutravidin strongly bind up to four biotin molecules and are forms of avidin without sugar residues. Both biotin-binding proteins form a linker between GUVs with biotinylated lipids and SLBs equipped with biotin [6, 50, 51] or biotin immobilized on glass [32]. Another receptor-ligand couple used in model systems is sialyl-Lewis^x and E-selectin. The soluble part of E-selectin was physisorbed on an aminosilane substrate and the molecule sialyl-Lewis^x, consisting of four sugars, was chemically bound to a lipid. Giant vesicles were prepared by electroformation (explained in 3.2) and their adhesion dynamics were observed with RICM [113, 192]. The third example for receptor-ligand complexes transferred to GUVs is the homophilic, lipid-anchored receptor contact site A which was inserted in lipid bilayers on glass and in GUVs also containing PEGylated lipids [94]. The problem of incorporating an insoluble transmembrane protein was circumvented by employing genetic engineering approaches to produce E-cadherin only comprised of its water-soluble part which was fused to a hexa-histidin-tag [50]. This so-called his-tag is formed out of six histidins which efficiently bind nitrilotriacetic acid (NTA) in presence of metal ions (most often nickel). NTA can be covalently attached to lipids that are inserted in SLBs or GUVs. This technique allows the attachment of many different proteins to lipid membranes [155].

Major difficulties and limitations of synthetic vesicles as minimal models for cellular systems are discussed in [33]: Immobilized specific ligands do not inevitably lead to specific adhesion of cells or GUVs even though they have the corresponding receptors in their membrane. The importance of PEG-lipids for the reduction of unspecific binding due to steric hindrance is particularly emphasized.

In all examples previously discussed no transmembrane protein was incorporated into an artificial membrane system. Rather adhesion molecules were coupled to lipids, emphasizing the scientific challenge of this enterprise.

2.3.1 Model Systems related to Actin or Integrin

In studies investigating integrin-mediated adhesion, most often integrin $\alpha_{\mathrm{IIb}}\beta_3$ is used. It can be readily purified from blood platelet concentrate in sufficient amounts since it is the most abundant protein in thrombocyte membranes. Giant vesicles containing lipids functionalized with the small peptide RGD are usually utilized as "synthetic cells". First experiments were conducted with integrin physisorbed on glass. Forces needed to unbind such vesicles from their support were measured by employing magnetic tweezers [69], whereas spreading kinetics were investigated by means of RICM [24]. Synthesizing a RGD-lipid linked to a fluorescent dye allowed to track the localization of RGD in zones of tight adhesion which were identified with the help of RICM [117].

Further improvement of the system led to the incorporation of full length integrins

in supported bilayers. Proteoliposomes, SUVs carrying membrane proteins, were prepared based on protocols developed earlier [139, 140]. These vesicles were used to generate SLBs helping to identify a two-step binding mechanism of fibrinogen to integrin $\alpha_{\mathrm{IIb}}\beta_3$ [123]. Clustering of integrin in SLB was shown upon fibrinogen binding [45]. An additional layer of cellulose between glass and membrane was added to foster integrin diffusion. The effect of enhanced diffusion on the adhesion energy was studied in dependence of increasing amounts of repellent PEG-lipids in the GUV membranes [66]. An increase in adhesion energy of a RGD-containing vesicle to integrin embedded in a double layer was found as well, when the bilayer was indirectly connected to the glass by a polymer spacer [156]. Introducing peptide spacers led to tethered bilayers on gold which made it possible to observe ligand binding directly with surface plasmon resonance [190]. Using cryo transmission electron microscopy, inter-vesicle-cross-linking was shown between small vesicles containing integrin or an RGD-lipid in their bilayer respectively [79]. Proteoliposomes with integrin incorporated were employed to elucidate the mechanism leading to integrin activation (see 2.2.1). No significant change in height of membrane-incorporated integrins was observable with cryoelectron tomography after activation by Mn^{2+} ions [225]. An *in vitro* model of integrin activation was established by embedding integrin in nanodiscs out of a small lipid bilayer with its hydrophobic edges shielded by a customized protein. The discs' diameter of around 15 nm prevented the insertion of more than two integrins. Intra- and extracellular part of the protein were accessible. It was shown that talin binding to the intracellular part of integrin activates and extends the receptor [224].

First attempts were made to establish a protocol to generate giant vesicles with full length integrins inserted in their bilayers [198,199]. The model system's adhesive properties were studied by RICM on glass coated with fibrinogen or casein as a control. However, preparation of integrin-GUVs was not very reliable and adhesion was not always reproducible.

In early studies, GUVs with enclosed actin were most commonly produced by electroformation. Actin shells, self-assembled at the membrane, were separated by 0.4 µm to 0.5 µm due to thermal oscillations of the bilayer [73]. The morphology of actin networks, cross-linked by α-actinin and filamin, was studied inside giant vesicles. Lowering the temperature led to the network's reorganization from a randomly linked conformation into spiderweb-like gels or ring-like bundles depending on the vesicle size [106]. Spatial organization of F-actin was observed to depend not only on the size of the vesicles but also the composition of membrane lipids [104]. Positively charged PEGylated lipids induced a coupling of actin filaments to the inner leaflet of the bilayer by electrostatic interactions. This coupling influences the viscoelastic moduli as measured with magnetic bead microrheometry [105]. The mechanical properties of GUVs filled with an actin-network without direct link to the membrane were probed using atomic force microscopy (AFM). Actin-filled giant vesicles had a four times higher Young's modulus than pure lipid GUVs [228]. A model containing

an actin mesh mimicking a cellular actin network was developed recently. NTA-lipids were utilized to bind his-tagged proteins promoting nucleation of actin to the inner leaflet of a giant vesicle. As a result, an actin cortex assembled right beneath the bilayer [151]. The spreading dynamics of this model system was studied using RICM. Low amounts of actin inside the vesicles almost did not influence spreading while a dense network led to spreading reminiscent of a cell [130]. The adhesion of actin-containing giant vesicles was also investigated. It was shown that salt buffers are sufficient for stable unspecific adhesion on glass or poly(dimethylsiloxane) (PDMS) [75]. Only lately, GUVs encapsulating an actin-myosin network were prepared in physiological buffers from hybrid agarose-lipid films [209]. These networks could exert contractile forces thereby controlling vesicle shape when linked to the bilayer via biotin-streptavidin. Model systems investigating the interaction of actin with SLBs are not discussed here, but can be found in [212].

3 Liposome Preparation and Membrane Protein Reconstitution

Understanding of transmembrane proteins is of high interest since a fraction of 27% of the whole human proteome belong to this class of proteins [8]. Proteome stands for the entirety of all proteins. Transmembrane proteins consist in part of strongly hydrophobic sequences. Either detergents are needed to bring them in aqueous solution or they have to be incorporated in lipid bilayers for a more natural environment. As seen in section 2.2.1, the response of integrin to external cues like Mn^{2+} is different when it is solubilized by detergent compared to integrin incorporated in a membrane. This is why membrane protein reconstitution into vesicles is an important way to gain new information about the function of these proteins.

Vesicles form spontaneously in aqueous environment due to the amphiphilic nature of phospholipids as already observed in 1965 [14]. Most of them self-assemble in a double layer exposing their hydrophilic headgroups and preventing the hydrophobic tails from getting in contact with water molecules. Such bilayers can be stacked one over another to form multilayer structures. In the following, various techniques to produce unilamellar vesicles are discussed. Methods to grow GUVs are described in the second part. In the third section of this chapter, an introduction to the incorporation of membrane proteins in liposomes is given largely based on the review of *J.L. Rigaud* and *D. Levy* [165]. The interested reader is referred to older overview articles [133,168,188] to catch the long way of membrane protein reconstitution from a kind of black art to more quantitative science. The last part then focuses on techniques which are suitable for the production of GUVs with protein inserted in their bilayer.

3.1 Small and Large Unilamellar Vesicles

In the late 1950s ultrasonic waves were used to disperse phospholipids in aqueous solutions [172]. Size and shape of "'micelles"' produced by this ultrasonic irradiation were analyzed by measuring viscosity and diffusion as well as determining the sedimentation coefficient with ultracentrifugation [175]. Sonication was frequently employed to prepare vesicles for characterization of their permeability to ions or to analyze their viscosity or sedimentation velocity [81, 137]. Lipids are commonly mixed in chloroform and dried at the bottom of a test-tube or beaker. Complete

evaporation of the solvent is ascertained by placing the tube in a desiccator under reduced pressure for at least two hours. An aqueous solution of choice is added to the dried lipids that are subsequently allowed to swell for about one hour resulting in a solution containing irregular lipid structures. Then, the container is placed in a bath type sonicator or a tip sonicator, that is directly introduced in the emulsion (see sketch in figure 3.1a), is utilized to produce SUVs. Their mean diameter is around 30 nm depending on the type of lipid and the duration of sonication [203]. Main problems are lipid degradation due to the high energy input (especially with a tip sonicator) and contamination with chips of metal from the tip.

A lipid solution prepared by evaporation of the organic solvent and rehydration with an aqueous solution, as described above, can be extruded several times through a membrane yielding SUVs or large unilamellar vesicles (LUVs) as determined by the membrane's pore size. The diameter of the liposomes is slightly larger than average pores. After about 10 passes through the membrane, vesicles usually are comprised of only one bilayer [129]. The process is sketched in figure 3.1b This method was originally introduced as an easy, reproducible way for preparation of unilamellar vesicles without detectable degradation of phospholipids [135].

A water-in-oil emulsion of phospholipids allows to enclose a high fraction of the aqueous phase in LUVs [202]. Lipids are first dissolved and mixed in an organic solvent (usually diethyl ether). Then a watery solution of choice is added and sonication yields a stable water-ether-emulsion. The organic solvent is evaporated under reduced pressure, as indicated in figure 3.1c. Aqueous buffer is added to the mixture shortly before complete removal of organic residues. This procedure yields LUVs in watery environment. Elaborate protocols are published for example in [203] and [43].

A fundamentally different method is the removal of detergent from lipid-detergent mixtures (figure 3.1d) [179]. It was introduced in the early seventies as a way to integrate hydrophobic proteins in vesicles [85]. Lipids and detergent are mixed in a buffer. The detergent is subsequently removed by either dialysis [120, 230] or gel filtration [44]. More details can be found in section 3.3.

Alternative methods are solvent evaporation [137], ethanol injection [16, 96] and ether infusion and subsequent evaporation [36, 177].

3.2 Giant Unilamellar Vesicles

Gentle Hydration

The first preparation of "'thin-walled"' vesicles was performed by *J.P. Reeves* and *R.M. Dowben* [162]. A solution of lipids in chloroform or a mixture of methanol and chloroform was dried at the bottom of a flask as sketched in figure 3.2a. Careful addition of an aqueous solution led to GUVs when the flask was left undisturbed for the swelling period. Therefore, the technique is called gentle hydration or gentle

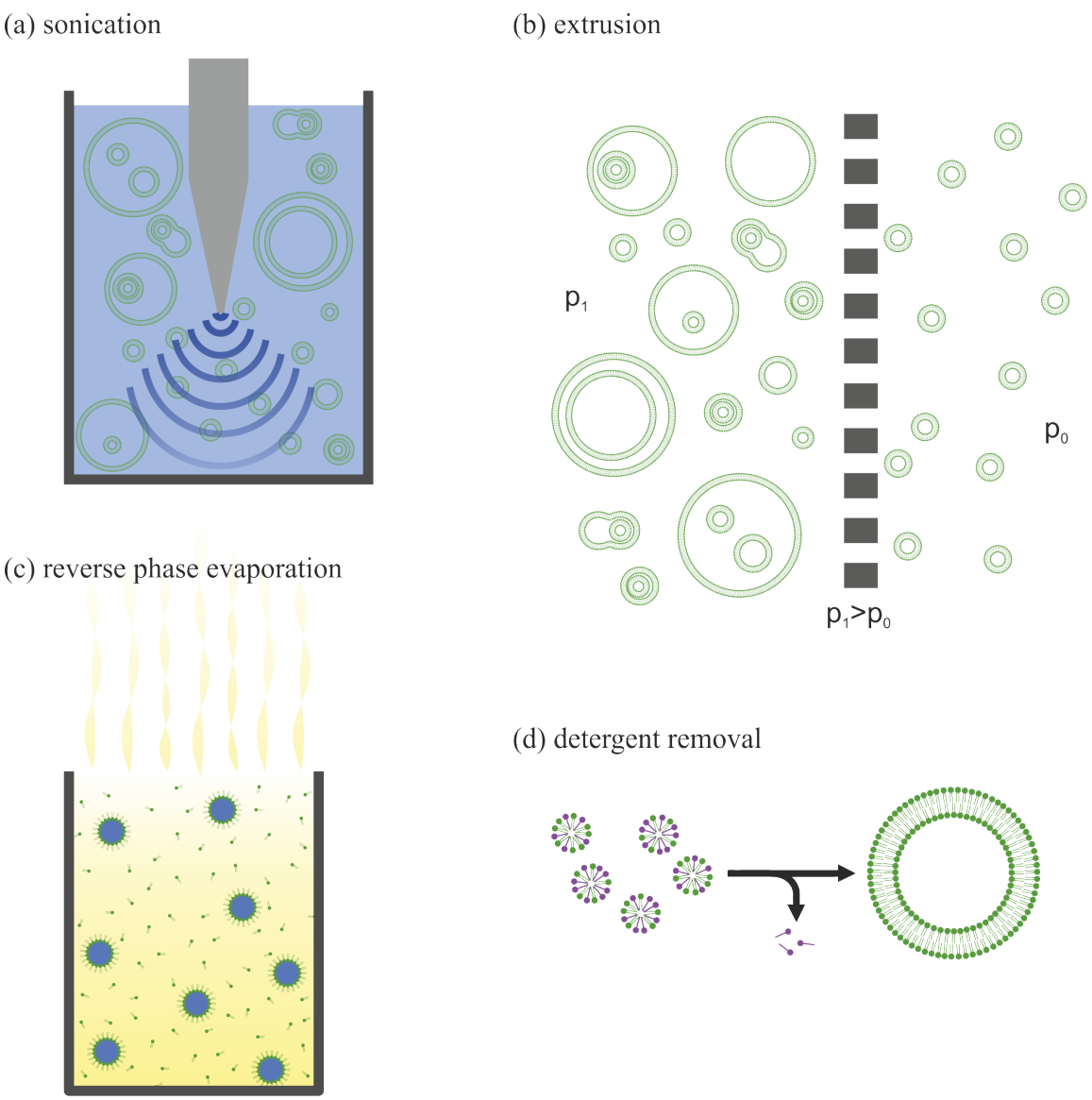

Figure 3.1: Different methods to prepare vesicles.

swelling. However, with this approach it was not possible to grow large liposomes when electrolytes were in solution. This problem was solved by including $10 - 20\%$ of negatively charged lipids in the lipid mixture. This slight adaption enabled the formation of GUVs under physiological conditions [4]. When negatively charged lipids were incorporated in a membrane, divalent ions prevented GUV formation while their growth was enhanced with neutral lipids when Ca^{2+} or Mg^{2+} were in solution [5]. It was discovered that it is possible to grow GUVs in solutions containing up to $2\,\mathrm{mol\,l^{-1}}$ of salt by addition of PEG-functionalized lipids [223]. Mixing of sugar (like glucose or fructose) in the solution of lipids in chloroform also supported preparation of GUVs from films of neutral lipids [210]. All additives mentioned above influence the interaction between bilayers. Sugar or PEGylated lipids enhance bilayer repulsion thereby facilitating their separation. On the other hand, ions tune the electrostatic interaction of charged membranes which can enhance or prevent their detachment from each other.

Electroformation

Another method starting from a dry film of lipids is electroformation (also called electroswelling) [10, 11, 39]. A thin lipid film is produced on electrodes by deposition of a lipid solution, as indicated in figure 3.2b, and evaporation of the organic solvent under a flow of nitrogen. The inert gas inhibits lipid oxidation. Platinum wires or glass slides coated with indium tin oxide (ITO), a transparent semiconductor, are usually employed as electrodes for the application of a direct current (DC) or alternating current (AC) electric fields. Frequencies of approximately 10 Hz are applied for salt solutions with ion concentrations below $10\,\mathrm{mmol\,l^{-1}}$. It was long believed that higher concentrations of salt would prevent GUV formation. Recently, giant vesicles were prepared under physiological conditions using a frequency of 500 Hz [124, 125, 152].

Growth of GUVs in flow chambers made it possible to exchange solutions. Glycerol solution, in which the vesicles were prepared, was substituted for an iso-osmolar salt solution. Surprisingly, even the solution inside the GUVs was replaced when growing them in glycerol solutions implying a quite permeable bilayer [47]. Since lipids might degenerate on electrodes due to oxidation, the lipid film was deposited on non-conductive substrates like a glass tube or a piece of a PET mesh. GUVs could be observed when these were put between two platinum wires or ITO-coated glass slides and an AC voltage was applied [132]. The growth of giant vesicles was also studied on silicon. Different surface properties after chemical treatment and surface structures had an influence on the preparation. The size distribution correlated with the size of micro-structures. Surface chemistry determined vesicle yield probably by changing the assembly of lipid layers [101]. Spin-coating of lipid solutions results in very homogeneous films with controllable thickness. This approach led in two times larger GUVs even with lipid mixtures that did not work with electroswelling before [46]. These results highlight the importance of the lipid layers' properties on giant vesicle growth.

GUV preparation depends on the AC electric field. It was shown that there exist upper boundaries for the field's frequency and strength of 10 kHz and 10 $V\,mm^{-1}$ respectively [148]. Radius' increase of GUVs was analyzed as a first-order kinetics. This study established membrane fluidity to be the dominant parameter in giant vesicle growth by electroformation [186]. The exact mechanism of GUV growth in electric field is still unclear. Even though, there exist some explanations and theories [10, 40, 184].

Comparison of gentle hydration with electroformation using fluorescence microscopy showed an increase in unilamellar vesicles and reduced number of defects for electroswelling. However, electroformation does not work if the amount of negatively charged lipids is too high. In this case gentle hydration is the method of choice to prepare giant vesicles [171].

Hybrid Agarose-Lipid Films

An interesting variation of the hydration technique starts from a hybrid film out of agarose and lipids [77]. First, a film of agarose is formed on a glass slide. Then, a lipid solution is deposited on top (see schematic in figure 3.2c). The organic solvent is evaporated in vacuum to guarantee its complete removal. Addition of water or buffer, even with physiological ionic strength, leads to the formation of GUVs by spontaneous swelling. This method has the advantage that macromolecules like actin can be enclosed in a high percentage of the vesicles [209].

Inverted Emulsions

Inverted emulsions of water in lipid-saturated oil were prepared. The water droplets coated with lipids were subsequently sedimented through a lipid monolayer at an oil/water interface. This procedure allowed to control the lipid composition of inner and outer leaflet of the bilayer independently [142]. The whole process is summarized in figure 3.2d Since an asymmetric lipid composition is common in cells and might influence cell signaling or membrane protein distribution, this might be important for drug delivery or imitation of natural structures. However, each ingredient has to be stable in organic environment. The inverted emulsion can also be produced by microfluidics resulting in a narrow size distribution of the asymmetric vesicles. Their size is dependent on the initial radius of the water droplets which is very reproducible when prepared by microfluidics [80].

Microfluidic Jetting

Unilamellar bilayers can be formed at the interface of two macroscopic water droplets in oil. GUVs were generated by blowing another aqueous solution through this bilayer in analogy to the production of soap bubbles [57, 58] as indicated in figure 3.2e. This technique, called microfluidic jetting, was further developed by incorporating proteins in the bilayer and analyzing the size dependence on the parameters of the inkjet pulse [196, 197]. Ultimately, the lipid composition of both leaflets was controlled independently from each other and oriented incorporation of membrane proteins was

achieved. Enclosure of solutions or emulsions of macromolecules of choice inside of the giant vesicles was shown to be feasible [164]. Nevertheless, traces of organic solvent were found in the vesicle membrane [92]. The solvent influences physical and chemical properties of the bilayer and might be detrimental to embedded proteins. Compared to the methods above, sophisticated equipment is needed with this technique.

GUVs can also be produced by fusion of small vesicles and they form under special circumstances using some of the methods to prepare small vesicles like detergent removal or ethanol injection [214].

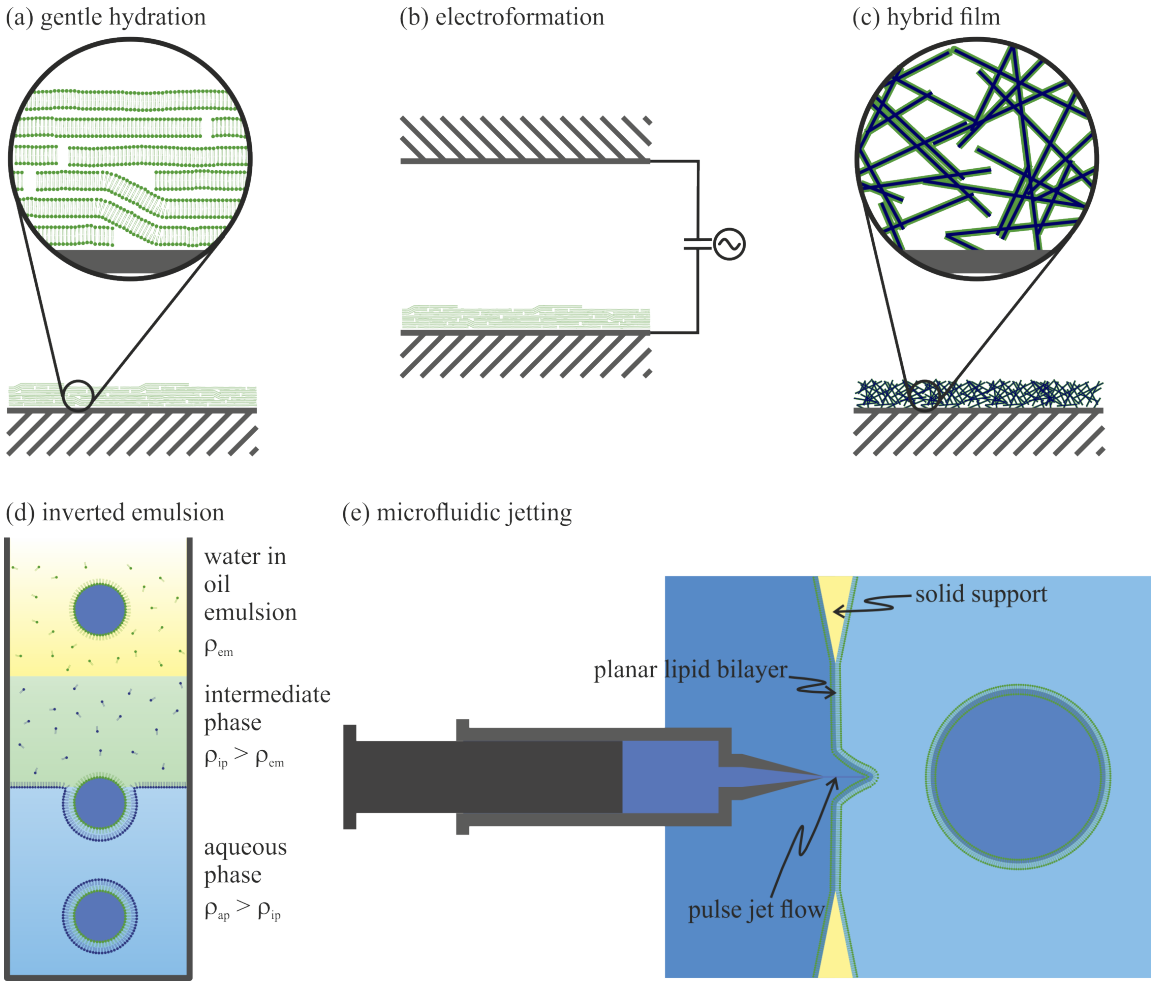

Figure 3.2: Different methods to prepare giant vesicles.

3.3 Liposomes with Incorporated Membrane Proteins

In principle, all strategies for the production of small unilamellar vesicles or large unilamellar vesicles that are discussed in section 3.1 also can be applied to prepare

proteoliposomes. However, one has to keep in mind, that treating lipid-protein-solutions by ultrasonic waves may lead to protein denaturing. Denaturation also occurs when mixing of lipids and membrane proteins in organic solvents. On the other hand, detergents usually are employed for the extraction of proteins from natural membranes. This is why detergent removal now is widely accepted as the method of choice for the production of proteoliposomes. The way how to remove the detergent might differ depending on the nature of the detergent.

The basic work flow of membrane protein reconstitution is illustrated in figure 3.3. Membrane proteins are solubilized by addition of detergent to native membranes. After protein purification, excess of lipids and detergent are mixed with the solubilized protein which leads to the formation of lipid-detergent-protein and lipid-detergent micelles. Gradually removing the detergent by different methods like dialysis, gel filtration, dilution or adsorption on polystyrene beads yields proteoliposomes.

Dilution works by adding buffer to a micellar lipid-detergent-protein solution until the detergent concentration is below the critical micelle concentration. The CMC corresponds to the concentration of a surfactant when micelles start to form from a solution of surfactant monomers. The method is very simple and fast. Control of the rate of detergent removal is feasible, but there are obvious drawbacks: first, complete removal of detergent is not possible and second, the sample always is very dilute in the end. Likewise, dialysis is only applicable to detergents with a high CMC. The method relies on the selective retention of molecules exceeding a certain size by the dialysis membrane. Only monomeric detergent diffuses across the membrane with a rate depending on the gradient in detergent concentration. The outside buffer has to be replaced several times and the whole procedure takes at least one or two days. Gel filtration on the other hand is quite fast. Depending on the sample volume it takes several minutes to hours. Owing to the rapidity of this approach there is a higher probability for proteins to be inserted incompletely and/or inhomogeneously. This is why gel chromatography is hardly used for membrane protein reconstitution anymore. After a thorough characterization of detergent removal via adsorption on hydrophobic, porous polystyrene beads [114, 115, 141, 167], this technique is now widely utilized. The commercial name “Bio-Beads”is often used synonymously for the hydrophobic beads. With some experience the method works for any detergent in a reproducible way. The main drawback is concomitant lipid adsorption which is why adsorptive capacity of beads for the different ingredients is an important quantity. In table 3.1 there is a summary of capacities for different detergents.

Fortunately, the capacity for detergent is around two orders of magnitude higher than for lipids or protein. A possible explanation is that (proteo)liposomes, micelles and protein scarcely enter the pores with a mean diameter of 9 nm as illustrated in figure 3.4. This extremely reduces the available surface for adsorption since the surface inside the pores is around 10000 times larger than the beads’ external surface.

According to a model for vesicle formation, removal of detergent from a solution of mixed micelles leads to the growth of micelles by fusion to disk-like structures

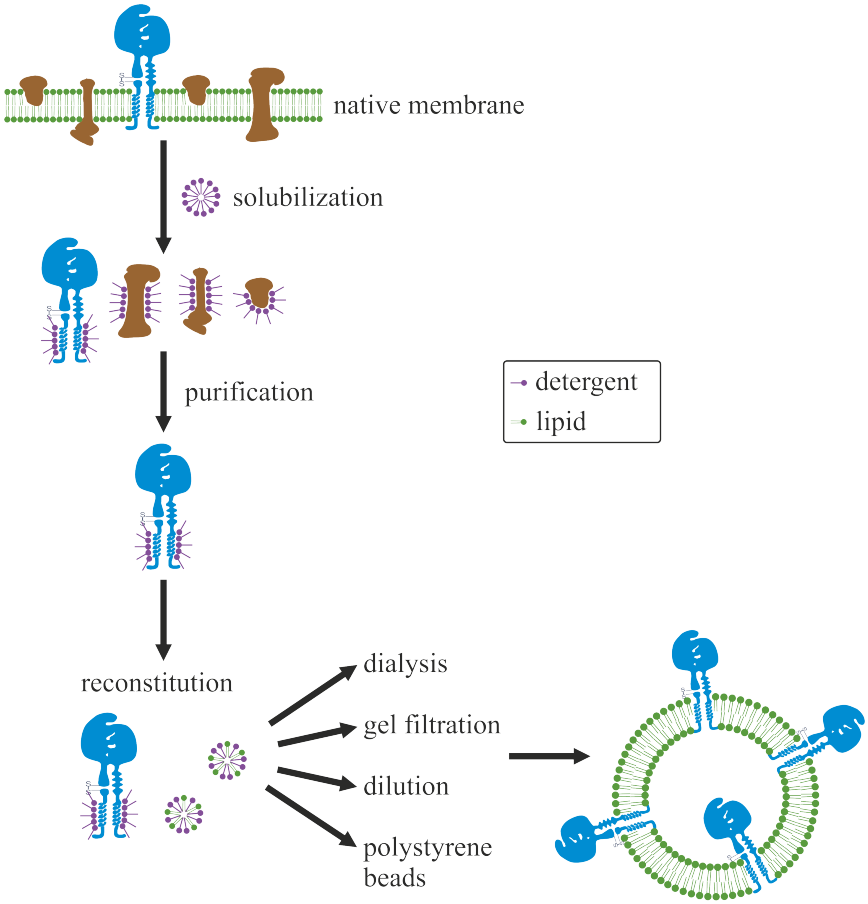

Figure 3.3: Work flow of membrane protein reconstitution mediated by detergents: Membrane proteins are solubilized by addition of detergent. After purification, excess of lipids and detergent are mixed with the solubilized protein which leads to the formation of lipid-detergent-protein and lipid-detergent micelles. Gradually removing the detergent by different methods like dialysis, gel filtration, dilution or adsorption on polystyrene beads yields proteoliposomes. Adapted from [165].

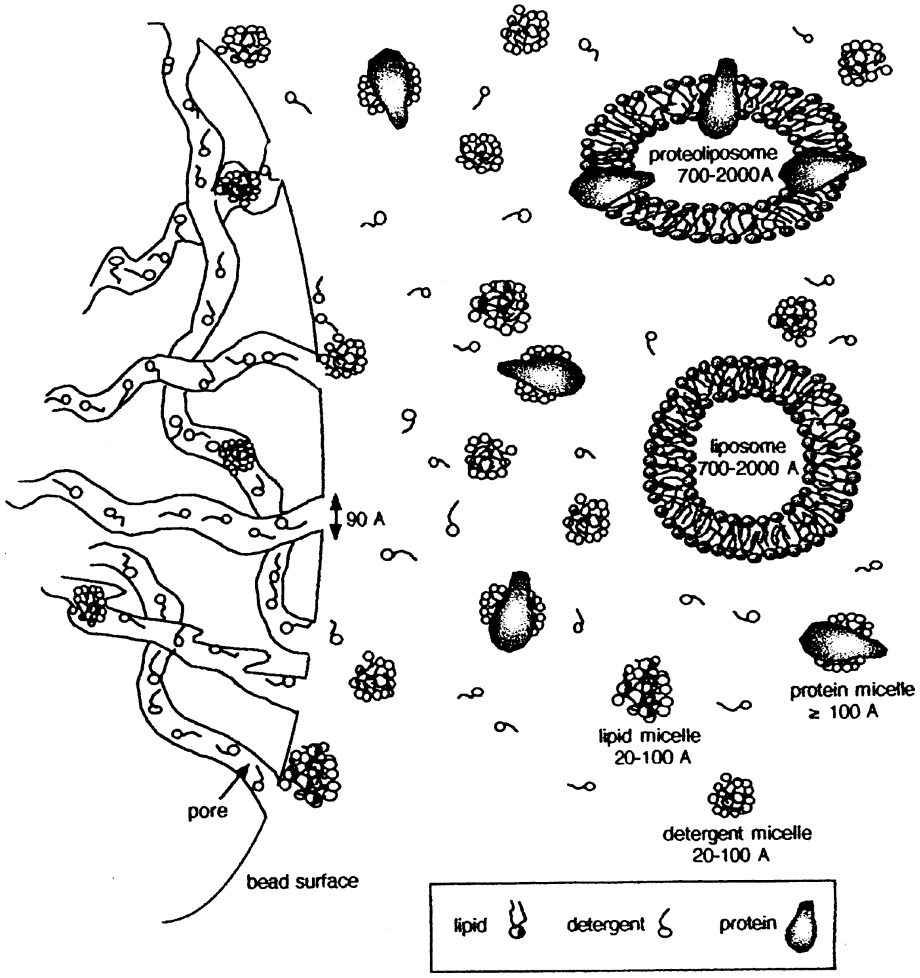

Figure 3.4: Illustration of the adsorption of detergents, lipids and proteins on the surface of porous polystyrene beads. Dissimilar accessibility of detergent monomer or micelle, lipid micelle or liposome and proteins as well as proteoliposomes to the pores results in very different binding capacities for the different constituents. Taken from [166].

Table 3.1: Adsorption capacities of Bio-Beads for chosen detergents, phospholipids and proteins. R_{sol} represents the effective detergent to lipid ratio needed for complete solubilization of preformed liposomes. For more information see the last paragraph in this section. Data from [166].

Compound	Adsorptive capacity (mg/g of beads)
Detergent:	
Triton X-100	185
$C_{12}E_8$	190
Octylglucoside	117
Dodecylmaltoside	105
Cholate	80
Phospholipid:	
Liposomes	1
Lipid-detergent micelles (R_{sol})	2
Lipid-detergent micelles ($3R_{sol}$)	4
Lipid-detergent-protein micelles	$0,5-1$
different *proteins*	$0-0,2$

with the detergent preferentially shielding the disks' edges [98]. These structures are called bilayered phospholipid fragments and they grow in size by further reducing detergent concentration. When reaching a certain critical radius, bending becomes energetically favorable. This is because of the relative reduction of the area of exposed hydrophobic chains at the disk's edge - which have to be shielded by detergent - compared to the bilayer's surface. In the end, the bilayer closes on itself. SUVs or LUVs are formed depending on the nature of lipids and detergent as well as the rate of detergent removal. As long as the amount of detergent is still high, the vesicles may undergo fusion thereby shifting the size distribution to larger values.

In order to obtain reproducible results for membrane protein reconstitution by detergent depletion, the step-by-step procedure was developed [165]. The process consists of four steps illustrated in figure 3.5, which are described in the following.

First, LUVs are preformed in an aqueous solution. Large vesicles are preferred because of their higher enclosed volume compared to SUVs. When growing them to GUVs, a homogeneous size and their lamellarity actually are not that important. Otherwise care should be taken in this regard. Reverse-phase evaporation or membrane extrusion are recommended for liposome production. The choice of phospholipids might also be crucial, especially since activity and function of some proteins depend on their interaction with lipids [27]. A certain (mostly small) fraction of charged (e.g. phosphatidylserine, phosphatidylglycerol or phosphatidic acid)

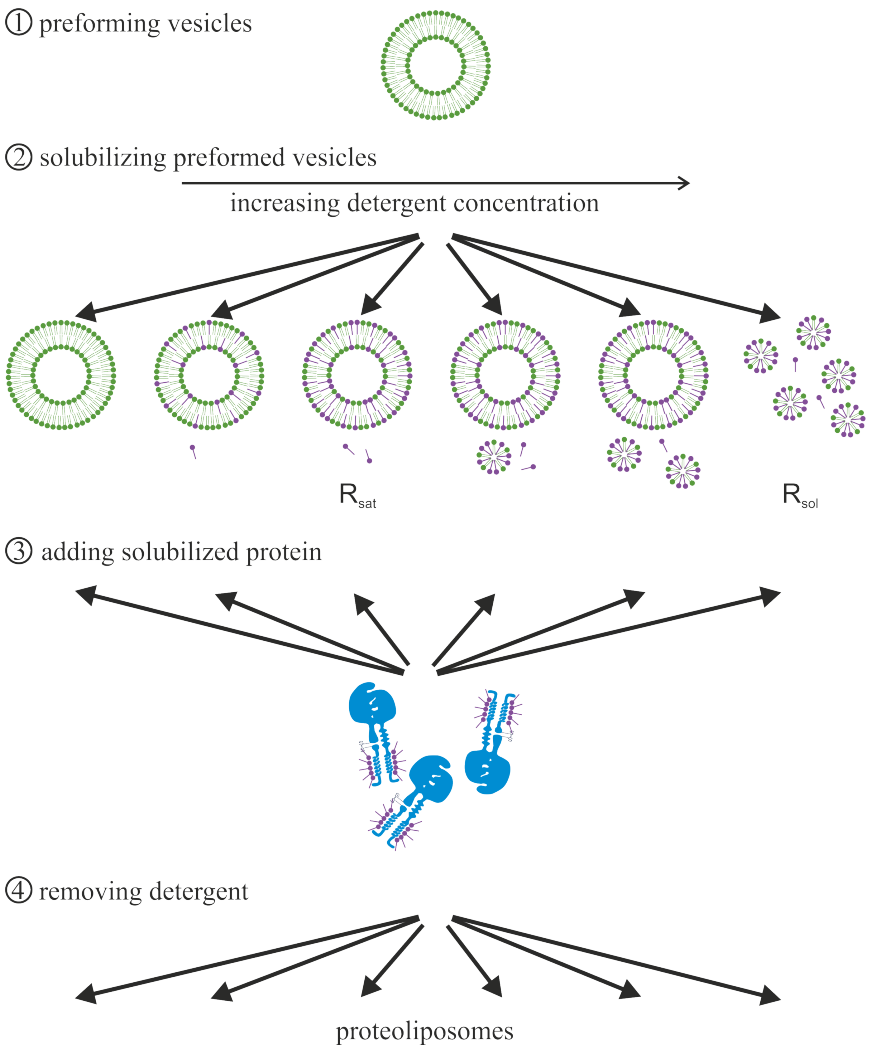

Figure 3.5: Scheme of the step-by-step procedure for membrane protein reconstitution. Vesicles are preformed in an aqueous solution and then solubilized by various amounts of detergent. In the next step, solubilized protein is added to each sample. Removal of detergent with one of the methods described above finally leads to the formation of proteoliposomes. Adapted from [165].

or non-bilayer forming lipids (e.g. phosphatidylethanolamine) might be needed for proper functioning of a protein. Second, detergent is added to the liposome suspension leading to a gradual solubilization with increasing amounts of detergent. The process of solubilization is described by equation (3.1) [103, 168]:

$$D_{\text{total}} = D_{\text{water}} + R\,L \tag{3.1}$$

where $D_{\text{total}} = D_{\text{water}} + D_{\text{bilayer}}$ is the overall detergent concentration, D_{water} the concentration of detergent in water/buffer, L the concentration of lipid and the ratio of detergent concentration in the bilayer to lipid concentration $R = D_{\text{bilayer}}/L$.

Progress of solubilization can be monitored by measuring the turbidity at a wavelength between 400 nm and 700 nm. At the beginning, detergent molecules incorporate into the lipid bilayer until it is saturated without destroying the vesicle. Turbidity is not changing very much in this stage. The ratio R of detergent to lipid concentration for which saturation occurs is labeled R_{sat}. Further on, small lipid-detergent micelles form. This is observed by a steady decrease of turbidity due to the reduction of the mean diameter of suspended particles. The suspension becomes optically transparent when all lipids are dissolved in detergent micelles after reaching the detergent/lipid ratio of complete solubilization R_{sol}. The dependence of turbidity on detergent concentration in a vesicle suspension is illustrated in figure 3.6.

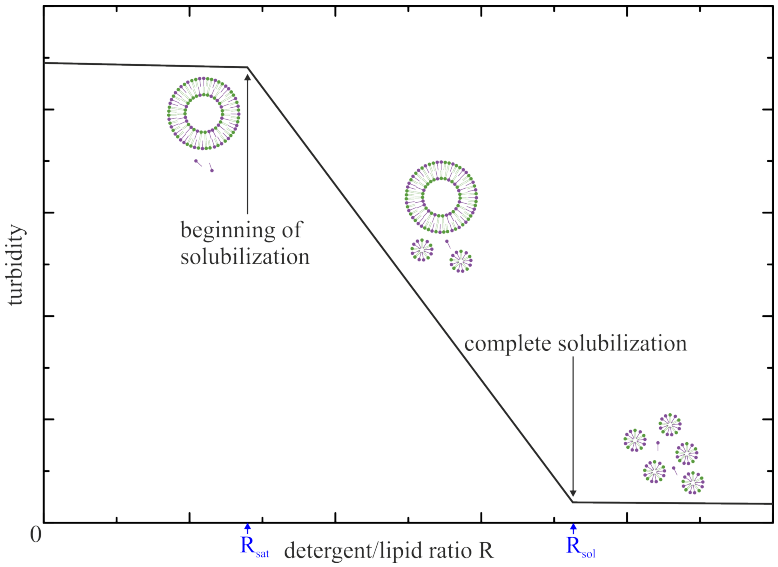

Figure 3.6: Schematic diagram of turbidity measured when detergent concentration is increasing in an aqueous suspension of liposomes.

For every detergent and membrane protein there is a certain point in the solubilization process where incorporation of protein works best. Therefore, it is advisable to test the addition of at least three different amounts of detergent: at the onset

of solubilization with detergent-saturated vesicles, at complete solubilization and in between. Table 3.2 lists the parameters describing solubilization of liposomes for a selection of detergents. After approximately one hour of incubation at room temperature, the sample should have reached equilibrium and the solubilized protein is added. This is the third step in the preparation method. The orientation of the protein is dependent on the degree of solubilization. Starting from a micellar solution results in completely statistical orientation. With decreasing amounts of detergent there is growing probability that the larger hydrophilic part of the protein - normally the extracellular part - is facing to the outer side. In the last stage of the procedure, detergent is removed by addition of Bio-Beads directly into the sample. Their amount determines the rate of removal and the time needed for complete removal. Afterwards, functional activity, protein incorporation and orientation as well as the size distribution of the vesicles, and their permeability need to be tested to ensure a successful reconstitution.

Table 3.2: Parameters describing solubilization of liposomes by a choice of detergents. Data from [165].

	D_{water}		R_{sat}		R_{sol}	
Detergent	mM	mg/ml	mol/mol	w/w	mol/mol	w/w
Triton X-100	0,18	0,12	0,64	0,5	2,5	2,0
$C_{12}E_8$	0,20	0,11	0,66	0,45	2,2	1,5
Octylglucoside	17	4,9	1,3	0,48	3,0	1,1
Dodecylmaltoside	0,3	0,15	1	0,65	1,6	1,0
Cholate	3	1,29	0,3	0,16	0,9	0,5

3.4 Preparation of Giant Vesicles containing Protein

First studies about proteins inserted in the membrane of giant vesicles employed gentle swelling of lipid-protein layers for vesicle production. Films were prepared by evaporating the organic solvent of a mixture of lipids and proteins [34]. With this approach, there is the risk of protein denaturation and only very hydrophobic membrane proteins can be used. The procedure of dehydration followed by gentle hydration was utilized for different channel proteins [22, 31] starting from a film of biological membranes or proteoliposomes mixed with liposomes. A more homogeneous size distribution was achieved producing GUVs containing bacteriorhodopsin with the help of electroformation instead of gentle hydration [116].

Fusion of GUVs prepared by electroswelling with proteoliposomes containing bacteriorhodopsin and a fusogenic peptide bound covalently to lipids also yielded giant

vesicles with inserted membrane proteins [86]. This method should work for any protein that can be incorporated in SUVs but the peptide inducing fusion will always be one constituent of the bilayer. When adding the proteoliposomes to a concentrated emulsion of GUVs, a transfer of material occurs from small vesicles to the giant ones even without special fusion molecules [211].

A general protocol was proposed for the reconstitution of membrane proteins in small liposomes using detergent removal (see 3.3) and their subsequent growth with electroformation. Partial dehydration of liposomes was performed under saturated vapor pressure of a saturated NaCl solution. The incorporation of the hydrophobic protein bacteriorhodopsin but also ATPase with a large hydrophilic part was demonstrated [65]. Water-insoluble SNARE proteins were also reconstituted in giant vesicles [13]. Detergent removal was done via gel filtration in contrast to Bio-Beads in the aforementioned work. Lipid-protein layers were dehydrated under vacuum at 4 °C. Another comprehensive and extensive study adapted the general protocol to the insertion of a voltage-gated potassium channel in giant vesicles [3]. The functional reconstitution of transporter proteins and a mechanosensitive ion channel was reported although dehydration was done in vacuum [42]. Addition of certain amounts of sucrose in the dehydration step reduced the risk of denaturing the protein.

The limitation of electroswelling to buffers with low salt content was recently overcome working at 500 Hz [125, 152] as also described in 3.2. Some membrane proteins need a high salt content for correct functioning. In addition, electroformation was applied to dry or partially dry layers of native membranes already containing membrane proteins [119, 125, 185]. This approach broadens

For some membrane proteins even direct incorporation in GUVs destabilized with detergent seems possible as it was shown for OmpF [95]. This protein is a non-specific transport channel that allows the diffusion of molecules with molecular weights up to 600 Da to 700 Da. Moreover, the direct insertion of bacterial mechanosensitive ion channels in giant vesicles was reported with more than 75% channel activity [15].

Although there are no publications yet on the use of agarose-proteoliposome hybrid films (see section 3.2), this method is interesting for proteo-GUV formation. As agarose forms a hydrogel always containing a certain amount of water there might be a protective effect on proteins incorporated in liposomes. It was already shown, that actin can effectively be enclosed in vesicles with this technique [209] paving the way to more complex model systems.

4 Methods

This chapter introduces basic tools for the production and investigation of GUVs with protein incorporated in their membranes. Most of these techniques are more common to biology or biochemistry than to the physics lab. Methods are sorted thematically. First, proteins and their purification are introduced. In the following, various methods of analytical biochemistry are discussed in detail. For the analysis of SUVs, density gradient centrifugation and dynamic light scattering are employed. Giant vesicles are analyzed by means of optical microscopy. High-resolution confocal microscopy and micro-interferometry, a technique termed reflection interference contrast microscopy (RICM), are described.

4.1 Proteins

4.1.1 Proteins and their Structure

Proteins and multiprotein complexes are a cell's machines or factories. They do not only produce other proteins and enzymes but also are responsible for energy production and storage. Proteins are involved in adhesion and maintaining a cell's structural integrity [20].

The basic building blocks of proteins are 20 amino acids. The sequence of amino acids constitutes the primary structure of a protein. Local structural elements form due to hydrogen bonds. Most common examples are α–helices, β–sheets and turns which are referred to as secondary structures. Their overall arrangement or, in other words, the native folding of a protein is called tertiary structure. It is stabilized by non-local interactions that lead for instance to the formation of a hydrophobic core in soluble proteins. Other examples for interactions are disulphide and hydrogen bonds as well as salt bridges. A protein's folding regulates its basic functions. Organization of two or more proteins into protein complexes leads to quaternary structures. As an example, all integrins are build by the non-covalent linkage of two tertiary protein structures, the α- and β-subunit.

4.1.2 Purification of Proteins

For the purification of a protein, first of all, a cellular material with a high concentration of the protein of interest is needed. Then the protein has to be released from

the cells [67] and the different parts of a cell have to be separated. This can be done with sequential steps of centrifugation with an increase of the rotational speed, a technique called differential centrifugation. The sedimented material in the pellet is removed and the supernatant is centrifuged once more. In this way, the fractionation of material with decreasing density or size is possible. When purifying a new protein, its concentration and activity in each fraction have to be measured with an appropriate assay. This is also the case for every subsequent step in the purification.

Proteins can be further separated according to their solubility, size, charge or specific binding. Solubility of most proteins decreases with increasing amounts of salt in solution. They precipitate at a certain salt concentration, a process termed salting-out. The salt or other small molecules can be removed by means of dialysis. A membrane holds back molecules larger than the cut-off molecular weight inside of the dialysis bag while smaller ones are released into solution.

Largest increase in purity is achieved with different chromatographic methods. A mixture of proteins passes a chromatographic column. The flow-through can be fractionated in adjustable volumes. Each column consists of a matrix of beads made from an inert, chemically and physically stable material like cross-linked dextran or agarose. Beads can be chemically modified to adjust interaction with the sample. The volume in between the beads is filled with a solution depending on the sample. Most often it is buffer in which the sample is applied to the column.

Ion-exchange Chromatography

Ion-exchange chromatography separates proteins based on their net charge. The column is filled with beads having either negatively charged carboxylate groups or positively charged amino groups on their surface. Proteins with an opposite net charge will then bind to the column material whereas polypeptide chains with the same charge pass through. By increasing the salt concentration in the buffer bound molecules are eluted. The higher their net charge, the higher the salt content needed.

Gel Filtration Chromatography

The following two methods, gel filtration and affinity chromatography were also used in this work for integrin purification. Gel filtration discriminates proteins according their size [70]. Columns for gel filtration have a matrix of inert, porous beads. Molecules in the sample solution are able to penetrate into the pores according to their size. The smaller they are, the longer they reside inside of the column because they have a larger available volume. All molecules too large to enter the pores go straight through and are not fractionated. A summary of the process is shown in figure 4.1. The separation range of a given column is determined by the beads' pore size distribution. There are materials for any range commercially available. Separation is also dependent on the volume of sample applied to a gel filtration column. The volume should not exceed 2% of the geometrical column volume V_c [25]. When using a mixture of proteins with known molecular weight it is possible to

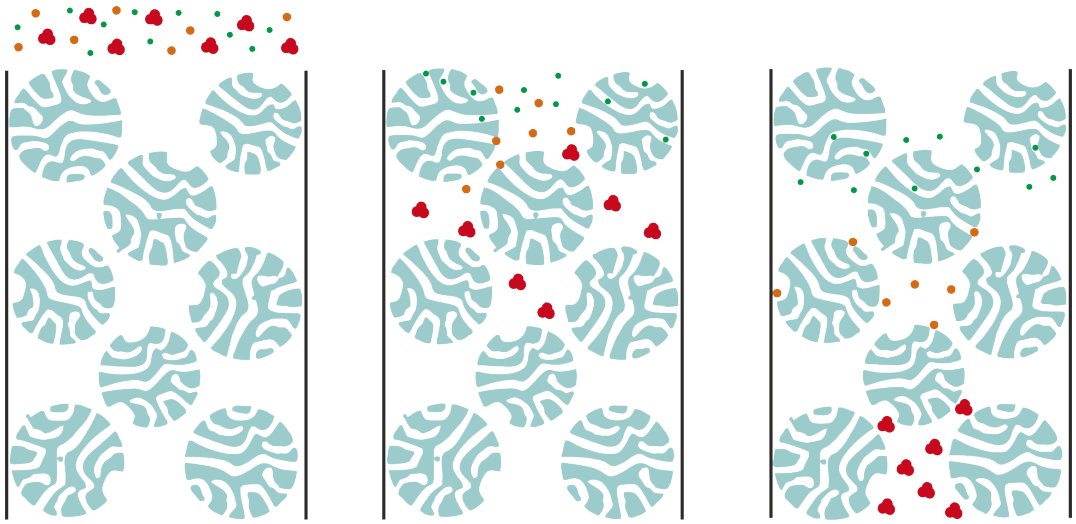

(a) Time t_0. **(b)** Time $t_1 > t_0$. **(c)** Time $t_2 > t_1$.

Figure 4.1: Schematic showing the principle of gel filtration chromatography: A sample consisting of three different proteins - the large ones in red, the medium-sized in orange and the small proteins in green - is applied to a gel filtration column at time t_0 (a). Over time, the proteins are separated due to the fact that smaller ones are able to diffuse into the pores of the matrix which slows them down. Medium-sized proteins can not enter the smallest pores. Their accessible area for diffusion is reduced while large proteins pass the column in between the porous beads (b,c).

calibrate a column. The elution volume V_e for the known proteins is measured and their partition coefficient K_{av} is calculated according to the following equation [99]

$$K_{av} = \frac{V_e - V_0}{V_c - V_0} \tag{4.1}$$

where V_0 denotes the column's void volume. K_{av} gives the fraction of the column volume available for a protein with elution volume V_e. The partition coefficient is related to the natural logarithm of molecular weight. In this way, an unknown protein's weight can be deduced from its elution volume.

Affinity Chromatography

In affinity chromatography specific ligands are bound to the column material to filter molecules out of the sample solution. For example, concanavalin A (ConA), a metalloprotein from the group of lectins, specifically binds carbohydrates [55] including glycoproteins like integrin. Bound material is eluted by applying high concentrations of the sugar mannose. On the other hand, unwanted bound molecules can be removed from the sample by using the flow through fraction. Heparin works like this in the purification of integrin by binding coagulation proteins like thrombospondin [54].

These proteins otherwise interact with integrin $\alpha_{\mathrm{IIb}}\beta_3$.

4.2 Biochemical Analysis of Proteins

Purified proteins are analyzed and characterized by various methods of biochemistry. Techniques relevant for this work are described in the following, namely sodium dodecyl sulfate (SDS)-polyacrylamide gel electrophoresis (PAGE), Western blotting enzyme linked immunosorbent assay (ELISA) and co-immunoprecipitation (co-IP). A nice introduction (in German) for someone not coming from the field to the methods in protein biochemistry can be found in [163].

4.2.1 Measuring Protein Concentration

Many different methods to measure the protein concentration are established [134]. A selection of techniques is briefly described in the following. Their results may show differences even though the same sample is probed. A certain assay may show varying sensitivity for certain amino acids. Thus, results are obtained deviating from the real concentration for different proteins. For instance, using $1\,\mathrm{mg\,ml^{-1}}$ bovine serum albumin, integrin or actin might lead to measured concentrations slightly above or below $1\,\mathrm{mg\,ml^{-1}}$ depending on the protein. In addition, substances like detergents or ions might interfere with the test. Keeping this in mind, not only the protein concentration should be reported but also the method used for its measurement should be mentioned.

The amino acids tryptophan and tyrosine absorb ultraviolet (UV) light. Their absorption can be used to determine protein concentration spectrophotometrically by measuring the extinction at 278 nm or 280 nm [68]. This method is a fast and easy. The amount of tryptophan and tyrosine in the protein sequence should not be too high. Other UV-absorbing ingredients in the buffer also influence the result. One example is the detergent Triton X-100 which contains a benzene ring.

The absorption maximum of the dye Coomassie brilliant blue G-250 is shifted from 465 nm to 595 nm upon its binding to a protein. This shift is exploited for the Bradford assay. The increase in absorption at 595 nm is taken as a measure for protein concentration. Results for different proteins show only minor variations but detergents (e.g. Triton X-100 or SDS), needed for solubilization of membrane proteins, hamper binding of Coomassie.

The molecule bicinchoninic acid (BCA) forms a colored complex with Cu^{2+}-protein complexes evolving in basic solutions. The complexation of proteins with Cu^{2+} in basic environment is called Biuret reaction. The absorbance of the BCA-Cu^{2+}-protein complex shows a maximum at 562 nm. A standard curve is generated with known amounts of bovine serum albumin (BSA) to relate absorption to concentration. This method is called BCA assay. Detergents such as Triton X-100 do not influence

the results, but, for example, the chelating agent ethylenediaminetetraacetic acid (EDTA), glucose or the reducing agent dithiotriole (DTT) distort them. Bradford as well as BCA assay can be performed in roughly under 2 h.

Another choice might be densitometry of images of SDS polyacrylamide gels. The sample is run alongside known, increasing amounts of BSA in SDS-PAGE. SDS-PAGE is explained in the following section 4.2.2. A standard curve is calculated from the intensities of BSA bands in the gel. The sample's concentration is deduced using this standard curve. Therefore, it should fall into the range of BSA concentrations. This requirement is also true for the BCA assay described above. Different sensitivity of the gel stain for BSA and the protein of interest has to be considered. Compared to the aforementioned methods, this procedure is very time consuming.

4.2.2 SDS-Polyacrylamide Gel Electrophoresis

SDS-PAGE is used for the analysis of samples containing a mixture of different proteins [59]. The small, amphiphile and negatively charged molecule SDS binds to proteins in a known weight ratio. Due to hydrophobic interaction with hydrophobic amino acids inside of the protein, the protein's tertiary structure additionally is unfolded. This process is enhanced by heating the sample. Subunits of proteins connected via disulphide bonds, are separated by adding reducing agents like β-mercaptoethanole or DTT. In the end, this treatment leads to proteins in an ellipsoidal form with a negative charge proportional to their length. It is also possible to work under non-denaturing and non-reducing conditions. There are many different protocols for this technique, called Native PAGE [176].

Acrylamide forms a porous hydrogel when cross-linked with methylenebisacrylamide. Additional ingredients in the gel mixture are buffer, ultra-pure water, a 10% (w/v) solution of ammonium persulfate (APS) and tetramethylethylenediamine (TEMED). Ultra-pure water denotes deionized water filtered through a membrane and sterilized with UV light. This special treatment results in a resistance of 10 MΩ. APS works as source of radicals, thereby initiating cross-linking. TEMED catalyzes the cross-linking reaction.

The non-cross-linked, liquid mixture is filled between two glass plates tightly pressed together in a special frame as shown in figure 4.2a. In a discontinuous gel, there is a separating gel with a certain polymer concentration and a low concentration stacking gel on top. The stacking gel focuses proteins in a sample allowing them to enter the separating gel approximately at the same time. A comb put in the stacking gel results in different wells for different samples when removed. A labeled photograph of a gel is shown in figure 4.2b.

The gel serves as a sieve with the size of the pores controlled by the concentration of polymer and cross-linker respectively. Median pore size is inversely related to the square root of acrylamide concentration [28]. The sample is prepared as described above. Additionally, glycerol is added to the sample buffer leading to a sedimentation

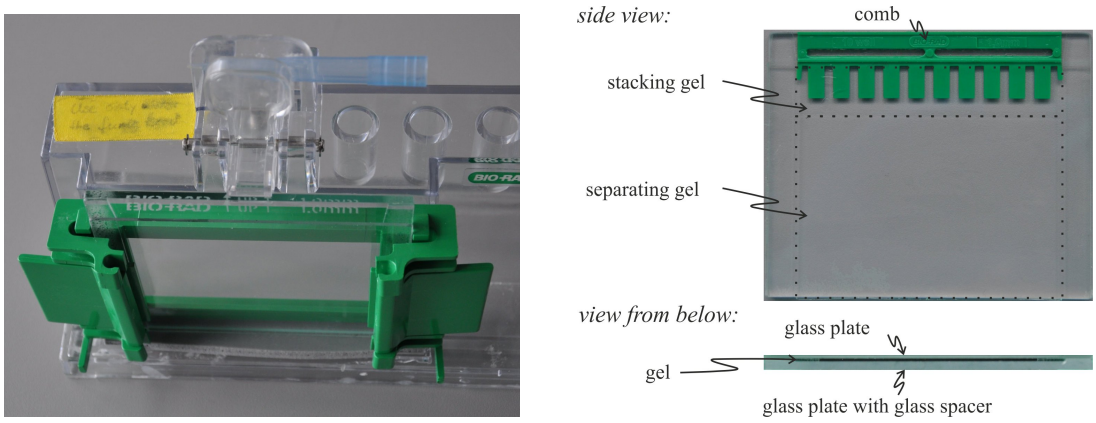

Figure 4.2: Casting a polyacrylamide gel between two glass plates:
(a) Setup for gel casting.
(b) Gel nomenclature.

of the sample solution in the well. This composition of sample buffer is known as Lämmli buffer system [97]. The sample is put in one of the different wells on top of the vertical slab of gel (see figure 4.3a). A direct current voltage is applied with the positive electrode at the bottom of the gel. This causes the negatively charged proteins with net charge z to enter the gel with a velocity given by

$$v = \frac{Ez}{f} \tag{4.2}$$

with the electric field strength E and the particle's frictional coefficient f. The frictional coefficient f is dependent on the particle's geometrical and mechanical properties as well as the gel's pore size. A charged particle's movement in an electric field is termed electrophoresis, thus the name SDS-PAGE. Figure 4.3b shows the gel put vertically in a tank filled with buffer. The two electrodes in the tank are connected to the power supply in the back.

The mesh of cross-linked acrylamide separates the macromolecules according to their size: the larger the proteins the more hindered their movement. The gel is taken from the tank when the sample reaches its bottom. Both glass plates are removed. Proteins are visualized with different stainings. Examples are the blue dye Coomassie or silver ions. Usage of a molecular weight standard, a mixture of proteins with known molecular weight, allows to deduce the size of proteins from their position in the gel.

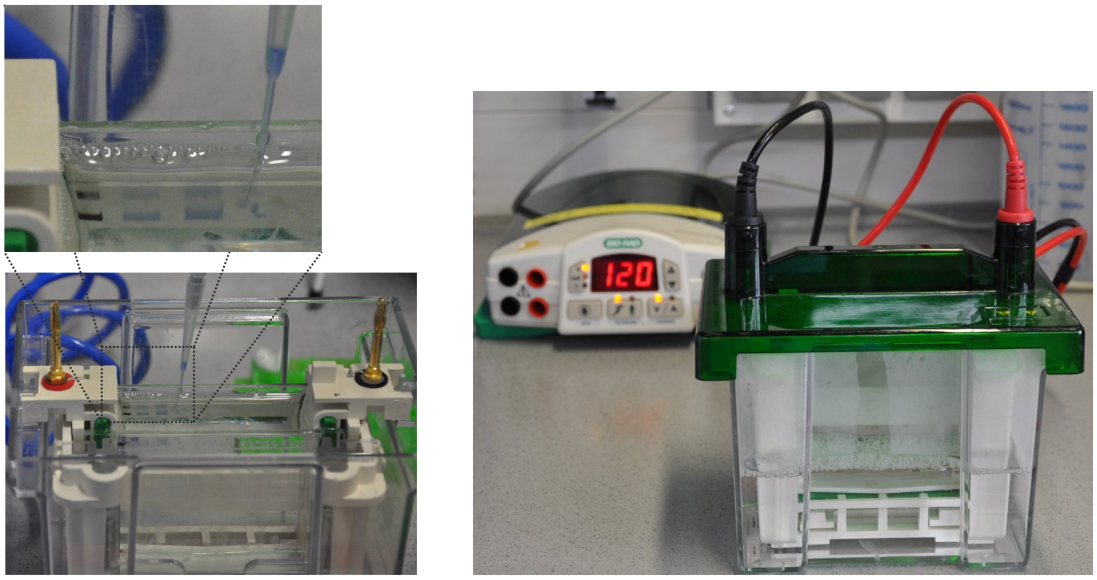

(a) (b)

Figure 4.3: SDS-PAGE:
(a) Application of a sample to a well using a pipette with a special tip.
(b) Photograph of the setup: the power supply is in the back with an applied voltage of 120 V and the tank with the gel can be seen in front.

4.2.3 Western Blotting

Western blotting is an immunological method for a protein's highly sensitive identification. Prerequisite is an antibody specifically binding the protein of interest. First, a protein mixture or cell lysate is separated with SDS-PAGE as described above. Then, an electric field is applied perpendicular to the gel. Proteins move in this field according to their charge and are transferred from the gel to a nitrocellulose or polyvinylidene fluoride (PVDF) membrane. Membrane and gel are put next to each other between filter papers and fiber pads to ensure complete contact between the two. Proteins are usually negatively charged after being separated with SDS-PAGE. Therefore, they migrate towards the anode in an electric field. This should be kept in mind for the insertion of the transfer sandwich between the electrodes.

The macromolecules stick to the membrane due to hydrophobic and/or electrostatic interaction but still are accessible to specific antibodies. All the membrane's free binding sites are blocked with BSA, casein or fat free milk prior to incubation with the primary antibody. This antibody is directed against the protein of interest. Washing removes excess of primary antibody. For detection a second antibody, functionalized with a dye or enzyme, is employed. In this work, I made use of alkaline phosphatase (AP) which cleaves the phosphate group from the substrate 5-bromo-4-chloro-3-indolyl phosphate (BCIP) added after extensive washing. The resulting

bromochloro indoxyl intermediate is then oxidized by p-nitro-tetrazolium blue (NBT) and forms a purple precipitate. On the other hand NBT is also reduced by the indoxyl producing an insoluble blue precipitate. Thereby, the membrane is specifically stained purple-blue where the primary antibody binds to the protein of interest. For a summary, please refer to the scheme in figure 4.4.

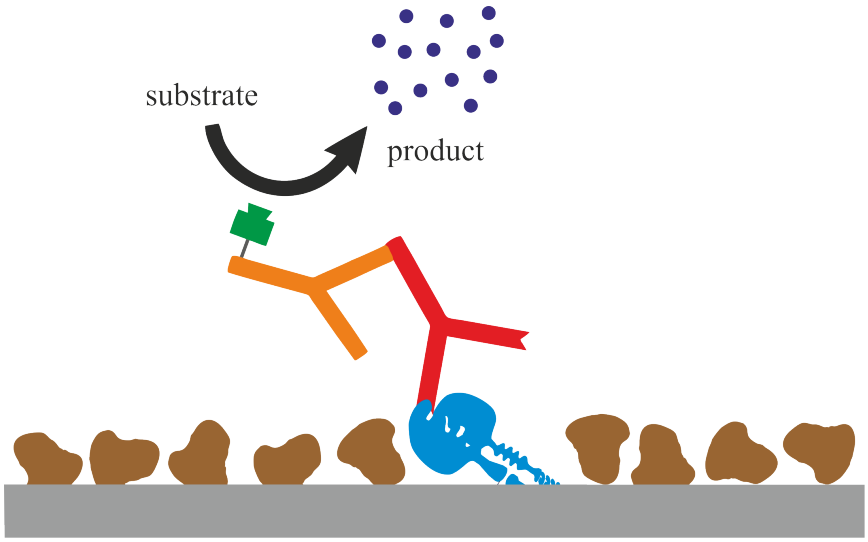

Figure 4.4: Principle of protein identification in Western blotting explained for the example of integrin. The scheme shows the arrangement of proteins and antibodies on the membrane (gray). Integrin (blue) and other proteins are transferred from an acrylamide gel to a nitrocellulose membrane by application of an electric field. Free binding sites of the membrane are blocked with BSA (brown) to prevent unspecific binding of the primary antibody (red). Blocking ensures specific interaction with the protein of interest. Detection is achieved with an enzyme (green) coupled to the secondary antibody (orange). The secondary antibody is directed specifically against the primary antibody's fc region. The enzyme catalyzes the conversion of a substrate to a colored precipitate.

4.2.4 Co-Immunoprecipitation

Co-immunoprecipitation helps to identify protein interactions. One member of a protein complex is fished out of solution by a specific antibody. This antibody is bound to a microsphere functionalized with protein G (or A, depending on the class of antibody). Protein G binds an antibody's fc-region with high affinity. Therefore, the antibody's fragment antigen binding (fab)-region is freely accessible for antigen binding. The whole complex out of functionalized microsphere, antibody and protein is extracted from solution by sedimentation/centrifugation or a magnetic field in case

of superparamagnetic beads[1]. The extracted complex is disassembled by, for instance, suspending it in SDS-PAGE sample buffer and heating the suspension. All steps are shown schematically in figure 4.5. The supernatant without the beads is be put directly on a polyacrylamide gel. Western blotting identifies the other presumed part of the protein complex with a specific antibody. In this way, it is possible to discern, if integrin $\alpha_{\mathrm{IIb}}\beta_3$ exists as heterodimer after purification from platelet membranes.

4.2.5 ELISA

An enzyme linked immunosorbent assay (ELISA) employs antibodies for the specific detection and quantification of proteins, peptides, hormones or other antibodies. The antigen of interest is adsorbed directly or indirectly to a solid surface. For indirect coating, another antibody or a protein which interacts with the antigen is bound to the surface first. Like in a Western blot, detection is achieved by the action of an enzyme linked to an antibody. The enzyme produces a quantitatively measurable product. Enzymes are either conjugated to a primary antibody directly binding to the antigen or to a secondary antibody detecting the primary one.

Binding activity of purified integrin $\alpha_{\mathrm{IIb}}\beta_3$ was studied in this work using ELISA. Therefore, the bottom of a 96-well plate is coated with its natural ligand fibrinogen and blocked with BSA. An antibody directed against the intracellular part of the integrin guarantees the specific detection. Alkaline phosphatase is coupled to the secondary antibody. The enzyme cleaves the phosphate group from para-nitrophenylphosphate (NPP) producing the faintly yellow para-nitrophenol. The concentration of para-nitrophenol is measured by a spectrophotometer according to Lambert-Beer's law. Thorough washing between each step ensures a specific detection. Figure 4.6 schematically illustrates the final arrangement in one a well. The detailed protocol of the assay, based on results in [144], is listed in appendix G.2.

4.3 Analysis of Small Vesicles

4.3.1 Dynamic Light Scattering

Dynamic light scattering (DLS) is an indirect method allowing the calculation of particle sizes from the time-dependent scattering intensity. Another name is photon correlation spectroscopy. When laser light is passing through an emulsion of particles, a small part of light is scattered at each particle in every direction. Maxima in intensity are measured in case of constructive interference of scattered rays from

[1]Superparamagnetic beads consist of polymeric microspheres with magnetite inclusions being so small that only one magnetic domain forms. Above a certain temperature, the orientation of magnetization is randomized over time without an external magnetic field. Therefore the beads show paramagnetic behavior with a magnetic saturation comparable to a ferromagnet.

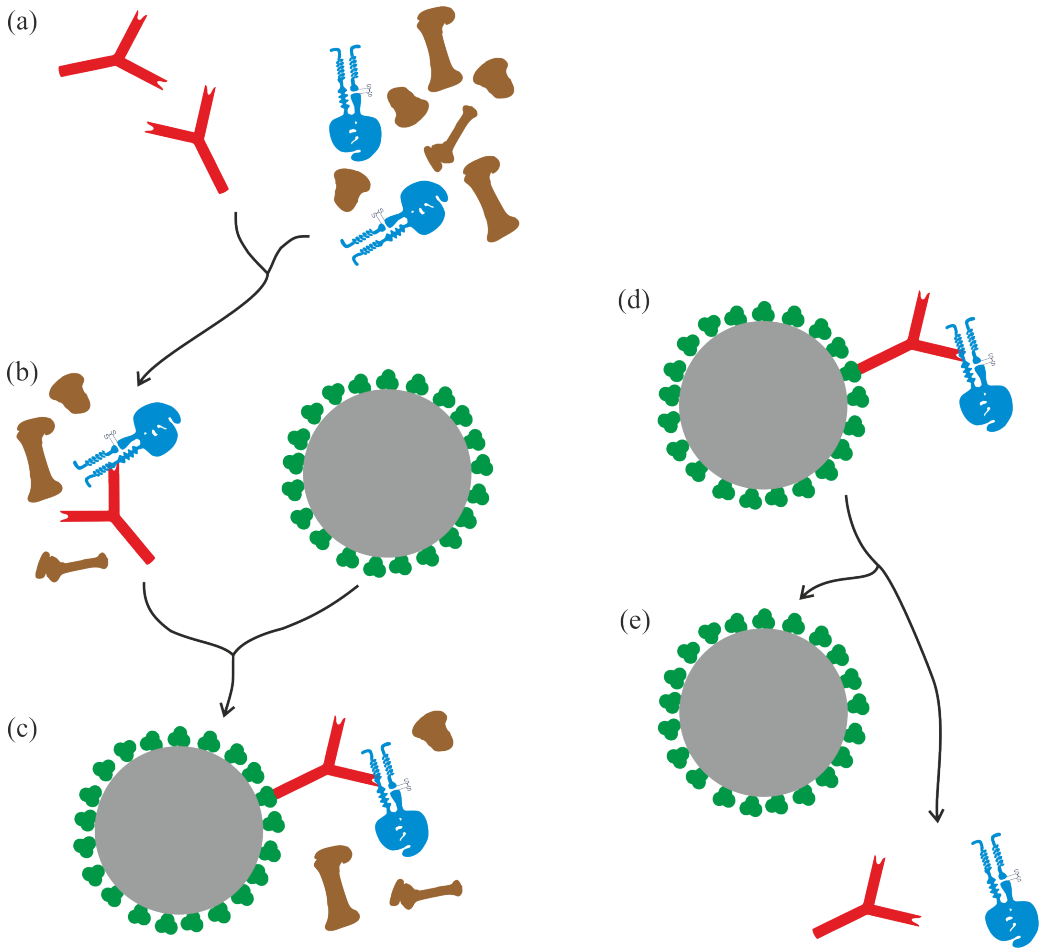

Figure 4.5: Course of events in co-immunoprecipitation. The protein mixture is incubated with an antibody (red) directed against the protein complex of interest (blue) (a). After binding of the antibody, microspheres (gray) coated with protein G (green) are added to the solution (b). Due to the high affinity of protein G for an antibody's fc-region, the antibody-protein complex readily associates with the beads (c). The large difference in density between proteins and beads allows their easy separation from the protein mixture by sedimentation or centrifugation. Another elegant way is the use of superparamagnetic beads. These are attracted by a magnet and the remaining solution can be removed (d). In the last step, protein and antibody are separated from the beads for further analysis (e).

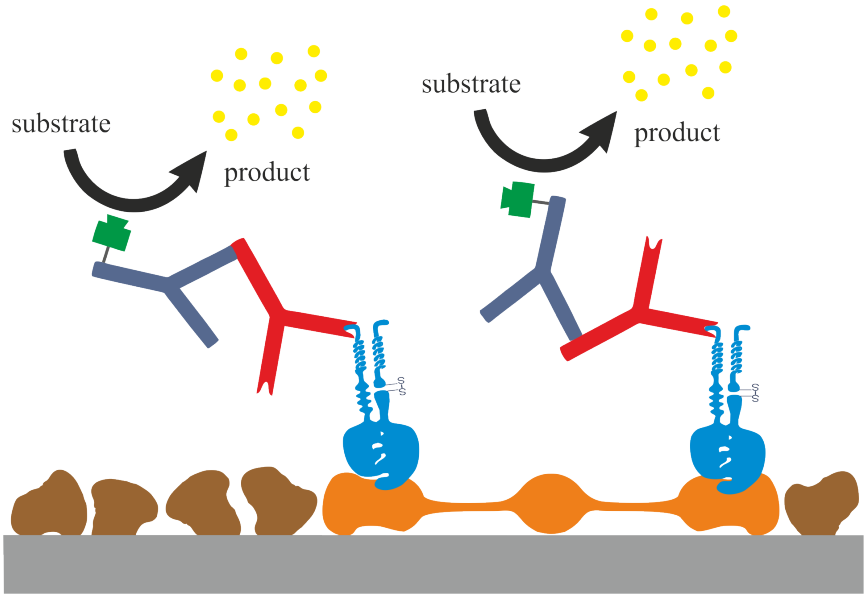

Figure 4.6: Schematic illustrating the principle of ELISA for the example of integrin (blue) binding to fibrinogen (orange) which is physisorbed at the bottom of a 96-well plate (gray). Blocking is done with BSA (brown). The primary antibody (red) binds the cytosolic tail of integrin and is detected by the secondary antibody (dark blue) coupled to the enzyme AP (green) that cleaves the phosphate group from NPP producing the faintly yellow para-nitrophenol.

different scattering centers. Due to brownian motion the particles' distance and orientation to each other change over time. These small variations lead to intensity fluctuations. The smaller the particles, the shorter the time scale of fluctuations because of the higher velocity of their movement. Fast fluctuations in turn are connected to a fast decay of correlation. There is a direct functional relation between the intensity's autocorrelation function $g^{(2)}(\tau)$ with delay time τ and the diffusion coefficient D of monodisperse particles in solution:

$$g^{(2)}(\tau) = B + \beta \ \exp\left(-2Dq^2\tau\right) \tag{4.3}$$

where B is a baseline value, β a factor depending on the experimental geometry and $q = (4\pi n/\lambda)\sin(\theta/2)$ the scattering wave vector. λ represents the wavelength of the laser in vacuum, n the refractive index of the medium and θ the scattering angle. By using the Stokes-Einstein equation

$$D = \frac{k_B T}{6\pi\eta r} \tag{4.4}$$

which is valid for spherical particles, the particles hydrodynamic radius r is calculated with Boltzmann's constant k_B, absolute temperature T and the solution's viscosity η.

4.3.2 Density Gradient Centrifugation

A density gradient is useful for separating cellular organelles or macromolecules like proteins but also small particles like SUVs. Separation is achieved due to weight or density in the enhanced gravitational field of a centrifuge. Many substances are applied as gradient media. Sugars (e.g. sucrose), non-ionic iodinated media (e.g. Nycodenz) or alkali metal salts (e.g. CsCl) are common examples among others. There are continuous or step gradients. The former is usually formed by gradient mixers where a light and a very dense solution are mixed in a linear way. Alternatively, steps are smoothed with time by diffusion. A step gradient is formed by layering solutions of different density on top of each other in a centrifugation tube starting with the densest liquid at the bottom. The sample can either be in the topmost layer or it is put at the bottom of the tube depending on the conditions (see below). For many applications it is easier to start with the lightest solution. Long pipette tips or syringe needles are employed to bring in denser ones below. This procedure most often reduces the risk of mixing the different layers.

A particle's movement in a gravitational field can be characterized by the sedimentation coefficient s. It is equal to the ratio of sedimentation velocity v and rotational acceleration $\omega^2 R$ with the rotors angular speed ω and the particle's distance R to

the axis of rotation. The equation is

$$s = \frac{v}{\omega^2 R} = \frac{m_p\,(1 - \rho_l/\rho_p)}{f} \tag{4.5}$$

where m_p and ρ_p are the particle's mass and density respectively, ρ_l the liquid's density and f the particle's frictional coefficient. The second relation represents a special form of the so-called Svedberg equation. It is obvious that heavier particles sediment faster than lighter ones. Since friction is influenced by the shape of a particle, there is also a separation due to shape. Rod shaped objects, for instance, move slower than spherical ones, provided they are of the same mass. The direction of motion is dependent on the ratio of liquid's to particle's density. If the object is lighter than the solution, it moves upwards and vice versa. In case of equal densities the particle comes to a halt.

Density gradient separation can be classified into two categories: Rate-zonal and isopycnic separation. In rate-zonal centrifugation the density of the material to be separated is higher than the densest gradient solution. The sample is layered on top of the gradient and centrifugation leads to a fractionation due to weight and shape. The sample solvent needs to be lighter than each gradient solution. A pellet is formed at the tube's base due to the high density of the sample, if centrifugation is too long.

When the density of solutes or particles in the sample is in the range of the gradient solutions, separation occurs according to density. This process is called isopycnic centrifugation. Particles stop at the position in the gradient, where their density equals that of the surrounding medium. Since this is an equilibrium process longer run times have no unfavorable effect if the sample is stable in the gradient solutions. In this work, the sample is dissolved or dispersed in the lowest layer of the gradient. Molecules or particles then rise corresponding to their density.

4.4 Analysis of Giant Vesicles – Microscopy

As giant vesicles are several tens of micrometers in size, they are imaged with an optical microscope. However, due to the small changes in intensity because of the thin shell of molecules barely absorbing light, they show only low contrast in bright field microscopy. This is why special contrast methods have to be used, which make changes in the phase of the illuminating light visible. The human eye is not sensitive to changes in the phase of incoming light, but interference is one way to convert phase differences in detectable differences in intensity. This principle is applied in phase contrast and differential interference contrast microscopy. Both techniques are discussed in detail in the appendix A. Furthermore fluorescent dyes can be utilized to label the samples on the molecular scale. Fluorescent molecules absorb light of a certain wavelength depending on their electronic and vibrational states leading to the excitation of an electron. The absorbed energy can be re-emitted through the

emission of a photon. Epifluorescence microscopy is also explained in A in more depth.

4.4.1 Confocal Laser Scanning Microscopy

In order to allow for optical sectioning even in thick samples, stray light is reduced in confocal laser scanning microscopy by using a pinhole in front of the detector and illuminating with a point source. The lateral and axial resolution are improved by a factor of about 1.4. In contrast to standard microscopy, that usually uses a charged coupled device (CCD) as detector, in confocal microscopy the sample is scanned point by point. The signal is recorded by a photomultiplier tube (PMT) or an avalanche photodiode (APD). As typical for scanning imaging techniques, the final image is rendered from the single signal intensities with a computer. Most often a laser is utilized for illumination. The reasons are its brightness and the narrow beam profile which makes it easy to focus to a point-like spot. After passing the illumination pinhole, which is omitted in some setups, one or more mirror galvanometers allow for the scanning of the sample in x- and y-direction. Excitation and emission are separated as in epifluoresence by appropriate filters and dichroic mirrors. On the other hand, in modern microscopes acousto-optical modulators and/or filters are used for a fast separation of different wavelengths without mechanically switching a filter cube. Electrically excited oscillations in a piezoelectric material result in acoustic waves in a coupled block of glass. This leads to periodic changes in the index of refraction acting as diffraction grating. Additionally, the intensity of light can be modulated by the sound wave's intensity thereby combining color selectivity with illumination power control. A simplified scheme of a confocal microscope is shown in figure 4.7.

4.4.2 Reflection Interference Contrast Microscopy

For the investigation of adhesion of cells or model systems like GUVs, optical techniques are utilized, that allow to obtain information specifically from surfaces of biofunctionalized substrates. In total internal reflection fluorescence (TIRF) microscopy the evanescent field of a totally reflected laser beam excites only fluorophores closer than approximately 200 nm to the bottom of an observation chamber. However, labeling of adhesion proteins with, for instance, fluorescent antibodies might interfere with the process of adhesion itself. The non-invasive micro-interferometric technique RICM is used to accurately measure distances from the surface of a glass slide with a precision of a few nanometers without the need of further treatment of the sample [108]. In the 1970ies, the method was used extensively in biology to study cell-substrate distances [64]. In the last 20 years, it was mostly applied to investigate adhesion of model systems [6, 50, 107, 113].

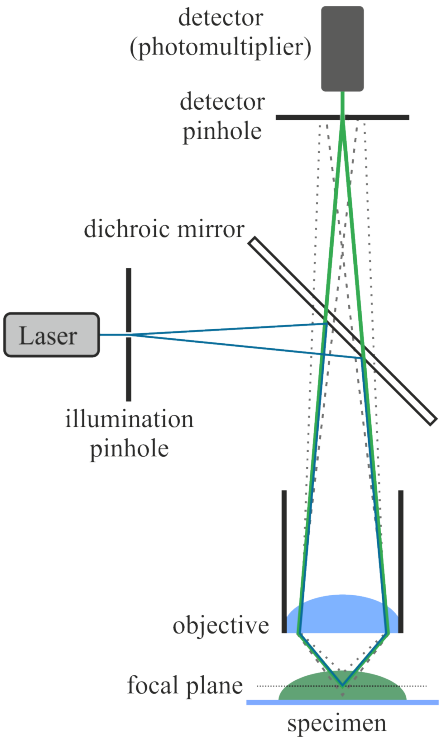

Figure 4.7: Simplified beam path in a confocal microscope. Fluorophores in the sample are excited by a wavelength of light shorter than the wavelength of their emission. Only light originating from points in a plane being confocal to the detector pinhole - the focal plane - substantially contributes to image formation. Light emitted from below or above this plane (indicated by gray broken lines) is not focused on the pinhole. Thereby, stray light is reduced. The drawing is not to scale.

Typically, an inverted microscope is modified to apply RICM. Monochromatic epi-illumination, meaning illumination and detection from the same side of the specimen, is used. Therefore, an interference filter protected by an anti-caloric filter selects one wavelength, usually 546 nm. Aperture and field diaphragm allow the establishment of Köhler illumination. A polarizer linearly polarizes the light. The quarter wave plate in front of the objective's lens renders linear polarization to circular polarization. Its orientation is rotated by 45° with respect to the orientation of the polarizer. Two different kinds of interfaces are encountered in the sample: Interfaces with decreasing or increasing index of refraction. For quasi-normal incidence, in both cases either parallel or perpendicular component of the electric field experience a phase shift of π, while the other component is not affected. The phase shift results in the reversal of direction of circular polarization. The second passing through the quarter wave plate transforms the reversed circularly polarized light to linearly polarized light. The light's polarization vector is perpendicular to the incident linear polarization. Thereby, light reflected in the sample is able to pass the crossed analyzer. Any stray light, that retains its original direction of polarization, is rejected by the combination of crossed polarizers and quarter wave plate. The image is formed through interference of light reflected at the different interfaces in the sample. The interferograms are recorded by a CCD camera. A scheme of the beam path is shown in figure 4.8.

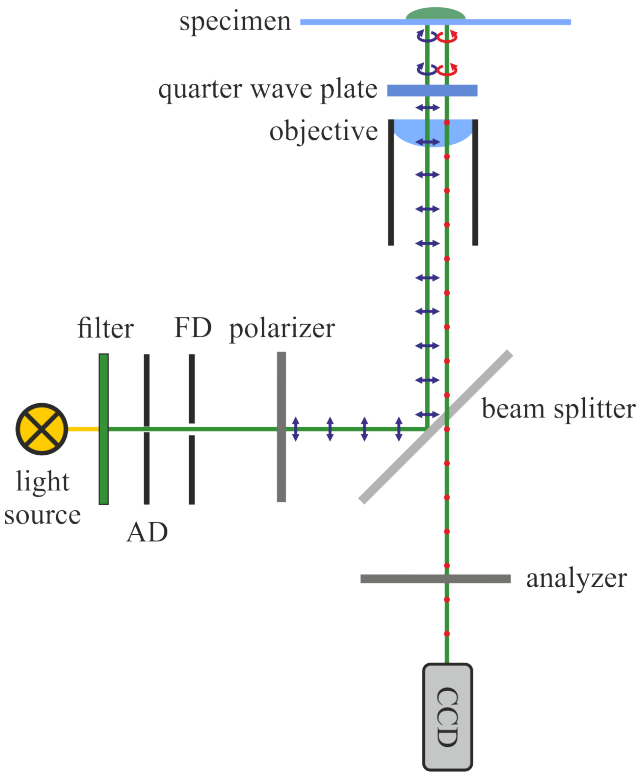

Figure 4.8: Beam path of reflection interference contrast microscopy. A band pass filter selects a wavelength, typically 546 nm, out of light from a mercury vapor pressure lamp. Aperture diaphragm (AD) and field diaphragm (FD) allow the establishment of Köhler illumination in reflected light mode. The polarizer linearly polarizes the light. Direction of polarization is indicated by blue (incident light) and red (reflected light) arrows or points. Arrows indicate circular polarization or polarization in the image plane, points show polarization perpendicular to this plane. A quarter wave plate in front of the objective's lens renders linear polarization to circular polarization or the other way round in the other direction. Polarization of light reflected at the sample afterwards is perpendicular to the incident polarization. Therefore, it passes the crossed polarizer. Images are recorded with a CCD camera.

Theory of Image Formation

In order to quantitatively measure the distance h between substrate and object from interference patterns acquired with RICM, theoretical models of image formation are needed. Relative changes of distances can then be determined with nanometer precision [159]. The absolute height is only accessible under special circumstances due to the periodicity of interference phenomena. This restriction can be overcome by using dual-wavelength RICM [126, 178].

The most simple model of image formation assumes perpendicular incidence of light and plane, parallel interfaces [160]. Curved surfaces are approximated by stepwise segments parallel to the glass surface. More complex theories include effects of finite aperture [64, 161, 217] with additional influences of polarization [207]. Curved interfaces are addressed in the so-called non-local theory [91], which was adapted to account even for finite aperture [30, 218]. However, finite aperture theories do not yield an analytical expression for the height profile in dependence of intensity. Illumination with finite aperture leads to stretching and damping of interference fringes. Non-local theory, on the other hand, is not applicable to objects with unknown shape and solution has to be done numerically. Curved or tilted interfaces result in reduced distance between fringes. Their intensity is also damped. The fringes are only visible as long as the interface's slope is smaller than a maximal slope due to the lateral resolution of the microscopy. In order to reconstruct the shape of giant vesicles in the vicinity of the substrate, a theory was used which accounts for reflections from three planar interfaces under the assumption of normal incidence [107]. A scheme of reflections at three interfaces is depicted in figure 4.9.

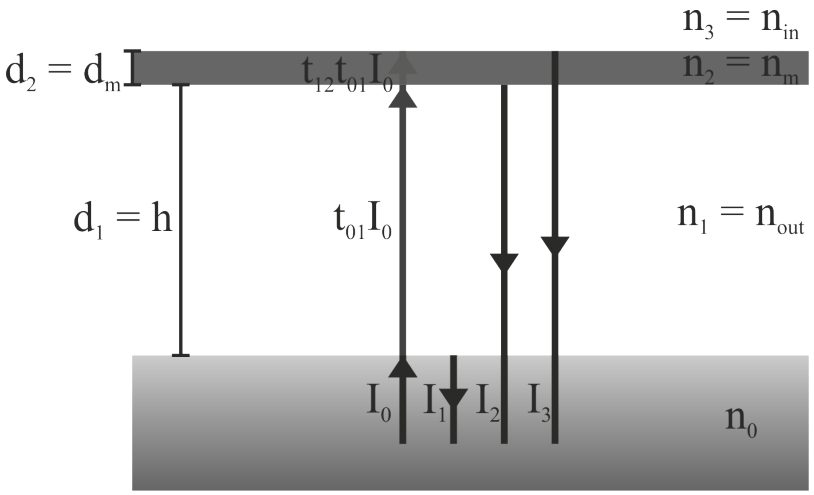

Figure 4.9: Reflection and transmission of light at three interfaces with normal incidence. The part of light reflected at interface ij is given by the respective reflection coefficient r_{ij}, while transmitted light is described by the transmission coefficient t_{ij}.

In RICM, an image is formed from the interference of light rays reflected at the different interfaces in the system. The reflection of an electromagnetic wave at an interface is described by the Fresnel equations. The (angle-independent) reflection

coefficient r_{ij} of the interface between layers i and j for normal incidence is given by

$$r_{ij} = \frac{n_i - n_j}{n_i + n_j}, \tag{4.6}$$

where n_i and n_j denote the refractive indexes of layers i and j respectively. The overall amplitude of the reflected field E can be calculated as the product of incident amplitude E_0 and the complex, effective reflection coefficient R

$$E_{\text{refl}} = R\ E_0. \tag{4.7}$$

Equation (4.7) implies for the measurable quantity intensity I

$$I = R^* R\ E_0^2 = R^* R\ I_0 \tag{4.8}$$

with * indicating the complex conjugate. The optical path length L_i for light passing twice layer i with local thickness $d_i\,(x, y)$ is

$$L_i = 2\ n_i\ d_i\,(x, y) \tag{4.9}$$

where (x, y) indicates the position on the substrate. The system under study consists of a GUV membrane with thickness $d_{\text{m}} = d_2$ and refractive index $n_{\text{m}} = n_2$ of the membrane enclosing inner buffer with refractive index $n_{\text{in}} = n_3$. The vesicle is immersed in outer buffer with refractive index $n_{\text{out}} = n_1$. The membrane's distance to the substrate surface is denoted $h = d_1$. If multiple reflections are neglected, the effective reflexion coefficient R reads for this specific situation

$$R = r_{01} + \left(1 - r_{01}^2\right) \exp\left(4\pi i n_{\text{out}} h/\lambda\right) \left(r_{12} + r_{23}\left(1 - r_{12}^2\right) \exp\left(4\pi i n_{\text{m}} d_{\text{m}}/\lambda\right)\right). \tag{4.10}$$

The local intensity $I\,(x, y) = I\,(h\,(x, y)) = I\,(h)$ is then given by

$$2\ I\,(h) = (I_{\max} + I_{\min}) - (I_{\max} - I_{\min}) \cos\left(\frac{4\pi n_{\text{out}}}{\lambda}\,(h - h_0)\right) \tag{4.11}$$

with $I_{max} = I_1 + I_2 + 2\sqrt{I_1 I_2}$ and $I_{min} = I_1 + I_2 - 2\sqrt{I_1 I_2}$ being the observed maximum and minimum intensities of the interference pattern. The local distance h therefore depends on the local intensity $I\,(x, y)$ as

$$h\,(x, y) = h_0 + \frac{\lambda}{4\pi n_{\text{out}}} \arccos\left(\frac{I_{\max} + I_{\min} - 2I(x, y)}{I_{\max} + I_{\min}}\right). \tag{4.12}$$

The distance of minimal intensity is shifted to h_0 due to the reflection at the membrane/inner buffer interface as compared to simpler methods of evaluation of RICM [18, 94]. The shift depends on values of indexes of refraction for inner and outer

buffer. The analytical expression for h_0 is

$$h_0 = \frac{-\lambda}{4\pi n_{\text{out}}} \arctan\left(\frac{\gamma \sin d_{\text{m}}}{1 + \gamma \sin d_{\text{m}}}\right) \tag{4.13}$$

with $\gamma = \frac{r_{23}}{r_{12}}\left(1 - r_{12}^2\right)$ following [107].

Valuable insight about resolution and influence of coherence, which is not treated here, can be gained from the theoretical discussion in [153].

Part II

Experimental Design and Measurement Techniques

5 The Minimal System

The minimal system of cell adhesion reduces the cellular complexity to three essential components. To this end, an adhesion protein was incorporated in the membrane of a GUV. These structures were filled with an emulsion of a polymeric protein, which is part of the cytoskeleton. Due to their diameter of more than 10 µm, GUVs were easily investigated by means of optical microscopy. Phase contrast allowed the detailed study of overall morphology, while RICM was used to determine the shape of the membrane in the vicinity of nano-structured and bio-functionalized substrates thereby enabling characterization of adhesion.

The cell plasma membrane was imitated by giant unilamellar vesicles. Main lipid components were phosphatidylcholine (PC) and phosphatidic acid (PA), both purified from egg yolk (eggPC and eggPA respectively). Due to their natural source, they contain a variety of saturated and unsaturated fatty acid tails. This mixture leads to a phase transition temperature below room temperature. PA renders the bilayer negatively charged. Lipids functionalized with the polymer poly(ethylene glycol) served as a mimic of the cell's glycocalyx. These lipids prevent unspecific adhesion. The concentration in the bilayer of adhesion receptor and PEG-functionalized lipid control the adhesive properties of the model system. Specifically, dipalmitoyl (DP) phosphatidylethanolamine (PE) functionalized with PEG 2000 was used. PEG 2000 is poly(ethylene glycol) with an average molecular weight of $2000\,\mathrm{g\,mol^{-1}}$.

Protein components were the adhesion molecule integrin $\alpha_{\mathrm{IIb}}\beta_3$ from human platelet membranes and the cytoskeletal constituent actin purified from rabbit muscle. These specific proteins were chosen because of the availability of respective raw material. Integrin $\alpha_{\mathrm{IIb}}\beta_3$ was incorporated in the bilayer of GUVs, while G-actin was enclosed inside of the vesicles. The ionophore A23187, also known as calcimycin, was added to the lipid mixture permitting the polymerization of actin by addition of magnesium ions to the outer buffer. A23187 inserts in bilayers and forms stable complexes with divalent ions. Thereby, it allows their transport across membranes. The schematic in figure 5.1 illustrates the assembly of components.

The following sections introduce methods and assays that were applied to obtain the desired minimal system. The design of experiments is explained explicitly. A detailed list of chemicals, reagents and other material used in this study is found in appendix D.

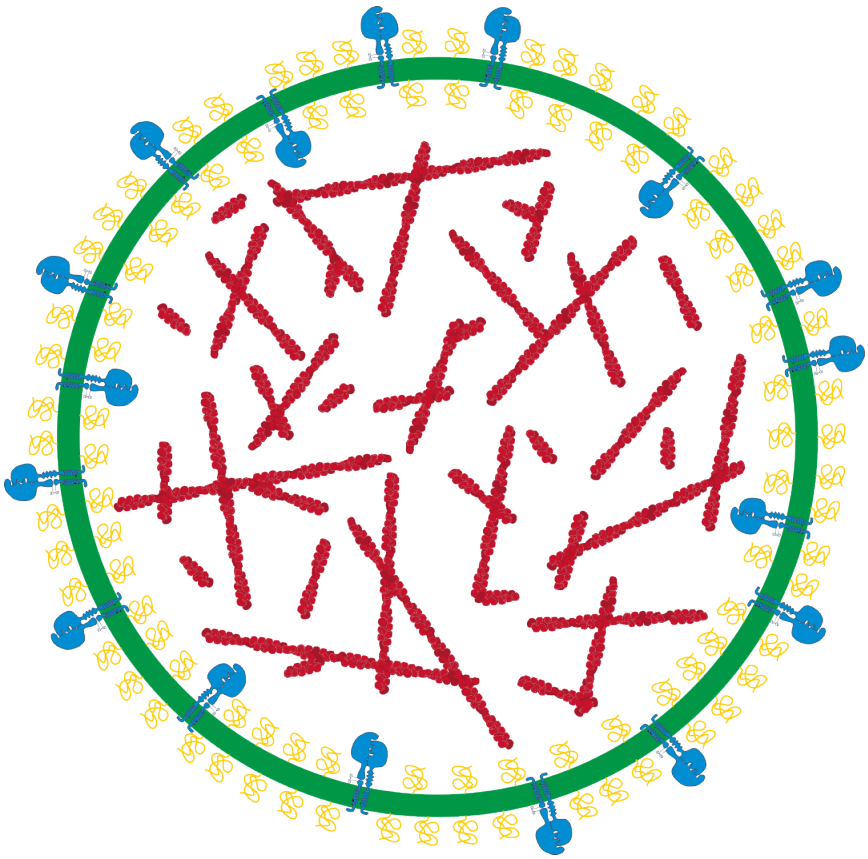

Figure 5.1: Schematic illustration of the minimal system. Integrin $\alpha_{\mathrm{IIb}}\beta_3$ (blue) is incorporated in the lipid membrane (green) of a GUV. Actin (red) is enclosed in buffer. In addition, lipids functionalized with PEG (yellow) mimic a cell's glycocalyx and prevent unspecific adhesion. The ionophore A23187, allowing polymerization of actin inside of vesicles, is not shown in this scheme. The drawing is not to scale.

6 Preparation of Small and Giant Vesicles

6.1 Small Unilamellar Vesicles

Sonication and membrane extrusion were used in this work to prepare small and large unilamellar vesicles. First, solutions of different lipids in chloroform were mixed in ratios as listed in table 10.1 with Hamilton syringes (detailed volumes for lipid mixtures see appendix E). All lipids employed in this study were obtained from Avanti Polar Lipids unless otherwise stated. Phosphatidylcholine labeled with the fluorescent dye BODIPY (BODIPY-PC, #D3793, life technologies) was added at 0.1 to 0.4% (w/w) for fluorescence microscopy studies. As chloroform is a strong solvent, care was taken to avoid its contact with potential solutes. Lipids or lipid mixtures were stored at $-20\,^{\circ}\mathrm{C}$ in glass test tubes with glass joint caps protected from light or in small, brown glass bottles with screw caps and teflon septum (all Carl Roth). To prevent oxidation of unsaturated lipids, argon was layered on top of lipid solutions. Oxidation leads to a saturation of double bonds in fatty acid chains. When taken from the freezer, containers were opened only after temperature equilibration to avoid condensation of water inside of the bottles. Water leads to hydrolysis of lipids, that is the cleavage of fatty acid from the glycerol backbone of a lipid. All the following steps to prepare vesicles were performed above the highest phase transition temperature of all the components in the mixture.

The lipid mixtures were transferred to a small glass bottle. The exact volume depends on the concentration of the lipid solution in chloroform and the desired concentration in the aqueous emulsion of vesicles to be prepared. Chloroform was evaporated under a gentle stream of nitrogen till an opaque gel formed and no fluid was left anymore. Lipids were spread on the maximal available surface, which depends on the amount of aqueous solution added later on. To remove even slight traces of chloroform, the flask was put in a desiccator (figure 6.1a). The desiccator was filled with argon and connected to a small diaphragm pump (KNF, Laboport, N86KT.18) for 2 h at a minimum. Afterwards, water or buffer was added to the dried lipid films which were allowed to swell for at least 1 h in the dark. Typically, $20\,\mathrm{mmol\,l^{-1}}$ Trehalose (#5151.3, Carl Roth) was used as swelling solution. A tip sonicator (Bandelin Sonopuls, Bandelin electronic, HD 2070 equipped with sonotrode MS72) was used to produce SUVs (figure 6.1b). Pulses of 0.1 s duration were applied three times for

20 s each with a frequency of 1 Hz. Short pauses decrease heating of the sample. SUVs and LUVs were prepared with the Avanti Mini Extruder (figure 6.1c;#610000, Avanti Polar Lipids) employing hydrophilic polycarbonate membranes with pore sizes of 50 nm. 100 nm and 200 nm (most often 100 nm). The solution of swollen lipid was filled in one of the two syringes and both were connected to the teflon connector holding the membrane. By pushing the solution back and forth several times the vesicles' size distribution becomes more and more narrow and monodisperse emulsions of SUVs can be produced. A minimum of thirteen passes through the membrane was performed resulting in monodisperse samples as verified by dynamic light scattering (DLS). When working with large amounts of lipid, clumps of lipid sometimes formed in the swelling period before extrusion. Short immersion, 30 s at a maximum, in a bath sonicator (Bandelin Sonorex, Bandelin electronic, RK 102 H) was generally sufficient to disperse lipids.

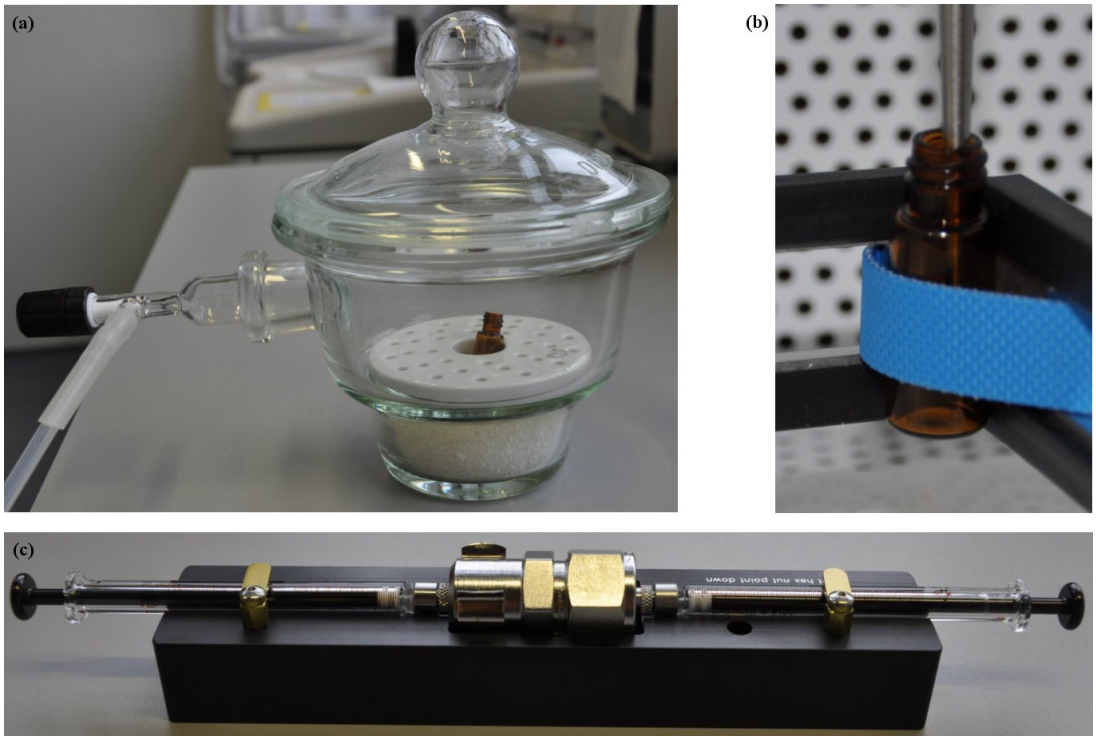

Figure 6.1: Preparation of SUVs.
(a) Small bottle with dried lipid films in a desiccator connected to a vacuum pump.
(b) Tip of a tip sonicator inserted in a small bottle filled with an emulsion of swollen lipid in water/buffer.
(c) Avanti Mini Extruder: Two Hamilton syringes are connected via teflon element with a polycarbonate membrane inside.

6.2 Giant Unilamellar Vesicles

Giant unilamellar vesicles were mostly prepared employing electroformation. In another approach, agarose-lipid-hybrid films were also tested for their possibilities in producing GUVs from proteoliposomes.

Electroformation

Electrically conductive and transparent ITO-coated glass slides (#CEC010S, PGO) and platinum wire (#PT005145, Goodfellow) were used as electrodes. ITO was used with lipid films from lipid mixtures dissolved in chloroform, while lipid films on platinum wire were mostly produced from aqueous liposome or proteoliposome emulsions.

20 µl lipid solution in chloroform was spread on about 2 cm^2 on ITO with a Hamilton syringe (figure 6.2b). Glasses were put in desiccator to ensure complete evaporation of chloroform. Each ITO-coated glass had a teflon spacer with a thickness of 0.5 mm and copper tape (#1181, 3M) on top of the spacer on one side, as shown in figure 6.2a. Two such glasses build a small capacitor, when put next to each other. To form closed chamber sigillum wax (#9120101, Hirschmann Laborgeräte) was used. An about 1.5 mm thick, "sausage-like" object was shaped. The wax was laid around the dry lipid layers and two ITO-coated glasses were pressed together between two brass blocks (about 6x9x1.5 cm^3). A completed chamber is depicted in figure 6.2c. The chamber was filled with water or buffer and closed with sigillum wax. Voltage was applied between the two copper strips (see figure 6.2d).

Pt-wire electrodes were employed to grow liposomes or proteoliposomes to GUVs. Figure 6.3 illustrates different designs of swelling chambers. The chamber in figure 6.3a is made from teflon and is closed using vacuum grease and two 24x60 mm^2 cover slides. The following description refers to one of the three wells of this swelling chamber.

One side of the chamber was closed with grease and a cover glass. A 3 ml syringe (#4616025 V, B. Braun) with a 1.2 mm thick needle (#4665120, B. Braun) was used to apply the vacuum grease. In total, 2 µl of liposome emulsion with a concentration around 5 mg ml^{-1} were applied to the wires in small droplets with a 2.5 µl pipette. The small pipette allows precise dosage to ensure small droplets. After 1 to 2 min, droplets were spread on the wire with the pipette. Remaining fluid was aspirated and once more applied in small droplets. This process was repeated two to three times until only a thin film of liquid remained. This film was allowed to dry in ambient atmosphere at room temperature to complete dryness for liposomes (typically at least 45 min). For proteoliposomes, drying was more elaborate: The remaining liquid film was allowed to dry until the glossy appearance of a wet wire was lost, taking about 5 min. Proteoliposomes were dried further for another 10 min. Too long drying leads to the denaturation of incorporated membrane proteins. Too short drying results in the detachment of the lipid film from the wire when an aqueous solution is added for

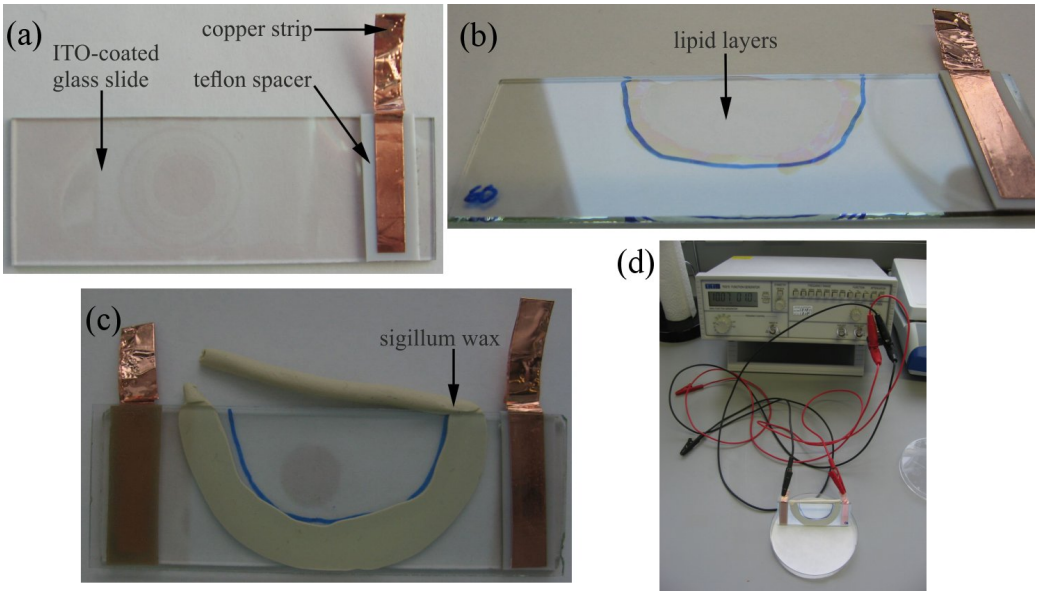

Figure 6.2: Electroformation using ITO-coated glass slides.
(a) Assembly of teflon spacer and copper strip on the ITO-coated side of the glass.
(b) Lipid layers on ITO-coated glass.
(c) Assembly of the swelling chamber.
(d) Swelling chamber connected to a function generator.

electroformation. While drying, each well was framed by vacuum grease on the teflon surface. 415 µl ultra-pure water or buffer were added to each well. The chamber was closed with another glass slide trying to avoid air bubbles inside of the wells. An sinusoidal potential was applied between the two wires.

A sine wave AC electric field was generated with a function generator (TTi, #TG315) using a frequency of 10 Hz for low salt conditions (below approximately 10 mmol l^{-1}) or 500 Hz for higher salt concentrations. Typically, 1 V peak-to-peak voltage per 1 mm distance between platinum wire electrodes was applied. When employing ITO-coated glass slides as electrodes, the electric field was about 2 V mm^{-1} (peak-to-peak). The osmolality of all solutions was checked with a cryoscopic osmometer (gonotec GmbH, Osmomat 030) by comparison of the sample's freezing point to the freezing point of pure water. Osmolality is important in case of dilution or exchange of the buffer outside of the GUVs. Dilution or exchange allow, for example, to control membrane tension by taking advantage of osmosis. The membrane is tense or flaccid depending on whether the outer solution has lower or higher osmolality. If the difference in osmolality is too large, this can even lead to the destruction of vesicles especially for outside buffers with lower osmolality. Furthermore, giant vesicles filled with a sucrose solution sediment to a glass slide when diluted in an iso-osmolar solution of glucose due to the difference of density.

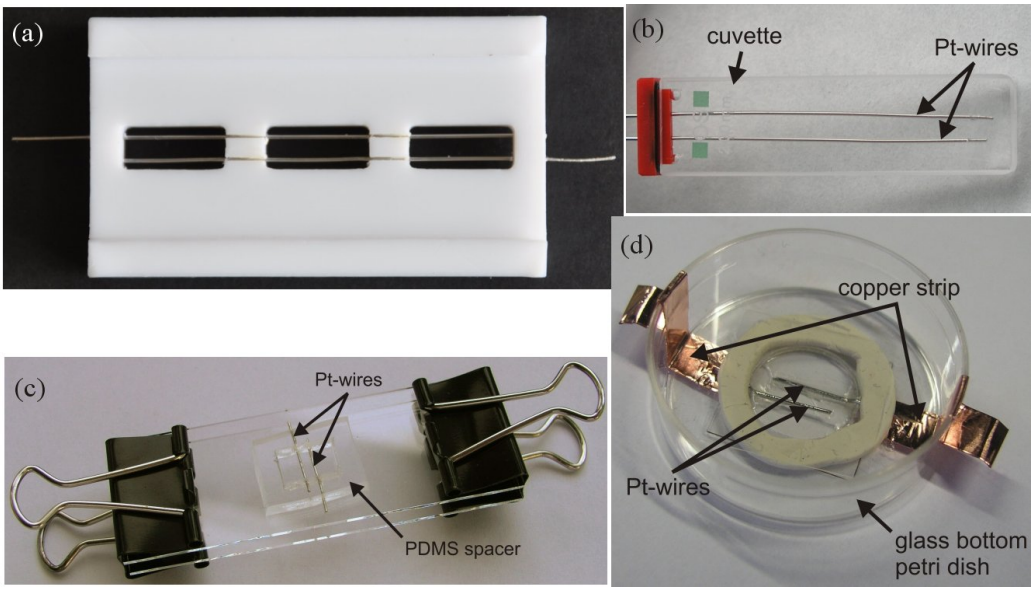

Figure 6.3: Swelling chambers for electroformation using platinum wire.
(a) Most used, current design. The main frame was cut from a teflon block and platinum wire was inserted through small holes and slits. These small recesses were sealed with sigillum wax to avoid exchange of fluid between wells. Swelling chambers were closed with vacuum grease and two cover glasses as described in the text.
(b) Design with maximum wire surface area.
(c)&(d) Preliminary designs.

Cleaning of the Pt-wire Swelling Chamber

Platinum-wire swelling chambers were thoroughly cleaned to assure consistent surface properties as summarized in table 6.1. In short, manual cleaning with spatula, Kimwipes (Kimberly Clark) and solvents removed most of sigillum wax and vacuum grease. The chamber was subsequently immersed in chloroform, ethanol and ultra-pure water successively in an ultrasonic bath. Electrolysis of $1\,\mathrm{mol\,l^{-1}}$ NaCl eliminated last traces of contaminants prior to use.

Table 6.1: Summary of the cleaning procedure of the Pt-wire swelling chamber.

duration	action	solution/tool
-	manual cleaning	Kimwipe
-	manual cleaning	Kimwipe + 70% ethanol (technical grade)
-	remove sigillum wax	use spatula
-	manual cleaning	Kimwipe + chloroform
5 min	ultrasound treatment	chloroform
5 min	ultrasound treatment	ethanol
-	thorough rinsing	ultra-pure water
5 min	ultrasound treatment	about 1% Hellmanex
-	thorough rinsing	ultra-pure water
5 min	ultrasound treatment	ultra-pure water
-	drying	flow of nitrogen
1 min	electrolysis of $1\,\mathrm{mol\,l^{-1}}$ NaCl	function generator: sine wave, 1 Hz, $7\,\mathrm{V_{rms}}$
-	thorough rinsing	ultra-pure water

Agarose-Lipid-Hybrid Films

Ultra-low gelling agarose (#A2576, Sigma Aldrich) was used to prepare agarose films on glass slides. Agarose films were subsequently coated by lipid layers and GUVs were grown from these hybrid films by addition of water or buffer. Coating was done with a spin-coater (WS-400B 6NPP-Lite, Laurell Technologies).

A 1% (w/v) solution of agarose was prepared. Agarose was weighed and dissolved in the appropriate amount of ultra-pure water in a 50 ml plastic tube (#227261, Greiner Bio-One). The tube was weighed once more, before it was put in a microwave oven (#MW7823, Severin) with an additional plastic tube filled with ultra-pure water. Liquids were heated at 800 W for 10 s. The agarose solution was manually shaken to mix the components and both liquids were heated at 800 W for about 5 s to 15 s until the agarose solution became clear. The Falcon tube with agarose solution was weighed. Evaporated water was replaced by warm water from the additional Falcon tube. The solution can be stored in the dark at room temperature for several weeks.

Melting was achieved by heating with microwaves and evaporated water was replaced as described above.

Glass slides (20x20 mm^2) were cleaned prior to spin-coating in 1% (w/v) Hellmanex, ethanol and ultra-pure water respectively in an ultrasonic bath for 5 min. Glass slides were dried under a stream of nitrogen. 200 µl of agarose solution were spin-coated at 600 rpm (also tested: 300, 900 and 1200 rpm) for 30 s. Agarose was partly dried in an oven at 37 °C for 1 h. 100 µl of liposome emulsion with a lipid concentration of about 5 mg ml^{-1} was spin-coated at 1200 rpm for 5 min. The hybrid film was partly dried as before at 37 °C for 1 h. For some experiments, lipid solutions in chloroform/methanol according to [209] were spin-coated (1200 rpm, 5 min) on top of an agarose film. This agarose film was produced at 1200 rpm for 30 s. To remove even slight traces of organic solvents, the coated glass slides were put in a desiccator for 1.5 h.

The coated glass slide was placed in a self-made petri dish, which is described below. 1.5 ml of buffer were added and the petri dish was covered by a round glass with a diameter of 35 mm. From the start of observation at a microscope, GUVs were observed which grew over periods of several hours.

Since no container with a volume of roughly 1 ml could be found for agarose-lipid-coated glass slides, small petri dishes were assembled by gluing a glass ring (outer diameter 34 mm, height 4 mm) to a round cover glass (diameter 35 mm). The glue (Norland Optical Adhesive, NOA61) was cured with UV light at a wavelength of $\lambda = 365$ nm. A photograph of the petri dish is shown in figure 6.4.

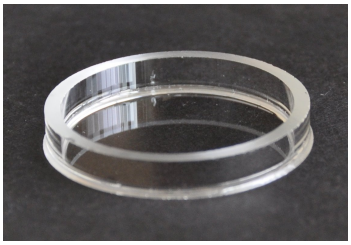

Figure 6.4: Photograph of a self-made petri dish used to grow GUVs from agarose-lipid-hybrid films.

6.3 Protein Incorporation in GUVs

Measuring Binding Capacity of Bio-Beads for Triton X-100

In literature, different maximum amounts of Triton X-100 adsorbed to 1 g of Bio-Beads SM2 (#152-8920, Bio-Rad) are reported: 70 mg g^{-1} [76] and 185 mg g^{-1} [114]. Therefore, an easy experiment was realized to measure binding capacity of the beads. The result was used to decide which value to use in the calculation of the amount of Bio-Beads added for detergent removal.

Bio-Beads were washed prior to use at least once in methanol and thrice in ultra-pure water. Therefore, around 5 g of beads were put in a 50 ml Falcon tube and

approximately 45 ml of solvent were added. The dispersion was shaken manually for about 1 min and was subsequently centrifuged for 1 min at 1000 rpm at room temperature in a Heraeus Multifuge 1S-R (Thermo Scientific). The supernatant was discarded each time and, after all four washing steps, sedimented beads were dispersed in ultra-pure water.

Different amounts m_i of Bio-Beads were added to 1 ml of a 8 mg ml^{-1} solution of Triton X-100. The mixture was stirred for the whole experiment. After certain time intervals, samples of 10 µl were removed from the supernatant. Concentration of Triton X-100 in the sample was deduced from its absorption at 280 nm. Absorption was measured typically three times with a spectrophotometer (Nanodrop, PeqLab). Data was fitted with an exponential decay:

$$f(t) = A \exp\left(\frac{t}{\tau}\right) + c \tag{6.1}$$

with time t, a constant A and the plateau value c. The binding capacity C_B was determined from the ratio of plateau value c to amount m_i of Bio-Beads:

$$C_B = \frac{c}{m_i} \tag{6.2}$$

Solubilization of Vesicles by Triton X-100

The successful insertion of membrane proteins in the bilayer of preformed SUVs relies on the destabilization of the bilayer by detergent. Increasing amounts of detergent first lead to a saturation of the bilayer with detergent molecules. Lipid-detergent micelles form on further addition of detergent until vesicles are completely solubilized. This process is monitored by measuring the turbidity of the sample, which decreases with progressive solubilization.

Samples of a 5 mg ml^{-1} SUV emulsion were treated with various amounts of Triton X-100 solution with a concentration of 0.43 mol l^{-1} in 0.5 ml Eppendorf tubes. Diluted Triton is pipetted more easily than pure Triton due to reduced viscosity, especially when working with small volumes. Samples were incubated for 30 min stirring with small magnetic stirs. Three times 50 µl of each sample were pipetted in a microwell plate. Extinction was measured at 500 nm with a spectrophotometer (Infinite 200M, Tecan).

Protein Reconstitution

The general principle of protein reconstitution is described in section 3.3. In the following description, volumes are adjusted for subsequent density gradient centrifugation, but can be scaled in the range of 100 µl to several milliliter.

600 µl of preformed liposomes with a lipid concentration of 5 mg ml^{-1} were mixed with 5, 13 or 22.5 µl of 0.43 mol l^{-1} Triton X-100. The three different volumes correspond to 3.6, 9.1 and 15.5 mmol l^{-1} of Triton X-100 leading to saturated bilayers,

intermediate and complete solubilization (see figure 3.6). The mixture was allowed to equilibrate for half an hour. Then, 100 µg of solubilized integrin was added. After 1 h of incubation, detergent was removed by addition of 9, 20 or 34 mg of Bio-Beads depending on the volume of Triton X-100 added at the beginning. This amount corresponds to 1 mg Bio-Beads per 185 µg of Triton X-100 [114] plus 1 mg to ensure complete removal. Removal was done at room temperature overnight. The process is sketched in figure 6.5.

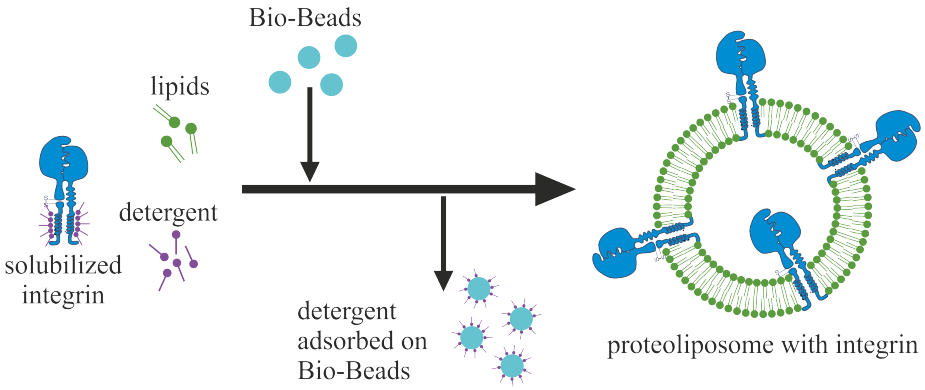

Figure 6.5: First step in preparation: Proteoliposomes are formed from an aqueous solution of lipid vesicles, solubilized integrin and Triton X-100 by detergent adsorption on porous, hydrophobic polystyrene beads called Bio-Beads.

Growing Proteo-GUVs

Electroformation was used to grow GUVs from these proteoliposomes or from purified platelet membranes. Actin was enclosed in the vesicles by adding G-actin to the buffer in which the GUVs were grown in. The ionophore A23187, also called calcimycin, allowed the polymerization of actin inside of the GUVs by addition of $MgCl_2$ to the outer buffer. A23187 transports divalent cations across the membrane. Polymerization in the outside buffer was prevented either by addition of DNase I in equimolar ratio to actin or by dilution with iso-osmolar buffer below the critical polymerization concentration of actin. Below this critical concentration, nucleation of several actin monomers is highly unlikely which prohibits polymerization [7]. DNase I is an enzyme binding to G-actin [100] thereby preventing formation of F-actin. Actin was fluorescently stained using phalloidin Alexa Fluor 647 (#A22287, life technologies). Phalloidin is a toxin from the death cap mushroom specifically binding to actin and thereby stabilizing F-actin. The schematic in figure 6.6 illustrates the second step in producing integrin-GUVs containing actin.

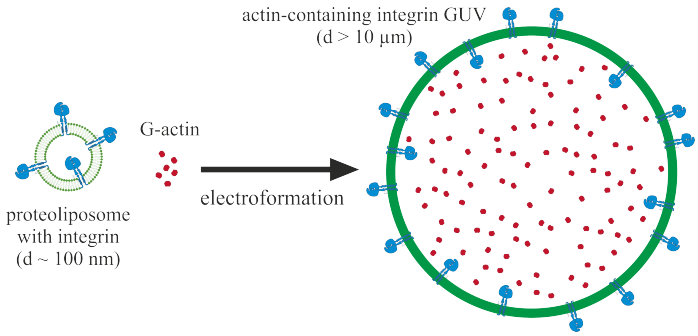

Figure 6.6: Second step in preparation: GUVs were grown from proteoliposomes with the help of electroformation as described in section 6.2.

7 Characterization of Vesicles

7.1 Size Measurement with Dynamic Light Scattering

Dynamic light scattering was performed employing a Malvern Zetasizer Nano ZS. A helium-neon laser with $\lambda = 633\,\text{nm}$ is used for illumination. An attenuator allows to control illumination intensity to avoid overload of the detector. Scattered light is detected under $\theta = 173°$ by an APD. This so-called backscatter detection reduces effects of multiple scattering as well as influence of light scattered by large particles. Large particles mainly scatter in forward direction. The intensity autocorrelation function is obtained from the signal by a correlator, a digital signal processing board. Data was analyzed on a computer with the Zetasizer software. The setup is shown in figure 7.1.

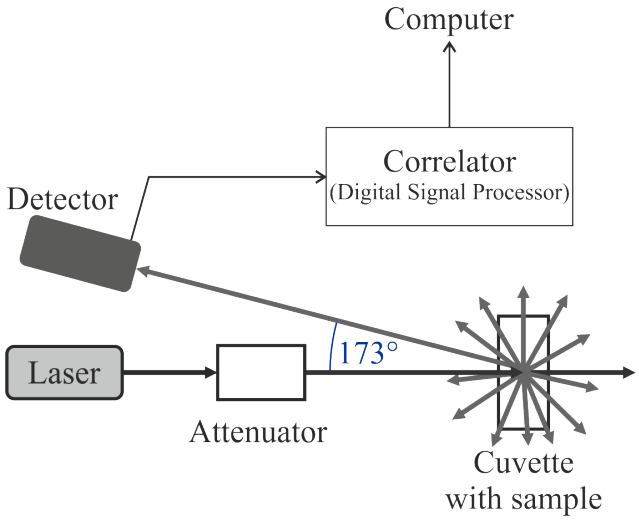

Figure 7.1: Setup for DLS of the Malvern Zetasizer Nano ZS. Adapted from the Zetasizer Manual.

The intensity size distribution is generated from the measured intensity autocorrelation function, but the software allows the conversion to volume and number distribution. For monodisperse samples, the mean size does not change much for the different distributions. However, the intensity size distribution of a mixture of small and large particles is dominated by the larger particles, as scattering in the Rayleigh regime increase with the sixth power of particle diameter. Therefore, the comparison of intensity and number size distribution sometimes results in a better characterization of polydisperse samples.

Depending on the concentration, between 20 and 50 µl of liposome suspension were diluted to approximately 1.5 ml with ultra-pure water in 12 mm square polystyrene cuvettes (Malvern, #DTS0012). Each sample was allowed to equilibrate for 2 min before starting a measurement.

7.2 Density Gradient Centrifugation of Liposomes and Proteoliposomes

Density gradients were prepared as step gradients in 4 ml centrifugation tubes (Beckman, Ultra-Clear, 11x60 mm, #344062). Each step was deposited at the bottom of the tube starting with the least dense solution using a syringe (B. Braun, Injekt-F, Tuberculin, #9166017V) with a long, thin cannula (B. Braun, Sterican, 0, 6x80 mm, #4665635) as shown in figure 7.2a. A gradient consisted of buffer - most often integrin buffer without Triton X-100 - as well as 5% (w/v) and 10% (w/v) of Nycodenz (Axis Shield, #1002424) in the same buffer 1 ml each. At last, the sample was mixed with 40% (w/v) Nycodenz at equal volume to yield a 20% solution. This solution was put at the very bottom of the tube. Figure 7.2b shows a density gradient with a liposome sample. Centrifugation was performed in an ultracentrifuge (Beckman Coulter, Optima L-80 XP) with a Beckman SW60 Ti rotor at 4 °C and 44000 rpm for 2 h. If the concentration of liposomes was high enough, different bands were observed in the tube after centrifugation (see figure 7.2c). Pictures of all tubes were taken with a Nikon D5000 digital camera for documentation. Each position of a sample was marked on the tube with the samples number. Samples were carefully removed from the gradient with a pipette equipped with a long tip - for example one as shown in figure 4.3a - beginning from the top. Analysis was performed with SDS-PAGE as described in section 4.2.2. Before application on the gel, samples were mixed 1:1 (v/v) with 2x Lämmli buffer.

7.3 Light Microscopy to Study Giant Unilamellar Vesicles

7.3.1 Phase Contrast, differential interference contrast (DIC), Fluorescence and Confocal Microscopy

Analysis of giant vesicles was always performed using an inverted microscope looking from below on vesicles, that sedimented to the surface of the glass substrate. Phase contrast images were acquired with various microscopes (Zeiss Axiovert 40CFL, AxioVert 200M and AxioImager) using 10x/0.25 NA, 10x/0.3 NA, 20x/0.4 NA LD or 40x/0.6 NA objectives. LD denotes long distance, meaning objectives with extended

Figure 7.2: Density gradients centrifugation tubes.
(a) Preparation of a step gradient: Starting with the least dense solution subsequent (denser) layers are deposited at the bottom of the tube through a long needle.
(b) Prepared gradient with a liposome sample at the bottom ready for centrifugation.
(c) Liposome sample in a density gradient after centrifugation: different bands are clearly visible.

working distance. Zeiss software AxioVision was used for image acquisition from the camera AxioCam MRm. Fluorescence microscopy was done with an inverted Zeiss AxioVert 200M microscope equipped with appropriate filter cubes and a mercury vapor arc lamp (X-Cite 120).

For confocal microscopy, an inverted Zeiss AxioObserver microscope connected to an UltraView Spinning Disc system (Perkin Elmer) was used. Confocal laser scanning was performed utilizing a Leica TCS SP5 with an inverted DMI6000 stage and white light source. The pinhole was set to one Airy unit. DIC microscopy was also done with this system without using the confocal scan head, but the Leica CCD camera instead.

Typically, images were contrast enhanced without cutting any data. Other treatments of an image are described in the figure's caption accordingly.

Preparation of Observation Chambers

Versatile, customizable chambers were assembled by two glass slides separated by Parafilm (Bemis Company) for the observation of samples in optical microscopes. Parafilm was folded to end up with several layers of Parafilm on top of each other. The number of layers determines the thickness of the chamber and thereby its volume. One layer roughly corresponds to 120 µm in the end as averaged from measured thicknesses of different numbers of layers with a vernier caliper. Typically, six layers were used. The folded Parafilm can be cut to any shape with scissors or a scalpel.

(a) **(b)**

Figure 7.3: Preparation of an observation chamber for microscopy.
(a) Observation chamber lying on a hot plate protected by aluminum foil.
(b) Several layers of u-shaped Parafilm are put with tweezers on top of a glass slide lying on a hot plate.

Most often, an u-shaped spacer was employed as depicted in figure 7.3b. The hot plate was covered with aluminum foil for its protection and heated to 130 °C. One glass slide (typically: Carl Roth, 24x50 mm, thickness #1, 1871) was put on top of the hot plate followed by the Parafilm layers and a second glass slide (typically: Carl Roth, 20x20 mm, thickness #1, H873). The slides were joined together by the melting Parafilm gently pressing on the top glass with the tweezers. The chamber can be sealed with mineral oil or vacuum grease that is not soluble in water.

7.3.2 Reflection Interference Contrast Microscopy

High resolution shape analysis of giant vesicles was performed by reflection interference contrast microscopy to study the process of adhesion of integrin-coated GUVs to bio-functionalized substrates. RICM was carried out with an inverted Zeiss AxioImager microscope using a 63x/1.25 NA oil immersion Antiflex-objective. A filter cube with two polarizers, oriented perpendicular to each other, and beamsplitter was inserted in the beam path. Two motorized iris diaphragms allowed to achieve Köhler illumination in reflected light mode. The sample was illuminated with a mercury vapor arc lamp (Zeiss HBO100) filtered with a bandpass filter transmitting at $\lambda = 546\,\text{nm}$. The quarter wave plate in front of the objective was adjusted for maximal intensity of reflected light. The optical axis of the quarter wave plate is then oriented at 45° with respect to polarizer and analyzer. The aperture diaphragm was adjusted to the smallest opening possible , which leads to the best contrast in RICM by a small numerical aperture of illumination. The field diaphragm opened, that its shadow just vanished from the field of view. For each sample, at least one phase

contrast image was also acquired. Semi-automatic and quantitative image processing was done as described in section 7.3.1.

Preparation of Homogeneously-Coated Substrates for RICM

To study adhesion of giant vesicles with incorporated integrin to functionalized substrates, glass slides were homogeneously coated with casein or fibrinogen. The glass was cleaned in ethanol and 1% (w/v) Hellmanex using an ultrasonic bath for 5 min respectively. After each step, glass slides were thoroughly rinsed with ultra-pure water. Immersion in Piranha solution for 10 min, produced by mixing one part hydrogen peroxide (30%) with two parts sulfuric acid (98%), removed organic material and rendered the glass surface hydrophilic. Glass slides were stored until further use in ultra-pure water. Prior to each experiment, glass slides were dried under a flow of nitrogen and treated in oxygen plasma for 5 min at 0.4 bar and 150 W (plasma system 100, PVA TePla). This procedure ascertains reproducible surface properties of the glass. The positively charge amino acid poly-L-lysine (PLL) was physisorbed on the slide by incubation of 100 µl PLL solution (#P8920, Sigma Aldrich) covered with Parafilm for 10 min. The covering with Parafilm prevents evaporation and ensures complete wetting of the surface. The proteins casein and fibrinogen were dissolved in 10 mmol l^{-1} HEPES with pH 7.4 at 1 mg ml^{-1}. Fibrinogen is a natural ligand for integrin and casein is known to minimize adhesion of integrin-coated GUVs [198]. Solutions of casein or fibrinogen were incubated for 1 h by coverage of 100 µl of solution with Parafilm. Surfaces were rinsed thoroughly with HEPES buffer and stored in the same solution. Observation chambers were assembled with coated glass slides as described above after drying under a flow of nitrogen.

Preparation of Nano-Structured and Bio-Functionalized Substrates to Control Ligand Density

More sophisticated substrates were prepared on glass by block copolymer micelle nanolithography [195], which enables to tune the average distance of nanometer-sized gold dots with nanometer precision [112]. Gold dots were specifically bio-functionalized with the small peptide RGD by using thiol-ene chemistry. RGD specifically binds to integrin $\alpha_{\mathrm{IIb}}\beta_3$ [145]. Thereby it was possible to control the density of ligands in the range of approximately 3000 down to 30 ligands per µm^2. Substrates with average interparticle distances between gold dots of 38 ± 8 nm and 93 ± 22 nm were employed corresponding to ligand densities of about 800 ("high") and 100 ("low") ligands per µm^2. The glass surface between gold dots was passivated by binding of PEG, which minimizes adhesion of cells [23].

Reconstruction of Vesicle Shape from RICM Images

A typical example of a GUV hovering above the substrate surface is depicted in figure 7.4, as imaged in phase contrast and RICM. In short, the general scheme for reconstruction of the giant vesicle's height profile is the following: First, the intensity of light reflected at three interfaces is calculated in dependence of the distance be-

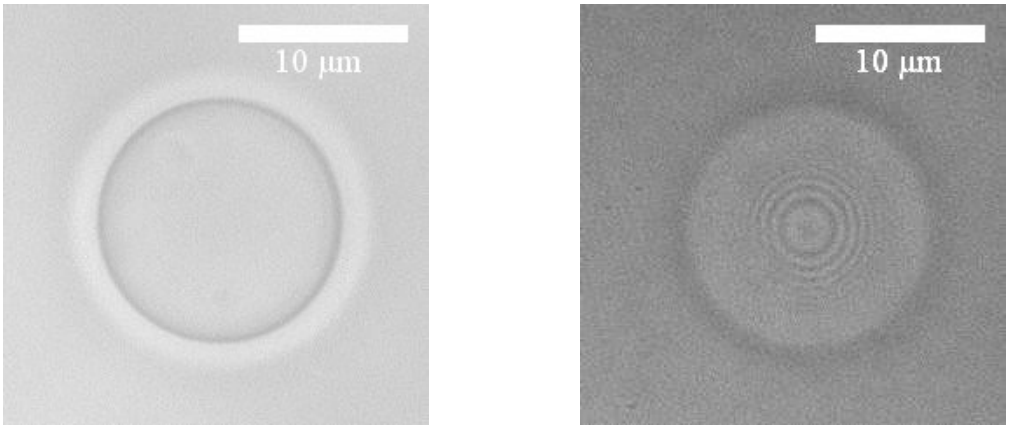

Figure 7.4: Example of a GUV imaged with phase contrast (a) and RICM (b). The bright region around the GUV is a result of phase contrast, called "halo-effect". For a spherical object, the interference pattern acquired with RICM exhibits alternating bright and dark rings leading to a periodic intensity distribution in radial direction.

tween the first (glass substrate/outer buffer) and second interface (outer buffer/lipid bilayer). An analytical expression is then fitted to this data to obtain parameters, which are subsequently used to calculate the height corresponding to the intensity measured with RICM.

The theoretically reflected intensity was calculated with subtraction of the background intensity $I_{\text{refl}}^{\text{bg}}$, stemming from the reflection at the glass/buffer interface, and normalizing to the intensity of the background:

$$\tilde{I}_{\text{refl}}^{\text{theo}} = \frac{I_{\text{refl}}^{\text{theo}} - I_{\text{refl}}^{\text{bg}}}{I_{\text{refl}}^{\text{bg}}} = \frac{R^2 - r_{01}^2}{r_{01}^2}, \tag{7.1}$$

where r_{01} is the reflection coefficient of the glass/buffer interface and R the effective reflexion coefficient, defined in equation (4.10). The theoretically calculated intensity of reflected light is plotted in figure 7.5 up to a substrate-membrane distance of 500 nm. The periodic function

$$\tilde{I}_{\text{refl}}^{\text{theo}}(h) = y_0 - A\ \cos\left(4\pi \frac{n_{\text{out}}}{\lambda}\ (h - h_0)\right) \tag{7.2}$$

was fitted to this data to obtain the parameters y_0, A and h_0, as this function describes the intensity along lines perpendicular to the interference pattern [107]. An analytical expression for h_0 is given in equation (4.13) and A can be calculated according to

$$A = 2\ \frac{r_{12}}{r_{01}}\ \left(r_{01}^2 - 1\right) \sqrt{1 + \gamma^2 + 2\ \gamma\ \cos L_m}$$

with reflection coefficients r_{ij} and $\gamma = \frac{r_{23}}{r_{12}}\ (1 - r_{12}^2)$. The phase shift of light with

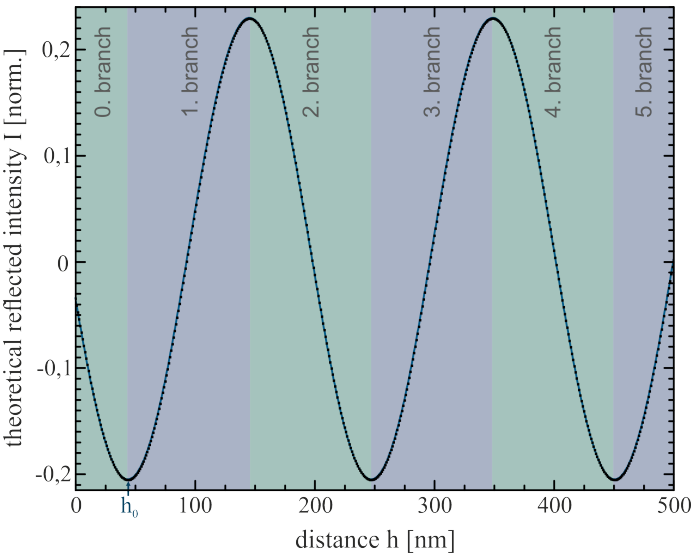

Figure 7.5: Reflected intensity in dependence of the distance h between substrate and membrane as calculated using equation (7.1). The first minimum of intensity occurs at a distance h_0. Data is in excellent agreement with the fit according to equation (7.2) illustrated in dark blue.

wavelength λ passing twice the membrane with thickness d_m and refractive index n_m is given by

$$L_m = 4\pi \; n_m d_m \; / \; \lambda.$$

The parameter h_0 describes the distance of substrate and membrane, that results in a minimum of reflected light intensity. The fitted curve is depicted in blue in figure 7.5 showing an excellent agreement with data.

Images were analyzed semi-automatically with Matlab 2011a (MathWorks) utilizing self-written code (appendix C). Parts of the routines are based on work of Tobias Hofmann done in his master thesis [75]. Each image was cropped to a rectangular region of interest around the observed giant vesicle to reduce the amount of data. In order to correct data for inhomogeneous illumination, an image of the background was subtracted from the raw data image. Therefore, illumination had to be interpolated in the area covered by the giant vesicle. The vesicle was masked and pixels inside of the mask were set to NaN ("Not a Number"). The background was theoretically calculated by the Matlab-implemented function "inpaint_nans" [38]. This function solves a partial differential equation in areas of pixels with NaN values by using the intensity of pixels surrounding these areas as a boundary condition. For instance, one model for this calculation uses the linear heat equation: pixel intensity "diffuses into" the masked area from the boundaries. Other models are described in the instruction for this Matlab function. After background correction, pixel intensities of the resulting image were normalized to the corresponding pixels of the background. Six lines were drawn interactively for each GUV perpendicular to the interference patterns (figure 7.6).

Intensity profiles along these lines (figure 7.6b) were evaluated using equation (7.2) and taking the periodicity of the cosine into account. Thus, the shape of giant vesicles was reconstructed in the different branches $j \in \mathbb{N}$ with intervals

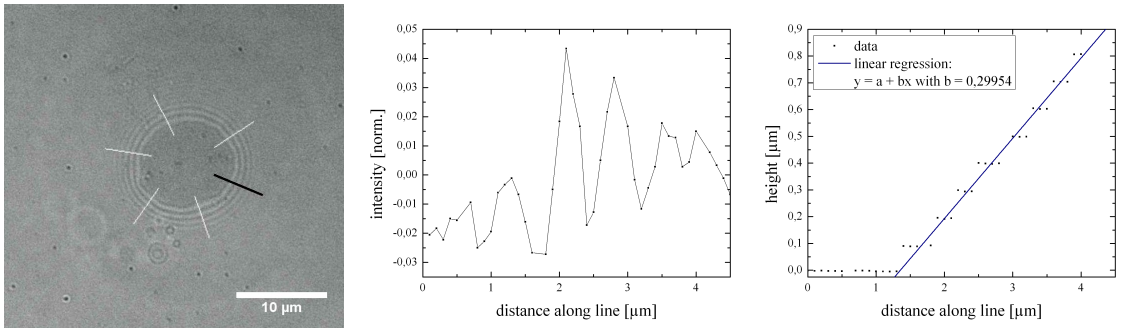

Figure 7.6: Image from RICM with six lines perpendicular to the interference pattern (a), intensity profile along one of these lines (b) which was used to calculate the height profile (c).

$\left[h_0 + \frac{j\lambda}{4n_{\text{out}}}, h_0 + \frac{(j+1)\lambda}{4n_{\text{out}}}\right]$ by

$$h = h_0 + (j-1)\ \frac{\lambda}{4\ n_{\text{out}}} \pm \frac{\lambda}{4\pi\ n_{\text{out}}}\ \arccos\left(\frac{y_0 - \tilde{I}_{\text{refl}}}{A}\right). \tag{7.3}$$

$\tilde{I}_{\text{refl}}$ represents the measured, background-corrected and normalized intensity. The plus sign was used for uneven branches j, the minus sign for even branches. As illustrated by the graph in figure 7.5, the second summand in equation (7.3) had to be set to 0 in the 0th branch and the term with the arc cosine was subtracted from h_0. A typical height profile is illustrated in figure 7.6c as calculated from the intensity profile depicted in figure 7.6b. Refractive indexes of inner and outer buffer (listed in appendix F.4) were measured with a refractometer (DR201-95, Krüss Optronic) and are summarized in table 7.1.

Table 7.1: Measured refractive indexes of inner and outer buffer, n_{in} and n_{out} respectively. Indexes of refraction of glass n_0 and lipid membrane n_m are reported in literature [108,159].

n_{in}	n_{out}	n_0	n_m
1.3447	1.3423	1.525	1.486

Bending of the lipid bilayer becomes negligible farther away from the area of contact than the so-called capillary length, which is of the order of 1 µm [173]. The height profile of the GUV can then be approximated by a line. The slope of this line gives the macroscopic contact angle of the vesicle. An effective adhesion energy can be estimated with this contact angle using

$$W = \sigma\ (1 - \cos\vartheta) \tag{7.4}$$

with the membrane tension σ. Each of the six height profiles was plotted with Origin 8.6 (OriginLab Corp.). Linear regression was used in the linearly increasing part of the height profile to measure the slope of the bilayer of the GUV. The arc tangent of the slope gave the contact angle in degrees, which was employed to estimate the effective adhesion energy according to equation (7.4). A membrane tension of $\sigma = 1 \times 10^{-6}\,\mathrm{N\,m^{-1}}$ was used for this estimation [130].

8 Biochemistry

8.1 Protein and Platelet Membrane Purification

Protein Purification

Integrin $\alpha_{\mathrm{IIb}}\beta_3$ was purified from outdated human platelet concentrate which was obtained from donor blood (kindly provided by Katharinenhospital Stuttgart). Platelet concentrate can only be used for transfusion within five days after blood donation. First, contaminating other (larger) cells like red and white blood cells were removed by centrifugation. Platelets were pelleted and serum was replaced by washing buffer. Platelets were washed three times. Therefore, each time platelets were pelleted by centrifugation, supernatant was discarded, washing buffer was added and the emulsion was mixed with a pipette. Platelets were subsequently broken by shear forces with a homogenizer. Membranes were pelleted by centrifugation and the supernatant containing platelet cytosol and organelles was discarded. Membrane proteins were solubilized by addition of Triton X-100. To prevent degradation of proteins by proteinases, a mixture of proteinase inhibitors was added. After centrifugation, the supernatant was applied to a ConA column (GE Healthcare) binding glycoproteins. Bound proteins were eluted with the sugar mannose. Coagulation proteins were afterwards bound by a heparin affinity column (GE Healthcare). The flow-through was fractionated by gel filtration on a Superdex 200 column (GE Healthcare). All columns were used in combination with the chromatography systems ÄKTA purifier (figure 8.1) and ÄKTA prime plus (both GE Healthcare). A detailed protocol for the purification of integrin $\alpha_{\mathrm{IIb}}\beta_3$ is given in appendix G.1. This procedure allows the purification of about 5 mg of integrin $\alpha_{\mathrm{IIb}}\beta_3$ from approximately 2.5 l platelet concentrate. The protein was stable for at least six month if it was stored at 80 °C.

Actin was purified from rabbit muscle according to [138].

Purification of Platelet Membranes

Platelet membranes were purified following an adapted version of a protocol previously described [194]. Larger contaminating cells were removed by centrifugation before platelets were pelleted. Serum was changed for buffer and platelets were washed two times. The sample was placed in the pressure chamber of a cell disruption bomb (Parr Instrument) after adding a mixture of protease inhibitors. A pressure of about 83 bar was applied by connecting a high-pressure nitrogen bottle. Contents were discharged into a glass beaker. Membranes were sedimented by centrifugation and

Figure 8.1: Photograph of the ÄKTA purifier system equipped with a heparin column. The setup contains a pump to apply sample and buffer to the column and various analytical instruments like spectrophotometer to monitor absorption or pH-meter to measure the pH.

Table 8.1: Summary of integrin purifications from platelet concentrate performed in this study.

date	January 2009	March 2009	August 2009	March 2010
label	A	B	C	D
date	August 2010	March 2011	May 2011	May 2011
label	E	F	G	H
date	August 2011	August 2011	February 2012	
label	I	J	K	

resuspended in buffer. A solution of 21,5% (w/v) Nycodenz, a gradient medium, was layered below the sample in a centrifugation tube. After centrifugation, membranes were harvested from the interface between buffer and Nycodenz. Membranes were resuspended in buffer and centrifuged once more to remove remaining Nycodenz. The pellet was weighed and suspended buffer to yield a concentration of roughly $30\,\mathrm{mg\,ml^{-1}}$. The detailed protocol is given in appendix G.4.

Platelet membranes can also be purified by stopping integrin purification with the centrifugation after homogenizing the platelets. Membranes are further purified as described above by a Nycodenz cushion and another centrifugation to remove Nycodenz.

8.2 Measuring the Concentration of Purified Integrin

The overall concentration of protein in the different fractions was determined after purification of integrin $\alpha_{\mathrm{IIb}}\beta_3$ from human platelet membranes. Determination was done on the one hand with the BCA assay and on the other hand by measuring the extinction at 280 nm with a spectrophotometer (Infinite 200, Tecan). The BCA test was performed as described by the manufacturer. For spectrophotometry, Triton X-100 had to be replaced by its reduced form having a cyclohexane ring instead of a benzene ring. This reduced form has a substantially decreased absorption in the UV spectrum without significantly changed solubilizing properties [208]. An extinction coefficient of $1.18\,\mathrm{ml\,mg^{-1}\,cm}$ [158] was used for the calculation of the concentration. The exact concentration of integrin was deduced from each fraction's purity. Purity was obtained with SDS-PAGE as the ratio of added intensity of both integrin bands compared to overall intensity per lane. Since concentration might change during freezing, for example, due to adsorption of protein to tube walls, it was measured once more spectrophotometrically after thawing.

8.3 SDS-Polyacrylamide Gel Electrophoresis

Bio-Rad's Mini-Protean 3 system (Bio-Rad, Electrophoresis System, #165-3301) was employed for SDS-PAGE using the Lämmli buffer system. Ready-to-use mixtures of acrylamide and bisacrylamide were used (#3029.2, Carl Roth). Gels with different polymer concentrations were prepared according to the supplier's manual. Gels were run at 110 V and stopped after about 85 min, when the dye front reached the gel's bottom. As a rule of thumb 0.5 µg to 5 µg of protein were applied per well depending on whether purified protein or a mixture of proteins is used. This amount ensures visible and clear staining with Coomassie (Bio-Rad, Bio-Safe Coomassie Stain, 161-0786), even though amounts as low as 8 ng per band can be detected with this dye. On the other hand, the lanes are not overloaded. Too much protein leads for

example to smeared protein bands. Digital images of stained gels were taken with the luminescent image analyzer LAS-3000 (Fujifilm). If not stated otherwise, 10% polyacrylamide gels usually were utilized.

Images of gels were evaluated employing built-in plugins of Fiji, an image processing package based on ImageJ. Each lane was specified by a rectangular region of interest. The intensity profile was plotted along the running direction of samples. The area under peaks of proteins was then utilized as a measure of protein amount. The position of a protein in the gel was determined from the position of the maximum of its peak in the intensity profile.

8.4 Specific Detection of Integrin

After separating the integrin samples with SDS-PAGE as described in 8.3, proteins were transferred to the membrane. Transfer was performed at 100 V for 60 min (Mini-Protean 3 system, Bio-Rad, Cell and Mini Trans-Blot module, #165-3317). The blotting sandwich was arranged as shown in figure 8.2. For this order of layers, the correct orientation in the blotting tank is depicted in figure 8.3a. Afterwards, the membrane was stained for 5 min with the dye Ponceau S to check transfer of protein. Excess dye was removed by washing with ultra-pure water and a photograph was taken for documentation.

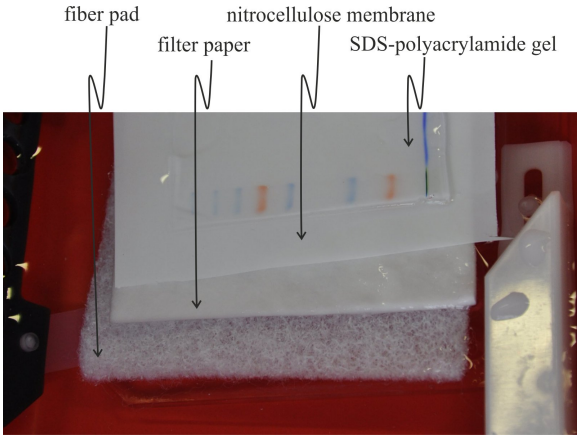

Figure 8.2: Assembly of the transfer sandwich for Western blotting: Before the plastic cassette is closed an additional filter paper is put on top of the gel followed by one more fiber pad. Filter paper and fiber pad on both sides of membrane and gel ensure their complete contact when the cassette is closed for the transfer. Air bubbles or a separation could impair the proteins' transfer from the gel to the membrane.

Blocking was done with 5% (w/v) BSA in TBS-T buffer (table F.11). The membrane was incubated with BSA solution for approximately 2 h at room temperature, followed by three washes with TBS-T for 10 min each. Then, the primary antibody was applied to the membrane at 4 °C overnight. Incubation with antibody was always executed with the membrane sealed in plastic film as shown in figure 8.3b.

The following antibodies were diluted as specified in 5% (w/v) BSA in TBS-T:

1. anti-integrin α_{IIb} (human), abcam, ab63323, mouse, monoclonal, 1:200 (v/v);

Figure 8.3: (a) Transfer sandwich in the tank for blotting. For an assembly as shown in figure 8.2 with the membrane closer to the transparent side of the plastic cassette than the gel, the transparent side has to face to the anode. With this arrangement negatively charged proteins are transferred to the membrane.
(b) Application of the antibody solution to the membrane. In order to reduce the amount of antibody solution needed for incubation, the membrane is sealed in plastic film.

2. anti-integrin β_3 (human), Chemicon, CBL479, mouse, monoclonal, 1:100 (v/v).
3. anti-fibrinogen (human), Sigma Aldrich, F4639, mouse, monoclonal, 1:1000 (v/v).

The membrane was washed once more three times with TBS-T for 5 min each. The secondary antibody (anti-mouse, APconjugate, life technologies, G21060) was applied at room temperature for 1 h sealed in plastic film. Before staining of the membrane by addition of the substrate BCIP/NBT (Sigma-Aldrich, B1911), unbound antibody was removed by washing three times for 5 min with TBS-T. A photograph was taken for documentation as shown for example in figure 9.2.

Table 8.2: Summarized protocol for Western blotting of integrin α_{IIb} or integrin β_3 with antibodies specified above.

action	conditions	solution/buffer
SDS-PAGE	see section 8.3	-
transfer	100 V, 60 min	-
Ponceau S staining	5 min, room temperature (r.t.)	Ponceau S solution
destain background	about 3 min, r.t.	ultra-pure water
photograph	-	-
blocking	2 h, r.t.	5% (w/v) BSA in TBS-T
3x washing	10 min, r.t.	TBS-T
primary antibody	overnight, 4 °C	antibody in 5% (w/v) BSA in TBS-T
3x washing	5 min, r.t.	TBS-T
secondary antibody	1 h, r.t.	antibody in 5% (w/v) BSA in TBS-T
3x washing	5 min, r.t.	TBS-T
staining	about 3 min, r.t.	BCIP/NBT
photograph	-	-

8.5 Co-Immunoprecipitation of Integrin

In order to check whether integrin α_{IIb} was bound to integrin β_3 and vice versa, co-immunoprecipitation was performed. 10 µl of antibody was added to 500 µl integrin sample in a 1.5 ml Eppendorf tube. Anti-integrin α_{IIb} (human, mouse monoclonal, Sigma-Aldrich, #I9660) or anti-integrin β_3 (human, rabbit monoclonal, abcam, #ab119992) were used. The sample was incubated for 2 h at 4 °C under rotation with a MACSmix tube rotator (Miltenyi Biotec, #130-090-753). 100 µl of

Dynabeads Protein G (life technologies, #10003D) were added and carefully mixed with a pipette. Incubation was done overnight at 4 °C while rotating. Three washes with 500 µl of integrin buffer (table F.4) ensured removal of free integrin and antibody. Washing was performed as follows: after addition of buffer, the sample was carefully mixed with a pipette. Beads were then accumulated with a strong magnet (supermagnete.de, #K-19-C) and the supernatant was removed. Integrin and antibody were separated from Protein G and each other by addition of 35 µl integrin buffer and 35 µl 2x Lämmli sample buffer (table F.9). Subsequently the whole mixture was heated to 95 °C for 5 min. 30 µl per well were applied to a 10% polyacrylamide gel for separation at 110 V for about 80 min. The sample was further analyzed by Western blotting as described in 8.4 to verify the co-precipitation of integrin α_{IIb} or β_3 respectively. The procedure is summarized in table 8.3.

Table 8.3: Summarized protocol for co-IP of integrin α_{IIb} or integrin β_3 with antibodies specified above.

action	conditions	remarks
add 10 µg antibody	-	to 500 ul sample
or 1:50 dilution		in 1.5 ml eppi
incubation	1 h, 4 °C	rotate with MACSmix
add 100 µl Dynabeads	-	mix with pipette
incubation	overnight, 4 °C	rotate with MACSmix
3x washing	r.t.	500 ul integrin buffer
		mix with pipette
		accumulate beads with magnet
remove supernatant	-	-
add 35 µl integrin buffer	r.t.	-
add 35 µl 2x Lämmli	r.t.	mix with pipette
heating	5 min, 60 °C	-
Western blotting	see table 8.2	use supernatant
vs. α_{IIb} and β_3		divide in two 30 ul samples

Part III

Results and Discussion

9 Characterization of Purified Platelet Integrin

In this and the following two chapters, key findings obtained in this work are presented. At the end of each section, results are discussed.

9.1 Identification of Proteins Purified from Platelet Membranes

9.1.1 SDS-PAGE

Integrin $\alpha_{\mathrm{IIb}}\beta_3$ was purified from donated and outdated human platelet membranes as described in section 8.1. Performed purification procedures are summarized in table 8.1. A representative Coomassie-stained gel is depicted in figure 9.1 with samples of four fractions after gel filtration. Each lane shows a variety of protein bands.

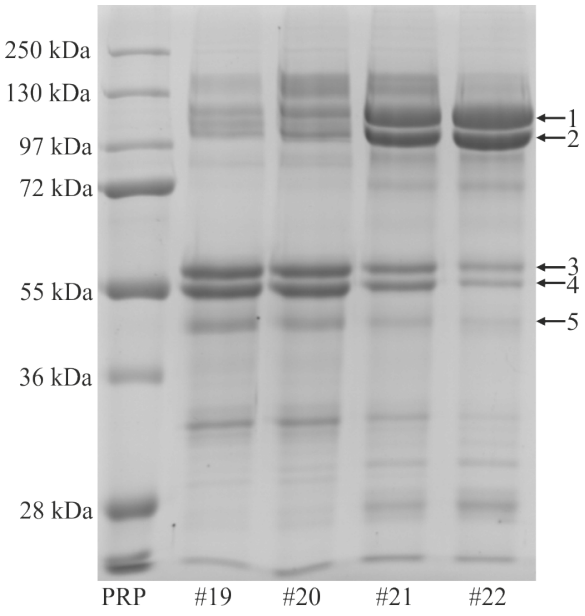

Figure 9.1: Exemplary image of a Coomassie-stained SDS polyacrylamide gel. Protein bands are marked by numbers for later reference. The four lanes to the right show different fractions of a gel filtration with a Superdex 200 10/300 GL column of integrin purification D. The molecular weight marker (PRP) was applied in the first lane from the left.

The molecular weight of proteins was calculated from the calibration curve deduced from molecular weight marker proteins. Results for the protein bands marked

in figure 9.1 are summarized in table 9.1. Determination of protein position, as described in section 8.3, is very precise and does not lead to significant errors. However, calibration with the molecular weight marker does not always result in a linear relationship of gel position with the logarithm of the molecular weight. Accuracy of determination of molecular weight is therefore estimated to ±3 kDa.

Table 9.1: Molecular weight of selected proteins found in integrin samples fractionated by gel filtration. Accuracy is estimated to be ±3 kDa.

band #:	1	2	3	4	5
molecular weight / kDa:	126	107	63	52	43

Molecular weight of protein bands 1 and 2, 126 kDa and 107 kDa, agrees very well with values for integrin α_{IIb} and integrin β_3 reported in literature. Integrin α_{IIb} and integrin β_3 migrate in SDS-PAGE under reducing conditions with a molecular weight of 125 kDa and 108 kDa respectively [54]. Other reported contaminants of integrin purification from platelets, found in SDS-polyacrylamide gels, are fragments of fibrinogen at about 60 kDa, actin at 42 kDa and a subunit of talin at 37 kDa [54,157]. These weights suggest bands 3 and 4 with 63 kDa and 52 kDa to be subunits of fibrinogen and band 5 with 43 kDa to be actin. The calculation of the approximate molecular weight of the γ-chain of fibrinogen from its 411 amino acids [128], results in a weight of around 53 kDa by assuming an average weight of 130 Da per amino acid. Both proteins, actin and γ-chain of fibrinogen, are known to interact directly or indirectly with integrin $\alpha_{\mathrm{IIb}}\beta_3$ [19, 219].

9.1.2 Western Blot

Western blots were performed to unambiguously identify the proteins in the fractions after gel filtration. Figure 9.2 depicts the results of the optimized Western blots against integrins α_{IIb} and β_3. Reversible staining of the membrane with Ponceau S (see left images in figures 9.2a and 9.2b) shows all proteins on the membrane. Given a complete transfer of proteins from the SDS-polyacrylamide gel, Ponceau S-stained membranes display the same protein bands as Coomassie-stained gels. There is a shift of band 1 from below 130 kDa under reducing conditions to above 130 kDa, when not reduced. On the other hand, band 2 shifts from above 100 kDa under reducing conditions to below 100 kDa under non-reducing conditions. After Western blotting, band 1 is specifically stained with an antibody directed against integrin α_{IIb}, while an integrin β_3 antibody binds to band 2, as can be seen in images on the right-hand side of figures 9.2a and 9.2b.

In the negative control (figure 9.3), the primary antibody was omitted, but otherwise the same procedure was followed as above. Protein bands visible with Ponceau

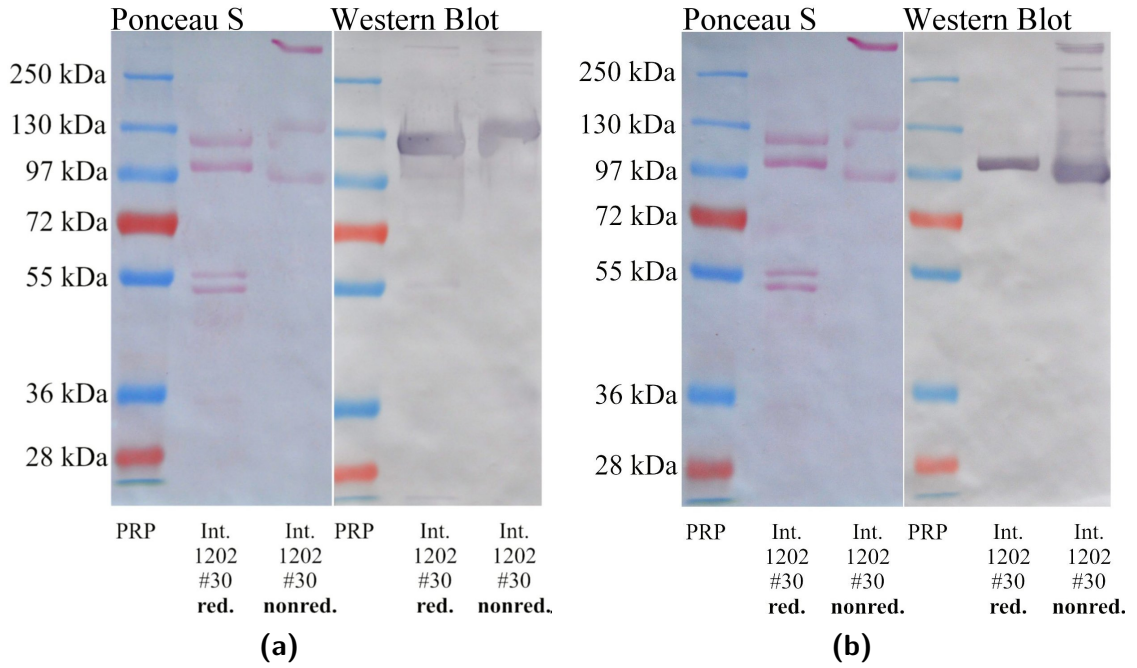

Figure 9.2: Images of membranes stained with Ponceau S and after Western blot against integrin α_{IIb} showing a signal at approximately 130 kDa (a) and integrin β_3 at about 100 kDa (b). In the middle the sample was reduced by β-mercaptoethanol, while on the right the sample was not reduced. The molecular weight marker PRP was applied in the first lane from the left.

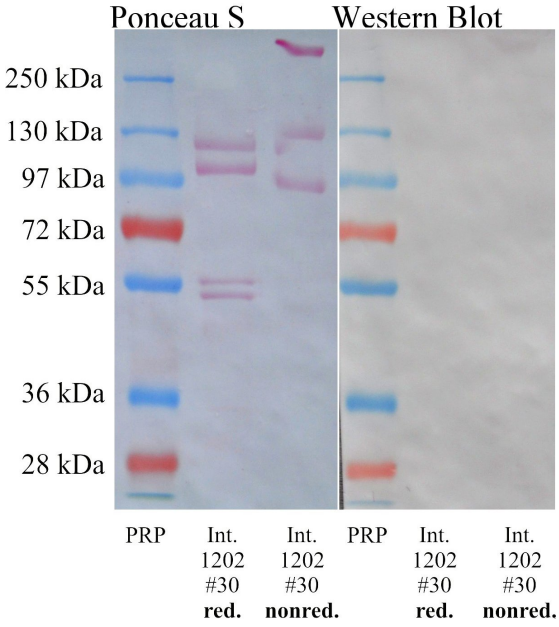

Figure 9.3: Negative control: Ponceau S stained membrane and Western blot negative control without usage of a primary antibody. The secondary antibody does not bind non-specifically to the nitrocellulose membrane. In the middle the sample was reduced by β-mercaptoethanol, while on the right the sample was not reduced. The molecular weight marker PRP was applied in the first lane from the left.

S staining (figure 9.3, left) are not stained after the Western blot, as illustrated in figure 9.3 on the right.

Western blot with an anti-fibrinogen antibody led to the staining of band 4, as shown in figure 9.4 for three different fractions of an integrin purification. A solution of fibrinogen was applied in lane 2 of the gel as positive control.

The shift of bands 1 and 2 under non-reducing conditions is an indication for these proteins to be integrin α_{IIb} and integrin β_3. Reported molecular weights of integrins α_{IIb} and β_3 are 136 kDa and 97 kDa respectively, when not reduced [54]. Both Western blots in figure 9.2 confirm these indications. The negative control without primary antibody does not show any stained protein bands, ruling out non-specific interactions of the secondary antibody. The membrane is stained where the secondary antibody coupled to alkaline phosphatase is bound. Therefore, band 1 is identified as integrin α_{IIb} and band 2 as integrin β_3. One contaminant, band 4, is a subunit of fibrinogen as demonstrated by the specific staining in the Western blot against fibrinogen (fg) in figure 9.4. According to the manufacturer, the anti-fibrinogen antibody binds to the γ-chain of fibrinogen, which is in agreement with the molecular weight determined above in 9.1.1 for band 4. Integrin $\alpha_{\mathrm{IIb}}\beta_3$ also binds directly to the fibrinogen γ-chain [128]. The protein visible at around 25 kDa in the gel shown in figure 9.6 almost certainly is the light chain of integrin α_{IIb}. Light and heavy chain of integrin α_{IIb} are linked via a disulphide bond [29], which is cleaved under reducing conditions of SDS-PAGE [170]. Thus, integrins α_{IIb} and β_3 are purified from human platelet membranes with contamination below 15% by the fibrinogen-γ-chain, possibly actin and an unknown protein with a molecular weight of 63.1 kDa. Contamination by fibrinogen and actin does not interfere with integrin

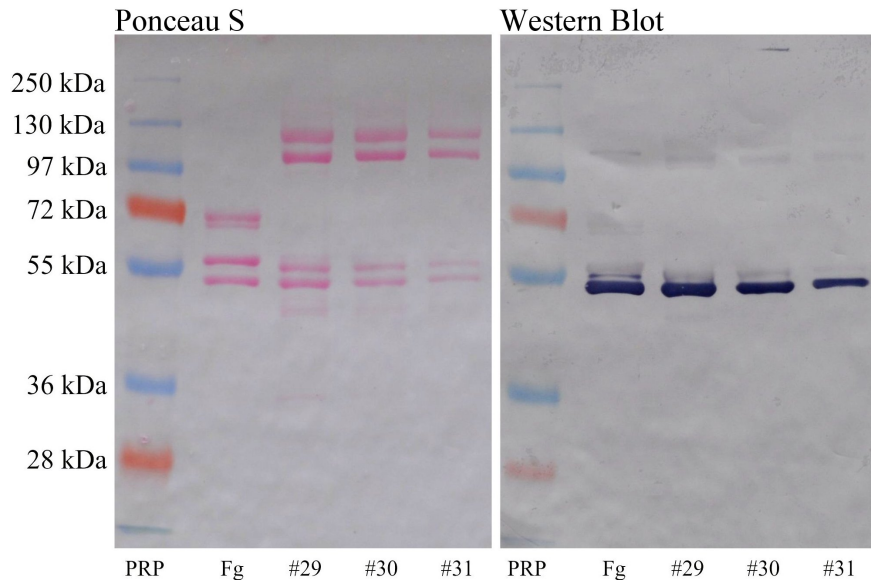

Figure 9.4: Western blot against fibrinogen with samples reduced by β-mercaptoethanol. Samples are from left to right: fibrinogen, fractions #29, #30 and #31 of purification K. The molecular weight marker PRP was applied in the first lane from the left.

reconstitution in vesicle membranes. Both proteins are water-soluble not exposing hydrophobic domains that are necessary for insertion in bilayers.

9.2 Purity and Yield of Purified Integrin

The overall concentration of protein in each fraction was measured after purification by UV absorption and the BCA assay. Results of both methods are compared in the diagram in figure 9.5. Concentrations as measured with the UV absorption are higher than concentrations deduced from BCA assay by a factor of 1.08 to 1.17 in this case. However, the BCA assay generally resulted in higher values than UV absorption. Typically, concentrations different fractions were in the range of $0.1\,\mathrm{mg\,ml^{-1}}$ to $1.0\,\mathrm{mg\,ml^{-1}}$.

Figure 9.6 shows an exemplary SDS polyacrylamide gel of fractions after the final gel filtration of two integrin purifications. The high molecular weight contamination slightly below 250 kDa in fractions #28-A and #29-B might be fragments of talin. Talin links integrin to actin and is formed from two subunits with molecular weights of 47 kDa and 220 kDa respectively [127], which is in good correspondence with observed protein bands.

Each fraction's purity was determined by densitometry as the ratio of added intensity of both integrin bands to the overall intensity of bands per lane. Table 9.2 summarizes the results for the samples of the gel depicted in figure 9.6.

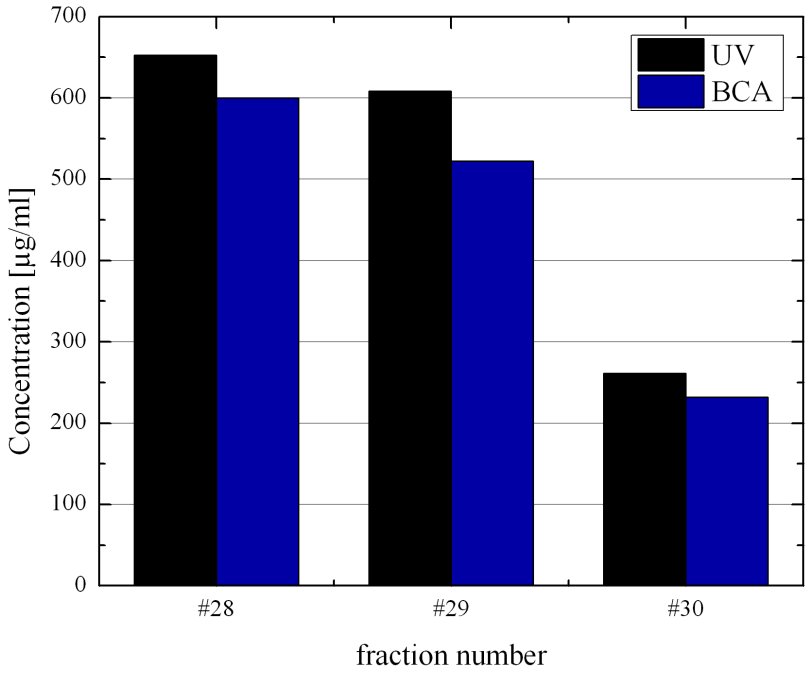

Figure 9.5: Concentration of integrin $\alpha_{\mathrm{IIb}}\beta_3$ in different fractions of purification I. The graph shows results from UV absorption measurement (black) and BCA assay (dark blue).

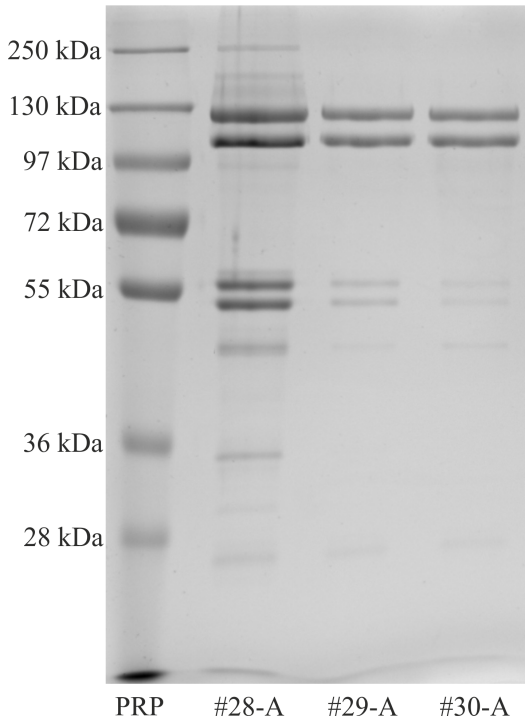

Figure 9.6: Coomassie-stained SDS-gel of fraction of the final gel filtration step of integrin purification. The lanes show fractions #28, #29 and #30 of the gel filtration with a HiLoad 26/60 Superdex 200 prep grade column of purification I. The molecular weight marker was applied in the first lane from the left.

Table 9.2: Purity of fractions after gel filtration of integrin purification I. Purity was obtained from evaluation of Coomassie-stained gels as the ratio of intensity of integrin $\alpha_{\mathrm{IIb}}\beta_3$ bands to the overall intensity per lane.

fraction:	#28-A	#29-A	#30-A	#29-B	#30-B	#31-B	#32-B
purity:	39%	77%	88%	39%	60%	75%	73%

Overall yield of pure integrin $\alpha_{\mathrm{IIb}}\beta_3$ was calculated by multiplication of concentration (figure 9.5), purity (table 9.2) and a volume of 5 ml per fraction. Purification I yielded 4.5 mg pure integrin, which was typical for integrin purification in this study.

Reconstitution of integrin $\alpha_{\mathrm{IIb}}\beta_3$ in SUVs generally was done with concentrations of integrin higher than $0.5\,\mathrm{mg\,ml^{-1}}$to avoid excessive dilution of preformed vesicles. Aliquots of adequate fractions were used. If integrin concentration was too low, integrin samples were concentrated by centrifugal filtering using membranes with a molecular weight cutoff of 50 kDa. Depending on the spin time, filtering typically results in a ten times higher concentration of protein with minimal loss of sample. Therefore, purification of integrin $\alpha_{\mathrm{IIb}}\beta_3$ yields samples with concentrations sufficient for this study.

Integrin $\alpha_{\mathrm{IIb}}\beta_3$ of highest purity over 85% was usually found in fraction #30 of each purification. Purity could be increased by an additional step of gel filtration, but was sufficient for incorporation of integrin in vesicle membranes. The overall yield of about 5 mg pure integrin $\alpha_{\mathrm{IIb}}\beta_3$ per purification process allowed time intervals of three month in between purifications. Even several density gradient centrifugation experiments can be performed that require high amounts of protein (roughly 0.5 mg). Thus, integrin $\alpha_{\mathrm{IIb}}\beta_3$ was purified with sufficient yield from human platelet membranes.

9.3 Molecular State of Purified Integrin

9.3.1 Calibrated Gel Filtration

In order to elucidate whether integrins α_{IIb} and β_3 are associated with each other, gel filtration columns were calibrated to be able estimate the size of purified proteins. A mixture of globular, water-soluble proteins with known molecular weight was used to calibrate a Superdex 200 10/300 GL gel filtration column. This column serves more analytical purposes compared the much larger HiLoad 26/60 Superdex 200 prep grade, which was used in the final step of purification owing to large sample volume. The chromatogram of a calibration run is depicted in figure 9.7.

The partition coefficient K_{av} of the proteins is calculated as described in section 4.1 with a column volume $V_c = 23.562$ ml given by the manufacturer and a measured void volume $V_0 = 8.0$ ml. In general, a sigmoid relationship exists between K_{av} and

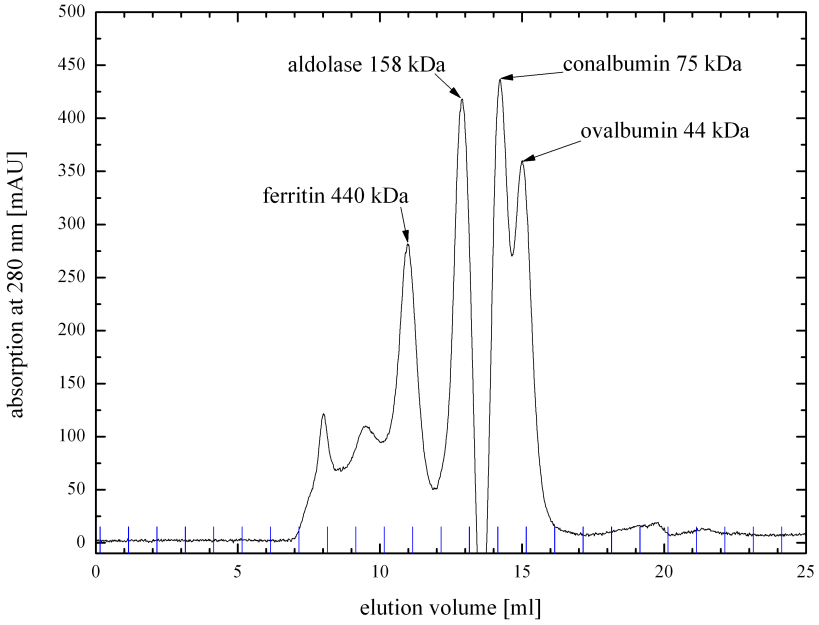

Figure 9.7: Chromatogram of the calibration of a Superdex 200 10/300 GL column.

$\ln M_\mathrm{R}$ when considering the whole separation range of a column, but in the middle part of this range the relation is linear [9]. On the other hand, $\sqrt{-\ln K_{av}}$ linearly depends on r_St [99, 187]. Therefore, data in both diagrams is fitted using linear regression. Figure 9.8a shows the plotted partition coefficient K_{av} over the natural logarithm of molecular weight $\ln M_\mathrm{R}$. Additionally, the square-root of the negative natural logarithm of the partition coefficient, $\sqrt{-\ln K_{av}}$, is plotted over the Stokes radius r_St as shown in figure 9.8b.

The elution volume V_e of integrin is deduced from the chromatogram of an integrin sample, which is shown in figure 9.9a. SDS-PAGE allows the determination of the fraction with the highest concentration of integrin (figure 9.9b). Thus, integrin is assigned to the second peak of the two peaks at about 10 ml with its maximum at $V_e = 10.97\,\mathrm{ml}$.

The molecular weight $M_\mathrm{R}^\mathrm{integrin}$ is calculated from the linear regression in figure 9.8a with the partition coefficient of integrin K_{av}^integrin:

$$M_\mathrm{R}^\mathrm{integrin} = 523\,\mathrm{kDa} \tag{9.1}$$

The calculation of the Stokes radius r_St of integrin results in

$$r_\mathrm{St}^\mathrm{integrin} = 6.5\,\mathrm{nm} \tag{9.2}$$

Errors for both values are estimated to be at about 10% due to the use of soluble

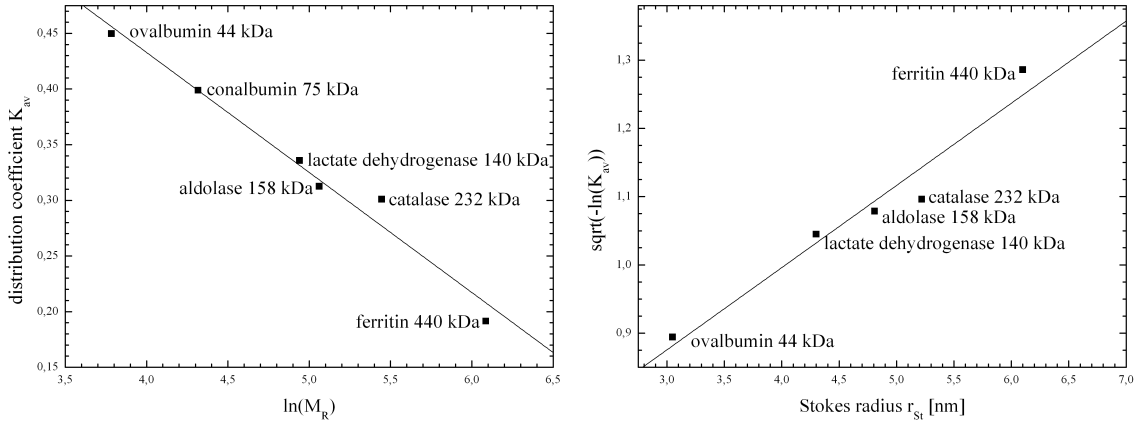

Figure 9.8: Data from calibration of a Superdex 200 10/300 GL column with a fit (red) using linear regression.
(a) Partition coefficient K_{av} over the natural logarithm of molecular weight $\ln M_{\mathrm{R}}$.
(b) Square-root of the negative natural logarithm of the partition coefficient, $\sqrt{-\ln K_{av}}$, over Stokes radius r_{St}.

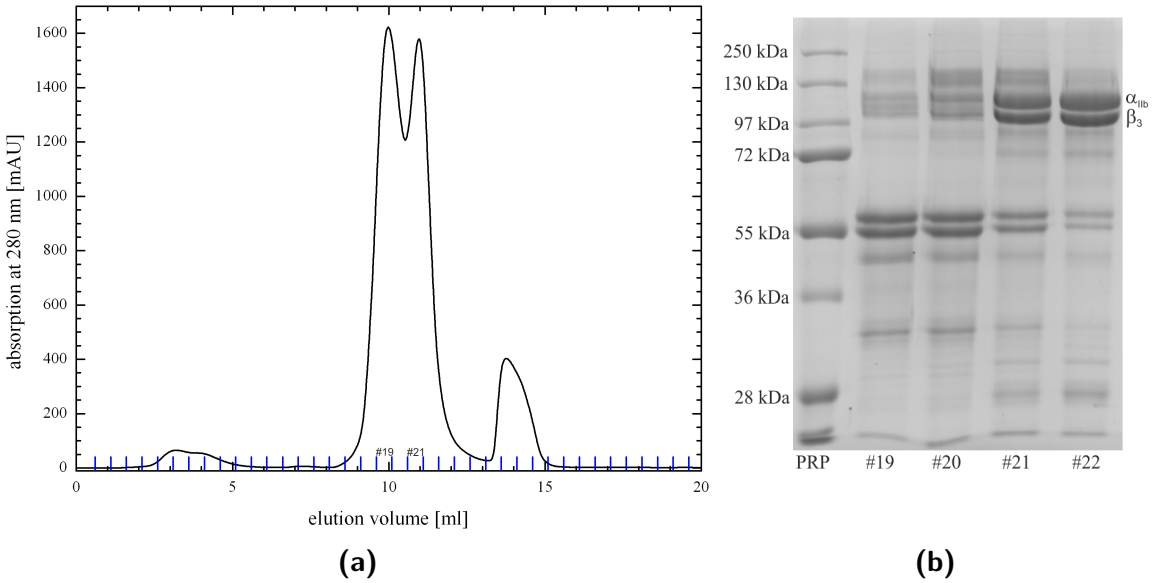

Figure 9.9: Chromatogram of an integrin sample separated with a Superdex 200 10/300 GL column (a) and Coomassie-stained gel (b) of various fractions of the double peak at about 10 ml. Different fractions are indicated in the chromatogram by blue lines perpendicular to the x-axis and fractions #19 and #21 are emphasized specifically.

proteins for calibration which might not be suitable for membrane proteins.

Table 9.3 summarizes data of the calibration of the HiLoad 26/60 Superdex 200 prep grade column used for purification of integrin from platelets. Its void volume V_0 was measured to be 113.75 ml and the column volume V_c is 319.1 ml.

Table 9.3: Proteins used for calibration of a HiLoad 26/60 Superdex 200 prep grade column. Their molecular weight M_{R} and elution volume V_e are listed. Error of elution volume V_e is due to reading error in chromatograms printed on paper with a x-y plotter.

protein	M_{R} (kDa)	V_e (ml)
thyroglobulin	669	$134,75 \pm 1$
ferritin	440	$151,0 \pm 1$
aldolase	158	$180,5 \pm 1$
conalbumin	75	$203,25 \pm 1$
ovalbumin	44	$221,0 \pm 1$

Calculation of molecular weight M_{R} and Stokes radius r_{St} using the integrin's average elution volume $V_e = 143.25$ ml leads to

$$M_{\mathrm{R}}^{\mathrm{integrin}} = 533\,\mathrm{kDa} \tag{9.3}$$

and

$$r_{\mathrm{St}}^{\mathrm{integrin}} = 7.3\,\mathrm{nm} \tag{9.4}$$

Thyroglobulin deviated substantially from the linear dependence of $\sqrt{-\ln K_{av}}$ on Stokes radius r_{St} exhibited by the other proteins. Calibration results in a Stokes radius r_{St} of 6.7 nm when not considering thyroglobulin.

The molecular weight of integrin of about 530 kDa, calculated from calibration curves of gel filtration columns, is more than two times higher than the molecular weight of 230 kDa deduced from its amino acid sequence. Glycoproteins such as integrin often elute earlier in gel filtration as their actual molecular weight implies, that is with a higher apparent molecular weight. The earlier elution might be due to a stronger hydration of glycosylated proteins as reported by other groups [9]. In buffer containing 0.2% (w/v) Triton X-100, integrin $\alpha_{\mathrm{IIb}}\beta_3$ additionally binds 0.38 mg Triton per 1 mg of integrin increasing the weight of the protein complex [170]. Some authors even doubt in general a direct dependence of elution volume on molecular weight of proteins, but they propose a correlation of Stokes radius and elution volume only [187]. Non-specific interactions of integrin $\alpha_{\mathrm{IIb}}\beta_3$ with the column medium could lead to a retardation of integrin's elution.

At the same time, Stokes radius of detergent-solubilized membrane proteins is overestimated by gel filtration compared to data from analysis of ultracentrifugation [102]. When thyroglobulin is not considered for calibration, Stokes radii of both

columns used for gelfiltration agree reasonable well with each other. Both values are slightly larger than 6.2 nm as measured with calibrated gel filtration [170]. However, they are smaller than 7.4 nm calculated according to [205] using molecular weight and sedimentation coefficient [170]. This finding suggests the purification of integrin $\alpha_{\mathrm{IIb}}\beta_3$ as a monomer.

Even though the molecular weight determined by gel filtration is too high, Stokes radius is not significantly increased as would be expected for integrin $\alpha_{\mathrm{IIb}}\beta_3$ aggregated in a dimer or multimer. Thus, integrin $\alpha_{\mathrm{IIb}}\beta_3$ heterodimer is most likely purified in its monomeric form from platelet membranes.

Static light scattering allows the precise determination of molecular weight not requiring calibration. Therefore, this method might be one way to ascertain the purification of integrin $\alpha_{\mathrm{IIb}}\beta_3$ as a monomer. Calibration of a HiLoad 26/60 Superdex 200 prep grade at the European Molecular Biology Laboratory results in the elution of standard proteins about 15 ml ahead of elution volumes determined in this study [154].

9.3.2 Co-Immunoprecipitation of Platelet Integrin

Co-immunoprecipitation was performed to elucidate whether integrin $\alpha_{\mathrm{IIb}}\beta_3$ is purified as a heterodimer or as two separated subunits. Figure 9.10 shows the result of the subsequent Western blot for sample analysis. In figure 9.10a the primary antibody was directed against integrin α_{IIb}. For the Western blot in figure 9.10b an anti-integrin β_3 antibody was utilized. The prestained marker on the left was not affected by Western blot. In the second lane, an integrin sample was applied as positive control. Starting in lane three, samples of different immunoprecipitations (IPs) were applied: (1) IP with anti-β_3 antibody, (2) IP with anti-α_{IIb} antibody, (3) IP with anti-α_{IIb} antibody without integrin and, in the last lane on the right, (4) IP with integrin but without antibody.

The integrin sample showed the specific staining of integrin α_{IIb} or integrin β_3 at 97 kDa and 130 kDa respectively. More protein bands are visible in figure 9.10a than in figure 9.2a due to a longer incubation with the substrate of the enzyme in Western blotting to detect smaller amounts of proteins. Integrin α_{IIb} was clearly stained in samples (1) and (2) and practically not stained in samples (3) and (4) (figure 9.10a). Integrin β_3 was colored purple-blue in sample (2), but is barely visible in sample (1) and not at all in both lanes on the right (figure 9.10b). In both Western blots, two protein bands at around 25 kDa and 50 kDa were stained in samples (2) and (3). Very faint bands can be found in samples (2) and (3) and maybe in (1) at around 30 kDa in the Western blot for integrin β_3 (figure 9.10b).

Protein bands at around 25 kDa and 50 kDa show fragments of the antibody used for immunoprecipitation (IP), as they are clearly visible in samples (2) and (3) in both Western blots, but not in other lanes. The antibody employed for IP of sample (1) was produced in rabbit. Thereby, it is not detected by secondary anti-mouse

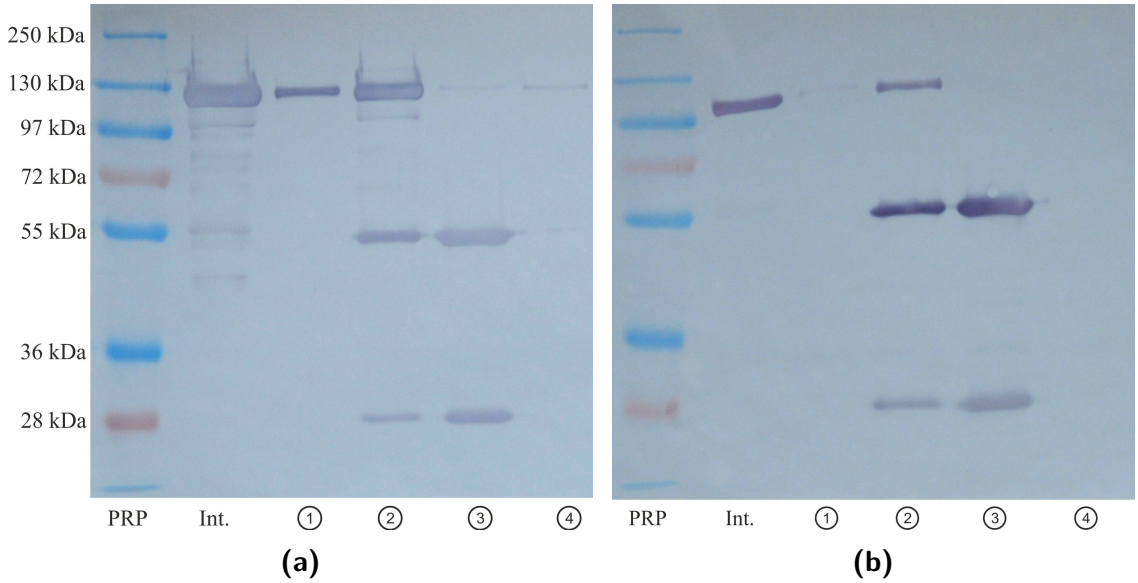

Figure 9.10: Western blot against integrin α_{IIb} (a) and β_3 (b) after co-IP. Samples are from left to right: molecular weight standard (PRP), integrin $\alpha_{\mathrm{IIb}}\beta_3$ (Int.), sample of immunoprecipitation with antibody vs. β_3 (1), sample of immunoprecipitation with antibody vs. α_{IIb} (2), sample of immunoprecipitation without integrin (3), sample of immunoprecipitation without antibody (4).

antibody of Western blotting. Sample (4) did not contain any antibody.

The band at around 30 kDa represents most likely recombinant protein G, which migrates in SDS-PAGE with the same molecular weight [49]. Protein G is detached almost certainly to some extent from the beads by treatment with Lämmli buffer and heating. It binds antibodies in general, as described in section 4.2.4, and might thereby be stained in Western blots.

Samples (3) and (4) are negative controls. They rule out significant non-specific binding of integrin to the protein G-coated beads, even though integrin α_{IIb} is slightly visible (figure 9.10a). As only buffer and no integrin was in sample (3), the visible α_{IIb} band might indicate that maybe sample run over from a neighboring well in SDS-PAGE due to high sample volumes.

Integrin β_3 is bound to integrin α_{IIb}, as can be deduced from the staining of both integrins in sample (2). On the other hand, integrin α_{IIb} is co-immunoprecipitated with integrin β_3, since it is clearly found in sample (1) (figure 9.10a). It might be possible, that the anti-β_3 antibody of immunoprecipitation was not dissociated from its antigen by addition of Lämmli buffer and heating. This antibody might block the binding region of the antibody used for Western blotting. Thus, with the utmost probability, integrin $\alpha_{\mathrm{IIb}}\beta_3$ is purified as heterodimer.

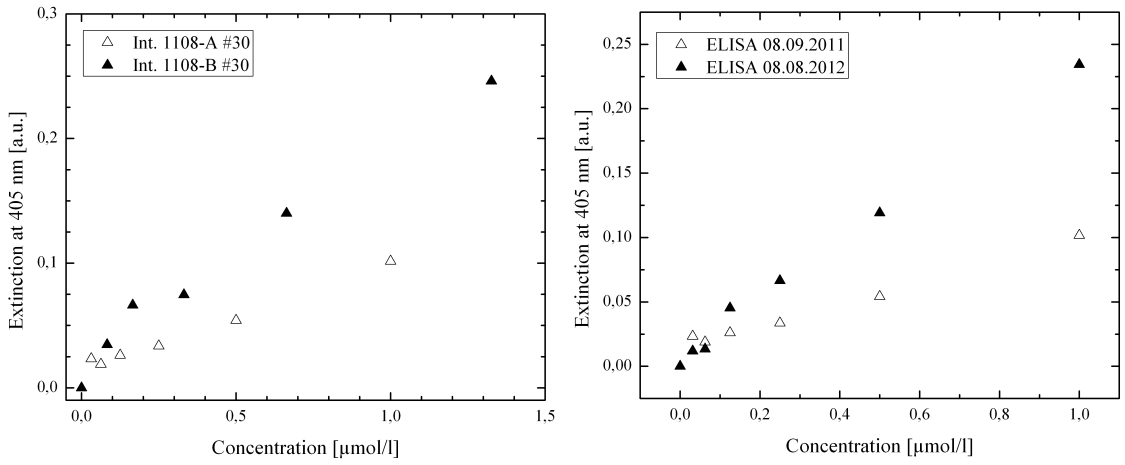

(a) **(b)**

Figure 9.11: (a) ELISA data from the same fractions of different purifications showing binding activities differing by a factor of two.
(b) ELISA data on the effect of storage at −85 °C on integrin activity. One sample was assayed directly after purification, the other after almost one year of storage at −85 °C. Except from storage conditions, identical samples were used.

9.4 Functionality of Purified Integrin

As integrin $\alpha_{\mathrm{IIb}}\beta_3$ is purified as a heterodimer from platelet membranes with sufficient yield, its functionality has to be tested. ELISA was used to measure the binding of purified integrin to its natural ligand fibrinogen. The procedure is described in section 4.2.5 with a detailed protocol in appendix G.2.

A sample without integrin did not lead to a measurable signal in ELISA (not shown). When the same fraction of two different purifications was tested, varying binding activities were measured (figure 9.11a). To test stability of integrin, the influence of storage of the purified integrin at −85 °C on binding was addressed testing the same sample before and after storage for about one year. Binding to fibrinogen was found to be higher for the stored sample (figure 9.11b).

Integrin was labeled with the dye carboxytetramethylrhodamine (TAMRA) for reconstitution experiments to demonstrate the incorporation of integrin in the membrane of GUVs by fluorescence. Hence, binding of TAMRA-labeled integrin was compared to binding of non-labeled integrin (figure 9.12a). Labeling reduced signal in ELISA by one half. As manganese ions activate integrin resulting in higher binding to its ligands [83], this effect was also detected for two different fractions of integrin purified from platelets (figure 9.12b). The addition of manganese increased binding of integrin to fibrinogen by a factor of two to three.

Integrin $\alpha_{\mathrm{IIb}}\beta_3$ is purified from natural material, in particular, human platelet

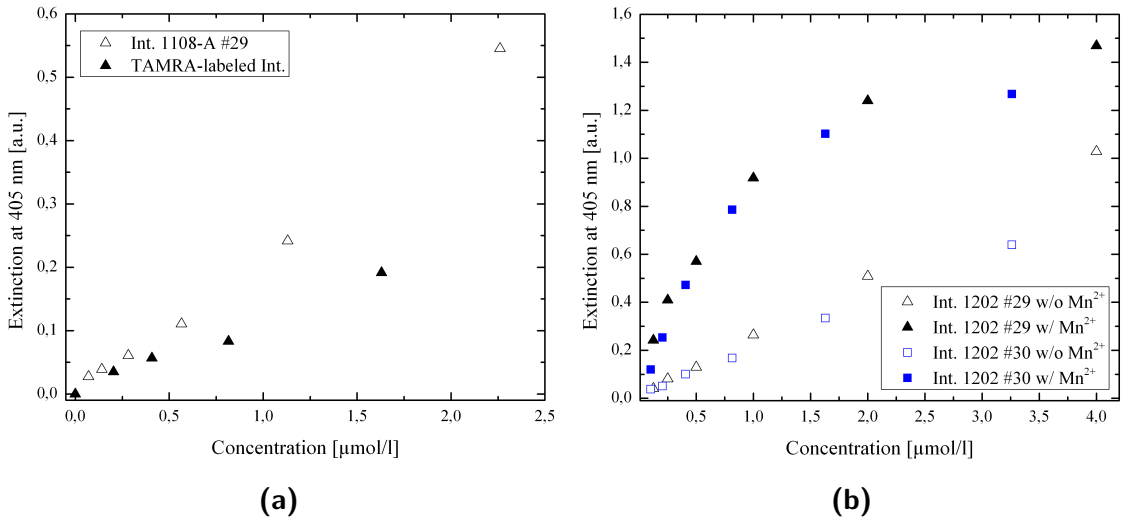

Figure 9.12: (a) ELISA data for TAMRA-labeled integrin and non-labeled integrin. Labeling reduces the activity roughly by a factor of two.
(b) ELISA data from two fractions of a purification with and without Mn^{2+} in solution showing the activating effect of manganese ions.

concentrate coming from various donors. Integrin of different purifications thereby shows differing binding activity by virtue of its source. It is not clear, why integrin stored for several month causes a higher signal in ELISA. One explanation might be, that freezing and thawing lead to activation of integrin. On the other hand, for results of different experiments being comparable, the signal needs to be normalized to a sample which was present in both experiments [144]. Otherwise, slight changes of experimental conditions might influence the result, even though the same sample was used. Data of ELISA compared in figure 9.11b was not normalized to each other.

Decrease of binding activity of TAMRA-labeled integrin can be explained by steric effects. The chemical reaction used for labeling couples the dye non-specifically to free amino groups of the protein. Coupling might also occur in the binding region of integrin hampering accessibility for ligands. This effect is no problem in reconstitution experiments, but has to be kept in mind, when adhesion is investigated.

Activation of purified integrin by manganese ions is one more hint to the successful purification of the receptor. Addition of Mn^{2+} can be used to control the adhesive properties of the model system in studies of its adhesion to surfaces.

ELISA is not suitable to measure binding constants due to the non-linear dependence of the signal on integrin concentration. Non-linearity arises, for instance, from the amplification of signal by using an enzyme reaction for detection or unknown and differing antibody concentrations. The non-linear detection is quantitatively demonstrated in literature [206].

For binding of integrin $\alpha_{\mathrm{IIb}}\beta_3$ to fibrinogen to occur, the integrin's presence as a

heterodimer is a prerequisite. Therefore, a signal in ELISA once more demonstrates the presence of heterodimers. In conclusion, integrin $\alpha_{\mathrm{IIb}}\beta_3$ is purified as a functional heterodimer from human platelets.

10 Results on Small and Giant Liposomes

10.1 Size Distribution of SUVs

In order to better understand the preparation of SUVs the size of SUVs and LUVs was measured using dynamic light scattering. The very high curvature of vesicles smaller than 50 nm might also influence incorporation of proteins. However, vesicle size was determined in qualitative way rather than measuring absolute values of the diameter. The absolute diameter depends on the exact optical properties like index of refraction and the geometry of the particles and requires sophisticated mathematical models for its calculation.

Vesicles were prepared by sonication or extrusion. Figure 10.1 shows a typical size distribution of liposomes extruded through a membrane with a pore size of 100 nm. SUVs are slightly larger than the pore size of the membrane with a narrow size distribution (PDI < 0.1) indicating a monodisperse sample (note the linear scale in figure 10.1). The mean diameter of the intensity size distribution was approximately 130 nm and did not deviate much from the mean diameter of the number size distribution of roughly 110 nm.

Measurement of size was also used to investigate the colloidal stability of sonicated and extruded SUVs containing PEGylated lipid. To check, if there was significant fusion of SUVs leading to larger diameters, the size distribution was measured 0 h, 1 h, 24 h and 48 h after preparation. The average diameter of sonicated vesicles was between 40 nm to 45 nm, whereas vesicles extruded through membrane with 100 nm pore size measured 105 nm to 110 nm in diameter. The number size distribution was used to deduce the vesicle diameter which did not change significantly over time. The intensity size distribution of vesicles, prepared by sonication, exhibited two peaks at about 40 nm and 180 nm. Since a mean diameter of 35 nm is reported for SUVs prepared by sonication [213], number-based values were considered to be more reliable for sonicated vesicles.

Three different lipid mixtures were tested on their incorporation of integrin. Their composition is listed in table 10.1. The *Standard* mixture was derived from [198, 199] with addition of the ionophore A23187. To elucidate possible influence of the type of the negatively charged headgroup on integrin insertion, the lipid eggPA was changed for brainPS in the *PS* mixture. The name brainPS specifies the source

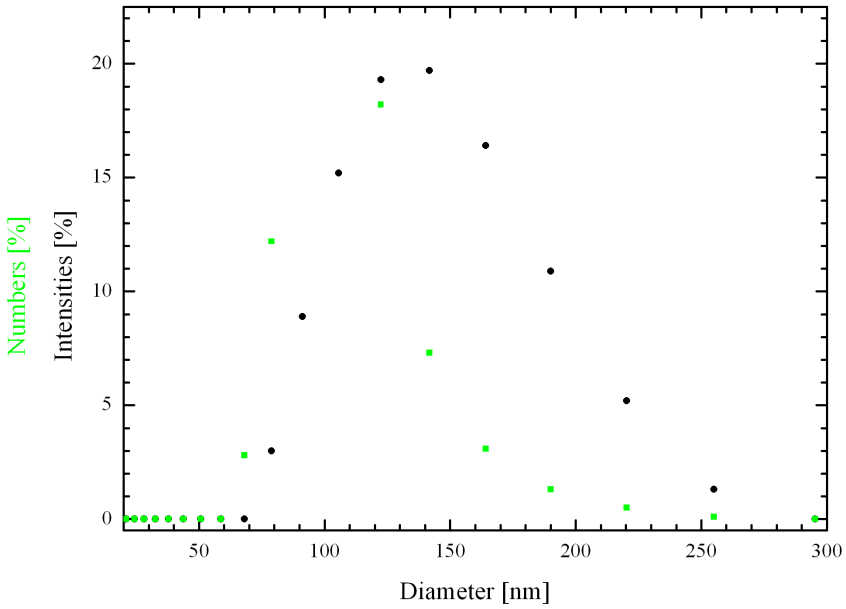

Figure 10.1: Size distribution of SUVs extruded through a membrane with 100 nm pore size. Intensity and number size distribution are given.

phosphatidylserine (PS) which is purified from porcine brain. The composition of the *Platelet* mixture was adjusted to mimic the composition of platelet membranes according to data in [191]. This mixture included cholesterol in addition to brainPS.

Unilamellar vesicles were produced by sonication and extrusion using *Standard*, *PS* and *Platelet* mixtures. Membrane pore sizes of 50 nm, 100 nm and 200 nm were employed for extrusion. Vesicle size did not significantly depend on the lipid mixture as size variations between different mixtures were about 10% (table 10.2). Extruded vesicles were slightly larger than 50 and 100 nm pores, but SUVs measured only

Table 10.1: Composition of different lipid mixtures used in this work: *Standard*, *PS* and *Platelet* mixture.

lipid	Standard (mol%)	PS (mol%)	Platelet (mol%)
eggPC	82, 5	82, 5	43, 1
eggPA	10, 0	-	-
brainPS	-	10, 0	14, 4
DPPE PEG2000	5, 0	5, 0	3, 1
chol	-	-	37, 8
A23187	2, 5	2, 5	1, 6

Table 10.2: Average diameter $\bar{d}$ and polydispersity index PDI and average diameter $\bar{d}_{num}$ of the number based size distribution. The PDI is a measure for the width of the intensity based size distribution. Liposomes were prepared from the lipid mixture *Standard*, *PS* and *Platelet* by sonication (US) and extrusion (extr). Pore size p of the membranes used for extrusion is also given. The lipid composition of the mixtures can be found in table 10.1. Given diameters and PDI are averages of two independent measurements.

prepared by	lipid mix	p (nm)	$\bar{d}$ (nm)	$\bar{d}_{num}$ (nm)	PDI (a.u.)
US	Standard	n.a.	127	41	0,295
US	PS	n.a.	120	44	0,388
US	Platelet	n.a.	154	50	0,442
extruder	Standard	50	100	85	0,079
extruder	Standard	100	170	121	0,103
extruder	Standard	200	169	129	0,080
extruder	PS	50	85	73	0,070
extruder	PS	100	119	89	0,120
extruder	PS	200	142	100	0,218
extruder	Platelet	50	94	84	0,058
extruder	Platelet	100	137	104	0,089
extruder	Platelet	200	153	113	0,091

around 120 nm for membranes with a pore size of 200 nm. Sonication produced polydisperse samples indicated by a PDI ≥ 0.3, but the predominant population of vesicles was about 40 nm in diameter for all lipid mixtures (first three lines in table 10.2).

The size distribution of SUVs is controlled by the technique used for their preparation. The lipid compositions investigated in this study led to minor size variations in the range of 10%. Sonication yielded polydisperse samples as two populations of vesicles were mixed. Very small, highly curved vesicles with a diameter of about 35 nm constitute the major part of the mixture. LUVs sized around 180 nm were also found in the samples. This population might be due to inhomogeneous ultrasonic waves caused by reflections inside of the small bottle used for vesicle preparation with the tip sonicator. Extrusion through membranes with pore sizes of 50 nm and 100 nm produced monodisperse vesicles slightly larger than the pore size, while 200 nm membranes lead to vesicles smaller than the pore size with a mean diameter of approximately 120 nm. The pressure required for extrusion through membranes is inversely correlated to pore size. Due to increased risk of leakage of the Avanti Mini Extruder at high pressure, membranes with 100 nm pores were used to produce monodisperse samples.

10.2 Analysis of Integrin Reconstitution in Small Vesicles

Density gradient centrifugation was performed to separate free, solubilized integrin $\alpha_{\mathrm{IIb}}\beta_3$, vesicles without incorporated integrin and proteoliposomes. The lipid mixtures *Standard*, *PS* and *Platelet* were used for protein reconstitution as described in section 6.3.

Figure 10.2 depicts photographs of density gradients with vesicles prepared by extrusion through a membrane with 100 nm pore size using the *Standard* mixture. Besides three samples of proteoliposomes, two control samples, solubilized integrin and vesicles without integrin, were used. Coomassie-stained gels of samples marked in figure 10.2 are illustrated in figure 10.3. Solubilized integrin was found exclusively at the bottom of the centrifugation tube (figure 10.3a). As expected, no protein bands were detected in samples of the gradient with pure lipid vesicles (figure 10.3a,b). All visible bands of vesicles in gradients with samples from reconstitution contained integrin, although roughly 50% of integrin was found at the bottom of the tubes (figure 10.3b,c,d). The distribution of proteoliposomes in gradients and incorporation of integrin did not change significantly with the size of SUVs used for reconstitution (data not shown). Integrin was still found in samples of vesicles bands visible in gradients.

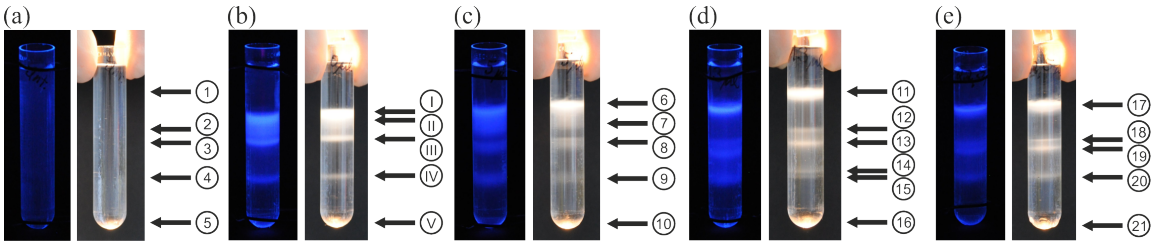

Figure 10.2: Photos of centrifugation tubes after density gradient centrifugation illuminated with daylight and UV light ($\lambda = 365\,\mathrm{nm}$). The *Standard* lipid mixture was used to prepare SUVs by extrusion through a membrane with 100 nm pore size. Solubilized integrin (a) and pure SUVs (b) were used to control their distribution in density gradients. Vesicles from reconstitution of integrin $\alpha_{\mathrm{IIb}}\beta_3$ are denoted with the volume of Triton X-100 added to preformed SUVs. Preformed vesicles were saturated with detergent (c) and they were partly (d) or completely (e) solubilized before reconstitution of integrin. Positions of samples gathered from the gradients are marked and numbered.

Density gradient centrifugation of SUVs after reconstitution of integrin $\alpha_{\mathrm{IIb}}\beta_3$ clearly shows, that integrin is interacting with bilayers of vesicles. However, around 50% of integrin is found at the bottom of the centrifugation tubes. Incorporation of integrin seems to work slightly better starting either with detergent-saturated vesicles or with lipid-detergent micelles, in the case of completely solubilized SUVs. At an

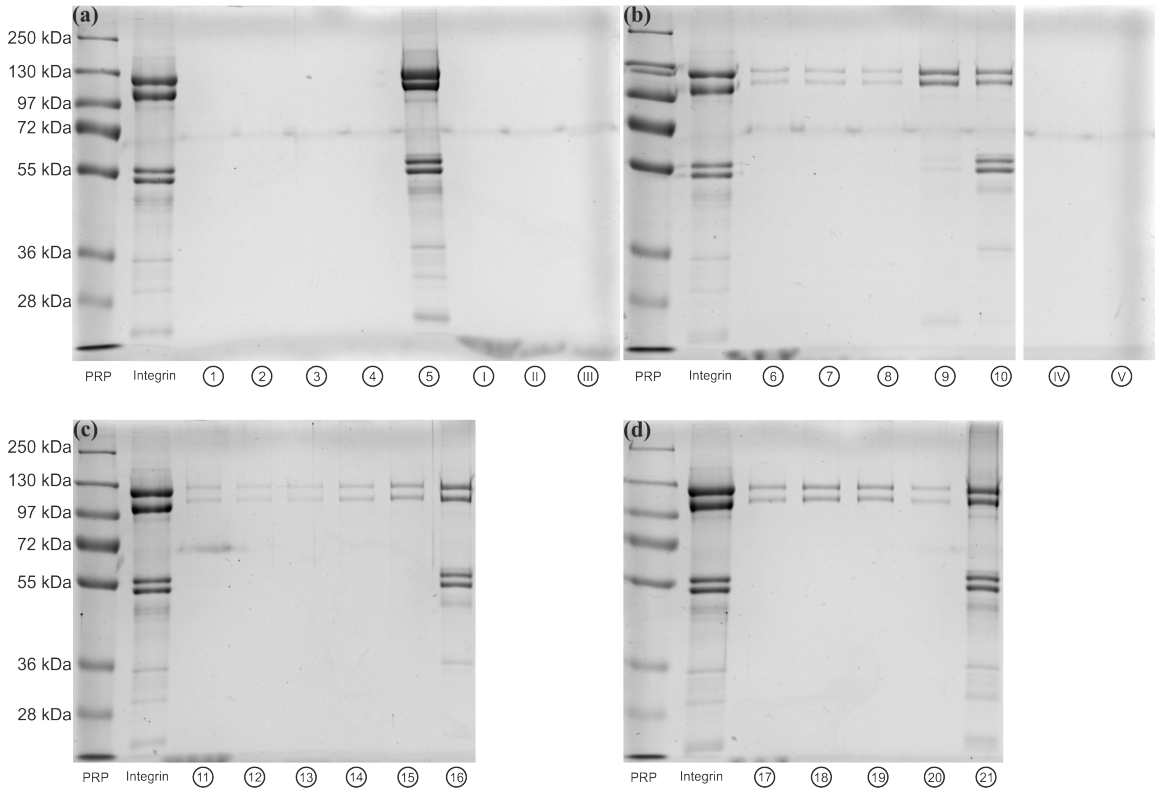

Figure 10.3: SDS-polyacrylamide gels of samples from density gradient centrifugation. Samples are specified in figure 10.2.

intermediate point of solubilization samples from the gradient exhibit slightly lower intensity of integrin bands in Coomassie-stained gels. Complete solubilization of preformed vesicles results in a statistical insertion of integrin in the bilayer as vesicles assemble from protein-lipid-detergent micelles. About 50% of integrins are oriented outside-out, while the extracellular part of the other half points to the interior of the vesicles. On the other hand, integrin should be incorporated predominantly outside-out in vesicles which are only destabilized by detergent due to its very large extracellular part. A passage of the hydrophilic extracellular part through the hydrophobic bilayer remains highly unlikely even though Triton might shield exposed edges. Therefore, reconstitution using low amounts of Triton X-100 is preferred over complete solubilization.

In the range of diameter of SUVs examined in this study (around 40 to 150 nm), size distribution does not affect integrin incorporation in vesicles.

The *PS* mixture also yields integrin-coated vesicles after reconstitution as determined with density gradient centrifugation. A slightly higher integrin content was found in vesicles destabilized or completely solubilized by detergent compared to intermediate stages of solubilization. This behavior is similar to findings with the *Standard* mixture. The type of negatively charged lipid is thus of minor importance for the incorporation of integrin in bilayers. However, the negatively charged headgroup might influence the yield of electroformation in a subsequent growth to GUVs. Cholesterol, which was included in the *Platelet* mixture, influences the solubilization process in a more fundamental way. Satisfying insertion of integrin was achieved only with 22.5 µl of Triton X-100, which leads to complete solubilization of SUVs from the *Standard* mixture. However, it is not clear if solubilization is merely shifted to higher concentrations of detergent due to the stiffer cholesterol-containing bilayers. Another explanation could be a direct interference of cholesterol with protein incorporation at low detergent concentrations.

Preliminary data by cryo-TEM indicated merely low amounts of integrin incorporated in vesicles. Due to short time and limited access to the instrument located in Zurich, further investigation was not realizable. This finding suggests, that integrin is potentially not inserted, but only attached to the bilayer of vesicles. It is not possible to discern by density gradient centrifugation whether proteins are attached to or incorporated in vesicle membranes.

Integrin reconstitution in SUVs, according to work of Pia Streicher in her PhD thesis [198, 199], was also examined utilizing density gradients. No integrin bands were visible in SDS-polyacrylamide gels with samples from the gradients. However, concentration of integrin (and lipid) is five times lower in this protocol compared to reconstitution described in section 6.3. Staining of gels with Coomassie might be not sensitive enough to detect such low amounts of integrin. Furthermore, bands of vesicles in the gradient after centrifugation were not clearly visible due to lower lipid concentration making the identification of potential samples in the gradient quite difficult.

In conclusion, integrin $\alpha_{\mathrm{IIb}}\beta_3$ is interacting or attached to the bilayers of preformed SUVs. Confocal images of GUVs grown from proteoliposomes even suggests insertion of integrin. The mere attachment of integrin to membranes should be ruled out in further experiments using cryo-TEM.

10.3 Preparation of GUVs using Different Methods

10.3.1 Electroformation

Electroformation is one way to grow giant unilamellar vesicles from (partially) dry lipid films. Phospholipid bilayers oscillate in an externally applied alternating electric field depending on its frequency and amplitude. When working with frequencies around 1 Hz and amplitudes up to 10 V, the movement of bilayers was easily observed at the microscope (see Movie 1, appendix B). The oscillations help to separate bilayers allowing water to penetrate between these bilayers more easily. Mechanical stimulation of bilayers eventually led to fusion of GUVs (see Movie 2, appendix B). Swelling and subsequent fusion of bilayers might be one mechanism how GUVs grow from lipid layers.

Various ways of deposition of lipid layers were tested. Spin-coated lipid layers did not lead to GUVs employing electroformation, while dip-coating did not enhance GUV yield compared to simple deposition with the Hamilton pipette. Spreading of lipids on surface using a wet Kimwipe did not produce more or larger GUVs as well. The most practical way to produce lipid layers is described in section 6.2. Giant unilamellar vesicles were prepared with electroformation using lipid layers from chloroform solution on ITO-coated glass (figure 10.4a,b). When platinum wires were employed as electrodes, better results were obtained with lipid layers deposited from emulsions of SUVs (figure 10.4d,e). The use of proteoliposomes is discussed in more detail in section 10.5.3. An alternating electric field with frequency of 500 Hz allowed to prepare GUVs in buffers with physiological salt concentration (figure 10.4c,f)

Electroformation is a versatile technique to prepare giant unilamellar vesicles as previously demonstrated (figure 10.4). Largest vesicles up to several 100 µm were obtained in ultra-pure water, with only trace amounts of ions, without additives like sucrose. More complex buffers for swelling in general reduce the size and increase the time of growth. If buffers with physiological concentrations of salt are needed, increase of the frequency of the electric field to 500 Hz still allows preparation of giant vesicles. The effect of the high-frequency electric field on integrin functionality remains to be tested. Despite all these restrictions, electroformation is a promising and straight forward tool to prepare GUVs with integrin $\alpha_{\mathrm{IIb}}\beta_3$ inserted in their bilayer.

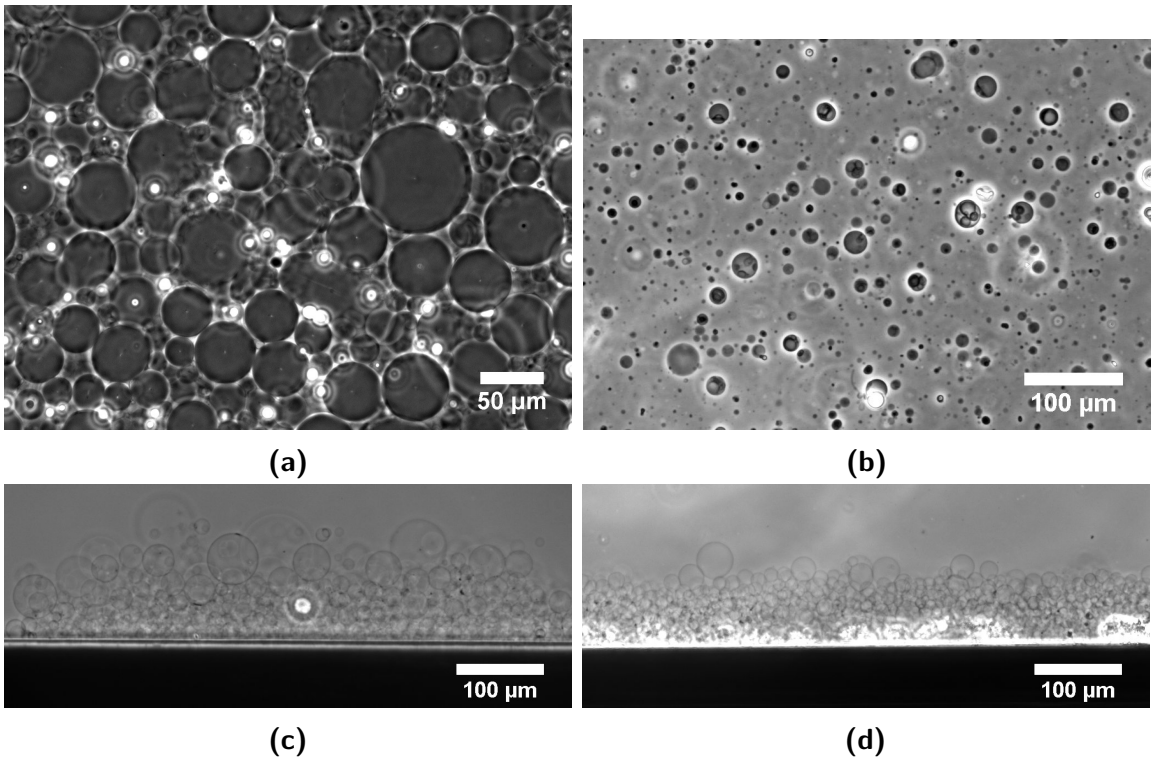

Figure 10.4: GUVs produced by electroformation using ITO (a,b) or platinum (c,d) electrodes. Lipid layers were prepared from lipid solutions in chloroform (a,b) and emulsions of SUVs (c,d). Employing an alternating electric field with a frequency of 500 Hz instead of 10 Hz, giant vesicles were produced in buffers containing physiological salt concentrations (b,d). The sample was already removed from the swelling chamber in (b).

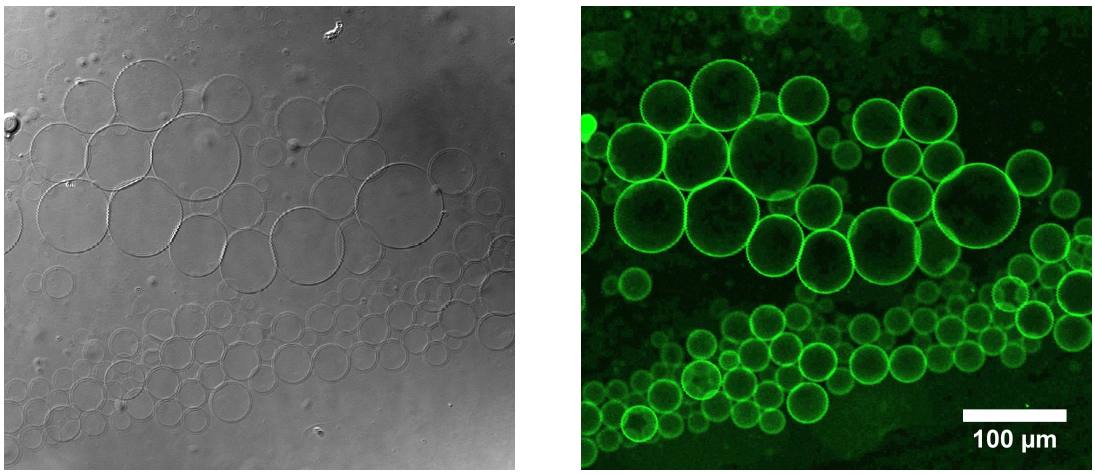

(a) (b)

Figure 10.5: GUVs produced with agarose-lipid-hybrid films from lipid solutions in methanol and chloroform. Lipid solution contained 0.27% (w/w) of fluorescent BODIPY-PC. DIC (a) and confocal fluorescence (b) images of the same sample are shown.

10.3.2 Agarose-Lipid-Hybrid Films

Agarose-lipid-hybrid films were investigated as a second method for their potential to grow giant vesicles with integrin $\alpha_{\mathrm{IIb}}\beta_3$ inserted in their bilayers. GUVs spontaneously formed by addition of water or buffer to an agarose-lipid film. Agarose was therefore coated with a solution of lipids in a 9:1 (v/v) mixture of chloroform and methanol. Formation worked with high yield and GUVs were produced as large as 80 µm in diameter (figure 10.5).

Lipid films on top of agarose were also prepared from emulsion of SUVs and proteoliposomes. Application of proteoliposomes for agarose-coating is discussed in section 10.5.3. Lipid films from SUVs emulsions resulted in dense clusters of giant vesicles with a maximum diameter of about 65 µm (figure 10.6).

The crucial step in electroformation is the partial drying of lipid layers, which might be deleterious for proteins embedded in bilayers of small vesicles. As agarose forms hydrogels, which always contain a certain amount of water, the agarose-lipid-hybrid film technique might help to preserve the natural structure of proteins. GUVs evolve spontaneously with high yield and sufficient diameter by swelling of hybrid films, as depicted in figures 10.5 and 10.6. The growth of GUVs was not restricted by any buffer ingredient used in this study. Thus, this method is applicable to prepare giant vesicles with integrin $\alpha_{\mathrm{IIb}}\beta_3$ functionally inserted in their bilayer.

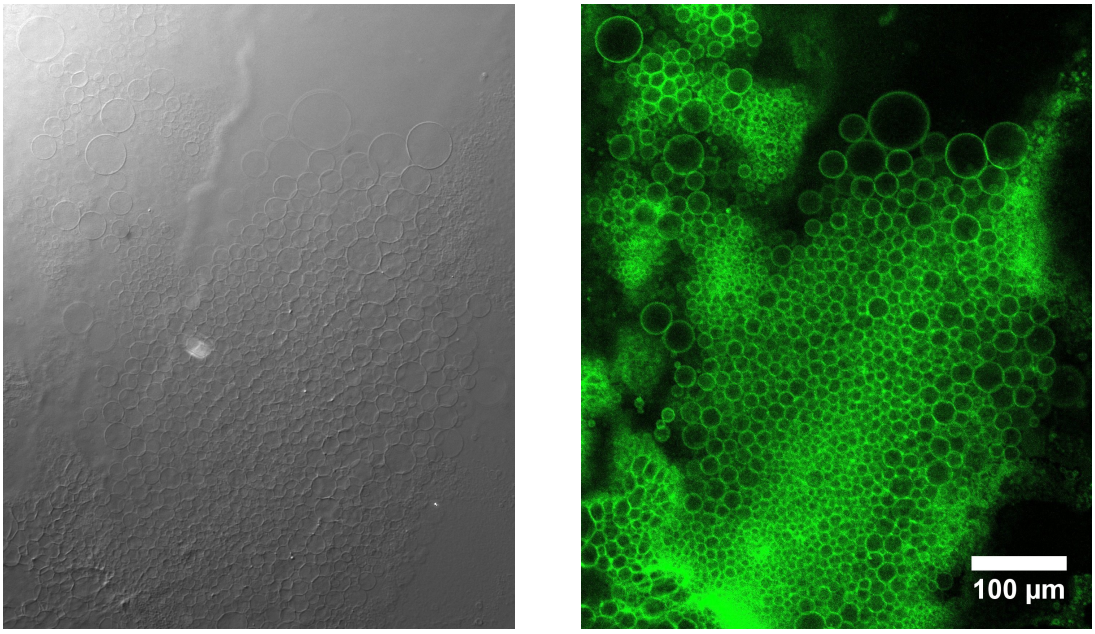

Figure 10.6: GUVs produced with agarose-lipid-hybrid films from SUV emulsions in water. Lipid solution contained 0.13% (w/w) of fluorescent BODIPY-PC. DIC (a) and confocal fluorescence (b) images of the same sample are shown. Brightness of the DIC image was increased by image processing in addition to the usual contrast enhancement.

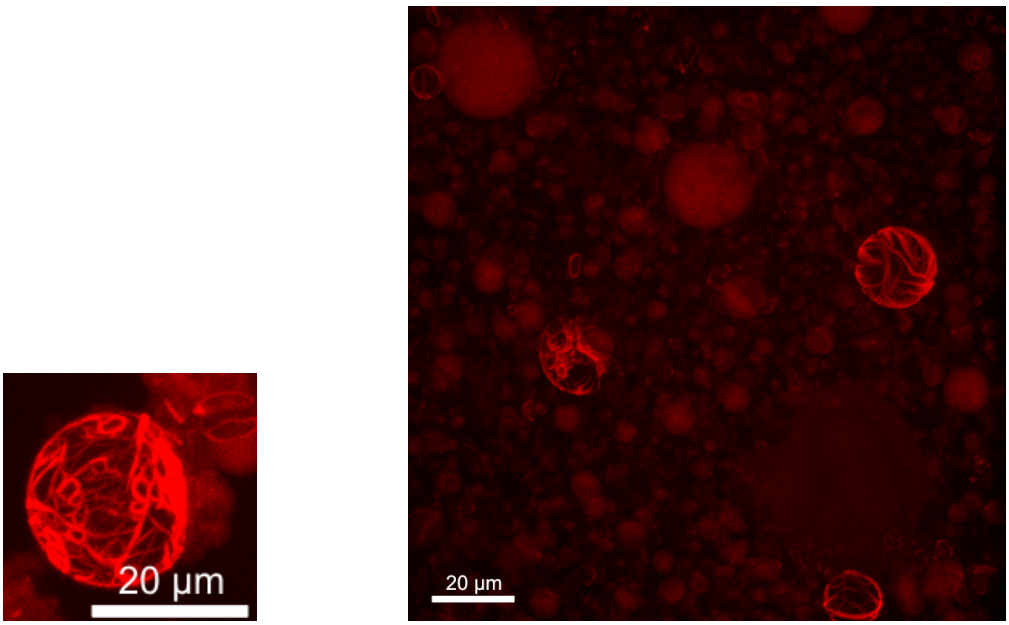

Figure 10.7: Examples of GUVs filled with actin. Z-stacks imaged with the confocal spinning disc microscope were projected into one plane with image processing software (Volocity, Perkin Elmer). Actin was stained with Alexa Fluor 647 phalloidin.
(a) A single GUV enclosing an actin network.
(b) Broader overview of the sample depicting GUVs of various diameters with homogeneous actin distribution or actin networks inside.

10.4 Enclosure of Actin in GUVs

The cytoskeletal protein actin was enclosed in GUVs by electroformation on ITO-coated glass. Actin was added in its monomeric form to the buffer in which giant vesicles were grown. When platinum wires were utilized as electrodes instead of ITO, no actin could be detected inside of GUVs by staining of actin with fluorescently-labeled phalloidin. Actin was polymerized inside of the GUVs by addition of $MgCl_2$ to the outer buffer and the transport of the divalent cations was enabled across the membrane by the ionophore A23187 (figure 10.7). Some GUVs exhibited interconnected actin networks visualized with fluorescent staining of actin (figure 10.7a,b), while others showed homogeneous fluorescence indicating that no polymerization occurred (figure 10.7b).

GUVs filled with actin were produced employing electroformation with ITO-coated glass slides. No dependence of the morphology of actin networks was observed in this study, as suggested in [104]. GUVs larger than 20 µm exhibited homogeneous fluorescence of fluorescently labeled phalloidin, but most smaller vesicles did so, too. However, the organization of actin networks was not investigated in detail. The

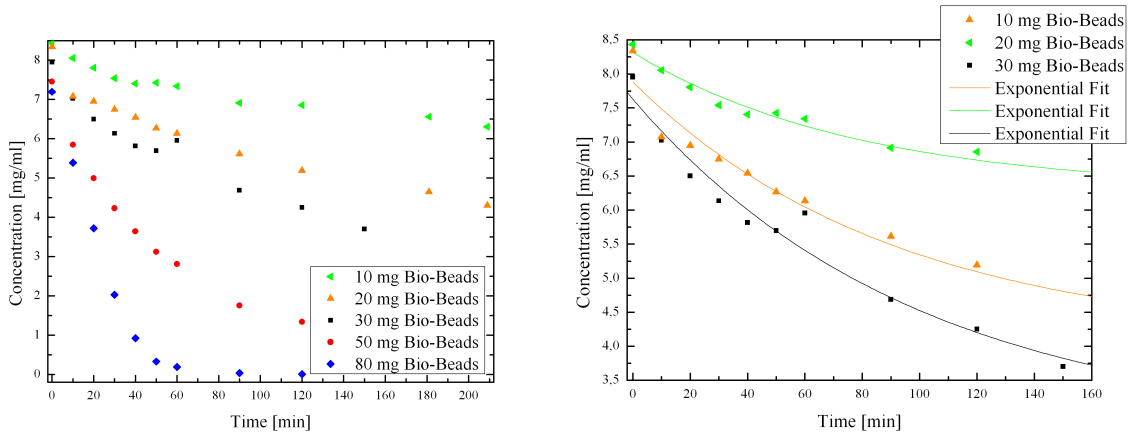

Figure 10.8: (a) Adsorption kinetics of Triton X-100 to various amounts of Bio-Beads. (b) Fit of an exponential decay to adsorption kinetics of Triton X-100 to Bio-Beads.

enclosure of actin in giant vesicles most likely did not work with platinum wires due to the much smaller surface area of lipid layers compared to ITO-coated glass slides. The smaller area reduces the probability to enclose large amounts of actin. As only F-actin is easily detectable with fluorescent phalloidin, GUVs might even contain monomeric actin inside with a concentration below the critical polymerization concentration.

10.5 Preparation of Integrin-GUVs from Proteoliposomes

10.5.1 Adsorption of Triton X-100 to Bio-Beads

The kinetics of adsorption of Triton X-100 on Bio-Beads was measured. Five different amounts of beads were added to a solution of Triton X-100. Higher amounts of beads not only adsorbed more Triton X-100 from solution, but also led to faster kinetics. Below 50 mg of beads, part of Triton remained in solution and its concentration reached a plateau. The difference of the plateau to initial concentration of Triton led to corresponding binding capacities. Addition of 50 mg and 80 mg Bio-Beads resulted in the removal of Triton X-100 below the limit of detection (figure 10.8a).

An exponential decay (equation (6.1)) was fitted to the data and the binding capacity was calculated from plateau value and amount of beads according to equation (6.2). Measured capacities are summarized in table 10.3.

The average amount of Triton X-100 adsorbed on 1 g of Bio-Beads was calculated

Table 10.3: Binding capacity C_B of Bio-Beads for Triton X-100 as measured with different amounts m_i of beads added to 1 ml of a $8\,\mathrm{mg\,ml^{-1}}$ Triton X-100 solution.

m_i/mg	C_B/ (mg g^{-1})
10	213
20	214
30	175

as the mean of binding capacities in table 10.3 resulting in:

$$\bar{C}_B = 201 \pm 22\mathrm{mg\,g^{-1}} \tag{10.1}$$

In this control experiment, a binding capacity of Bio-Beads for Triton X-100 of $201\,\mathrm{mg\,g^{-1}}$ was measured. This result confirms a binding capacity of $185\,\mathrm{mg\,g^{-1}}$ obtained by more accurate and more complex measurements using radioactive labeling of Triton X-100 [114]. An earlier reported value of $70\,\mathrm{mg\,g^{-1}}$ [76] can be ruled out. The former value was therefore used to calculate the amount of Bio-Beads, that had to be added to emulsions of SUVs treated with different amounts of Triton X-100.

10.5.2 Solubilization of Vesicles by Triton X-100

Preformed vesicles are mixed with detergent. Depending on the amount of detergent they are partly or completely solubilized to allow the insertion of membrane proteins. Solubilization depends on the detergent and the lipid mix of the vesicles' bilayer (section 3.3). Measurement of turbidity of vesicle emulsions allows the determination of the degree of solubilization. Turbidity was measured at 500 nm with a spectrophotometer. Three experiments were performed with a concentration of lipid of $6.25\,\mathrm{mg\,ml^{-1}}$ and one experiment with $5\,\mathrm{mg\,ml^{-1}}$. Data was normalized to the turbidity without detergent and turbidity at $20\,\mathrm{mmol\,l^{-1}}$ was subtracted as blank value. This subtraction is the reason for negative values of turbidity, which were not measured in experiment and have no physical meaning. Except from experiment A, turbidity decreased even at lowest concentrations of added Triton X-100 (figure 10.9). Emulsions became transparent, corresponding to complete solubilization of SUVs, between 7 and $13\,\mathrm{mmol\,l^{-1}}$. As kinetics of solubilization depend on temperature [53], samples were adjusted to 25 °C throughout experiment D. No significant change of solubilization was detected despite temperature control. The theoretical curve shown in figure 3.6 was nicely reproduced in experiment A. First, the addition of detergent did not change turbidity very much indicating mostly intact SUVs. Decrease of turbidity, as a sign of disintegration of vesicles, started at about $5\,\mathrm{mmol\,l^{-1}}$ Triton X-100, finally resulting in the complete solubilization of SUVs at approximately $15\,\mathrm{mmol\,l^{-1}}$ of Triton (data depicted in red in figure 10.9).

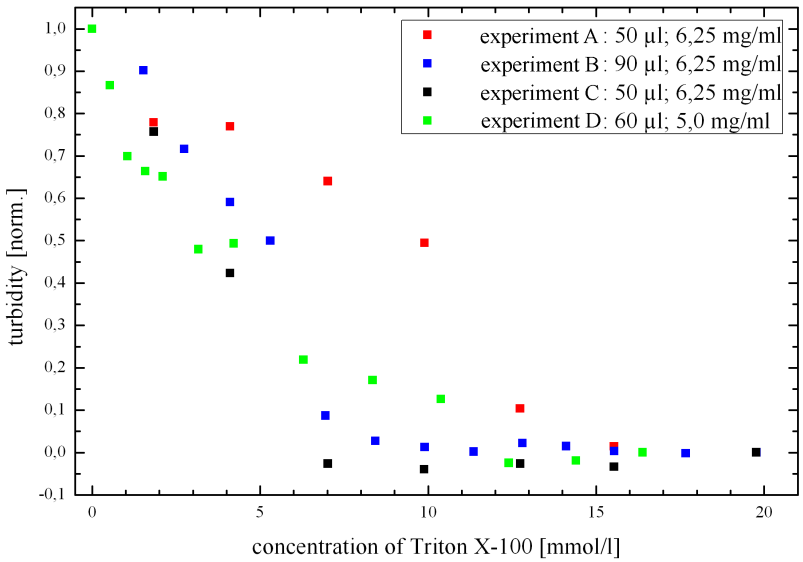

Figure 10.9: Solubilization of SUVs by addition of Triton X-100. Turbidity of emulsions of SUVs was measured with increasing amounts of detergent. Three experiments were performed with a concentration of lipid of 6.25 mg ml^{-1} and one experiment with 5 mg ml^{-1}. The legend specifies the date of the experiment, the volume of sample per well of the microwell plate and the concentration of lipid in the vesicle emulsion.

Small vesicles prepared with the *Standard* lipid mixture (see table 10.1) at a concentration of $5\,\mathrm{mg\,ml^{-1}}$ are saturated with Triton X-100 at a concentration of about $4\,\mathrm{mmol\,l^{-1}}$ using detergent-lipid ratios reported in literature [165]. Complete solubilization should occur at approximately $15\,\mathrm{mmol\,l^{-1}}$. The molar concentration of lipid is calculated using an average molecular weight deduced from molar ratios and molecular weight of the mixture's lipid components. The measurement of turbidity of SUV emulsions with increasing amounts of Triton X-100 confirms these values by tendency. Below $4\,\mathrm{mmol\,l^{-1}}$ of Triton, most of the SUVs seem to be still intact as inferred from the still high turbidity. Above $15\,\mathrm{mmol\,l^{-1}}$ of Triton, vesicles are destroyed and lipids are dissolved in mixed lipid-detergent micelles leading to a transparent sample. Thus, volumes of diluted solutions of Triton X-100 added to SUV emulsions were adjusted to result in final concentrations of about 4.0, 9.0 and $15.5\,\mathrm{mmol\,l^{-1}}$ for the reconstitution of integrin $\alpha_{\mathrm{IIb}}\beta_3$.

10.5.3 Preparation of Integrin-GUVs from Proteoliposomes Using Electroformation or Agarose-Lipid-Hybrid Films

GUVs were prepared by electroformation according employing proteoliposomes as starting material. Proteoliposomes contained integrin $\alpha_{\mathrm{IIb}}\beta_3$ as indicated by density gradient centrifugation. For the reconstitution, Triton X-100 was added to a final concentration of $10.0\,\mathrm{mmol\,l^{-1}}$ to preformed SUVs. Integrin was fluorescently labeled to allow its detection with confocal microscopy. Fluorescent BODIPY-PC was additionally added to the lipid mixture in order to visualize the bilayer. Images acquired with laser scanning microscopy showed a co-localization of integrin and lipid fluorescence (figures 10.10 and 10.11). Some of the lipid layers detached from the platinum wires and allowed giant vesicles to grow in between the wires (figure 10.10).

Bright spots of TAMRA fluorescence were observed directly at the platinum wires even in areas where the fluorescent signal of BODIPY was not significantly increased (see arrows in figure 10.11). The overall intensity of fluorescence inside of the membranes of GUVs was quite low regardless of whether TAMRA or BODIPY emission was detected. Cross-talk between different fluorescence channels was excluded by sequential scanning and non-overlapping absorption and emission spectra of the dyes utilized for labeling.

Agarose-lipid-hybrid films were also checked for their use to prepare GUVs from proteoliposomes. Giant vesicles showed very inhomogeneous fluorescence. Clusters of high intensity of fluorescently labeled integrin were observed without vesicle-like structures being detectable in the vicinity by DIC (see arrows in figures 10.12b and 10.12d). Some GUVs did not contain any fluorescent integrin (encircled in figures 10.12b and 10.12d). Multilamellar and vesicle-inside-vesicle structures were also found in the samples (especially 10.12b, for example inside of the white rectangle).

Images above clearly show that GUVs can be prepared from proteoliposomes either

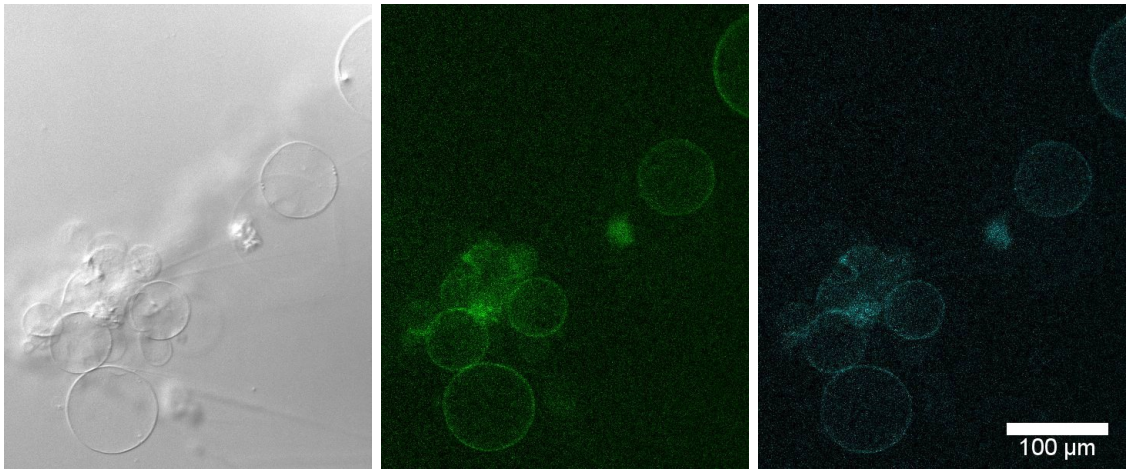

Figure 10.10: GUVs prepared from proteoliposomes using electroformation with platinum wires. The giant vesicles, shown in the image, grew in solution between the wires not directly on the electrodes. The lipid bilayer was labeled using BODIPY-PC. Integrin $\alpha_{\mathrm{IIb}}\beta_3$ was conjugated to the dye TAMRA for visualization. DIC (a), BODIPY (b) and TAMRA fluorescence (c) are shown. Fluorescence of TAMRA is depicted in false color.

by electroformation or by agarose-lipid-hybrid films. Both methods produced giant vesicles with diameters around 30 µm. Fluorescence of TAMRA-labeled integrin co-localized with the bilayer of vesicles. Spontaneous swelling of agarose-lipid-hybrid films also produced structures which were not unilamellar. The parameters of the agarose-method should thus be investigated in more detail.

10.5.4 Characterization of Proteo-GUVs

As shown above, GUVs were prepared from proteoliposomes with integrin $\alpha_{\mathrm{IIb}}\beta_3$ embedded in their membrane. Images of these giant vesicles acquired with confocal laser scanning microscopy strongly indicate, that fluorescently labeled integrin was also incorporated in their bilayer (figures 10.10, 10.11 and 10.12). However, intensity of fluorescence was close to the detection limit. Electrical amplification of the signal, measured with the photomultiplier tube of the confocal microscope, was almost at its maximum (at about 1100 V of 1250 V). Even though, contrast of images had to be enhanced using image processing software for integrin fluorescence to be easily visible. Fluorescent integrin seems to agglomerate in clusters, especially at the platinum wire (figure 10.11b), but also with agarose-lipid-hybrid films highly fluorescent spots were observed (figures 10.12b and 10.12d).

To clarify whether integrin was inserted in membranes or not, immuno-staining of integrin was attempted. Only few GUVs were found in micro-channels used for

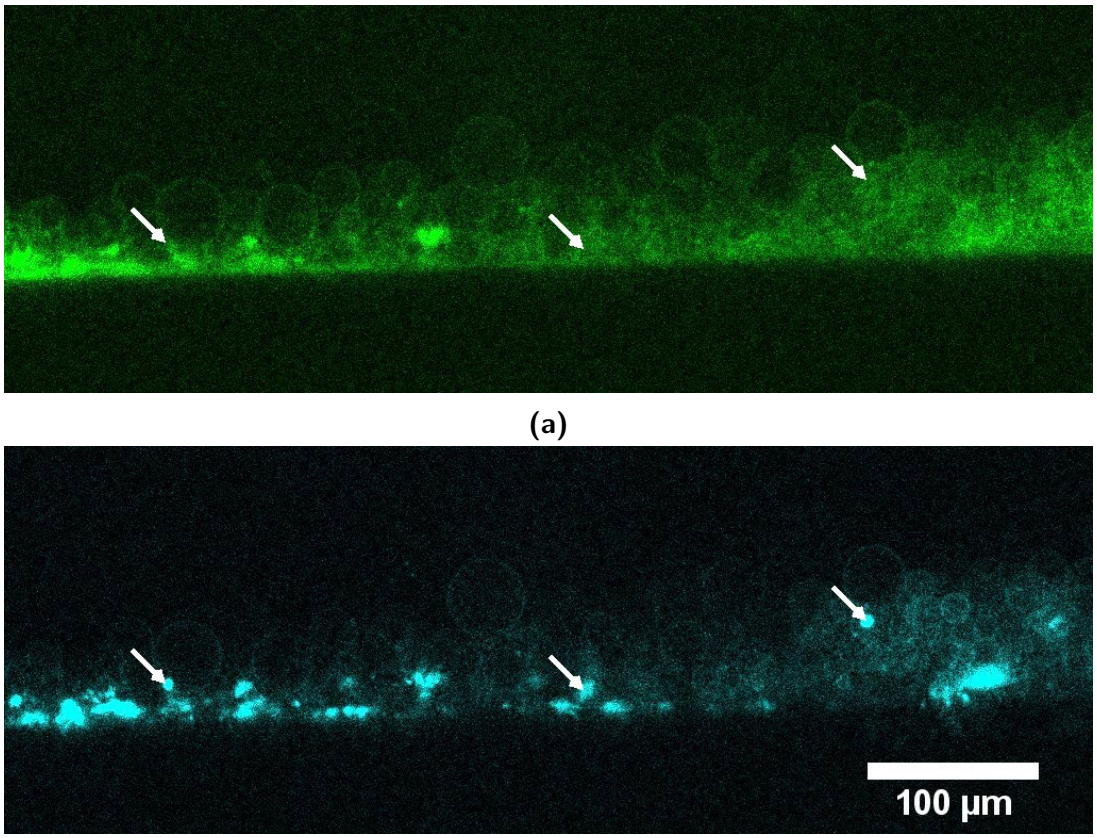

Figure 10.11: Giant vesicles from proteoliposomes attached to platinum wires that were used to grow them via electroformation. BODIPY fluorescence (a) marks lipid bilayers while integrin was labeled with TAMRA (b; false color). Arrows mark selected positions of high fluorescence of TAMRA without a corresponding increase of BODIPY intensity.

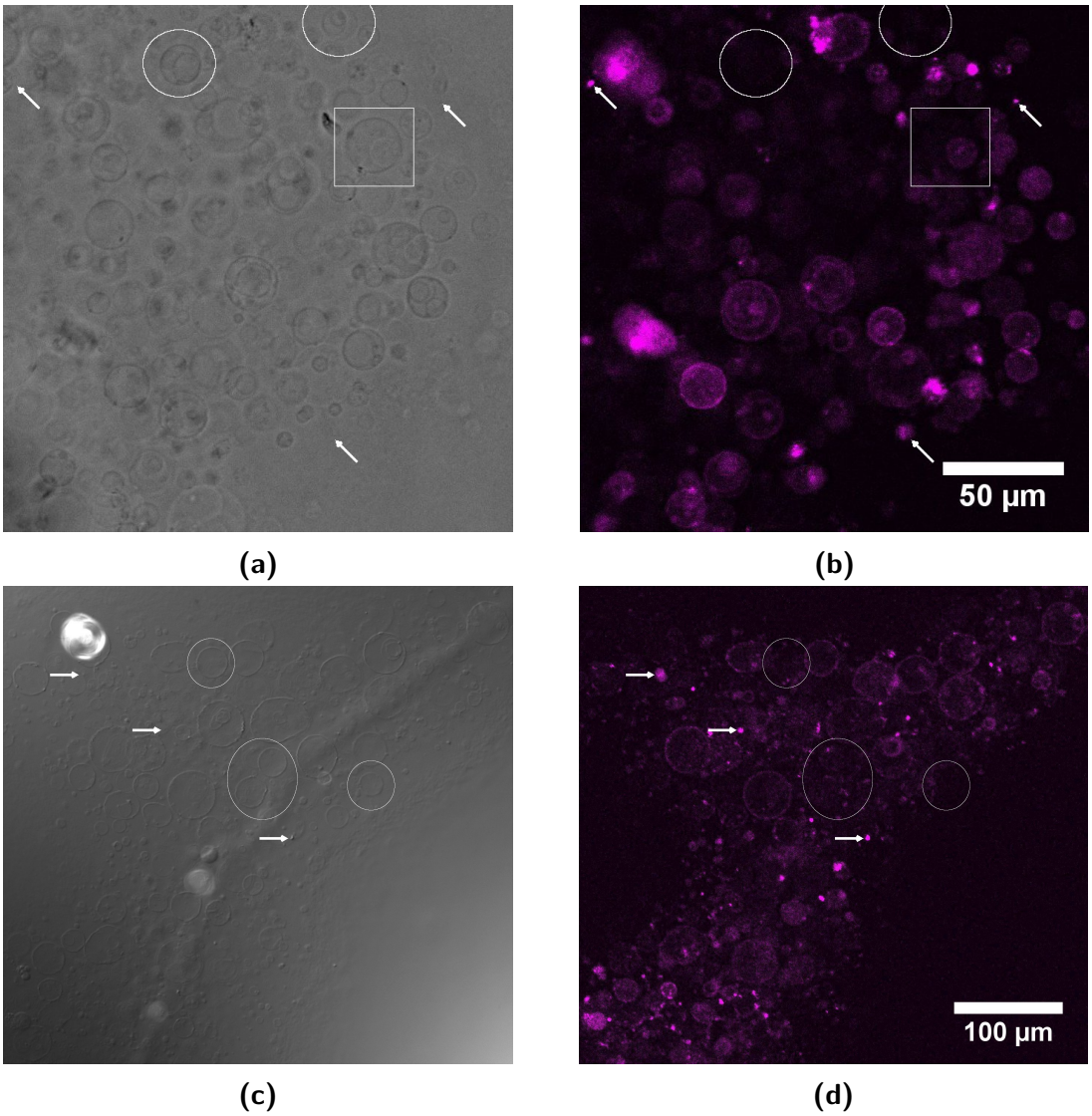

Figure 10.12: GUVs prepared from agarose-proteoliposome-hybrid films. Integrin $\alpha_{\mathrm{IIb}}\beta_3$ was labeled with the dye TAMRA for visualization. DIC (a,c) and TAMRA fluorescence (b,d; false color) are shown. Arrows mark selected positions of high fluorescence of TAMRA without a visible signal in DIC. Circles indicate areas, where GUVs were observed in DIC, but no fluorescence of TAMRA was detected. In the region framed by a white rectangle, a smaller fluorescent vesicle is enclosed in a giant vesicle without fluorescently labeled integrin in its bilayer.

staining after a complicated procedure with several steps of washing. No fluorescence of the secondary, fluorescently labeled antibody could be detected.

Integrin $\alpha_{\mathrm{IIb}}\beta_3$ was reconstituted into giant unilamellar vesicles, as illustrated by images from fluorescence microscopy using fluorescently labeled integrin (figures 10.10, 10.11 and 10.12). However, results indicate only a low concentration of integrin in the bilayer of these GUVs. Their adhesion was not sufficient on surfaces homogeneously coated with fibrinogen in micro-channels to withstand low flow rates. These micro-channels were used for immuno-labeling of integrin in bilayers of GUVs. Immuno-staining also could not verify the presence of integrin in the membrane of giant vesicles. However, a minimum amount of integrin inserted in bilayers of giant vesicles is a prerequisite to induce measurable effects in experiments investigating the adhesion of integrin-containing GUVs on adhesive surfaces. Thus, preparation of GUVs from purified platelet membranes was examined in more detail.

10.6 Preparation of GUVs from Platelet Membranes

GUVs were prepared from native platelet membranes, which were purified as described in section 8.1. Electroformation allowed the production of GUVs either with ITO-coated glass slides (figure 10.13a) or platinum wire (figure 10.13b) as electrodes. Generally, platinum wires were employed because of their higher yield of giant vesicles. As concentration of platelet membranes could not be determined very accurately, different concentrations of membranes were tested regarding their GUV yield after each purification. Typically, an emulsion of about $10\,\mathrm{mg\,ml^{-1}}$ platelet membranes in buffer produced largest vesicles up to $40\,\mu\mathrm{m}$ in diameter with the highest yield. Even though, preparation of GUVs from platelet membranes was never equally effective as preparation from suspensions of vesicles with or without integrin incorporated in their bilayers.

Purified platelet membranes contain a high amount of integrin $\alpha_{\mathrm{IIb}}\beta_3$ besides other, unidentified membrane proteins as observed in SDS-PAGE. In intact platelets, the average distance between two molecules of integrin $\alpha_{\mathrm{IIb}}\beta_3$ is about 20 nm [29]. GUVs from purified platelet membranes are therefore expected to contain more integrin in their bilayer than giant vesicles produced with proteoliposomes, in which integrin was reconstituted. The presence of integrin in the bilayers of giant vesicles prepared from platelet membranes was examined indirectly by comparison of their adhesion on passivated and adhesive surfaces.

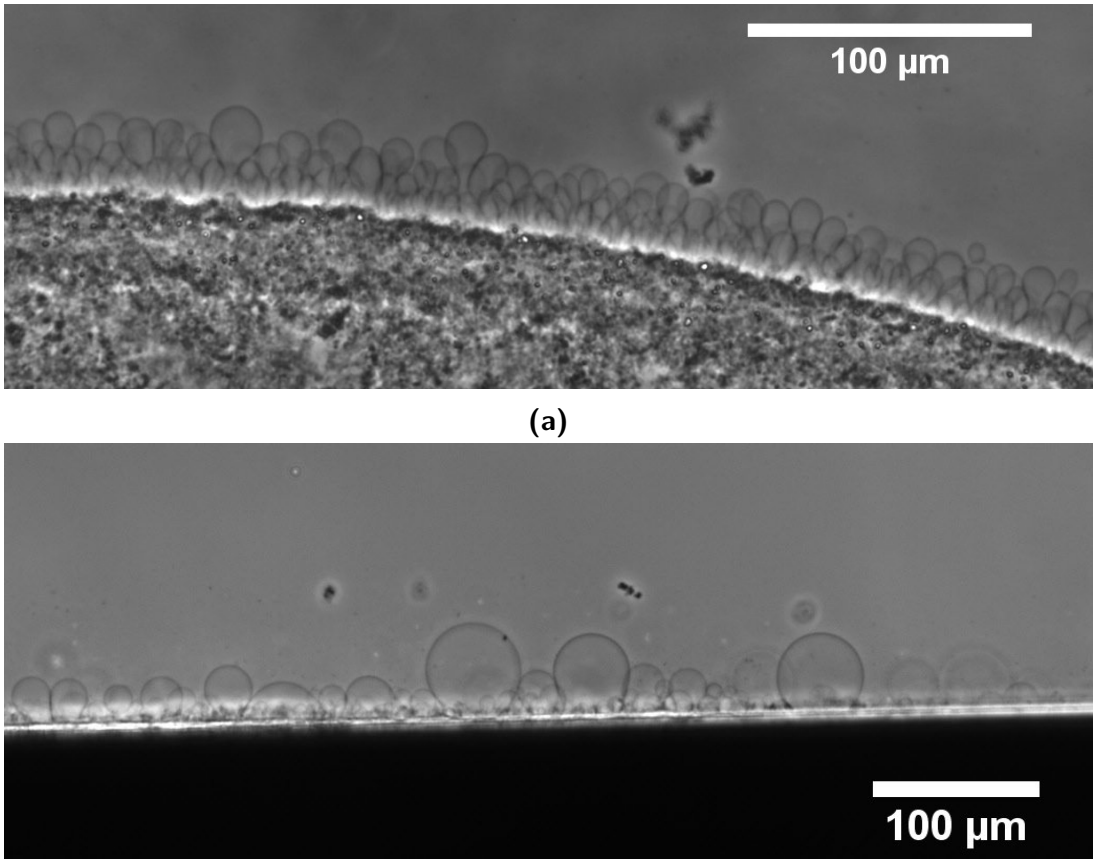

Figure 10.13: GUVs produced from native platelet membranes on ITO-coated glass (a) and platinum wire (b).

11 Adhesive Properties of the Model System

In order to characterize the adhesion of platelet membrane derived GUVs to various surfaces, these GUVs were allowed to sediment to biologically functionalized substrates. Preliminary experiments showed, that around 90% of GUVs burst upon interaction with bare glass surfaces. Additionally, enhanced contrast in phase contrast microscopy due to different indexes of refraction of inner and outer buffer was lost in most giant vesicles over a time span of about 15 min. This loss of contrast indicates leakage of vesicles: The sucrose-containing inner buffer and the glucose-containing outer buffer mixed because of diffusion and osmotic gradients. The membrane structure of platelets is known to allow the passage of small molecules [169].

Glass surfaces, homogeneously coated with casein or fibrinogen, were tested for their passivating or adhesive properties for "platelet-GUVs". On fibrinogen, those giant vesicles making contact with the surface burst and spread on the substrate in less than 2 min. The spreading was most likely caused by the strong interaction of integrin $\alpha_{\mathrm{IIb}}\beta_3$ with fibrinogen. GUVs were stable on casein for about one day, but took the form of a spherical cap after incubation for several hours. This half-sphere shape suggests an, albeit weak, interaction between casein and platelet membrane proteins or lipids present in the bilayer of the GUVs. Therefore, casein is not suitable for passivation in adhesion experiments with platelet derived GUVs. Spreading on fibrinogen prevented investigation of adhesion. To be able to tune interaction strength by control of ligand density, bio-functionalized, nano-structured glass surfaces were studied.

11.1 GUVs from Platelet Membranes on Nanostructured Surfaces

To elucidate the dependence of adhesion energy on ligand density, RGD-functionalized nano-patterns were utilized exhibiting "low" and "high" ligand density as defined in section 7.3.2. As a control, adhesion of platelet giant vesicles was investigated on nano-structured surfaces passivated with PEG without a ligand molecule.

In each experiment, giant vesicles were assigned floppy or tense vesicles according to their morphology in phase contrast images. Floppy GUVs exhibited strongly os-

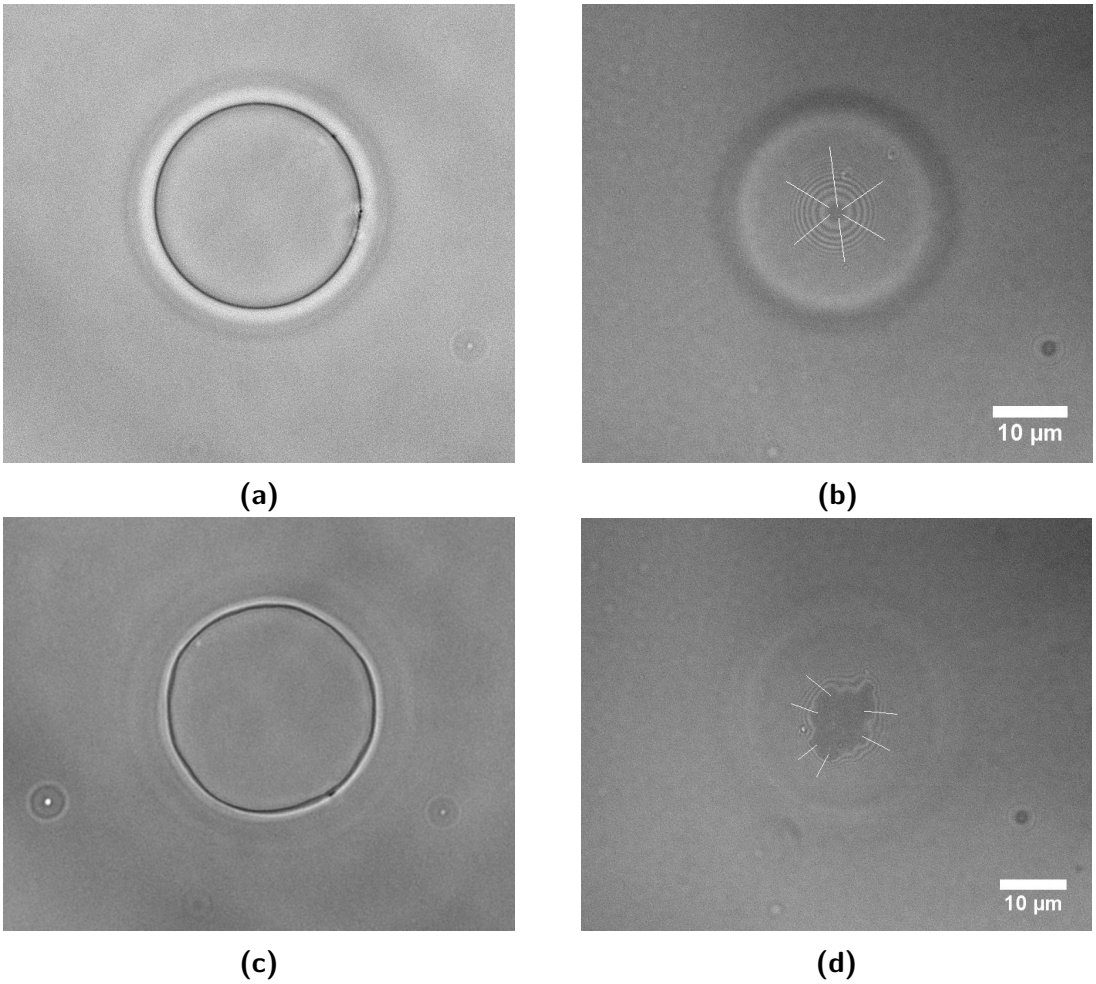

Figure 11.1: Representative phase contrast (a,c) and RICM (b,d) images of typical tense (a,b) and floppy (c,d) giant unilamellar vesicle that lay on PEG-passivated nano-structured glass surfaces.

cillating bilayers (figures 11.1c and 11.2c), while tense vesicles were strictly spherical (figures 11.1a and 11.2a). About 30 to 40% of a sample were floppy giant vesicles. The interference pattern of tense GUVs was built from concentric circular rings (figures 11.1b and 11.2b) in contrast to more tattered shapes of floppy giant vesicles (figures 11.1d and 11.2d). This overall appearance did not depend on the surface functionalization and was observed for both tested distances of ligands. The size of giant vesicles also did not substantially influence the geometry of interference fringes. However, no floppy GUVs larger than 20 µm in diameter were observed on RGD-functionalized substrates.

To quantify adhesion, a number of four giant vesicles was measured for the passivated, "low" and "high" density substrates and membrane morphology. On pas-

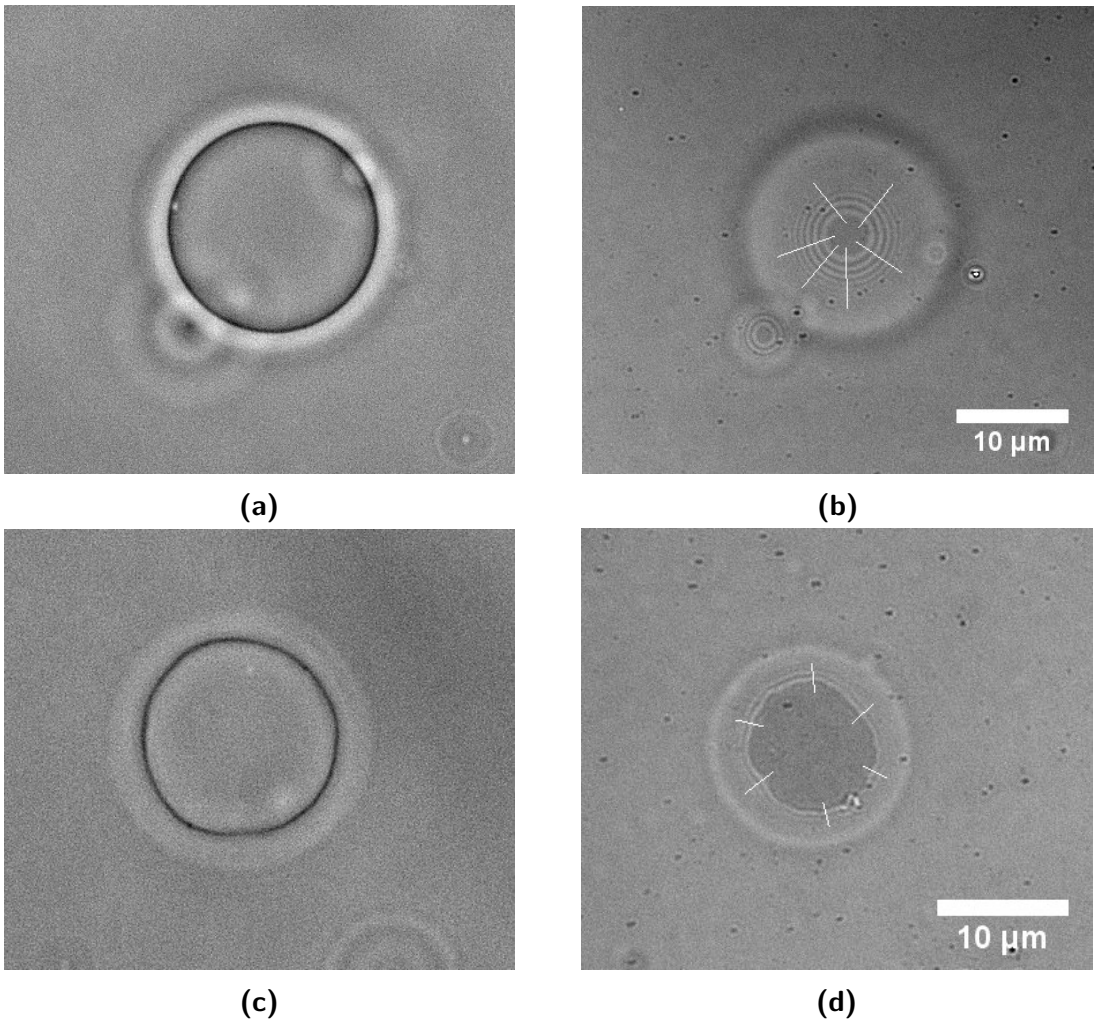

Figure 11.2: Representative phase contrast (a,c) and RICM (b,d) images of tense (a,b) and floppy (c,d) giant vesicles on "high" density, RGD-functionalized nano-structured glass surfaces. The general shape of vesicles and contact area did not significantly depend on ligand density.

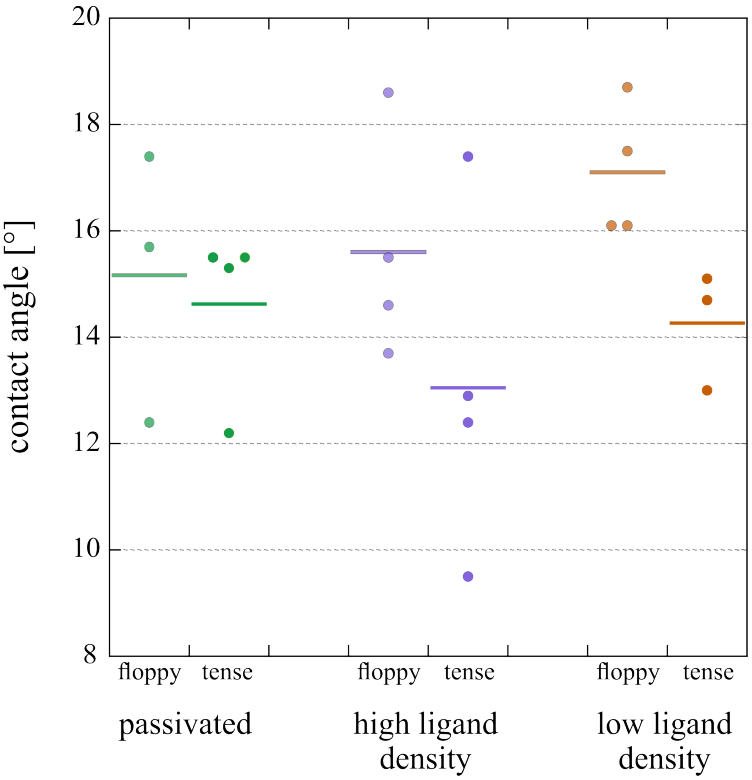

Figure 11.3: Contact angle of GUVs from platelet membranes on PEG-passivated and RGD-functionalized nano-structured surfaces. GUVs were differentiated into floppy and tense giant vesicles depending on the morphology of their membrane in phase contrast microscopy. Average contact angles of individual GUVs determined from six height profiles are depicted by dots. The horizontal line indicates the mean contact angle.

sivated surfaces only three floppy giant vesicles were found. For tense vesicles on "low" density substrates only three measurements were done. Due to the low yield of GUV preparation from platelet membranes, samples contained only low numbers of giant vesicles. The low concentration of vesicles made it extremely difficult to find suitable GUVs in the small field of view of the 63x oil-immersion objective. For each GUV, an average contact angle was calculated from six height profiles along lines perpendicular to the interference pattern, as shown for instance in figure 11.2d. This macroscopic contact angle is a measure for the strength of a vesicle's interaction with a surface. The mean contact angle of all GUVs of one measurement did not significantly deviate from 15° regardless of substrate properties or membrane morphology (figure 11.3). By tendency, the contact angle of floppy GUVs was slightly larger of tense giant vesicles on adhesive surfaces. The morphology of the membrane did not affect the contact angle of giant vesicles on passivated surfaces.

The effective adhesion energy was estimated to 1.4×10^{-7} to $2 \times 10^{-6}\,\mathrm{J\,m^{-2}}$ using a membrane tension of $1 \times 10^{-6}\,\mathrm{N\,m^{-1}}$ [130].

Adhesion of GUVs from platelet membranes apparently did not lead to specific adhesion of the giant vesicles to RGD as indicated by not significantly different contact angles between passivated and adhesive substrates. Adhesion leads to an increase of the area of contact, which in turn leads to a growing membrane tension. In equilibrium membrane tension balances adhesion energy. Therefore, floppy vesicles naturally have larger contact areas and higher contact angles than vesicles with a tense membrane. The estimated effective adhesion energy is not very instructive, because its order of magnitude solemnly depends on the membrane tension. The membrane tension should be measured independently.

Leakage and subsequent loss of contrast in the phase contrast images of GUVs did not interfere with the determination of the contact angle, because no absolute heights were measured. The change of the refractive index of the inner buffer affects the value of the constant h_0, but not the determination of the overall shape of giant vesicles.

12 Conclusive Remarks and Further Experiments

Understanding of cell adhesion is important not only for basic research, but also it has major implications in medical sciences potentially leading to new therapies. Simplified model systems are a prerequisite for experimental analysis of physical mechanisms underlying cell adhesion. Such a system was developed in this study reducing cellular complexity to three essential components: the lipid bilayer, the cell adhesion molecule integrin and the cytoskeletal protein actin.

Established protocols for the purification of integrin $\alpha_{\mathrm{IIb}}\beta_3$ and muscle actin were adapted to the equipment and conditions in the lab. Relevant methods for the biochemical analysis of these proteins were optimized and refined. The newly conceived protocol for Western blotting of integrin $\alpha_{\mathrm{IIb}}\beta_3$ allowed its highly specific detection. Using ELISA, calibrated gel filtration and co-immunoprecipitation, it could be demonstrated that integrin was purified as a functional heterodimer. Purified actin assembled to F-actin by addition of adenosine triphosphate and calcium ions confirming purification of a functional form of G-actin. Thus, preparation of sufficient amounts of functional protein was set up allowing to use integrin and actin as starting material for further investigations.

Efficiency of incorporation of integrin in small vesicles was enhanced by determination of crucial parameters for integration. To this end, incorporation was analyzed in dependence of lipid composition, vesicle size and detergent concentration employing density gradient centrifugation. Interaction of integrin with membranes of SUVs was unequivocally shown.

Integrin-coated small vesicles were grown to giant unilamellar vesicles by two different approaches. Electroformation and spontaneous swelling on agarose-lipid films were compared. Formation of GUVs was investigated by means of confocal laser scanning microscopy confirming successful integration of fluorescently labeled integrin into the bilayer of the giant vesicles.

Knowledge from the detailed investigation of electroformation was used and transferred to establish a novel method for the preparation of GUVs from purified platelet membranes. Purification of platelet membranes was optimized. Concentration of membranes and preparation of homogeneous lipid layers on platinum electrodes were found to be key parameters for the successful production of giant vesicles with good yield. Interaction of these "platelet-GUVs" with nano-structured and biofunctionalized surfaces was investigated in detail. Their adhesion was characterized

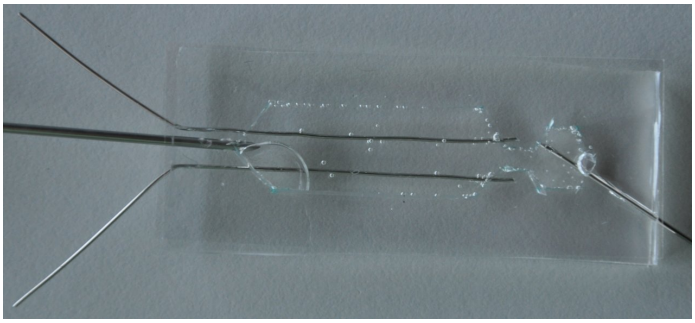

Figure 12.1: Preliminary design of swelling chamber with platinum wires allowing the exchange of buffer.

for the first time by RICM, which allowed estimation of an average adhesion energy.

This work lays a broad and solid basis for further research in the field of synthetic model systems of cell adhesion and cell mechanics. It is a first, essential step on the way to more complex model systems.

However, insertion of integrin in GUVs has to be verified by cryo-transmission electron microscopy. Preliminary experiments were already conducted in the group of Prof. O. Medalia at the University of Zurich. The mere attachment of integrin to the bilayer of vesicles could also be ruled out by alkaline wash, urea treatment and partitioning of Triton X-114 [60]. Samples could then be analyzed for their protein content in SDS-PAGE. Immunostaining directly in swelling chamber could also help to proof integrin incorporation. A preliminary design of a flow cell combined with platinum wires for electroformation is depicted in figure 12.1. Antibodies or RGD-peptides functionalized with quantum dots might lead to bright and stable fluorescence allowing to detect even low amounts of integrin in GUVs bilayers.

For a more insightful characterization of the adhesion of the model systems, the evaluation of RICM images should be optimized by numerically interpolating the data obtained from intensity-line-profiles. So far, the number of data points is limited by the number of pixels along one line (see figure 7.6b). Interpolation would increase the number of data points and allow a more precise determination of the position of extrema. Thereby, smoother height profiles could be obtained, as compared to, for example, figure 7.6c. The "local" membrane tension could then be determined by deducing the capillary length from the height profile [6] and measuring the bending stiffness of the membrane in a separate experiment using micro-pipette aspiration [48] or flicker analysis [122]. This procedure would give a more useful estimation of adhesion energy. Additionally, contrast in RICM could be enhanced by coating of glass surfaces with MgF_2 [161, 217]. For high precision measurements of the height profiles, thickness-corrected glass slides should be used.

The bottom-up approach used in this study of course allows to add more proteins to mimic focal adhesions [226, 227]. Talin should be one of the first candidates as it is an adaptor protein linking integrin and actin. Furthermore, regulatory effects of lipids like phosphoinositides could also be addressed using the developed model system [118, 136].

It is well known, that platelets influence tumor progression and metastasis [61]. The model system "platelet"-GUVs might help to dissect the effect and influence of integrin $\alpha_{\mathrm{IIb}}\beta_3$ and other factors without interference of active biological processes. As human platelets cannot be produced *in vitro* or cultured [169], GUVs from purified platelet membranes might even have therapeutic use.

Abbreviations

2D	two dimensional
3D	three dimensional
AP	alkaline phosphatase
AC	alternating current
AFM	atomic force microscopy
APD	avalanche photodiode
APS	ammonium persulfate
BCA	bicinchoninic acid
BCIP	5-bromo-4-chloro-3-indolyl phosphate
brainPS	phosphatidylserine purified from porcine brain
BSA	bovine serum albumin
CAM	cell adhesion molecule
CCD	charged coupled device
CMC	critical micelle concentration
ConA	concanavalin A
DC	direct current
DIC	differential interference contrast
co-IP	co-immunoprecipitation
DLS	dynamic light scattering
DNA	deoxyribonucleic acid
DP	dipalmitoyl
DTT	dithiotriole
ELISA	enzyme linked immunosorbent assay
ECM	extracellular matrix
EDTA	ethylenediaminetetraacetic acid
eggPA	phosphatidic acid purified from egg yolk
eggPC	phosphatidylcholine purified from egg yolk
FA	focal adhesion
fab	fragment antigen binding
fc	fragment crystallizable
fg	fibrinogen
GUV	giant unilamellar vesicle
IP	immunoprecipitation
ITO	indium tin oxide
LUV	large unilamellar vesicle

NBT	p-nitro-tetrazolium blue
NTA	nitrilotriacetic acid
PA	phosphatidic acid
PAGE	polyacrylamide gel electrophoresis
PALM	photoactivated localization microscopy
PC	phosphatidylcholine
PE	phosphatidylethanolamine
PS	phosphatidylserine
NPP	para-nitrophenylphosphate
PDMS	poly(dimethylsiloxane)
PEG	poly(ethylene glycol)
PET	poly(ethylene terephthalate)
PLL	poly-L-lysine
PMT	photomultiplier tube
PVDF	polyvinylidene fluoride
RGD	arginine-glycine-aspartic acid
RICM	reflection interference contrast microscopy
r.t.	room temperature
SDS	sodium dodecyl sulfate
SLB	supported lipid bilayer
SUV	small unilamellar vesicle
TAMRA	carboxytetramethylrhodamine
TEM	transmission electron microscopy
TEMED	tetramethylethylenediamine
TIRF	total internal reflection fluorescence
UV	ultraviolet

List of Figures

List of Tables

Bibliography

The bibliography is sorted by name of first author. For documents from the internet their URL is specified. The availability of the homepages was last checked on September 24th 2012.

[1] Abedin, M., and King, N. Diverse evolutionary paths to cell adhesion. *Trends in Cell Biology 20*, 12 (2010), 734–742. doi:10.1016/j.tcb.2010.08.002.

[2] Adair, B., and Yeager, M. Three-dimensional model of the human platelet integrin $\alpha_{IIb}\beta_3$ based on electron cryomicroscopy and x-ray crystallography. *Proceedings of the National Academy of Sciences 99*, 22 (2002), 14059–14064. doi:10.1073/pnas.212498199.

[3] Aimon, S., Manzi, J., Schmidt, D., Larrosa, J., Bassereau, P., and Toombes, G. Functional reconstitution of a voltage-gated potassium channel in giant unilamellar vesicles. *PloS one 6*, 10 (2011), e25529. doi:10.1371/journal.pone.0025529.

[4] Akashi, K., Miyata, H., Itoh, H., and Kinosita, K. Preparation of giant liposomes in physiological conditions and their characterization under an optical microscope. *Biophysical Journal 71*, 6 (1996), 3242–3250. doi:10.1016/S0006-3495(96)79517-6.

[5] Akashi, K., Miyata, H., Itoh, H., and Kinosita, K. Formation of giant liposomes promoted by divalent cations: Critical role of electrostatic repulsion. *Biophysical Journal 74*, 6 (1998), 2973–2982. doi:10.1016/S0006-3495(98)78004-X.

[6] Albersdörfer, A., Feder, T., and Sackmann, E. Adhesion-induced domain formation by interplay of long-range repulsion and short-range attraction force: a model membrane study. *Biophysical Journal 73*, 1 (1997), 245–257. doi:10.1016/S0006-3495(97)78065-2.

[7] Alberts, B., Johnson, A., Lewis, J., Raff, M., Roberts, K., and Walter, P. *Molecular Biology of the Cell*, 4. ed. Garland Science, 2002.

[8] Almén, M., Nordström, K., Fredriksson, R., and Schiöth, H. Mapping the human membrane proteome: a majority of the human membrane

proteins can be classified according to function and evolutionary origin. *BMC Biology 7*, 1 (2009), 50. doi:10.1186/1741-7007-7-50.

[9] Andrews, P. Estimation of molecular size and molecular weights of biological compounds by gel filtration. *Methods of Biochemical Analysis 18* (1970), 1–53. doi:10.1002/9780470110362.ch1.

[10] Angelova, M., and Dimitrov, D. Liposome electroformation. *Faraday Discussions of the Chemical Society 81* (1986), 303–311. doi:10.1039/DC9868100303.

[11] Angelova, M., and Dimitrov, D. A mechanism of liposome electroformation. *Progress in Colloid and Polymer Science 76* (1988), 59–67.

[12] Avanti Polar Lipids. Critical Micelle Concentrations. Website. `http://avantilipids.com/index.php?option=com_content&view=article&id=1703&Itemid=422`.

[13] Bacia, K., Schuette, C., Kahya, N., Jahn, R., and Schwille, P. Snares prefer liquid-disordered over "raft"(liquid-ordered) domains when reconstituted into giant unilamellar vesicles. *Journal of Biological Chemistry 279*, 36 (2004), 37951. doi:10.1074/jbc.M407020200.

[14] Bangham, A., Standish, M., and Watkins, J. Diffusion of univalent ions across the lamellae of swollen phospholipids. *Journal of Molecular Biology 13*, 1 (1965), 238–252. doi:10.1016/S0022-2836(65)80093-6.

[15] Battle, A., Petrov, E., Pal, P., and Martinac, B. Rapid and improved reconstitution of bacterial mechanosensitive ion channel proteins mscs and mscl into liposomes using a modified sucrose method. *FEBS Letters 583*, 2 (2009), 407–412. doi:10.1016/j.febslet.2008.12.033.

[16] Batzri, S., and Korn, E. Single bilayer liposomes prepared without sonication. *Biochimica et Biophysica Acta - Biomembranes 298*, 4 (1973), 1015–1019. doi:10.1016/0005-2736(73)90408-2.

[17] Bausch, A., and Kroy, K. A bottom-up approach to cell mechanics. *Nature Physics 2*, 4 (2006), 231–238. doi:10.1038/nphys260.

[18] Behrisch, A., Dietrich, C., Noegel, A., Schleicher, M., and Sackmann, E. The actin-binding protein hisactophilin binds in vitro to partially charged membranes and mediates actin coupling to membranes. *Biochemistry 34*, 46 (1995), 15182–15190. doi:10.1021/bi00046a026.

[19] Bennett, J. Platelet-fibrinogen interactions. *Annals of the New York Academy of Sciences 936*, FIBRINOGEN: XVIth INTERNATIONAL FIBRINOGEN WORKSHOP (2001), 340–354. doi:10.1111/j.1749-6632.2001.tb03521.x.

[20] Berg, J., Tymoczko, J., and Stryer, L. *Biochemie*, 5. ed. Spektrum Akademischer Verlag, Heidelberg, Berlin, 2003.

[21] Berg, R. The indigenous gastrointestinal microflora. *Trends in Microbiology 4*, 11 (1996), 430–435. doi:10.1016/0966-842X(96)10057-3.

[22] Berrier, C., Coulombe, A., Houssin, C., and Ghazi, A. A patch-clamp study of ion channels of inner and outer membranes and of contact zones of e. coli, fused into giant liposomes: Pressure-activated channels are localized in the inner membrane. *FEBS Letters 259*, 1 (1989), 27–32. doi:10.1016/0014-5793(89)81486-3.

[23] Blümmel, J., Perschmann, N., Aydin, D., Drinjakovic, J., Surrey, T., Lopez-Garcia, M., Kessler, H., and Spatz, J. Protein repellent properties of covalently attached peg coatings on nanostructured sio_2-based interfaces. *Biomaterials 28*, 32 (2007), 4739–4747. doi:10.1016/j.biomaterials.2007.07.038.

[24] Boulbitch, A., Guttenberg, Z., and Sackmann, E. Kinetics of membrane adhesion mediated by ligand-receptor interaction studied with a biomimetic system. *Biophysical Journal 81*, 5 (2001), 2743–2751. doi:10.1016/S0006-3495(01)75917-6.

[25] Bärmann, M. private communication, 2009.

[26] Calvete, J. On the structure and function of platelet integrin αIIbβ3, the fibrinogen receptor. *Proceedings of the Society for Experimental Biology and Medicine 208*, 4 (1995), 346–360. doi:10.3181/00379727-208-43863A.

[27] Ces, O., and Mulet, X. Physical coupling between lipids and proteins: a paradigm for cellular control. *Signal Transduction 6*, 2 (2006), 112–132. doi:10.1002/sita.200500079.

[28] Chrambach, A., and Rodbard, D. Polyacrylamide gel electrophoresis. *Science 172*, 3982 (1971), 440–451. doi:10.1126/science.172.3982.440.

[29] Coller, B., and Shattil, S. The GPIIb/IIIa (integrin αIIb β3) odyssey: a technology-driven saga of a receptor with twists, turns, and even a bend. *Blood 112*, 8 (2008), 3011–3025. doi:10.1182/blood-2008-06-077891.

[30] Contreras-Naranjo, J., Silas, J., and Ugaz, V. Reflection interference contrast microscopy of arbitrary convex surfaces. *Applied Optics 49*, 19 (2010), 3701–3712. doi:10.1364/AO.49.003701.

[31] Criado, M., and Keller, B. A membrane fusion strategy for single-channel recordings of membranes usually non-accessible to patch-clamp pipette electrodes. *FEBS Letters 1* (1987), 172–176. doi:10.1016/0014-5793(87)80442-8.

[32] Cuvelier, D., and Nassoy, P. Hidden dynamics of vesicle adhesion induced by specific stickers. *Physical Review Letters 93*, 22 (2004), 228101. doi:10.1103/PhysRevLett.93.228101.

[33] Cuvelier, D., Vezy, C., Viallat, A., Bassereau, P., and Nassoy, P. Mimicking cell/extracellular matrix adhesion with lipid membranes and solid substrates: requirements, pitfalls and proposals. *Journal of Physics: Condensed Matter 16* (2004), 2427–2438. doi:10.1088/0953-8984/16/26/016.

[34] Darszon, A., Vandenberg, C., Schönfeld, M., Ellisman, M., Spitzer, N., and Montal, M. Reassembly of protein-lipid complexes into large bilayer vesicles: perspectives for membrane reconstitution. *Proceedings of the National Academy of Sciences 77*, 1 (1980), 239–243.

[35] Davidson, M.W. (Florida State University). Optical microscopy primer. Website. `http://micro.magnet.fsu.edu/primer/index.html`.

[36] Deamer, D., and Bangham, A. Large volume liposomes by an ether vaporization method. *Biochimica et Biophysica Acta - Biomembranes 443*, 3 (1976), 629–634. doi:10.1016/0005-2736(76)90483-1.

[37] Deibler, M. *Maintaining integrity: Force-induced optimization responses in cells subjected to cyclic tensile strain.* PhD thesis, University of Heidelberg, 2011.

[38] D'Errico, J. inpaint_nans. MATLAB Central File Exchange. `http://www.mathworks.com/matlabcentral/fileexchange/4551`.

[39] Dimitrov, D., and Angelova, M. Swelling and electroswelling of lipids: Theory and experiment. *Studia Biophysica 113*, 1–2 (1986), 15–20.

[40] Dimitrov, D., and Angelova, M. Lipid swelling and liposome formation mediated by electric fields. *Journal of Electroanalytical Chemistry and Interfacial Electrochemistry 19*, 2 (1988), 323–336. doi:10.1016/0022-0728(88)87069-4.

[41] Division of Cell Physiology and Scientific Film, University of Vienna. Lichtmikroskopie online - Theorie und Anwendung. Website. `http://www.univie.ac.at/mikroskopie/index.htm`.

[42] Doeven, M., Folgering, J., Krasnikov, V., Geertsma, E., van den Bogaart, G., and Poolman, B. Distribution, lateral mobility and function of membrane proteins incorporated into giant unilamellar vesicles. *Biophysical Journal 88*, 2 (2005), 1134–1142. doi:10.1529/biophysj.104.053413.

[43] Düzgünes, N. *Liposomes, Part A*, vol. 367 of *Methods in Enzymology*. Academic Press, 2003, ch. Preparation and Quantitation of Small Unilamellar Liposomes and Large Unilamellar Reverse-Phase Evaporation Liposomes, pp. 23–27.

[44] Enoch, H., and Strittmatter, P. Formation and properties of 1000-a-diameter, single-bilayer phospholipid vesicles. *Proceedings of the National Academy of Sciences 76*, 1 (1979), 145–149.

[45] Erb, E., Tangemann, K., Bohrmann, B., Müller, B., and Engel, J. Integrin $\alpha_{IIb}\beta_3$ reconstituted into lipid bilayers is nonclustered in its activated state but clusters after fibrinogen binding. *Biochemistry 36*, 24 (1997), 7395. doi:10.1021/bi9702187.

[46] Estes, D., and Mayer, M. Electroformation of giant liposomes from spin-coated films of lipids. *Colloids and Surfaces B: Biointerfaces 42*, 2 (2005), 115–123. doi:10.1016/j.colsurfb.2005.01.016.

[47] Estes, D., and Mayer, M. Giant liposomes in physiological buffer using electroformation in a flow chamber. *Biochimica et Biophysica Acta - Biomembranes 1712*, 2 (2005), 152–160. doi:10.1016/j.bbamem.2005.03.012.

[48] Evans, E., and Rawicz, W. Elasticity of "fuzzy" biomembranes. *Physical Review Letters 79*, 12 (1997), 2379–2382. doi:10.1103/PhysRevLett.79.2379.

[49] Faulmann, E., Otten, R., Barrett, D., and Boyle, M. Immunological applications of type iii fc binding proteins comparison of different sources of protein g. *Journal of Immunological Methods 123*, 2 (1989), 269–281. doi:10.1016/0022-1759(89)90231-7.

[50] Fenz, S., Merkel, R., and Sengupta, K. Diffusion and intermembrane distance: Case study of avidin and e-cadherin mediated adhesion. *Langmuir 25*, 2 (2009), 1074–1085. doi:10.1021/la803227s.

[51] Fenz, S., Smith, A., Merkel, R., and Sengupta, K. Inter-membrane adhesion mediated by mobile linkers: Effect of receptor shortage. *Soft Matter 7* (2011), 952–962. doi:10.1039/C0SM00550A.

[52] Feynman, R. There's plenty of room at the bottom. *Engineering and Science 23*, 5 (1960), 22–36.

[53] Fiammengo, R. private communication, 2011. discussion on 07.07.2011.

[54] Fitzgerald, L., Leung, B., and Phillips, D. A method for purifying the platelet membrane glycoprotein IIb-IIIa complex. *Analytical Biochemistry 151*, 1 (1985), 169–177. doi:10.1016/0003-2697(85)90067-3.

[55] Freeze, H. Lectin-affinity chromatography. *Current Protocols in Protein Science 0* (1995), 9.1.1–9.1.9. doi:10.1002/0471140864.ps0901s00.

[56] Frolov, V., Shnyrova, A., and Zimmerberg, J. Lipid polymorphisms and membrane shape. *Cold Spring Harbor Perspectives in Biology 3*, 11 (2011), a004747. doi:10.1101/cshperspect.a004747.

[57] Funakoshi, K., Suzuki, H., and Takeuchi, S. Lipid bilayer formation by contacting monolayers in a microfluidic device for membrane protein analysis. *Analytical Chemistry 78*, 24 (2006), 8169–8174. doi:10.1021/ac0613479.

[58] Funakoshi, K., Suzuki, H., and Takeuchi, S. Formation of giant lipid vesiclelike compartments from a planar lipid membrane by a pulsed jet flow. *Journal of the American Chemical Society 129*, 42 (2007), 12608–12609. doi:10.1021/ja074029f.

[59] Gallagher, S. One-dimensional SDS gel electrophoresis of proteins. *Current Protocols in Protein Science 0* (1995), 10.1.1–10.1.34. doi:10.1002/0471140864.ps1001s00.

[60] Garcia-Saez, A., Mingarro, I., Perez-Paya, E., and Salgado, J. Membrane-insertion fragments of bcl-xl, bax, and bid. *Biochemistry 43*, 34 (2004), 10930–10943. doi:10.1021/bi036044c.

[61] Gay, L., and Felding-Habermann, B. Contribution of platelets to tumour metastasis. *Nature Reviews Cancer 11*, 2 (2011), 123–134. doi:10.1038/nrc3004.

[62] Geiger, B., Spatz, J., and Bershadsky, A. Environmental sensing through focal adhesions. *Nature Reviews Molecular Cell Biology 10*, 1 (2009), 21–33. doi:10.1038/nrm2593.

[63] George, J., Caen, J., and Nurden, A. Glanzmann's thrombasthenia: the spectrum of clinical disease. *Blood 75*, 7 (1990), 1383–1395.

[64] Gingell, D., and Todd, I. Interference reflection microscopy. a quantitative theory for image interpretation and its application to cell-substratum separation measurement. *Biophysical Journal 26*, 3 (1979), 507–526. doi:10.1016/S0006-3495(79)85268-6.

[65] Girard, P., Pecreaux, J., Lenoir, G., Falson, P., Rigaud, J., and Bassereau, P. A new method for the reconstitution of membrane proteins into giant unilamellar vesicles. *Biophysical Journal 87*, 1 (2004), 419–429. doi:10.1529/biophysj.104.040360.

[66] Goennenwein, S., Tanaka, M., Hu, B., Moroder, L., and Sackmann, E. Functional incorporation of integrins into solid supported membranes on ultrathin films of cellulose: Impact on adhesion. *Biophysical Journal 85*, 1 (2003), 646–655. doi:10.1016/S0006-3495(03)74508-1.

[67] Goldberg, S. Mechanical/physical methods of cell disruption and tissue homogenization. *Methods in Molecular Biology 424* (2008), 3–22. doi:10.1007/978-1-60327-064-9_1.

[68] Grimsley, G., and Pace, C. Spectrophotometric determination of protein concentration. *Current Protocols in Protein Science 33* (2003), 3.1.1–3.1.9. doi:10.1002/0471140864.ps0301s33.

[69] Guttenberg, Z., Bausch, A., Hu, B., Bruinsma, R., Moroder, L., and Sackmann, E. Measuring ligand- receptor unbinding forces with magnetic beads: Molecular leverage. *Langmuir 16*, 23 (2000), 8984–8993. doi:10.1021/la000279x.

[70] Hagel, L. Gel-filtration chromatography. *Current Protocols in Protein Science 0* (1998), 8.3.1–8.3.30. doi:10.1002/0471140864.ps0803s14.

[71] Hantgan, R., Braaten, J., and Rocco, M. Dynamic light scattering studies of $\alpha_{IIb}\beta_3$ solution conformation. *Biochemistry 32*, 15 (1993), 3935. doi:10.1021/bi00066a013.

[72] Harburger, D., and Calderwood, D. Integrin signalling at a glance. *Journal of Cell Science 122*, 2 (2009), 159. doi:10.1242/jcs.018093.

[73] Häckl, W., Bärmann, M., and Sackmann, E. Shape changes of self-assembled actin bilayer composite membranes. *Physical Review Letters 80*, 8 (1998), 1786–1789. doi:10.1103/PhysRevLett.80.1786.

[74] Helfrich, W. Elastic properties of lipid bilayers: theory and possible experiments. *Zeitschrift fur Naturforschung Teil C Biochemie Biophysik Biologie Virologie 28*, 11 (1973), 693–703.

[75] Hofmann, T. Membrangebundene Aktinnetzwerke in Riesenvesikeln als biomimetisches Modell des Aktin-Cortex. Master's thesis, Universität Heidelberg, 2009.

[76] Holloway, P. A simple procedure for removal of triton X-100 from protein samples. *Analytical Biochemistry 53*, 1 (1973), 304–308. doi:10.1016/0003-2697(73)90436-3.

[77] Horger, K., Estes, D., Capone, R., and Mayer, M. Films of agarose enable rapid formation of giant liposomes in solutions of physiologic ionic strength. *Journal of the American Chemical Society 131*, 5 (2009), 1810–1819. doi:10.1021/ja805625u.

[78] Horwitz, A. Integrine. *Spektrum der Wissenschaft 1* (1998), 86–95.

[79] Hu, B., Finsinger, D., Peter, K., Guttenberg, Z., Bärmann, M., Kessler, H., Escherich, A., Moroder, L., Bohm, J., Baumeister, W., Sui, S., and Sackmann, E. Intervesicle cross-linking with integrin $\alpha_{IIb}\beta_3$ and cyclic-RGD-lipopeptide. A model of cell-adhesion processes. *Biochemistry 39*, 40 (2000), 12284–12294. doi:10.1021/bi000144q.

[80] Hu, P., Li, S., and Malmstadt, N. Microfluidic fabrication of asymmetric giant lipid vesicles. *ACS Applied Materials and Interfaces 3* (2011), 1434–1440. doi:10.1021/am101191d.

[81] Huang, C. Phosphatidylcholine vesicles. Formation and physical characteristics. *Biochemistry 8*, 1 (1969), 344–352. doi:10.1021/bi00829a048.

[82] Humphries, J., Byron, A., and Humphries, M. Integrin ligands at a glance. *Journal of Cell Science 119*, 19 (2006), 3901. doi:10.1242/jcs.03098.

[83] Hynes, R. Integrins bidirectional, allosteric signaling machines. *Cell 110*, 6 (2002), 673–687. doi:10.1016/S0092-8674(02)00971-6.

[84] Ingber, D. Mechanobiology and diseases of mechanotransduction. *Annals of Medicine 35*, 8 (2003), 564–577. doi:10.1080/07853890310016333.

[85] Kagawa, Y., and Racker, E. Partial resolution of the enzymes catalyzing oxidative phosphorylation. *Journal of Biological Chemistry 246*, 17 (1971), 5477–5487.

[86] Kahya, N., Pécheur, E., de Boeij, W., Wiersma, D., and Hoekstra, D. Reconstitution of membrane proteins into giant unilamellar vesicles via peptide-induced fusion. *Biophysical Journal 81*, 3 (2001), 1464–1474. doi:10.1016/S0006-3495(01)75801-8.

[87] Kalb, E., Frey, S., and Tamm, L. Formation of supported planar bilayers by fusion of vesicles to supported phospholipid monolayers. *Biochimica et Biophysica Acta - Biomembranes 1103*, 2 (1992), 307–316. doi:10.1016/0005-2736(92)90101-Q.

[88] Kanchanawong, P., Shtengel, G., Pasapera, A., Ramko, E., Davidson, M., Hess, H., and Waterman, C. Nanoscale architecture of integrin-based cell adhesions. *Nature 468* (2010), 580–584. doi:10.1038/nature09621.

[89] Kasza, K., Rowat, A., Liu, J., Angelini, T., Brangwynne, C., Koenderink, G., and Weitz, D. The cell as a material. *Current Opinion in Cell Biology 19*, 1 (2007), 101–107. doi:10.1016/j.ceb.2006.12.002.

[90] Kenworthy, A., Hristova, K., Needham, D., and McIntosh, T. Range and magnitude of the steric pressure between bilayers containing phospholipids with covalently attached poly (ethylene glycol). *Biophysical journal 68*, 5 (1995), 1921–1936. doi:10.1016/S0006-3495(95)80369-3.

[91] Kühner, M., and Sackmann, E. Ultrathin hydrated dextran films grafted on glass: Preparation and characterization of structural, viscous, and elastic properties by quantitative microinterferometry. *Langmuir 12* (1996), 4866–4876.

[92] Kirchner, S., Ohlinger, A., Pfeiffer, T., Urban, A., Stefani, F., Deak, A., Lutich, A., and Feldmann, J. Membrane composition of jetted lipid vesicles: a raman spectroscopy study. *Journal of Biophotonics 5*, 1 (2012), 40–46. doi:10.1002/jbio.201100058.

[93] Kleinman, H., Philp, D., and Hoffman, M. Role of the extracellular matrix in morphogenesis. *Current Opinion in Biotechnology 14*, 5 (2003), 526–532. doi:10.1016/j.copbio.2003.08.002.

[94] Kloboucek, A., Behrisch, A., Faix, J., and Sackmann, E. Adhesion-induced receptor segregation and adhesion plaque formation: A model membrane study. *Biophysical Journal 77*, 4 (1999), 2311–2328. doi:10.1016/S0006-3495(99)77070-0.

[95] Kreir, M., Farre, C., Beckler, M., George, M., and Fertig, N. Rapid screening of membrane protein activity: electrophysiological analysis of OmpF reconstituted in proteoliposomes. *Lab Chip 8*, 4 (2008), 587–595. doi:10.1039/b713982a.

[96] Kremer, J., Van der Esker, M., Pathmamanoharan, C., and Wiersema, P. Vesicles of variable diameter prepared by a modified injection method. *Biochemistry 16*, 17 (1977), 3932–3935. doi:10.1021/bi00636a033.

[97] Laemmli, U. Cleavage of structural proteins during the assembly of the head of bacteriophage T4. *Nature 227*, 5259 (1970), 680–685. doi:10.1038/227680a0.

[98] Lasic, D. The mechanism of vesicle formation. *Biochemical Journal 252* (1988), 1–11.

[99] Laurent, T., and Killander, J. A theory of gel filtration and its experimental verification. *Journal of Chromatography A 14* (1964), 317–330. doi:10.1016/S0021-9673(00)86637-6.

[100] Lazarides, E., and Lindberg, U. Actin is the naturally occurring inhibitor of deoxyribonuclease i. *Proceedings of the National Academy of Sciences 71*, 12 (1974), 4742–4746.

[101] Le Berre, M., Yamada, A., Reck, L., Chen, Y., and Baigl, D. Electroformation of giant phospholipid vesicles on a silicon substrate: Advantages of controllable surface properties. *Langmuir 24*, 6 (2008), 2643–2649. doi:10.1021/la703391q.

[102] le Maire, M., Rivas, E., and Møller, J. Use of gel chromatography for determination of size and molecular weight of proteins: further caution. *Analytical Biochemistry 106*, 1 (1980), 12–21. doi:10.1016/0003-2697(80)90112-8.

[103] Lichtenberg, D. Characterization of the solubilization of lipid bilayers by surfactants. *Biochimica et Biophysica Acta - Biomembranes 821*, 3 (1985), 470–478. doi:10.1016/0005-2736(85)90052-5.

[104] Limozin, L., Bärmann, M., and Sackmann, E. On the organization of self-assembled actin networks in giant vesicles. *The European Physical Journal E-Soft Matter 10*, 4 (2003), 319–330. doi:10.1140/epje/i2002-10118-9.

[105] Limozin, L., Roth, A., and Sackmann, E. Microviscoelastic moduli of biomimetic cell envelopes. *Physical Review Letters 95*, 17 (2005), 178101. doi:10.1103/PhysRevLett.95.178101.

[106] Limozin, L., and Sackmann, E. Polymorphism of cross-linked actin networks in giant vesicles. *Physical Review Letters 89*, 16 (2002), 168103. doi:10.1103/PhysRevLett.89.168103.

[107] Limozin, L., and Sengupta, K. Modulation of vesicle adhesion and spreading kinetics by hyaluronan cushions. *Biophysical Journal 93*, 9 (2007), 3300–3313. doi:10.1529/biophysj.107.105544.

[108] Limozin, L., and Sengupta, K. Quantitative Reflection Interference Contrast Microscopy (RICM) in Soft Matter and Cell Adhesion. *ChemPhysChem 10*, 16 (2009), 2752–2768. doi:10.1002/cphc.200900601.

[109] Linkenheld, C. Pfad durch die Lichtmikroskopie. Website. `http://mikroskopie.de/pfad/index.html`.

[110] Liu, A., and Fletcher, D. Biology under construction: in vitro reconstitution of cellular function. *Nature Reviews Molecular Cell Biology 10*, 9 (2009), 644–650. doi:10.1038/nrm2746.

[111] Lodish, H., Berk, A., Zipursky, S., Matsudaira, P., Baltimore, D., and Darnell, J. *Molecular Cell Biology*, 4. ed. W. H. Freeman and Company, 2000.

[112] Lohmüller, T., Aydin, D., Schwieder, M., Morhard, C., Louban, I., Pacholski, C., and Spatz, J. Nanopatterning by block copolymer micelle nanolithography and bioinspired applications. *Biointerphases 6* (2011), MR1–MR12. doi:10.1116/1.3536839.

[113] Lorz, B., Smith, A., Gege, C., and Sackmann, E. Adhesion of Giant Vesicles Mediated by Weak Binding of Sialyl-Lewis X to E-Selectin in the Presence of Repelling Poly(ethyleneglycol) Molecules. *Langmuir 23*, 24 (2007), 12293–12300. doi:10.1021/la701824q.

[114] Lévy, D., Bluzat, A., Seigneuret, M., and Rigaud, J. A systematic study of liposome and proteoliposome reconstitution involving Bio-Bead-mediated Triton X-100 removal. *Biochimica et Biophysica Acta - Biomembranes 1025*, 2 (1990), 179. doi:10.1016/0005-2736(90)90096-7.

[115] Lévy, D., Gulik, A., Bluzat, A., and Rigaud, J. Reconstitution of the sarcoplasmic reticulum Ca2+-ATPase: mechanisms of membrane protein insertion into liposomes during reconstitution procedures involving the use of detergents. *Biochimica et Biophysica Acta - Biomembranes 1107*, 2 (1992), 283–298. doi:10.1016/0005-2736(92)90415-I.

[116] Manneville, J., Bassereau, P., Ramaswamy, S., and Prost, J. Active membrane fluctuations studied by micropipet aspiration. *Physical Review E 64*, 2 (2001), 021908. doi:10.1103/PhysRevE.64.021908.

[117] Marchi-Artzner, V., Lorz, B., Gosse, C., Jullien, L., Merkel, R., Kessler, H., and Sackmann, E. Adhesion of Arg-Gly-Asp (RGD) Peptide Vesicles onto an Integrin Surface: Visualization of the Segregation of RGD Ligands into the Adhesion Plaques by Fluorescence. *Langmuir 19*, 3 (2003), 835–841. doi:10.1021/la026227k.

[118] Martel, V., Racaud-Sultan, C., Dupe, S., Marie, C., Paulhe, F., Galmiche, A., Block, M., and Albiges-Rizo, C. Conformation, localization, and integrin binding of talin depend on its interaction with phos-

phoinositides. *Journal of Biological Chemistry 276*, 24 (2001), 21217–21227. doi:10.1074/jbc.M102373200.

[119] Merkle, D., Kahya, N., and Schwille, P. Reconstitution and anchoring of cytoskeleton inside giant unilamellar vesicles. *ChemBioChem 9*, 16 (2008), 2673–2681. doi:10.1002/cbic.200800340.

[120] Milsmann, M., Schwendener, R., and Weder, H. The preparation of large single bilayer liposomes by a fast and controlled dialysis. *Biochimica et Biophysica Acta - Biomembranes 512*, 1 (1978), 147–155. doi:10.1016/0005-2736(78)90225-0.

[121] Mizejewski, G. Role of integrins in cancer: Survey of expression patterns. *Experimental Biology and Medicine 222*, 2 (1999), 124–138.

[122] Méléard, P., Gerbeaud, C., Pott, T., Fernandez-Puente, L., Bivas, I., Mitov, M., Dufourcq, J., and Bothorel, P. Bending elasticities of model membranes: influences of temperature and sterol content. *Biophysical Journal 72*, 6 (1997), 2616–2629. doi:10.1016/S0006-3495(97)78905-7.

[123] Müller, B., Zerwes, H., Tangemann, K., Peter, J., and Engel, J. Two-step binding mechanism of fibrinogen to alpha iib beta 3 integrin reconstituted into planar lipid bilayers. *Journal of Biological Chemistry 268*, 9 (1993), 6800–6808.

[124] Montes, L., Ahyayauch, H., Ibarguren, M., Sot, J., Alonso, A., Bagatolli, L., and Goñi, F. Electroformation of giant unilamellar vesicles from native membranes and organic lipid mixtures for the study of lipid domains under physiological ionic-strength conditions. *Methods in Molecular Biology 606* (2010), 105. doi:10.1007/978-1-60761-447-0_9.

[125] Montes, L., Alonso, A., Goni, F., and Bagatolli, L. Giant unilamellar vesicles electroformed from native membranes and organic lipid mixtures under physiological conditions. *Biophysical Journal 93*, 10 (2007), 3548–3554. doi:10.1529/biophysj.107.116228.

[126] Monzel, C., Fenz, S. F., Merkel, R., and Sengupta, K. Probing biomembrane dynamics by dual-wavelength reflection interference contrast microscopy. *ChemPhysChem 10* (2009), 2828–2838. doi:10.1002/cphc.200900645.

[127] Moser, M., Legate, K. R., Zent, R., and Fässler, R. The tail of integrins, talin, and kindlins. *Science 324*, 5929 (2009), 895. doi:10.1126/science.1163865.

[128] Mosesson, M. Fibrinogen and fibrin structure and functions. *Journal of Thrombosis and Haemostasis 3*, 8 (2005), 1894–1904. doi:10.1111/j.1538-7836.2005.01365.x.

[129] Mui, B., Chow, L., and Hope, M. *Liposomes, Part A*, vol. 367 of *Methods in Enzymology*. Academic Press, 2003, ch. Extrusion Technique to Generate Liposomes of Defined Size, pp. 3–14.

[130] Murrell, M., Pontani, L.-L., Guevorkian, K., Cuvelier, D., Nassoy, P., and Sykes, C. Spreading dynamics of biomimetic actin cortices. *Biophysical Journal 100* (2011), 1400–1409. doi:10.1016/j.bpj.2011.01.038.

[131] Needham, D., and Kim, D. PEG-covered lipid surfaces: bilayers and monolayers. *Colloids and Surfaces B: Biointerfaces 18*, 3-4 (2000), 183–195.

[132] Okumura, Y., Zhang, H., Sugiyama, T., and Iwata, Y. Electroformation of giant vesicles on a non-electroconductive substrate. *Journal of the American Chemical Society 129*, 6 (2007), 1490–1491. doi:10.1021/ja068127x.

[133] Ollivon, M., Lesieur, S., Grabielle-Madelmont, C., and Paternostre, M. Vesicle reconstitution from lipid–detergent mixed micelles. *Biochimica et Biophysica Acta - Biomembranes 1508*, 1-2 (2000), 34–50. doi:10.1016/S0304-4157(00)00006-X.

[134] Olson, B., and Markwell, J. Assays for determination of protein concentration. *Current Protocols in Protein Science 48* (2007), 3.4.1–3.4.29. doi:10.1002/0471140864.ps0304s48.

[135] Olson, F., Hunt, C., Szoka, F., Vail, W., and Papahadjopoulos, D. Preparation of liposomes of defined size distribution by extrusion through polycarbonate membranes. *Biomembranes 557*, 1 (1979), 9–23. doi:10.1016/0005-2736(79)90085-3.

[136] Pande, G. The role of membrane lipids in regulation of integrin functions. *Current Opinion in Cell Biology 12*, 5 (2000), 569–574. doi:10.1016/S0955-0674(00)00133-2.

[137] Papahadjopoulos, D., and Watkins, J. Phospholipid model membranes. ii. permeability properties of hydrated liquid crystals. *Biochimica et Biophysica Acta - Biomembranes 135*, 4 (1967), 639–652. doi:10.1016/0005-2736(67)90095-8.

[138] Pardee, J., and Spudich, J. Purification of muscle actin. *Methods in Enzymology 85* (1982), 164–181. doi:10.1016/0076-6879(82)85020-9.

[139] Parise, L., and Phillips, D. Platelet membrane glycoprotein IIb-IIIa complex incorporated into phospholipid vesicles. preparation and morphology. *Journal of Biological Chemistry 260*, 3 (1985), 1750.

[140] Parise, L., and Phillips, D. Reconstitution of the purified platelet fibrinogen receptor. fibrinogen binding properties of the glycoprotein IIb-IIIa complex. *Journal of Biological Chemistry 260*, 19 (1985), 10698–10707.

[141] Paternostre, M., Roux, M., and Rigaud, J. Mechanisms of membrane protein insertion into liposomes during reconstitution procedures involving the use of detergents. 1. solubilization of large unilamellar liposomes (prepared by reverse-phase evaporation) by triton X-100, octyl glucoside, and sodium cholate. *Biochemistry 27*, 8 (1988), 2668–2677. doi:10.1021/bi00408a006.

[142] Pautot, S., Frisken, B., and Weitz, D. Engineering asymmetric vesicles. *Proceedings of the National Academy of Sciences 100*, 19 (2003), 10718–10721. doi:10.1073/pnas.1931005100.

[143] Pellegrin, S., and Mellor, H. Actin stress fibres. *Journal of Cell Science 120*, 20 (2007), 3491–3499. doi:10.1242/jcs018473.

[144] Peter, K. *Isolation und Charakterisierung des Zellrezeptors Integrin $\alpha_{IIb}\beta_3$ - Studie zur Bindung an zytosolische Proteine und biokompatible Oberflächen.* PhD thesis, TU München, 1999.

[145] Pfaff, M., Tangemann, K., Müller, B., Gurrath, M., Müller, G., Kessler, H., Timpl, R., and Engel, J. Selective recognition of cyclic RGD peptides of NMR defined conformation by alpha IIb beta 3, alpha V beta 3, and alpha 5 beta 1 integrins. *Journal of Biological Chemistry 269*, 32 (1994), 20233–20238.

[146] Phillips, R., Kondev, J., and Theriot, J. *Physical Biology of the Cell*, 1. ed. Garland Science, 2009.

[147] Pokutta, S., and Weis, W. Structure and mechanism of cadherins and catenins in cell-cell contacts. *Annual Review of Cell and Developmental Biology 23* (2007), 237–261. doi:10.1146/annurev.cellbio.22.010305.104241.

[148] Politano, T., Froude, V., Jing, B., and Zhu, Y. Ac-electric field dependent electroformation of giant lipid vesicles. *Colloids and Surfaces B: Biointerfaces 79* (2010), 75–82. doi:10.1016/j.colsurfb.2010.03.032.

[149] Pollard, T. The cytoskeleton, cellular motility and the reductionist agenda. *Nature 422*, 6933 (2003), 741–745. doi:10.1038/nature01598.

[150] Pollard, T., and Cooper, J. Actin, a central player in cell shape and movement. *Science 326*, 5957 (2009), 1208–1212. doi:10.1126/science.1175862.

[151] Pontani, L., van der Gucht, J., Salbreux, G., Heuvingh, J., Joanny, J., and Sykes, C. Reconstitution of an actin cortex inside a liposome. *Biophysical Journal 96*, 1 (2009), 192–198. doi:10.1016/j.bpj.2008.09.029.

[152] Pott, T., Bouvrais, H., and Méléard, P. Giant unilamellar vesicle formation under physiologically relevant conditions. *Chemistry and Physics of Lipids 154*, 2 (2008), 115–119. doi:10.1016/j.chemphyslip.2008.03.008.

[153] Prechtel, A.-K. *Wetting and interdiffusion: establishment of a biocompatible system and studies of its dynamics.* PhD thesis, TU München, 2005.

[154] Protein Expression and Purification Core Facility, EMBL Heidelberg. Calibration of HiLoad 26/60 Superdex 200 prep grade. website. `http://www.embl.de/pepcore/pepcore_services/protein_purification/chromatography/hiload26-60_superdex200/`.

[155] Puech, P., Feracci, H., and Brochard-Wyart, F. Adhesion between giant vesicles and supported bilayers decorated with chelated E-cadherin fragments. *Langmuir 20*, 22 (2004), 9763–9768. doi:10.1021/la048682h.

[156] Purrucker, O., Gönnenwein, S., Förtig, A., Jordan, R., Rusp, M., Bärmann, M., Moroder, L., Sackmann, E., and Tanaka, M. Polymer-tethered membranes as quantitative models for the study of integrin-mediated cell adhesion. *Soft Matter 3*, 3 (2007), 333–336. doi:10.1039/b612069e.

[157] Qureshi, A., Chaoji, V., Maiguel, D., Faridi, M., Barth, C., Salem, S., Singhal, M., Stoub, D., Krastins, B., Ogihara, M., Zaki, M., and Gupta, V. Proteomic and phospho-proteomic profile of human platelets in basal, resting state: insights into integrin signaling. *PLoS One 4*, 10 (2009), e7627. doi:10.1371/journal.pone.0007627.

[158] Ramsamooj, P., Doellgast, G., and Hantgan, R. Inhibition of fibrin(ogen) binding to stimulated platelets by a monoclonal antibody specific for a conformational determinant of GPIIIa. *Thrombosis Research 58*, 6 (1990), 577–592. doi:10.1016/0049-3848(90)90304-U.

[159] Rädler, J., Feder, T., Strey, H., and Sackmann, E. Fluctuation analysis of tension-controlled undulation forces between giant vesicles and solid substrates. *Physical Review E 51*, 5 (1995), 4526–4536. doi:10.1103/PhysRevE.51.4526.

[160] Rädler, J., and Sackmann, E. On the measurement of weak repulsive and frictional colloidal forces by reflection interference contrast microscopy. *Langmuir 8*, 3 (1992), 848–853. doi:10.1021/la00039a019.

[161] Rädler, J., and Sackmann, E. Imaging optical thicknesses and separation distances of phospholipid vesicles at solid surfaces. *Journal de Physique II France 3* (1993), 727–748. doi:10.1051/jp2:1993163.

[162] Reeves, J., and Dowben, R. Formation and properties of thin-walled phospholipid vesicles. *Journal of Cellular Physiology 73*, 1 (1969), 49–60. doi:10.1002/jcp.1040730108.

[163] Rehm, H. *Proteinbiochemie/Proteomics*, 5. ed. Der Experimentator. Spektrum Akademischer Verlag, 2006.

[164] Richmond, D., Schmid, E., Martens, S., Stachowiak, J., Liska, N., and Fletcher, D. Forming giant vesicles with controlled membrane composition, asymmetry, and contents. *Proceedings of the National Academy of Sciences 108*, 23 (2011), 9431–9436. doi:10.1073/pnas.1016410108.

[165] Rigaud, J., and Levy, D. *Liposomes, Part B*, vol. 372 of *Methods in Enzymology*. Academic Press, 2003, ch. Reconstitution of membrane proteins into liposomes, pp. 65–86.

[166] Rigaud, J., Levy, D., Mosser, G., and Lambert, O. Detergent removal by non-polar polystyrene beads. *European Biophysics Journal 27*, 4 (1998), 305–319. doi:10.1007/s002490050138.

[167] Rigaud, J., Paternostre, M., and Bluzat, A. Mechanisms of membrane protein insertion into liposomes during reconstitution procedures involving the use of detergents. 2. incorporation of the light-driven proton pump bacteriorhodopsin. *Biochemistry 27*, 8 (1988), 2677–2688. doi:10.1021/bi00408a007.

[168] Rigaud, J., Pitard, B., and Levy, D. Reconstitution of membrane proteins into liposomes: application to energy-transducing membrane proteins. *Biochimica et Biophysica Acta - Bioenergetics 1231*, 3 (1995), 223–246. doi:10.1016/0005-2728(95)00091-V.

[169] Risitano, A., Beaulieu, L., Vitseva, O., and Freedman, J. Platelets and platelet-like particles mediate intercellular rna transfer. *Blood 119*, 26 (2012), 6288–6295. doi:10.1182/blood-2011-12-396440.

[170] Rivas, G., Aznarez, J., Usobiaga, P., Saiz, J., and González-Rodríguez, J. Molecular characterization of the human platelet integrin GPIIb/IIIa and its constituent glycoproteins. *European Biophysics Journal 19*, 6 (1991), 335–345. doi:10.1007/BF00183324.

[171] Rodriguez, N., Pincet, F., and Cribier, S. Giant vesicles formed by gentle hydration and electroformation: A comparison by fluorescence microscopy. *Colloids and Surfaces B: Biointerfaces 42*, 2 (2005), 125–130. doi:10.1016/j.colsurfb.2005.01.010.

[172] Rouser, G. Phospholipids and blood coagulation. *The American Journal of Clinical Nutrition 6*, 6 (1958), 681–687.

[173] Sackmann, E., and Bruinsma, R. Cell adhesion as wetting transition? *ChemPhysChem 3*, 3 (2002), 262–269. doi:10.1002/1439-7641(20020315)3:3<262::AID-CPHC262>3.0.CO;2-U.

[174] Sackmann, E., and Merkel, R. *Lehrbuch der Biophysik*. Wiley VCH, Weinheim, 2009.

[175] Saunders, L., Perrin, J., and D., G. Ultrasonic irradiation of some phospholipid sols. *Journal of Pharmacy and Pharmacology 14*, 1 (1962), 567–572. doi:10.1111/j.2042-7158.1962.tb11141.x.

[176] Schägger, H. *A Practical Guide to Membrane Protein Purification*. Academic Press, 1994, ch. Native Gel Electrophoresis, pp. 81–104.

[177] Schieren, H., Rudolph, S., Finkelstein, M., Coleman, P., and Weissmann, G. Comparison of large unilamellar vesicles prepared by a petroleum ether vaporization method with multilamellar vesicles: ESR, diffusion and entrapment analyses. *Biochimica et Biophysica Acta - General Subjects 542*, 1 (1978), 137–153. doi:10.1016/0304-4165(78)90240-4.

[178] Schilling, J., Sengupta, K., Goennenwein, S., Bausch, A., and Sackmann, E. Absolute interfacial distance measurements by dual-wavelength reflection interference contrast microscopy. *Physical Review E 69*, 2 (2004), 21901. doi:10.1103/PhysRevE.69.021901.

[179] Schubert, R. *Liposomes, Part A*, vol. 367 of *Methods in Enzymology*. Academic Press, 2003, ch. Liposome Preparation by Detergent Removal, pp. 46–70.

[180] Schwartz, M. The importance of stupidity in scientific research. *Journal of Cell Science 121*, 11 (2008), 1771. doi:10.1242/jcs.033340.

[181] Schwartz, M. Integrins and extracellular matrix in mechanotransduction. *Cold Spring Harbor Perspectives in Biology 2*, 12 (2010), a005066. doi:10.1101/cshperspect.a005066.

[182] Schwille, P. Bottom-up synthetic biology: Engineering in a tinkerer's world. *Science 333*, 6047 (2011), 1252–1254. doi:10.1126/science.1211701.

[183] Seifert, U. Configurations of fluid membranes and vesicles. *Advances in Physics 46*, 1 (1997), 13–137. doi:10.1080/00018739700101488.

[184] Sens, P., and Isambert, H. Undulation instability of lipid membranes under an electric field. *Physical Review Letters 88*, 12 (2002), 128102. doi:10.1103/PhysRevLett.88.128102.

[185] Shaklee, P., Semrau, S., Malkus, M., Kubick, S., Dogterom, M., and Schmidt, T. Protein incorporation in giant lipid vesicles under physiological conditions. *ChemBioChem 11*, 2 (2010), 175–179. doi:10.1002/cbic.200900669.

[186] Shimanouchi, T., Umakoshi, H., and Kuboi, R. Kinetic study on giant vesicle formation with electroformation method. *Langmuir 25*, 9 (2009), 4835–4840. doi:10.1021/la8040488.

[187] Siegel, L., and Monty, K. Determination of molecular weights and frictional ratios of proteins in impure systems by use of gel filtration and density gradient centrifugation. application to crude preparations of sulfite and hydroxylamine reductases. *Biochimica et Biophysica Acta - Biophysics including Photosynthesis 112*, 2 (1966), 346–362. doi:10.1016/0926-6585(66)90333-5.

[188] Silvius, J. Solubilization and functional reconstitution of biomembrane components. *Annual Review of Biophysics and Biomolecular Structure 21*, 1 (1992), 323–348. doi:10.1146/annurev.bb.21.060192.001543.

[189] Singer, S., and Nicolson, G. The fluid mosaic model of the structure of cell membranes. *Science 175*, 4023 (1972), 720–731. doi:10.1126/science.175.4023.720.

[190] Sinner, E., Reuning, U., Kök, F., Saccą, B., Moroder, L., Knoll, W., and Oesterhelt, D. Incorporation of integrins into artificial planar lipid membranes: characterization by plasmon-enhanced fluorescence spectroscopy. *Analytical Biochemistry 333*, 2 (2004), 216–224. doi:10.1016/j.ab.2004.05.022.

[191] Sloan, S. Glycoprotein iib-iiia-liposomes bind fibrinogen but do not undergo fibrinogen-mediated aggregation. Master's thesis, McGill University Montreal, 1997.

[192] Smith, A., Lorz, B., Seifert, U., and Sackmann, E. Antagonist-induced deadhesion of specifically adhered vesicles. *Biophysical Journal 90*, 3 (2006), 1064–1080. doi:10.1529/biophysj.105.062166.

[193] Smith, A., and Sackmann, E. Progress in mimetic studies of cell adhesion and the mechanosensing. *ChemPhysChem 10*, 1 (2009), 66–78. doi:10.1002/cphc.200800683.

[194] Smyth, S., and Parise, L. Regulation of ligand binding to glycoprotein IIb-IIIa (integrin $\alpha_{IIb}\beta_3$) in isolated platelet membranes. *Biochemical Journal 292* (1993), 749–758.

[195] Spatz, J., Roescher, A., and Möller, M. Gold nanoparticles in micellar poly (styrene)-b-poly (ethylene oxide) films - size and interparticle distance control in monoparticulate films. *Advanced Materials 8*, 4 (1996), 337–340. doi:10.1002/adma.19960080411.

[196] Stachowiak, J., Richmond, D., Li, T., Brochard-Wyart, F., and Fletcher, D. Inkjet formation of unilamellar lipid vesicles for cell-like encapsulation. *Lab on a Chip 9*, 14 (2009), 2003–2009. doi:10.1039/b904984c.

[197] Stachowiak, J., Richmond, D., Li, T., Liu, A., Parekh, S., and Fletcher, D. Unilamellar vesicle formation and encapsulation by microfluidic jetting. *Proceedings of the National Academy of Sciences 105*, 12 (2008), 4697–4702. doi:10.1073/pnas.0710875105.

[198] Streicher, P. *Studying Integrin-Mediated Cell Spreading Using a Biomimetic System.* PhD thesis, Université Paris VI, 2008.

[199] Streicher, P., Nassoy, P., Bärmann, M., Dif, A., Marchi-Artzner, V., Brochard-Wyart, F., Spatz, J., and Bassereau, P. Integrin reconstituted in GUVs: A biomimetic system to study initial steps of cell spreading. *Biochimica et Biophysica Acta - Biomembranes 1788*, 10 (2009), 2291–2300. doi:10.1016/j.bbamem.2009.07.025.

[200] Streuli, C. Extracellular matrix remodelling and cellular differentiation. *Current Opinion in Cell Biology 11*, 5 (1999), 634–640. doi:10.1016/S0955-0674(99)00026-5.

[201] Stupack, D., and Cheresh, D. Get a ligand, get a life: integrins, signaling and cell survival. *Journal of Cell Science 115*, 19 (2002), 3729–3738. doi:10.1242/jcs.00071.

[202] Szoka, F., and Papahadjopoulos, D. Procedure for preparation of liposomes with large internal aqueous space and high capture by reverse-phase evaporation. *Proceedings of the National Academy of Sciences 75*, 9 (1978), 4194–4198.

[203] Szoka, F., and Papahadjopoulos, D. Comparative properties and methods of preparation of lipid vesicles (liposomes). *Annual Review of Biophysics and Bioengineering 9*, 1 (1980), 467–508. doi:10.1146/annurev.bb.09.060180.002343.

[204] Takagi, J., Petre, B., Walz, T., and Springer, T. Global conformational rearrangements in integrin extracellular domains in outside-in and inside-out signaling. *Cell 110*, 5 (2002), 599–611. doi:10.1016/S0092-8674(02)00935-2.

[205] Tanford, C., Nozaki, Y., Reynolds, J., and Makino, S. Molecular characterization of proteins in detergent solutions. *Biochemistry 13*, 11 (1974), 2369–2376. doi:10.1021/bi00708a021.

[206] Tangemann, K., and Engel, J. Demonstration of non-linear detection in ELISA resulting in up to 1000-fold too high affinities of fibronogen binding to integrin αIIbβ3. *FEBS Letters 358*, 2 (1995), 179–181. doi:10.1016/0014-5793(94)01411-S.

[207] Theodoly, O., Huang, Z., and Valignat, M. New modeling of reflection interference contrast microscopy including polarization and numerical aperture effects: Application to nanometric distance measurements and object profile reconstruction. *Langmuir 26*, 3 (2010), 1940–1948. doi:10.1021/la902504y.

[208] Tiller, G., Mueller, T., Dockter, M., and Struve, W. Hydrogenation of triton X-100 eliminates its fluorescence and ultraviolet light absorption while preserving its detergent properties. *Analytical Biochemistry 141*, 1 (1984), 262–266. doi:10.1016/0003-2697(84)90455-X.

[209] Tsai, F., Stuhrmann, B., and Koenderink, G. Encapsulation of active cytoskeletal protein networks in cell-sized liposomes. *Langmuir 27*, 16 (2011), 10061–10071. doi:10.1021/la201604z.

[210] Tsumoto, K., Matsuo, H., Tomita, M., and Yoshimura, T. Efficient formation of giant liposomes through the gentle hydration of phosphatidylcholine films doped with sugar. *Colloids and Surfaces B: Biointerfaces 68*, 1 (2009), 98–105. doi:10.1016/j.colsurfb.2008.09.023.

[211] Varnier, A., Kermarrec, F., Blesneac, I., Moreau, C., Liguori, L., Lenormand, J., and Picollet-D'hahan, N. A simple method for the reconstitution of membrane proteins into giant unilamellar vesicles. *Journal of Membrane Biology 233*, 1 (2010), 85–92. doi:10.1007/s00232-010-9227-8.

[212] Vogel, S., and Schwille, P. Minimal systems to study membrane–cytoskeleton interactions. *Current Opinion in Biotechnology 23* (2012), 1–8. doi:10.1016/j.copbio.2012.03.012.

[213] Volinsky, R., Cwiklik, L., Jurkiewicz, P., Hof, M., Jungwirth, P., and Kinnunen, P. Oxidized phosphatidylcholines facilitate phospholipid flip-flop in liposomes. *Biophysical Journal 101*, 6 (2011), 1376–1384. doi:10.1016/j.bpj.2011.07.051.

[214] Walde, P., Cosentino, K., Engel, H., and Stano, P. Giant vesicles: Preparations and applications. *ChemBioChem 11*, 7 (2010), 848–865. doi:10.1002/cbic.201000010.

[215] Wang, J., and Thampatty, B. An introductory review of cell mechanobiology. *Biomechanics and Modeling in Mechanobiology 5*, 1 (2006), 1–16. doi:10.1007/s10237-005-0012-z.

[216] Weisel, J., Nagaswami, C., Vilaire, G., and Bennett, J. Examination of the platelet membrane glycoprotein IIb-IIIa complex and its interaction with fibrinogen and other ligands by electron microscopy. *Journal of Biological Chemistry 267*, 23 (1992), 16637–16643.

[217] Wiegand, G., Jaworek, T., Wegner, G., and Sackmann, E. Studies of structure and local wetting properties on heterogeneous, micropatterned solid surfaces by microinterferometry. *Journal of Colloid and Interface Science 196*, 2 (1997), 299–312. doi:10.1006/jcis.1997.5193.

[218] Wiegand, G., Neumaier, K., and Sackmann, E. Microinterferometry: three-dimensional reconstruction of surface microtopography for thin-film and wetting studies by reflection interference contrast microscopy (ricm). *Applied Optics 37*, 29 (1998), 6892. doi:10.1364/AO.37.006892.

[219] Wiesner, S., Legate, K., and Fässler, R. Integrin-actin interactions. *Cellular and Molecular Life Sciences 62*, 10 (2005), 1081–1099. doi:10.1007/s00018-005-4522-8.

[220] Xiong, J., Stehle, T., Diefenbach, B., Zhang, R., Dunker, R., Scott, D., Joachimiak, A., Goodman, S., and Arnaout, M. Crystal structure of the extracellular segment of integrin $\alpha_v\beta_3$. *Science 294*, 5541 (2001), 339. doi:10.1126/science.1064535.

[221] Xiong, J., Stehle, T., Goodman, S., and Arnaout, M. New insights into the structural basis of integrin activation. *Blood 102*, 4 (2003), 1155–1159. doi:10.1182/blood-2003-01-0334.

[222] Xiong, J.-P., Goodman, S., and Arnaout, M. *Integrins*, vol. 426 of *Methods in Enzymology*. Academic Press, 2007, ch. Purification, Analysis, and Crystal Structure of Integrin, pp. 307–336.

[223] Yamashita, Y., Oka, M., Tanaka, T., and Yamazaki, M. A new method for the preparation of giant liposomes in high salt concentrations and growth of protein microcrystals in them. *Biochimica et Biophysica Acta - Biomembranes 1561*, 2 (2002), 129–134. doi:10.1016/S0005-2736(02)00338-3.

[224] Ye, F., Hu, G., Taylor, D., Ratnikov, B., Bobkov, A., McLean, M., Sligar, S., Taylor, K., and Ginsberg, M. Recreation of the terminal events in physiological integrin activation. *The Journal of Cell Biology 188*, 1 (2010), 157–173. doi:10.1083/jcb.200908045.

[225] Ye, F., Liu, J., Winkler, H., and Taylor, K. Integrin αIIbβ3 in a Membrane Environment Remains the Same Height after Mn2+ Activation when Observed by Cryoelectron Tomography. *Journal of Molecular Biology 378*, 5 (2008), 976–986. doi:10.1016/j.jmb.2008.03.014.

[226] Zaidel-Bar, R., and Geiger, B. The switchable integrin adhesome. *Journal of Cell Science 123*, 9 (2010), 1385–1388. doi:10.1242/jcs.066183.

[227] Zaidel-Bar, R., Itzkovitz, S., Ma'ayan, A., Iyengar, R., and Geiger, B. Functional atlas of the integrin adhesome. *Nature Cell Biology 9*, 8 (2007), 858–867. doi:10.1038/ncb0807-858.

[228] Zhang, Y., Cheng, C., Cusick, B., and LeDuc, P. Chemically encapsulated structural elements for probing the mechanical responses of biologically inspired systems. *Langmuir 23*, 15 (2007), 8129–8134. doi:10.1021/la700488p.

[229] Zhu, J., Boylan, B., Luo, B., Newman, P., and Springer, T. Tests of the extension and deadbolt models of integrin activation. *Journal of Biological Chemistry 282*, 16 (2007), 11914–11920. doi:10.1074/jbc.M700249200.

[230] Zumbuehl, O., and Weder, H. Liposomes of controllable size in the range of 40 to 180 nm by defined dialysis of lipid/detergent mixed micelles. *Biochimica et Biophysica Acta - Biomembranes 640*, 1 (1981), 252–262. doi:10.1016/0005-2736(81)90550-2.

Appendices

A Phase Contrast, Differential Interference Contrast and Fluorescence Microscopy

In phase contrast microscopy special kinds of apertures are inserted in the illuminating path and in the objective. When traveling through the specimen different light rays experience a phase shift because of dissimilar path lengths due to differences in the refractive index of, for example, cell nuclei or cytoplasm. These changes are usually too small to be detected against bright background. This is why light coming from the condenser has to be attenuated. An annular aperture is employed to achieve a ring-shaped illumination. In contrast to dark field microscopy, all light coming from the condenser is collected by the objective. A phase plate matching the condenser annulus in the back focal plane of the objective attenuates the direct illuminating light and additionally adds a phase shift to it. Light interacting with the sample normally is refracted or diffracted and therefore does not hit the phase ring why it is not modified any further. Phase-shifted light from the specimen and attenuated direct light interfere to form the intermediate image in the image plane according to the phasing when focused by the tube lens. The intermediate image is then observed through the eyepiece. Optimal contrast requires the right choice of phase shift and attenuation by the phase plate. The optical path in phase contrast microscopy is shown in figure A.1.

Another way to make small changes in refractive index visible is to work with DIC. As its name implies it also takes advantage of interference. Linearly polarized light from the polarizer is split into two beams with a polarization perpendicular to each other by a Nomarski prism. Like a Wollaston prism it consists of two birefringent crystal wedges glued together but cut in such a way that the focal point of both beams lies outside of the prism. This allows for the easy adjustment of contrast by the movement of the second Nomarski prism perpendicular to the optical axis. The two partial rays are rendered parallel by the condenser. They go through the specimen with a lateral offset – the so-called shear - smaller than the diffraction limit (hence the name differential). If they pass the same structures having the same refraction index and thickness, there will be no phase shift between them. On the other hand, if each of them traverses a material with different index of refraction, they have different optical path lengths associated with a phase shift. Both beams

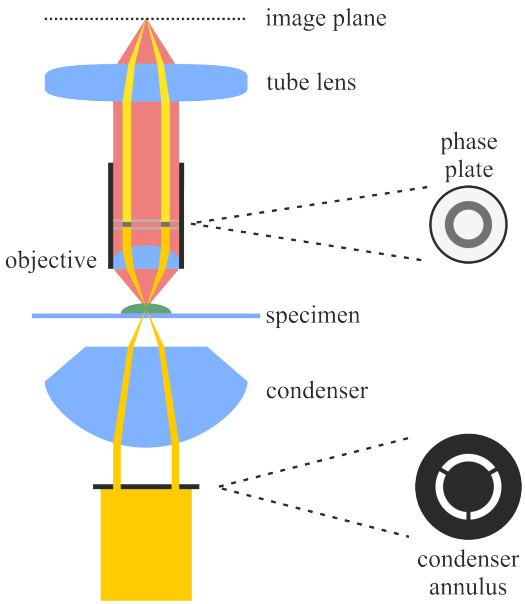

Figure A.1: Optical path in phase contrast microscopy. The whole pencil of rays passing the condenser annulus and illuminating the specimen is shown in the picture in yellow, as well as the direct light coming from the sample without an interaction. The direct light is attenuated and phase-shifted by the phase plate in the objective. The diffracted light is indicated in light red ignoring the light not reaching the objective. An image showing the different optical path lengths in the sample is finally formed when direct and diffracted light interfere in the image plane. The drawing is not to scale.

are recombined by the second Nomarski prism behind the objective. The analyzer oriented perpendicular to the polarizer renders the light linearly polarized once again. This enables the interference of the two beams in the plane of the intermediate image. Please refer to the beam path in figure A.2 for a better understanding. Contrary to phase contrast microscopy an image in DIC does not show directly the different optical path lengths in the specimen but rather gradients in path length. Since there is no contrast perpendicular to the shear the resulting image looks like a relief which represents not necessarily the real shape of the object. This has to be kept in mind when interpreting images from DIC. Figure 2.7 allows the comparison of GUVs imaged with both methods.

Fluorescent molecules absorb light of a certain wavelength depending on their electronic and vibrational states leading to the excitation of an electron. The absorbed energy can be re-emitted through the emission of a photon. Normally, the electron does not end up in the vibrational ground state of the excited state. On the one hand, transitions between vibrational states usually are non-radiative and on the other hand most often excess energy is lost to the environment in the form of heat. This explains the so-called Stokes shift meaning that a dye's emission wavelength is longer than the one for absorption. Using this effect allows for the discrimination of excitation and much weaker emission light employing different filters and a dichroic mirror. Light from an appropriate source (e.g. a xenon arc lamp or a mercury vapor lamp -> both gas-discharge lamps) passes the excitation filter selecting part of the spectrum for excitation. The dichroic mirror reflects the light to the specimen where it is partly absorbed. Emitted light from the sample is transmitted by the dichroic mirror and reaches the detector through the emission filter. The second filter assures a lower background and therefore a higher signal-to-noise ratio. Since fluorescent

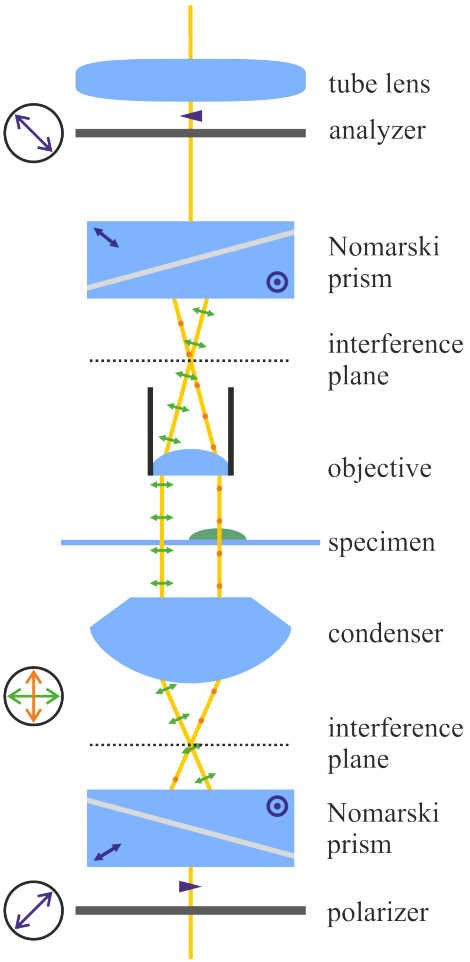

Figure A.2: Beam path in differential interference microscopy. The first Nomarski prism splits the polarized beam in two beams with their electric field vector oscillating perpendicular to each other. The direction of polarization in a plane perpendicular to the optical axis of the system is indicated by the arrows in the circles to the left of the drawing. When the two beams pass the specimen at points with different optical path lengths, they acquire a phase shift relative to each other. This results in contrast by interference in the image plane after both beams have been recombined by the second Nomarski prism and their polarization has been projected in the same plane by the analyzer. Please keep in mind that the drawing is not to scale.

dyes can be bound to many different molecules – antibodies, small peptide sequences or whole proteins to name but a few – very specific staining is possible. Furthermore structures smaller than the diffraction limit of light can be made visible by fluorescence even though they can not be resolved.

In my opinion, nice introductions (in German) to optical microscopy are given in [41] and especially in [109]. Even though I did not use it very often for myself, a good explanation of the basics of microscopy in English can be found in [35].

B Movies

Movie 1:
This movie depicts bilayers of GUVs oscillating in an alternating electric field. Frequency of the field was 0.7 Hz at the beginning, but was varied in the first two thirds of the movie in the range of 0.7 Hz to several Hz. In the last third of the movie, the amplitude of the field was varied from about 0.1 V to 10 V.

Movie 2:
This movie illustrates the fusion of GUVs in an alternating electric field of 10 Hz frequency with an amplitude of 1 V.

C Matlab Routines for Evaluation of RICM images

Some line breaks need to be formatted manually to ensure functioning code.

Main Program

All routines are started with this program, which uses several functions listed below.

```
%--------- Clearing screen and memory ---------------------------------

clear all; %Clears all variables
close all; %Closes open windows
clc; %Clears screen

%------ Stack or not?
commandwindow;
StackFlag = input('Do want to evaluate an image sequence produced...
from an image stack? Y/N [N]: ','s');
if isempty(StackFlag)
    StackFlag = 'N';
end

%------ Different cases for single image (StackFlag = 'N') or
%      stack (StackFlag = 'Y')
switch StackFlag

%-------------- single image ---------------
    case 'N'
        %------ find Raw Data
        [FileName,PATH] = uigetfile({'*.jpg;*.tif;*.png;*.gif',...
    'All Image Files'}, 'Select the image to evaluate: ',...
        'C:\Dokumente und Einstellungen\kreidler\Eigene Dateien\...
    Messungen\Mikroskop\');
        [pathstr, file, ext] = fileparts(fullfile(PATH,FileName));
        cd(PATH);

        dirOutput = dir(fullfile(PATH,strcat(file,ext)));

        %------ crop the image
        crop(PATH, file, ext, dirOutput);

```

```
34          %------ change filename to cropped image without number
35      %------ and file extension
36          file1=strcat(file,'_cut');
37          dirOutput1 = dir(fullfile(PATH,strcat(file1,'*',ext)));
38
39          %------ interpolate illumination in a ROI containing the
40      %------ object you are interested in
41          illucalc(PATH, file1, ext, dirOutput1);
42
43          %------ filename of cropped image with interpolated
44      %------ illumination without number and file extension
45          file2=strcat(file1,'_background');
46          dirOutput2 = dir(fullfile(PATH,strcat(file2,'*',ext)));
47
48          %------ average background images -> Does not change
49      %------ anything for one image...
50          average(PATH, file2, ext, dirOutput2);
51
52          %------ get line profiles and x-values of extrema
53          file3 = strcat(file1,'_01',ext);
54          bgname = strcat(file2,'_average',ext);
55          Image = imread(file3);
56          Background = imread(bgname);
57          Image_corr = (double(Image)-double(Background))./...
58      double(Background);
59          [c1x,c1y,c1,c2x,c2y,c2,c3x,c3y,c3,c4x,c4y,c4,c5x,c5y,c5,...
60      c6x,c6y,c6, xselect1,xselect2,xselect3,xselect4,xselect5,...
61      xselect6,yselect1,yselect2,yselect3,yselect4,yselect5,...
62      yselect6] = lineprofile(Image,Image_corr,PATH,file,ext);
63      % x- and y-values and intensities
64
65          %------ calculate height using intensity or refractive index
66      %------ method
67          commandwindow;
68          MethodFlag = input('Which method do you want to use to...
69      calculate height: min-max-intensity method [I] or...
70      refractive  index method [n]? Default: [I]: ','s');
71          if isempty(MethodFlag)
72              MethodFlag = 'I';
73          end
74          switch MethodFlag
75              case 'I'
76                  %------ calculation with subsequent plot
77                  [xH1,H1]=contact_angle_I(c1,c1x,c1y,xselect1,yselect1);
78                  figure(13);
79                  plot(xH1,H1, '-or');
80                  xlabel('distance in micrometer')
81                  ylabel('height in micrometer')
82                  title('Plot of heights along lines')
83                  hold on;
```

```
84                  [xH2,H2]=contact_angle_I(c2,c2x,c2y,xselect2,yselect2);
85                  plot(xH2,H2, '-og');
86                  [xH3,H3]=contact_angle_I(c3,c3x,c3y,xselect3,yselect3);
87                  plot(xH3,H3, '-ob');
88                  [xH4,H4]=contact_angle_I(c4,c4x,c4y,xselect4,yselect4);
89                  plot(xH4,H4, '-oc');
90                  [xH5,H5]=contact_angle_I(c5,c5x,c5y,xselect5,yselect5);
91                  plot(xH5,H5, '-om');
92                  [xH6,H6]=contact_angle_I(c6,c6x,c6y,xselect6,yselect6);
93                  plot(xH6,H6, '-oy');
94                  hleg1 = legend({'line 1','line 2','line 3','line 4',...
95          'line 5','line 6'},'Location','NorthWest');
96                  hold off;
97
98              case 'n'
99                  %------ calculation with subsequent plot
100                 [xH1,H1,A01,A0theo1,h01,h0theo1]=contact_angle_n(c1,...
101         c1x,c1y,xselect1);
102                 figure(42);
103                 plot(xH1,H1, '-or');
104                 xlabel('distance [\SI{}{\um}]')
105                 ylabel('height [\SI{}{\um}]')
106                 title('Plot of heights along lines')
107                 hold on;
108                 [xH2,H2,A02,A0theo2,h02,h0theo2]=contact_angle_n(c2,...
109         c2x,c2y,xselect2);
110                 plot(xH2,H2, '-og');
111                 [xH3,H3,A03,A0theo3,h03,h0theo3]=contact_angle_n(c3,...
112         c3x,c3y,xselect3);
113                 plot(xH3,H3, '-ob');
114                 [xH4,H4,A04,A0theo4,h04,h0theo4]=contact_angle_n(c4,...
115         c4x,c4y,xselect4);
116                 plot(xH4,H4, '-oc');
117                 [xH5,H5,A05,A0theo5,h05,h0theo5]=contact_angle_n(c5,...
118         c5x,c5y,xselect5);
119                 plot(xH5,H5, '-om');
120                 [xH6,H6,A06,A0theo6,h06,h0theo6]=contact_angle_n(c6,...
121         c6x,c6y,xselect6);
122                 plot(xH6,H6, '-oy');
123                 hleg1 = legend({'line 1','line 2','line 3','line 4',...
124         'line 5','line 6'},'Location','NorthWest');
125                 hold off;
126
127                 %------ Save parameters in parameters.txt file
128                 fid = fopen('parameters.txt', 'w');
129                 fprintf(fid, '%7.5f %7.5f %8.5f %8.5f \n %7.5f %7.5f...
130         %8.5f %8.5f \n %7.5f %7.5f %8.5f %8.5f \n %7.5f %7.5f...
131         %8.5f %8.5f \n %7.5f %7.5f %8.5f %8.5f \n %7.5f %7.5f...
132         %8.5f %8.5f', A01,A0theo1,h01,h0theo1, A02,A0theo2,h02,...
133         h0theo2, A03,A0theo3,h03,h0theo3, A04,A0theo4,h04,...
```

```
134         h0theo4, A05,A0theo5,h05,h0theo5, A06,A0theo6,h06,h0theo6);
135                 fclose(fid);
136         end
137 
138         %------ Save height and its x-values for each line in txt-files
139     %------ for ORIGIN evaluation
140         fid = fopen(strcat(file1,'_01','_heights_l1.txt'), 'w');
141         for m=1:length(H1)
142             fprintf(fid, '%7.1f %6.5f \n',xH1(m),H1(m));
143         end
144         fclose(fid);
145 
146         fid = fopen(strcat(file1,'_01','_heights_l2.txt'), 'w');
147         for m=1:length(H2)
148             fprintf(fid, '%7.1f %6.5f \n',xH2(m),H2(m));
149         end
150         fclose(fid);
151 
152         fid = fopen(strcat(file1,'_01','_heights_l3.txt'), 'w');
153         for m=1:length(H3)
154             fprintf(fid, '%7.1f %6.5f \n',xH3(m),H3(m));
155         end
156         fclose(fid);
157 
158         fid = fopen(strcat(file1,'_01','_heights_l4.txt'), 'w');
159         for m=1:length(H4)
160             fprintf(fid, '%7.1f %6.5f \n',xH4(m),H4(m));
161         end
162         fclose(fid);
163 
164         fid = fopen(strcat(file1,'_01','_heights_l5.txt'), 'w');
165         for m=1:length(H5)
166             fprintf(fid, '%7.1f %6.5f \n',xH5(m),H5(m));
167         end
168         fclose(fid);
169 
170         fid = fopen(strcat(file1,'_01','_heights_l6.txt'), 'w');
171         for m=1:length(H6)
172             fprintf(fid, '%7.1f %6.5f \n',xH6(m),H6(m));
173         end
174         fclose(fid);
175 
176 
177 %--------------- stack ------------------------------------------------------
178     case 'Y'
179         %------ find Raw Data
180         [FileName,PATH] = uigetfile({'*.jpg;*.tif;*.png;*.gif',...
181     'All Image Files'},...
182         'Select the first image of the sequence/stack: ',...
183         'C:\Dokumente und Einstellungen\kreidler\Eigene Dateien\...
```

```
184     Messungen\Mikroskop\');
185         [pathstr, name, ext] = fileparts(fullfile(PATH,FileName));
186         cd(PATH);
187 
188         prompt = {'Enter the "constant" part of the image name...
189     without underscore, e.g. for sequence "name_01.tif",...
190     "name_02.tif", ..., "name_29.tif" enter "name" : '};
191         dlg_title = 'Input for stacks';
192         num_lines = 1;
193         def = {name};
194         file_cell = inputdlg(prompt,dlg_title,num_lines,def);
195         file = file_cell{1};
196         %------ check input...
197         checkfileFlag = strcmp(name,file);
198         if checkfileFlag==1
199             prompt = {'Please delete numbers at the end of the...
200                filename!'};
201             file_cell = inputdlg(prompt,dlg_title,num_lines,def);
202             file = file_cell{1};
203             checkfileFlag = strcmp(name,file);
204                 if checkfileFlag==1
205                     prompt = {'Please delete the last...
206                    characters of the filename...
207                    to get "constant" part!'};
208                     file_cell = inputdlg(prompt,dlg_title,...
209                      num_lines,def);
210                     file = file_cell{1};
211                     checkfileFlag = strcmp(name,file);
212                     if checkfileFlag==1
213                         message = sprintf('Bloody idiot!');
214                         uiwait(msgbox(message));
215                     end
216                 end
217         end
218         dirOutput = dir(fullfile(PATH,strcat(file,'*',ext)));
219 
220         %------ crop the image
221         crop(PATH, file, ext, dirOutput);
222 
223         %------ filename of cropped image without number and file
224                 %------ extension
225         file1=strcat(file,'_cut');
226         dirOutput1 = dir(fullfile(PATH,strcat(file1,'*',ext)));
227 
228         %------ interpolate illumination in a ROI containing the
229                 %------ object you are interested in
230         illucal(PATH, file1, ext, dirOutput1);
231 
232         %------ filename of cropped image with interpolated
233     %------ illumination without number and file extension
```

```
234         file2=strcat(file1,'_background');
235         dirOutput2 = dir(fullfile(PATH,strcat(file2,'*',ext)));
236 
237         %------ average background images
238         average(PATH, file2, ext, dirOutput2);
239 end
```

Calculation of the Height Profile with the "Refractive Index Method"
This function is based on code of Tobias Hofmann. Only minor adaption were implemented.

```
function [xH,H,A0,A0theo,h0,h0theo]=...
                  contact_angle_n(c1,c1x,c1y,xselect1)

% REFRACTIVE INDEX MODEL
n = [1.525 1.3423 1.486 1.3447];% refractive indices [n_glass n_out...
                % n_m n_in]; m for membrane
d = 4;                          % Bilayer thickness (d(1)=h, d(2)=d)
lambda = 546;

r01 = (n(1)-n(2))/(n(1)+n(2));
r12 = (n(2)-n(3))/(n(2)+n(3));
r23 = (n(3)-n(4))/(n(3)+n(4));

gamma = (r23/r12)*(1-r12^2);
L_lipid = (4*pi*n(3)*d)/lambda;
A0theo = 2*(r12/r01)*(r01*r01-1)*sqrt(1+gamma^2+2*gamma*cos(L_lipid));
h0theo = (-lambda/(4*pi*n(2)))*atan((gamma*sin(L_lipid))/...
(1+gamma*sin(L_lipid)));

A0 = 0.21727; % A0, h0 and y0 from fit of theoretically calculated...
          % intensity (Inorm.m) in ORIGIN
h0 = 43.87617;% with Inorm(h) = y0 + A*cos(4*pi*n_out*(h-h0)/lambda)
y0 = 0.0118;  % using n_out=1.3423 and lambda=546 nm


dist = sqrt((c1x(2)-c1x(3))*(c1x(2)-c1x(3))+...
(c1y(2)-c1y(3))*(c1y(2)-c1y(3)));
x=(0:dist:dist*(length(c1)-1)); %eichung: 1384 pixel entsprechen...
                % 141,7 um -> 1px = 0,1024 um
                    % (siehe unten)

subplot(1,2,1);
ccc=(1:1:length(c1))*dist*0.1024;
plot(ccc,c1);

xextr = xselect1*dist; %[8, 16, 24, 32, 41, 48]; %xwerte der extrema,
               % (xmin xmax xmin xmax xmin ...)

count = 1;
index=1;

% Berechne Höhenprofil, indem den einzelnen Branches zwischen den
% Maxima die entsprechenden reziproken Funktion zugeordnet werden

while(count<length(xextr)) %gehe einzelne branches zw extrema durch
```

```
46      branch=count-1;
47
48  %       REFRACTIVE INDEX MODEL
49      if ((branch==0) | (mod(branch,2)==0)) %%if branch is even: 0,2,..
50          height = @(R_exp)-acos((y0-R_exp)/A0)/(4*pi*n(2)/lambda)+h0+...
51      branch/2*lambda/(2*n(2));
52      elseif (branch < 0)
53          disp('Not interested in negative Branches!');
54      else  %if branch is uneven
55          height = @(R_exp)acos((y0-R_exp)/A0)/(4*pi*n(2)/lambda)+h0+...
56      (branch-1)/2*lambda/(2*n(2));
57      end
58
59      while(x(index)≤xextr(count)) %erhöhe innerhalb eines branchs die
60                    % xwerte bis zum nächsten extremum
61          %if(mod(xextr,2)==0) Imin=Iextr; %falls xtremum gerade
62          H(index)=height(c1(index));%, Im, IM);
63          if imag(H(index))≠0
64              H(index)=NaN;
65              disp('NaN at branch ');
66              disp(count);
67          end
68          index=index+1;
69      end
70      count=count+1;
71  end
72
73  xH= x(1:length(H))*0.1024; %eichfaktor, längenangabe danach in um
74  H=H/1000; %angabe der höhe in mikrometern
```

Calculation of the Height Profile with the "Intensity Method"
This function is based on code of Tobias Hofmann. Only minor adaption were implemented.

```
function [xH,H]=contact_angle_I(c1,c1x,c1y,xselect1,yselect1)

lambda=546;
n2 = 1.3423;

dist = sqrt((c1x(2)-c1x(3))^2+(c1y(2)-c1y(3))^2);
x=(0:dist:dist*(length(c1)-1)); %eichung: 1384 pixel entsprechen
            % 141,7 um -> 1px = 0,1024 um (siehe unten)

subplot(1,2,1);
ccc=(1:1:length(c1))*dist*0.1024;
plot(ccc,c1);

xextr = xselect1*dist;%[8, 16, 24, 32, 41, 48]; %xwerte der extrema
Iextr = yselect1;
% beginne mit minimum ausserhalb der adhäsionsfläche, ab dem
% 1. branch gilt

count = 1; % nach erstem minimum liegt der zweite ast. bis zum
       % ersten der erste ast
index=1;

% Berechnung des Membran-Höhenprofils entlang der Linie nach der
% Min/Max-Methode:

while(count<length(xextr)) %gehe einzelne branches zw extrema durch
    branch=count;
    if (mod(branch,2)==0) %if branch is even: 2,4,..
        vz=-1;
        BRA = branch;
    elseif ((branch == 0) || (branch<0))
        disp('Not interested in negative Branches or zero!');
    else  %if branch is uneven
        vz=1;
        BRA = branch-1;
    end
    height = @(I, Imin, Imax)vz*acos((2*I-Imin-Imax)/(Imax-Imin))/...
    (4*pi*n2/lambda)+BRA/2*lambda/(2*n2);%definiere jeweilige höhenfkt

    while(x(index)<xextr(count)) % erhöhe innerhalb eines branchs die
                % xwerte bis zum nächsten extremum
        %if(mod(xextr,2)==0) Imin=Iextr; %falls xtremum gerade
        if count==1  %neu, falls in adhäsionsfläche
            IM=max(c1(1:xselect1)); % wähle max aus elementen vor
            % 1. minimum, d.h. in der adhäsionsfläche
```

```
46              Im=Iextr(1);
47          else
48              if(Iextr(count)>Iextr(count-1))
49                  IM=Iextr(count);
50                  Im=Iextr(count-1);
51              else Im=Iextr(count);
52                  IM=Iextr(count-1);
53              end
54          end
55          H(index)=height(c1(index), Im, IM);
56          if imag(H(index))~=0
57              H(index)=NaN;
58              disp('NaN');
59          end
60          index=index+1;
61      end
62      count=count+1;
63  end
64
65  xH= x(1:length(H))*0.1024; %eichfaktor, längenangabe danach in um
66  H=H/1000; %angabe der höhe in mikrometern
```

Acquire the Intensity along Six Lines

```
function [c1x,c1y,c1,c2x,c2y,c2,c3x,c3y,c3,c4x,c4y,c4,c5x,c5y,c5,...
      c6x,c6y,c6,xselect1,xselect2,xselect3,xselect4,xselect5,...
      xselect6,yselect1,yselect2,yselect3,yselect4,yselect5,...
      yselect6] = lineprofile(A,B,PATH,file,ext)

burnedImage = A;

figure, imshow(A);

% ----- interactively draw 6 lines and save starting and end point
% in variable "positioni"; double-click for next line

message = sprintf('Draw 6 lines interactively; double-click on the...
last drawn line to draw next line.');
uiwait(msgbox(message));

h1 = imline;
position1 = wait(h1);
binaryImage1 = h1.createMask(); % create mask of line
burnedImage(binaryImage1) = 255; % burn line into image

h2 = imline;
position2 = wait(h2);
binaryImage2 = h2.createMask(); % create mask of line
burnedImage(binaryImage2) = 255; % burn line into image

h3 = imline;
position3 = wait(h3);
binaryImage3 = h3.createMask(); % create mask of line
burnedImage(binaryImage3) = 255; % burn line into image

h4 = imline;
position4 = wait(h4);
binaryImage4 = h4.createMask(); % create mask of line
burnedImage(binaryImage4) = 255; % burn line into image

h5 = imline;
position5 = wait(h5);
binaryImage5 = h5.createMask(); % create mask of line
burnedImage(binaryImage5) = 255; % burn line into image

h6 = imline;
position6 = wait(h6);
binaryImage6 = h6.createMask(); % create mask of line
burnedImage(binaryImage6) = 255; % burn line into image

% ----- store image with burned lines
```

```
48 imwrite(burnedImage, fullfile(PATH,strcat(file,'_lines',ext)));
49
50 % ----- use averaged image (with a 3x3 average filter) to plot
51 % ----- lineprofile of each line
52 h = fspecial('average');
53 C = imfilter(B,h);
54 [c1x,c1y,c1]  = improfile(C, [position1(1,1) position1(2,1)],...
55 [position1(1,2) position1(2,2)]);
56 [c2x,c2y,c2]  = improfile(C, [position2(1,1) position2(2,1)],...
57 [position2(1,2) position2(2,2)]);
58 [c3x,c3y,c3]  = improfile(C, [position3(1,1) position3(2,1)],...
59 [position3(1,2) position3(2,2)]);
60 [c4x,c4y,c4]  = improfile(C, [position4(1,1) position4(2,1)],...
61 [position4(1,2) position4(2,2)]);
62 [c5x,c5y,c5]  = improfile(C, [position5(1,1) position5(2,1)],...
63 [position5(1,2) position5(2,2)]);
64 [c6x,c6y,c6]  = improfile(C, [position6(1,1) position6(2,1)],...
65 [position6(1,2) position6(2,2)]);
66
67 figure, plot((1:1:length(c1)),c1);
68 title('Lineprofile along line 1');
69 set(gcf, 'Position', get(0,'Screensize')); % Maximize figure.
70 message = sprintf('Click once to activate data selection tool and...
71 hold to select extremes. Start with maxiumum in adhesion area.');
72 uiwait(msgbox(message));
73 [¬,xselect1,yselect1] = selectdata('selectionmode','brush',...
74 'BrushSize',0.01,'BrushShape','rect');
75
76 figure, plot((1:1:length(c2)),c2);
77 title('Lineprofile along line 2');
78 set(gcf, 'Position', get(0,'Screensize')); % Maximize figure.
79 message = sprintf('Click once to activate data selection tool and...
80 hold to select extremes. Start with maxiumum in adhesion area.');
81 uiwait(msgbox(message));
82 [¬,xselect2,yselect2] = selectdata('selectionmode','brush',...
83 'BrushSize',0.01,'BrushShape','rect');
84
85 figure, plot((1:1:length(c3)),c3);
86 title('Lineprofile along line 3');
87 set(gcf, 'Position', get(0,'Screensize')); % Maximize figure.
88 message = sprintf('Click once to activate data selection tool and...
89 hold to select extremes. Start with maxiumum in adhesion area.');
90 uiwait(msgbox(message));
91 [¬,xselect3,yselect3] = selectdata('selectionmode','brush',...
92 'BrushSize',0.01,'BrushShape','rect');
93
94 figure, plot((1:1:length(c4)),c4);
95 title('Lineprofile along line 4');
96 set(gcf, 'Position', get(0,'Screensize')); % Maximize figure.
97 message = sprintf('Click once to activate data selection tool and...
```

```
hold to select extremes. Start with maxiumum in adhesion area.');
uiwait(msgbox(message));
[¬,xselect4,yselect4] = selectdata('selectionmode','brush',...
'BrushSize',0.01,'BrushShape','rect');

figure, plot((1:1:length(c5)),c5);
title('Lineprofile along line 5');
set(gcf, 'Position', get(0,'Screensize')); % Maximize figure.
message = sprintf('Click once to activate data selection tool and...
hold to select extremes. Start with maxiumum in adhesion area.');
uiwait(msgbox(message));
[¬,xselect5,yselect5] = selectdata('selectionmode','brush',...
'BrushSize',0.01,'BrushShape','rect');

figure, plot((1:1:length(c6)),c6);
title('Lineprofile along line 6');
set(gcf, 'Position', get(0,'Screensize')); % Maximize figure.
message = sprintf('Click once to activate data selection tool and...
hold to select extremes. Start with maxiumum in adhesion area.');
uiwait(msgbox(message));
[¬,xselect6,yselect6] = selectdata('selectionmode','brush',...
'BrushSize',0.01,'BrushShape','rect');
```

Calculation of the Background Intensity behind an Object which was Masked
A mask is interactively created in an image and pixels inside the mask are set to zero (black). Black pixels are converted to NaN and subsequently interpolated by the function inpaint_nans.m. This function can handle image stacks with less than 100 images.

```
function illucalc(PATH, file, ext, dirOutput)

% file ='timelapse_63nm_PEG_passiviert_GUV_01_t_cut'; % for testing...
% FOLDER = '2012_07_25_CO'; % for testing...

%dirOutput = dir(fullfile(PATH,file));
fileNames = {dirOutput.name}';

maxnumber = size(fileNames,1);

I = imread(fullfile(PATH,fileNames{1}));

figure, imshow(I);
axis on;
title('Cropped Image');
set(gcf, 'Position', get(0,'Screensize')); % Maximize figure.
message = sprintf('Draw a polygon around the object of interest...
by clicking\nwith the left mouse button at the polygon corners.');
uiwait(msgbox(message));
hIP = impoly();
% ----- Create a binary image ("mask") from the ROI object.
binaryImage = hIP.createMask();

for i=1:maxnumber
    I = imread(fullfile(PATH,fileNames{i}));
    J = medfilt2(I,[5,5]);

    objectMaskedImage = J;
    objectMaskedImage(binaryImage) = 0;

    % ----- set zeros to NaN
    backgr = im2double(objectMaskedImage);
    [y,x] = size(J);
    for k=1:1:x
        for l=1:1:y
            if backgr(l,k)==0
                backgr(l,k)=NaN;
            end
        end
    end
    backgr = inpaint_nans(backgr,4); % use 2 or 4, OR 3
                      % (run out of memory...)
```

```
43      background = uint8(backgr*255); % convert to image format;
44
45      % ----- set correct numbering for later storage of images
46      k0 ='0';
47      if i<10
48          k=strcat(k0, int2str(i));
49      elseif i<100
50          k=int2str(i);
51      end
52
53      backgrfile = strcat(file, '_background_', k, ext);
54
55      imwrite(background, fullfile(PATH, backgrfile));
56  end
57
58  close all;
```

Cropping of Images

The same area is cropped from all images of a stack and each cropped image is saved. This function can handle image stacks with less than 100 images.

```
function crop(PATH, file, ext, dirOutput)

% file ='timelapse_63nm_PEG_passiviert_GUV_01_t'; % for testing...
% FOLDER = '2012_07_25_CO'; % for testing...

%fileFolder = fullfile('C:', 'Dokumente und Einstellungen',...
%'kreidler', 'Eigene Dateien', 'Messungen', 'Mikroskop', FOLDER);
%dirOutput = dir(fullfile(fileFolder,strcat(file, '*.tif')));
fileNames = {dirOutput.name}';

maxnumber = size(fileNames,1);

I = imread(fullfile(PATH,fileNames{1}));
message = sprintf('Choose a rectangular ROI interactively. Then...
      double-click inside of the rectangle!');
uiwait(msgbox(message));
[I2 rect] = imcrop(I);

% ---------- store first cropped image
file1 = strcat(file, '_cut_01', ext);
imwrite(I2, fullfile(PATH, file1));

%---- crop the same area in alle other images and save cropped images
for i=2:maxnumber

    k0 ='0';
    if i<10
        k=strcat(k0, int2str(i));
    elseif i<100
        k=int2str(i);
    end

    I = imread(fullfile(PATH,fileNames{i}));
    I1 = imcrop(I, rect);
    file1 = strcat(file, '_cut_', k, ext);
    imwrite(I1, fullfile(PATH, file1));
end

close all;
```

Average Images

An average image is calculated from all images of a stack.

```
function average(PATH,file,ext,dirOutput)

%fileFolder = fullfile('C:', 'Dokumente und Einstellungen',...
%'kreidler', 'Eigene Dateien', 'Messungen', 'Mikroskop',..
%FOLDER, 'evaluation');
%dirOutput = dir(fullfile(fileFolder,strcat(file, '*.tif')));
fileNames = {dirOutput.name};

maxnumber = size(fileNames,1);

%if maxnumber==1
%    I = imread(fullfile(PATH,fileNames{1}));
%    J = im2double(I); % avoiding truncation at 255 when summing up
                % (as would be the case for uint8)
%    M=J;
%else
    for i=1:maxnumber
        I = imread(fullfile(PATH,fileNames{i}));
        J = im2double(I); % avoiding truncation at 255 when summing
              % up (as would be the case for uint8)
        if i==1 % adding up the images
            M=J;
        else
            M = M+J;
        end
    end
%end

im = M/maxnumber; % divide by the number of images
image = uint8(im*255); % convert to image format

averagefile = strcat(file,'_average',ext);
imwrite(image, fullfile(PATH, averagefile)); % save the averaged
                          % image as tif
```

Calculation of the Reflected, Normalized Intensity

The intensity of reflections at three interfaces is calculated and normalized to the background intensity.

```
function Itheo = Inorm(n,d_m,lambda)
%  h als vektor eingegeben, alle längen in nm angeben

L_m = 2*n(3)*d_m; %

interfaces = length(n);
k=2*pi/lambda;

r = zeros(1,interfaces-1); % eingefügt nach Tipp von Matlab;
                % CE 20.08.2012

for j=1:(interfaces-1)
    r(j)=(n(j)-n(j+1))/(n(j)+n(j+1));
end;

h = (0:500); % Abstände in nm, über die Rn berechnet werden soll:
          % hier 0-500nm
dim = length(h);
L = zeros(1,dim);

for l=1:dim
    L(l)=2*n(2)*h(l);
end;

R = r(1)+(1-r(1)^2)*exp(-1i*k*L)*r(2)+(1-r(1)^2)*(1-r(2)^2)...
*exp(-1i*k*(L+L_m))*r(3); % i geändert in 1i nach Tipp von Matlab;
               % CE 20.08.2012
Rn = (abs(R).^2-r(1)^2)/r(1)^2;
Itheo = [h;Rn];

%------ Save height and theoretical intensity in .txt files
fid = fopen('Inorm.txt', 'w');
for m=1:dim
    fprintf(fid, '%7.1f \t %6.5f\n',Itheo(:,m));
end
fclose(fid);
```

D Chemicals and Materials

D.1 General Equipment

- Eppendorf pipettes: Research and Reference
- Eppendorf tubes: 0.5 ml, 1.5 ml and 2.0 ml, normal and Protein LoBind
- plastic tubes: 15 ml and 50 ml, #188271 and #227261, Greiner Bio-One
- Parafilm, #PM-996, Bemis
- Kimwipe, #05511, Kimberly-Clark
- glass cover slips, #H873 (20x20 mm), #1871 (24x50 mm) and #H878 (24x60 mm), Carl Roth

D.2 Giant Vesicles

D.2.1 Lipids

- eggPC, #840051, Avanti Polar Lipids
- eggPA, #840101, Avanti Polar Lipids
- DPPE PEG2000, #880160, Avanti Polar Lipids
- brainPS, #840032, Avanti Polar Lipids
- cholesterol, #700000, Avanti Polar Lipids
- BODIPY-PC, #D3793, life technologies

D.2.2 Other Chemicals

- $CHCl_3$, #6340, Carl Roth
- MeOH, #4627, Carl Roth
- EtOH, #9065, Carl Roth
- manganese(II) chloride, #0276, Carl Roth
- D(+)-trehalose dihydrate, #5151, Carl Roth
- D(+)-sucrose, #177140010, Acros Organics
- D(+)-glucose, anhydrous, #G6152, Sigma-Aldrich
- Hellmanex II, #320.001, Hellma

D.2.3 Equipment

- brown glass bottles (#E160.1, Carl Roth) with screw caps (#E162.1, Carl Roth) and teflon septum (#E163.1, Carl Roth)
- sigillum wax #9120101, Hirschmann Laborgeräte
- ITO-coated glass slides, #CEC010S, Präzisions Glas & Optik
- platinum wire, #PT005145, Goodfellow
- copper foil shielding tape, electrical tape, 12 mm width, #1181, 3M
- tip sonicator, Bandelin Sonopuls, #HD 2070, Bandelin electronic equipped with sonotrode MS72
- Avanti Min Extruder, #610000, Avanti Polar Lipids
- Nuclepore Track-Etch membranes, PC MB 19 mm; pore sizes 50 nm (#800308), 100 nm (#800309) and 200 nm (#800281); Whatman
- Silicones, heavy duty high-vacuum grease, Wacker

D.2.4 Reconstitution of Integrin

1. Bio-Beads SM2 adsorbent, #152-8920, Bio-Rad
2. stirring bars, micro 5x2 mm, #442-0361, VWR

D.2.5 Density Gradient Centrifugation

- Nycodenz, #1002424, Axis Shield
- Ultra-Clear centrifugation tubes, #344062, Beckman Coulter

D.2.6 Homogeneously Coated Glass Slides to Study Adhesion of GUVs

- poly-L-lysine, 0.1% (w/v) in water, #P8920, Sigma-Aldrich
- 30% hydrogen peroxide, #8070, Carl Roth
- sulfuric acid, #X944, Carl Roth
- β-casein, #C6905, Sigma-Aldrich

D.3 Biochemical Methods

D.3.1 SDS-PAGE

- Rotiphorese Gel 30, #3029, Carl Roth
- TEMED, #2367, Carl Roth
- ammonium persulfate, #9592, Carl Roth

- Bio-Safe Coomassie, #161-0786, Bio-Rad
- β-2-mercaptoethanol, #2865, Serva
- Page Ruler Plus (PRP), prestained protein ladder, #26619, Thermo Scientific

D.3.2 Western Blotting

- Ponceau S, #161470250, Acros Organics
- anti-integrin α_{IIb}, mouse, monoclonal, #ab63323, abcam → not any more in product range → possible replacement: #ab134131, abcam
- anti-integrin β_3, mouse, monoclonal, #CBL479, Chemicon
- anti-fibrinogen, mouse, monoclonal, #F4639, Sigma-Aldrich
- anti-mouse IgG, AP-conjugated, goat, #G21060, life technologies

D.3.3 ELISA

- Tween 20, #9127, Carl Roth
- albumin bovine fraction V, #11924, Serva
- diethanolamine, #A13389, Alfa Aesar
- fibrinogen, #341578, Calbiochem
- anti-integrin α_{IIb}, rabbit, polyclonal, #AB1967, Chemicon
- anti-rabbit IgG, AP-conjugated, goat, #401312, Calbiochem
- p-nitrophenylphosphate, #4165, Carl Roth
- microplate, 96 F-bottom, #655101, Greiner Bio-One

D.3.4 Co-Immunoprecipitation

- Dynabeads Protein G, #100-03D, life technologies
- strong magnet, e.g. #K-19-C, www.supermagnete.de
- anti-integrin α_{IIb}, mouse, monoclonal, #I9660, Sigma-Aldrich
- anti-integrin β_3, rabbit, monoclonal, #ab119992, abcam

D.4 Protein Purification

D.4.1 Integrin

- Tris base, #4855, Carl Roth
- NaCl, #3957, Carl Roth
- EDTA dihydrate, #A2937, AppliChem

- acetylsalicylic acid, #A5376, Sigma-Aldrich
- $CaCl_2$ dihydrate, #208291, Calbiochem
- $MgCl_2$ hexahydrate, #012288, Alfa Aesar
- cOmplete EDTA-free protease inhibitor cocktail tablets, #05892791001, Roche
- Triton X-100, #93420, Fluka
- Triton X-100 reduced, #X100RS, Sigma-Aldrich
- NaN_3, #14314, Alfa Aesar
- methyl-α-D-manno-pyranoside, #M6882, Sigma-Aldrich
- Aprotinin, #3428, Sigma-Aldrich
- NaOH, #1.06498.0500, Merck
- ConA Sepharose 4B, #17-0440-01, GE Healthcare
- XK 16/20 column, #18-8773-01, GE Healthcare
- HiPrep Heparin FF 16/10, #28-9365-49, GE Healthcare
- Hiload 26/60 Superdex 200 prep grade, #17-1071-01, GE Healthcare

Measurement of Integrin Concentration

- BCA Protein Assay Kit, #23225, Thermo Scientific

Labeling of Integrin with the dye TAMRA

- Amicon Ultra-4 and -15, Ultracel-50K, #UFC805096 and #UFC905024, Millipore
- 5-(and-6)-carboxytetramethylrhodamine succinimidyl ester, #C1171, Molecular Probes
- PD-10 desalting columns, #17-0851-01, GE Healthcare

D.4.2 Actin

- ATP, #10920, Serva
- dithiothreitol, #39759, Serva
- DNase I, #11284932001, Roche
- A23187, #A2110, AppliChem
- phalloidin Alexa Fluor 488 and 647, #A12379 and #A22287, life technologies

D.5 Agarose-Lipid-Hybrid Films

- Agarose Type IX-A, ultra-low gelling temperature, #A2576, Sigma-Aldrich

E Lipid Mixtures

Typical concentrations of lipids are noted on the label of each glass flask and were the following: eggPC 25 mg ml^{-1}, eggPA 10 mg ml^{-1}, brainPS 10 mg ml^{-1}, DPPE 50 mg ml^{-1}, cholesterol 25 mg ml^{-1} and A23187 1 mg ml^{-1}.

Table E.1: Volumes of different ingredients to prepare lipid mixtures used in this work: *Standard*, *PS* and *Platelet* mixture.

lipid	Standard (µl)	PS (µl)	Platelet (µl)
eggPC	330	293	243
eggPA	95	-	-
brainPS	-	94	211.5
DPPE PEG2000	27.5	31.5	31
chol	-	-	108
A23187	173	150	149

F Buffers

In general, ingredients of buffers are dissolved in ultra-pure water of about 70% of the final volume of buffer. The pH value is adjusted by titration of either acid (typically hydrochloric acid) or base (typically sodium hydroxide) before ultra-pure water is added to the final volume.

F.1 Integrin

Table F.1: Platelet washing buffer.

ingredient	amount per l (g)
20 mM Tris/HCl pH 7.4	2.422 g
150 mM NaCl	8.766 g
1 mM EDTA	0.372 g
0.01% (w/v) acetylsalicylic acid	0.1 g

Table F.2: Platelet lysing buffer with Triton X-100. The same buffer was also prepared without Triton X-100.

ingredient	amount per 500 ml (g)
50 mM Tris/HCl pH 7.4	3.025 g
1 mM $CaCl_2$	0.5 ml of 1 M stock
1 mM $MgCl_2$	0.5 ml of 1 M stock
0.1% (w/v) Triton X-100	0.5 g

Table F.3: Buffer for equilibration of ConA and Heparin affinity columns.

ingredient	amount per 2 l (g)
20 mM Tris/HCl pH 7.4	4.84 g
100 mM NaCl	11.68 g
1 mM $CaCl_2$	2 ml of 1 M stock
1 mM $MgCl_2$	2 ml of 1 M stock
0.1% (w/v) Triton X-100	2 g
0.02% (w/v) NaN_3	2 ml of 20% stock

Elution of proteins bound to ConA is achieved by addition of 100 mM methyl-α-D-manno-pyranoside to 200 ml equilibration buffer, which is equivalent to 3.884 g.

Table F.4: Integrin buffer

ingredient	amount per 2 l (g)
20 mM Tris/HCl pH 7.4	4.84 g
150 mM NaCl	17.53 g
1 mM $CaCl_2$	2 ml of 1 M stock
1 mM $MgCl_2$	2 ml of 1 M stock
0.1% (w/v) Triton X-100	2 g
0.02% (w/v) NaN_3	2 ml of 20% stock
2 mg ml^{-1} Aprotinin	4 mg

F.2 Platelet Membranes

Table F.5: Platelet washing buffer 1.

ingredient	amount per l (g)
120 mM NaCl pH 7.0	7.01 g
13 mM trisodium citrate	3.82 g
30 mM dextrose	5.95 g

Table F.6: G buffer.

ingredient	amount per l (g)
2 mM Tris/HCl pH 8.0	0.242 g
0.2 mM ATP	0.110 g
0.2 mM $CaCl_2$	50 µl of 1 M stock
0.02% (w/v) NaN_3	1 ml of 20% stock
0.2 mM DTT (after titration)	0.03 g

Table F.7: G* buffer.

ingredient	amount per l (g)
2 mM Tris/HCl pH 8.0	0.242 g
0.2 mM ATP	0.110 g
0.05 mM $MgCl_2$	50 µl of 1 M stock
0.02% (w/v) NaN_3	1 ml of 20% stock
0.2 mM DTT (after titration)	0.03 g

F.3 Actin

F.4 Inner and Outer Buffer for Adhesion Experiments with Platelet-GUVs

Table F.8: Inner buffer.

ingredient	amount per l (g)
2 mM Tris/HCl pH 8.0	0.242 g
0.05 mM $MgCl_2$	50 µl of 1 M stock
0.02% (w/v) NaN_3	1 ml of 20% stock
200 mM sucrose	68.46 g

GUVs grown in the inner buffer were diluted 1:2 (v/v) in a buffer, for which 200 mM sucrose were replaced by 220 mM glucose and $CaCl_2$, $MgCl_2$ as well as $MnCl_2$ were added to a final concentration of 1.5 mM. Therefore, the outer buffer contained a mixture of sucrose and glucose as well as 1 mM of divalent calcium, magnesium and manganese ions. The osmolality was slightly higher than the inner buffer's osmolality.

F.5 SDS-PAGE and Western Blot

Lämmli Sample Buffer was purchased from Bio-Rad (#161-0737). Its composition is listed in table F.9.

Table F.9: 2x Lämmli sample buffer.

ingredient
62.5 mM Tris-HCl, pH 6.8
25% glycerol
2% SDS
0.01% Bromophenol Blue

Table F.10: Towbin buffer with SDS for blotting of SDS-polyacrylamide gels.

ingredient	amount per l (g)
25 mM Tris pH 8.3	3.03 g
192 mM glycine	14.4 g
20% (v/v) methanol	200 ml
0.1% (w/v) SDS	10 ml of 10% solution

Table F.11: Tris-buffered saline with Tween 20 (TBS-T).

ingredient	amount per l (g)
20 mM Tris/HCl pH 7.5	2.42 g
500 mM NaCl	29.24 g
0.05% (w/v) Tween 20	5 ml of 10% solution

G Protocols for Protein Purification and their Characterization

G.1 Purification of Integrin from Platelet Concentrate

All buffers used in column chromatography are thoroughly degassed before use.

Day 1

1. Start equilibrating the ConA-column with equilibration buffer (table F.3).
2. **Red cells removing:** (1 h)
   Outdated platelet concentrates (about 10 packages) are used within 14 days of venipuncture. Use plastic containers till cell breaking in step 4.
   Concentrate is put in six centrifugation tubes ($V \leq 450$ ml) which are weighed before. Centrifugation is done with the Sorvall RC6 centrifuge (Thermo Scientific) using the SLA 3000 rotor.
   Duration: 20 min
   Temperature: 22 °C
   Rotor: SLA 3000, 1400 rpm ($\hat{\approx}300\text{x}g$)
   Remove the **pellet** (red cells) $\hookrightarrow$ **waste**.
3. **Platelet washing:** (2.5 h)
   - Sedimentation of platelets:
     Duration: 30 min
     Temperature: 22 °C
     Rotor: SLA 3000, 4000 rpm ($\hat{\approx}2700\text{x}g$)
     Remove the **supernatant** and weigh the pellet.
   - The pellet (platelets) is resuspended in **platelet washing buffer** (table F.1) in two centrifugation tubes ($V \approx 100$ ml). This step is repeated three times and pellets are weighed in the end:
     Duration: 25 min
     Temperature: 22 °C
     Rotor: SLA 3000, 3100 rpm ($\hat{\approx}1600\text{x}g$)
4. **Cell breaking:** 4 °C (2 h)
   The pellets (washed platelets) are resuspended in about 100 ml of **platelet lysing buffer without Triton X-100** (table F.2) in a Schott bottle on ice. Platelets are broken with the Turrax homogenizer (20 s/time, two times). In the first round of cell breaking two tablets of cOmplete protease inhibitor are added and one tablet in the second round. The first sample of 1 ml is taken for documentation with SDS-PAGE. The resulting emulsion is centrifuged with an Optima L-80 XP ultracentrifuge (Beckman Coulter), that is also used in all following centrifugations.

Duration: 30 min
Temperature: 4 °C
Rotor: Beckman 45 Ti, 39 000 rpm (≈120 000xg)

5. **Membrane dissolving** (2.5 h)
   The pellets (lysed platelets) are resuspended in about 150 ml of **platelet lysing buffer** (table F.2) in a Schott bottle on ice. Platelet membranes are dissolved with the Turrax homogenizer (20 s/time, two times) adding two tablets of cOmplete protease inhibitor in each round. The resulting emulsion is rotated in 50 ml plastic tubes (Greiner Bio-One) for one hour at 4 °C. The second sample of 1 ml is taken for documentation with SDS-PAGE. Afterwards, the solution is centrifuged.
   Duration: 15 min
   Temperature: 4 °C
   Rotor: Beckman 45 Ti, 19 000 rpm (≈30 000xg)
   The pellet is disposed and 1 ml of the supernatant is kept as third sample for documentation.
6. **ConAs affinity chromatography** (2 h)
   The supernatant of step 5 (typically about 130 ml) is applied to the ConA column with the system pump at 0.5 ml min^{-1}. The column is subsequently washed overnight at 0.2 ml min^{-1}.
7. Equilibration of the HiLoad 26/60 Superdex 200 column is started with integrin buffer (table F.4).

Day 2

1. 200 ml of **elution buffer** is prepared for the ConA column by addition of 100 mM mannose to the equilibration buffer as stated below table F.3.
2. Bound glycoproteins on the ConA column are elute with aforementioned buffer:
   Flow rate: 0.5 ml min^{-1}
   Fraction size: 5 ml
3. The heparin column is equilibrated with **equilibration buffer** (table F.3)
4. The flow-through fractions of the peak are checked on their integrin content by SDS-PAGE. Fractions containing integrin are pooled and another sample is removed.
5. **Heparin affinity chromatography**
   The pooled flow-through of step 2 (typically about 80 ml) is applied to the heparin column with the system pump at 0.5 ml min^{-1}.
6. The flow-through fractions of the peak of the heparin column are checked on their integrin content by SDS-PAGE. Fractions containing integrin are pooled and another sample is removed.
7. The pooled flow-through is concentrated to within roughly 5 ml by ultrafiltration (Amicon Ultra-15, 50 kDa MWCO).
8. The concentrated flow-through is applied to the HiLoad 26/60 Superdex 200 column overnight:
   Flow rate: 1 ml min^{-1}
   Fraction size: 10 ml

Day 3

1. Peak fractions are analyzed by SDS-PAGE. Another sample of 1 ml is taken from one fraction for documentation with SDS-PAGE. Fractions with the highest concentration and purity of integrin $\alpha_{\mathrm{IIb}}\beta_3$ (typically fractions#29-30) are filtered through a membrane with 0.22 µm pore size and aliquots are stored at −80 °C

2. All columns are washed and regenerated according to the manufacturer.

G.2 ELISA for Integrin Binding Activity

Buffers:

- Integrin buffer without Triton X-100 (table F.4) denoted buffer A in the following
- Buffer A/Triton: buffer A plus 0,1% Triton X-100
- Buffer A/Tween: buffer A plus 0,04% Tween 20
- Blocking buffer: buffer A plus 3% BSA
- Antibody buffer: buffer A/Tween 3% BSA
- Buffer B: 10 mM diethanolamine/HCl pH 9.5, 0.5 mM MgCl2 (titration with 0.1 M HCl)
- EDTA: 100 mM EDTA/NaOH pH 8.5

Proteins/Antibodies/Materials:

- Fibrinogen $1\,\mathrm{mg\,ml^{-1}}$ in buffer A
- Integrin in buffer A/Triton X-100
- Primary antibody: 1:500 (v/v), anti-integrin α_{IIb}, rabbit, polyclonal, #AB1967, Chemicon
- Secondary Antibody: 1:500 (v/v), anti-rabbit IgG, AP-conjugated, goat, #L42008, Caltag
- Dye: p-nitrophenylphosphate (15 mg in 15 ml Buffer B)
- Microplate, 96 F-bottom, #655101, Greiner Bio-One

Volumes per step:

- Coating/incubation (Fibrinogen, 1st and 2nd AB, dye, EDTA) 100 µl
- Rinsing, blocking: 225 µl

Protocol:

1. Coating: 100 µl Fibrinogen per well, overnight at 4 °C
2. Rinse: 2 x 225 µl buffer A at room temperature
3. Blocking: 225 µl blocking buffer for 120 min at room temperature
4. Integrin incubation: 40 µl per well for 60 min
5. Rinse: 4 x 225 µl Buffer A/Tween
6. Incubation: Primary antibody, 100 µl per well for 60 min
7. Rinse: 4 x buffer A/Tween
8. Incubation: Secondary antibody, 100 µl per well for 60 min
9. Rinse: 4 x buffer A/Tween
10. Rinse: 2 x 225 µl buffer B
11. Dye: 100 µl of dye per well for 30 min
12. Stop: 100 µl EDTA Solution
13. As readout, the extinction is measured at 405 nm with a microplate reader

G.3 Labeling of Integrin with TAMRA

Nota bene: This protocol has been optimized for a 1:1 labeling rate per integrin dimer [144], but still it is necessary to determine dye/protein ratio and functionality by ELISA for each preparation.

Materials:

- Integrin $\alpha_{\mathrm{IIb}}\beta_3$, conc. $\geq 1\,\mathrm{mg\,ml^{-1}}$ in column buffer. Concentrate, if necessary by ultrafiltration (Amicon Ultra-4, 50 kDa MWCO)
- DMF, anhydrous
- TAMRA, SE (5-(and-6)-carboxytetramethylrodamine, succinimidyl ester; mixed isomers, #C1171, life technologies).
- PD-10 desalting column (GE Healthcare)
- Column buffer: 20 mM Tris/ HCl pH7.4, 150 mM NaCl, 1 mM CaCl2, 1 mM MgCl2, 0.1% Triton X-100, 0,02% NaN3, 2 mg Aprotinin/l.

Protocol:

1. Place about 1 ml integrin (1 to $5\,\mathrm{mg\,ml^{-1}}$ in column buffer pH 7.4) in a 2 ml Eppendorf tube.
2. Equilibrate PD-10 column against column buffer.
3. Dissolve $10\,\mathrm{mg\,ml^{-1}}$ TAMRA in anhydrous DMF.
4. Immediately add 50 µl dye solution drop-wise under slight shaking.
5. Rotate 1 h at r.t. in the dark.
6. Separate unbound dye from protein by gel filtration over PD-10 column.
7. Determine dye/protein ratio from molecular dye extinction ($\epsilon_{555} = 80\,000\,\mathrm{mol^{-1}\,cm}$ [144]) and protein absorption coefficient $1.18\,\mathrm{ml\,mg^{-1}\,cm}$ [158].
8. Determine functionality from ELISA binding test.

G.4 Purification of Platelet Membranes

Purification of platelet membranes was adapted following the protocol in [194]. Outdated platelet concentrate is used.

Day 1

1. Start equilibrating the ConA-column with equilibration buffer (table F.3).
2. **Red cells removing:**
   Centrifugation is done with the Sorvall RC6 centrifuge (Thermo Scientific) using the SLA 1500 rotor.
   Duration: 20 min
   Temperature: 22 °C
   Rotor: SLA 1500, 1200 rpm ($\approx$220xg)
   Remove the **pellet** (red cells) $\hookrightarrow$ **waste**.
3. **Platelet washing:**

- Sedimentation of platelets:
  Duration: 20 min
  Temperature: 22 °C
  Rotor: SLA 1500, 2150 rpm ($\hat{\approx}$700xg)
  Remove the **supernatant**.
- The pellet (platelets) is resuspended in **platelet washing buffer 1** (table F.5) in two centrifugation tubes ($V \approx 200$ ml). This step is repeated two times:
  Duration: 20 min
  Temperature: 22 °C
  Rotor: SLA 1500, 2150 rpm ($\hat{\approx}$700xg)

4. **Cell breaking with cell disruption bomb**
   The pellets (washed platelets) are resuspended in about 50 ml of **integrin buffer without Triton X-100** (table F.4, this buffer is denoted **buffer A** in the following) in a glass beaker. Two tablets of cOmplete protease inhibitor are added. The beaker is placed in the pressure chamber of a cell disruption bomb (#4635, Parr Instrument Co.). A pressure of 83 bar of nitrogen is applied for 30 min via a connected gas bottle. The resulting emulsion is centrifuged with an Optima L-80 XP ultracentrifuge (Beckman Coulter).
   Duration: 30 min
   Temperature: 4 °C
   Rotor: Beckman 45 Ti, 32 000 rpm ($\hat{\approx}$100 000xg)
   The supernatant is discarded. The **pellet** is resuspended in 20 ml **buffer A**.

5. **Nycodenz Cushion**
   20 ml of 21.5% Nycodenz are layered below 10 ml of sample. Nycodenz cushions are then centrifuged:
   Duration: 150 min
   Temperature: 4 °C
   Rotor: Beckman SW32 Ti, 28 000 rpm ($\hat{\approx}$100 000xg)
   Platelet membranes are recovered from the buffer/Nycodenz interface (about 5 ml per tube) and are mixed 1:5 (v/v) with **buffer A**.

6. **Removal of Nycodenz**
   Membranes are pelleted by centrifugation.
   Duration: 50 min
   Temperature: 4 °C
   Rotor: Beckman SW32 Ti, 28 000 rpm ($\hat{\approx}$100 000xg)
   The supernatant is discarded. The **pellet** is weighed and resuspended in **buffer A** with a concentration of approximately 30 mg ml^{-1}. Aliquots are stored at −80 °C.

Acknowledgment

This work took me on an interesting journey giving the opportunity to "dive" into the wide field of (protein-) biochemistry and coming into touch with biological science in general. I was able to learn a great deal about the "Importance of Stupidity in Scientific Research" [180]. Nevertheless, I also experienced moments of delight when experiments lead to new insights or when mere water droplets produced impressive images in the microscope. However, preparation of this thesis was only possible by the support of many people.

First, I would like to thank Prof. Joachim Spatz, who gave me the opportunity to work in his interdisciplinary group at the interface between biophysics, biochemistry and applied material science. Due to the availability of diverse and excellent equipment, I got the chance to learn many techniques for probing bio-inspired samples or investigating surfaces in general.

I am grateful to Prof. Rainer Fink, who kindly accepted to review my thesis.

I thank Michael Bärmann for initially providing me with this most exciting project and introducing me to protein purification as well as analytical biochemical methods.

Purification of proteins would not have been successful without the help of Christine Mollenhauer. She provided excellent work in the lab and delicious cake for moral support. Additionally, she was the link to my "indirect adviser" Jürgen Mollenhauer, who sometimes had to answer her questions after working hours. Many thanks to both of you!

I am indebted to Patricia Bassereau, Gilman Toombes and Sophie Aimon for fruitful discussions as well as for an instructive and pleasant stay in Paris. I am grateful, that I could get a taste of the special scientific atmosphere at Institut Curie.

Nano-structured bio-functionalized surfaces were prepared by Dennis Single, Martina Rau and Yvonne Schön. Thank you very much.

My fellow students and colleagues Ralf Kemkemer, Claudio Rolli, Martin Deibler, Jovana Matic, Borja Aragüés and Melih Kalafat were always there when advice was needed. Many thanks to them for all the fun and the great discussions at lunch. A big thanks goes to Claudio and Martin for proofreading of the manuscript of this thesis.

I also thank all the members of Spatz group in Heidelberg and Stuttgart for the good atmosphere, valuable discussions and all the help I received. I am grateful to Tobias Hofmann for his Matlab routines which were very helpful to evaluate images acquired by RICM.

Finally, my deep gratitude goes to my family, my wife Hanna and my friends for their support and patience during the last four years and especially the last four weeks.

Erklärung

Hiermit erkläre ich, dass ich die vorgelegte Dissertation selbst verfasst und mich keiner anderen als der von mir ausdrücklich bezeichneten Quellen und Hilfen bedient habe.

Stuttgart, den 01. Oktober 2012 . . . . . .

Christian Eberhard

Please insert this disk into your computer to see the movies.